Continuous direct ink jet printing.

Tay, Bee Yen

Continuous Direct Ink-Jet Printing

A thesis submitted for the degree of Doctor of Philosophy

by

Bee Yen Tay

Department of Materials

Queen Mary, University of London

Mile End Road, London E1 4NS

United Kingdom

July, 2001

Abstract

This thesis describes the preparation and continuous printing of zirconia ink under different conditions, as well as the development of silver inks, for the same purpose.

The dispersion of sub-micrometer zirconia powder in industrial methylated spirit using other additives such as dispersant and binder was investigated with different mixing methods and at varying powder and binder contents. The use of high shear mixing by triple roll milling followed by ultrasonic disruption as well as adequate sedimentation and filtration produced a homogeneous and stable ink of 2.5 vol. % ZrO_2. The ink could be printed directly and continuously on a commercial jet printer without interruption of any kind and the phenomena occurring during printing were investigated. The optimum modulation frequency for printing was determined with the generation of pear-shaped and symmetrical droplets. Printing was made on substrates of surface free energies lower and higher than the surface tension of the ZrO_2 ink. Powder migration was observed within a relic of the printed dot on the second type of substrate. Layers were also overprinted on the second type of substrate by varying the following: print resolution, printing interval, print area, drying conditions and ink powder loading. These series of prints were accompanied by the appearance of ridges, spattering and non-vertical walls and the effects were investigated.

The wettability and shrinkage of droplets of the ceramic ink was also studied in-situ by monitoring the evolution of contact angle, width of ink-substrate interface and droplet height with a video camera. The shape of the droplet experienced different dynamics on different types of substrate.

Lastly, the sedimentation behaviour of ethanol-based silver inks dispersed with different types of dispersant was investigated with respect to the sediment volume and half-value time. Deflocculated ink was obtained at a low dispersant level and powder loading.

Table of Contents

Acknowledgements

My supervisor, Professor Mohan Edirisinghe has been a counsellor and a mentor. If you have read the original drafts of the various papers, which have evolved from this research, you will appreciate the great pains he took in helping to get them in their final forms. I am deeply grateful – and, yes, also for his unyielding insistence on publishable papers, which has provided the requisite motivation to complete this work.

Thanks are also due to John Caulfield, Nigel Leyland, Zofia Luklinska, Tony Otten, Haroon Rashid and Bob Whitenstall for many constructive discussions and their helps related to this research work. Parts of the work were performed in the Institute of Polymer Technology and Materials Engineering, Loughborough University, Leicestershire and Linx Printing Technologies Plc., Cambridge. The assistance of Isla Mathieson, Frank Page and Susan Williams are acknowledged. Uniqema, Belgium is acknowledged for supplying all the dispersants used in this research; in particular, Bart Dehuvyne and Luc Mattheus are thanked for their helps and advice. I am also grateful to all the Drs-to-be in Room 236 for their friendship and laughter. I wish you all the best in your future endeavours.

The opportunity to pursue a post-graduate degree in the United Kingdom has been a far more educational experience than I wanted. This was made possible by the scholarship offered by the Gintic Institute of Manufacturing Technology, Singapore. The support given by L.C. Lee, Ian Pinwill and Choy, Chee Mun in the application and throughout the period of study is greatly appreciated.

My family has always been a bottomless well-spring of love and support. It is a blessing to be assured of their love wherever I go. Indeed, the thought of reuniting with them is an impetus for the completion of this endeavour. The constant encouragement and kindness, be it in words, prayers or deeds, of my wonderful friends: Ah Huay, Clara, Dorothy, Elsie, Gaby, Le Le Win, Roy, Siok Cheng, Wai Ying and Yee Lay meant a lot to me. My thanks also to Edwin for proofreading this thesis and giving me so much encouragement and love over the years. Thank you for convincing me that I could complete the work and keeping your faith in me at times when I was ready to give up.

Surely, no litany of thanks would be complete without my thanking to God, Father of my Lord Jesus Christ, who is my source of all love, wisdom, help and grace. I am grateful beyond all measure. It is He who began this work and will indeed bring it to completion (Philippians 1:6) and I know that His work in my life is still in progress.

Bee Yen Tay
July 2001

List of Tables and Figures

Figure **Pg**

Publications

Results of this research have been published/presented as follows:

1. TAY, B.Y., RASHID, H., WILLIAMS, S. and EDIRISINGHE, M.J., 1999. Direct ceramic ink-jet printing. *Poster session for 3rd UK-Ireland, Sol-Gel Group Meeting*, 14-15 June 1999, Loughborough University, UK.

2. RASHID, H., TAY, B.Y. and EDIRISINGHE, M.J., 2000. Dispersion of ceramic ink using an ultrasonic disruptor. *J. Mater. Sci. Lett.*, **19**(9), pp. 799-801.

3. TAY, B.Y., RASHID, H. and EDIRISINGHE, M.J., 2000. On the preparation of ceramic ink for continuous jet printing. *J. Mater. Sci. Lett.*, **19**(13), pp. 1151-1154.

4. TAY, B.Y. and EDIRISINGHE, M.J., 2000. Investigation of some phenomena occurring during ink-jet printing of ceramics. Presented orally at the *52nd Pacific Coast Regional and Basic Science Division Meeting,* American Ceramic Society, 6 – 9 Sep 2000, San Francisco, California, USA.

5. TAY, B.Y. and EDIRISINGHE, M.J., 2001. Investigation of some phenomena occurring during ink-jet printing of ceramics. *J. Mater. Res.*, **16**(2), pp. 373-384.

6. TAY, B.Y. and EDIRISINGHE, M.J.. Geometrical changes in a ceramic ink droplet. Submitted to *Proc. Royal Soc. A*.

7. TAY, B.Y. and EDIRISINGHE, M.J.. Solid freeform fabrication of ceramic. To be submitted to *Int. Mater. Rev.*.

8. TAY, B.Y. and EDIRISINGHE, M.J.. Dispersion and stability of silver inks. To be submitted to *J. Mater. Sci.*.

Chapter 1

Introduction

1.1 Background

Over the last two decades, a class of technologies, which has the capability of producing a complex solid directly from its computer model without the need for part-specific tooling, has emerged. The concept of its manufacturing opposes that of conventional production method. Instead of creating a solid object by removing material from stock, shaping in a die or mold, and/or adding units together, materials are added in a laminated fashion to build up the model. Collectively, these technologies represent a new material processing capability and is known as Solid Freeform Fabrication (SFF), layered manufacturing, automation fabrication, desktop manufacturing or fast free form manufacturing. Primarily, these methods have been applied for the rapid creation of models and prototypes and limited run manufacturing of engineering components with shapes that are too complicated to produce by conventional method. The more proliferate commercial SFF technologies include Stereolithoghrapy (SLA), Fused Deposition Modeling (FDM), Selective Laser Sintering (SLS), Laminated Object Manufacturing (LOM), Solid Ground Curing (SGC), Multiple Jet Solidification Process (MJS) and Three Dimensional Printing (3DP).

With its potential for revolutionary advances in speed, flexibility of product development and ability to produce complex net or near net-shape component, the focus of SFF in recent years has been shifted from its initial application on plastics component to others, and from visual or look-at prototype to more functional prototype. One of the most significant future applications of SFF is the direct production of advanced ceramic parts, which are difficult to fabricate with other techniques, and new processes and materials are developed to adapt SFF for it. Due to their hardness and brittleness, ceramics are normally processed in powder, slurry or suspension form, e.g. in powder metallurgy and gel casting, where the shape is formed (for example, in a mould) followed by densification at high temperature sintering. However, one of the perpetual challenges to this processing route is the difficulty to fabricate component to a net or near-net shape with the required dimensional tolerance due to the high shrinkage from green to sintered states. This is especially so during the development stage

where the ceramic materials are being evaluated at different testing conditions and designs are refined frequently. The concerns of high tooling cost and a likelihood of different actual behaviour from testing inevitably demand investment of time and resources in preparing physical models to investigate feasibility of the design concept. With SFF, these problems could be largely alleviated at the design stage and ceramic components with complex geometry can be fabricated rapidly with minimal or no need of tooling. Among the techniques used for freeforming ceramics are SLA, Fused Deposition of Ceramic, SLS, LOM, Computer-Aided Manufacturing of Laminated Engineering Materials, 3DP and Direct Ceramic Ink-Jet Printing (DCIJP). Encouraging results were achieved with monolithic ceramics such as SiC, Al_2O_3 and Si_3N_4. Highly complex ceramic parts for end-use and tooling have also been fabricated and demonstrated with these processes. Examples include ceramic casting mould with integral cores [Uziel, 1997], turbine blade [Cawley, 1997] and ceramic filters [Parish and Jeffery, 1995]. The benefits of SFF are not only restricted to design and performance optimisation purposes but has extended to low-quantity productions of complex shapes of piezoelectric ceramics and composites [Bandyopadhyay *et al.*, 1998] for which SFF was considered cost competitive compared to the conventional forming techniques.

Another opportunity offered by SFF for the processing of advanced ceramics is the control over local composition [Wang and Krstic, 1998]. This has led to the creation of parts with different compositions, microstructures and properties throughout the volume, which are difficult to do so using conventional forming techniques. Among these is the construction of composites of alternating layers of ZrO_2 and Al_2O_3 by CerLOM; the building of zirconate-titantate based mulitlayers with regions of different microstructures and properties by 3DP; the printing of a one-dimensional functionally graded ZrO_2/Al_2O_3 composite of 'continuous' gradient by DCIJP; the design and fabrication of ceramic mould with tailored surface texture for casting orthopaedic implants with bony ingrowth structures by 3DP.

Many of the SFF processes for ceramics build up materials in thin, discrete layers and this method of fabrication has proven to be extremely powerful [Rock *et al.*, 1997]. What distinguished these layered manufacturing methods from one another is the machinery and material used. Specific materials such as fluids, powders, wires or laminates are built up on equipment of different physical principles. Apart from selective laser chemical vapour deposition method, most of the SFF processes for ceramics utilise ceramic particles with binder.

In particular, the Direct Ceramic Ink-Jet Printing (DCIJP), pioneered by Evans, Edirisinghe and co-workers in 1995, then, at the Brunel University, UK, applies a commercially available printer and builds component by overprinting layers of 'ceramic ink'. Printing is considered 'direct' in contrast to 3DP, which also employs jet printer but dispenses only binder onto a powder bed and to be fused with it. Vital to DCIJP is the use of a ceramic ink prepared via colloidal processing to ensure the dissolution of all processing aids in the ink and enable the manipulation of inter-particle forces to yield a homogeneous and stable suspension. Such processing has already been used in many established industries, e.g. printing inks and paint and also in ceramic manufacturing.

As a SFF technique, DCIJP fabricates components without the use of a mould. Yet, unlike most SFF techniques, the use of jet printer precludes the involvement of high energy or lasers and is relatively cheaper. Further advantages offered by the jet printer are precise control of dispensed volumes, data-driven processing and environmental friendliness. As a non-contact deposition method, printing can be made on non-planar and curved surfaces. It has been utilised for depositing metal solders and polymer in display panels [Hayes *et al.*, 1998], patterning organic light emitting devices [Hebner *et al.*, 1998], making controlled released drug delivery devices for pharmaceuticals [Katstra *et al.*, 2000] and forming refractive microlenses made of hybrid organic-inorganic materials for optical systems [Biehl *et al.*, 1998].

The above mentioned characteristics of colloidal processing and jet printer thus endow the following advantages to DCIJP:

(i) more homogenous starting material can be prepared and this helps to eliminate many heterogeneities in ceramics traced to their sources, i.e. powder [Lange, 1989] and hence the production of parts free from agglomerates

(ii) a wide variety of ceramic inks can be adapted for printing and different single composition components such as TiO_2 [Xiang *et al.*, 1997; Kim and McKean, 1998], ZrO_2 [Slade and Evans, 1998; Song *et al.*, 1999], PZT [Windle and Derby, 1999] have been printed with either aqueous [Kim and McKean, 1998; Slade and Evans, 1998; Windle and Derby, 1999] or organic based [Mott *et al.*, 1999; Song *et al.*, 1999] inks

(iii) two or more different ceramic inks can be installed together in the printer leading to the construction of ceramic composites and functionally graded material [Mott and Evans, 1999]

(iv) patterns down to micrometer resolution can be attained with the small diameter of the jet nozzle (10 - 200 μm) [Yang *et al.*, 2000]. Furthermore, with the printer's precise control in droplet deposition, DCIJP has the potential of fabricating miniaturised components with control over local composition or microstructures [Edirisinghe, 1998]

(v) inks of different stoichiometry and chemistry from the final product can also be used - instead of printing inks containing the ceramic, that containing the constituents (precursors) of ceramics can be used, e.g. sol-gel ceramic ink [Atkinson *et al.*, 1997] and polymeric precursor ink [Mott and Evans, 2001]

(vi) material, especially the expensive one, can be efficiently utilised since each drop becomes a part of the component built.

The application of colloidal processing and jet printing in DCIJP does not just restrict the method to ceramic components. The method is highly versatile and could be adapted for metal in microcircuits [Teng and Vest, 1987], metallisation [Hong and Wagner, 2000], device materials [Teng *et al.*, 1990; Teng and Vest, 1988]. The versatility to print on almost any surface irrespective of shape allows great flexibility in these technologies. Many steps can be eliminated by direct printing with a saving in device and process materials.

1.2 Research Problem

Since its emergence, the work of DCIJP has been developing with the use of continuous and drop-on-demand jet printers. A continuous jet printer, as the name implied, forms droplets continuously even when there is no printing whereas a drop-on-demand device ejects ink droplets only when they are needed. Much of the developments in DCIJP has been concentrated on drop-on-demand printer - partly due to its low cost and small size. One of the reasons that the continuous jet printer does not develop as fast as the drop-on-demand printer in DCIJP lies in the printer's approach of droplet generation which entails complex droplet charging and deflection as well as start-up and shut-down procedures. However, with its high droplet generation rate (80 - 100 kHz) and hence fast printing speed, the use of continuous jet printer for DCIJP presents the technology not only as a rapid prototyping method but potentially as a manufacturing operation. So far the thickest part built by DCIJP is known to be 2.5 mm and this was printed with a continuous jet printer [Song *et al.*, 1999].

The first generation of DCIJP using continuous jet printer (or continuous DCIJP) employed a BioDot printer to demonstrate the viability of multilayer jet printing [Teng *et al.*, 1997; Teng and Edirisinghe, 1998; Song *et al.*, 1999]. However, printing was intermittent and far from 'continuous'. In due time, the printing process comes to a halt and the machine had to go through the iterative and tedious procedure of shutting-down and starting-up. The process is thus far from being a prototyping method.

So far, printing for both methods in DCIJP employs dilute ceramic ink of 80 - 95% (v/v) solvent with the remaining content consisting of ceramic particles, rheology control additives and/or conductive salt. This poses challenges to drying before the next layer can be printed, presenting a barrier to rapid production and handling of prints. In most cases, an organic base solvent is used for accelerated drying. The first layer has to be printed on a substrate for handling and those known to be used for DCIJP are ashless filter paper [Windle and Derby, 1999], silicone release paper [Mott and Evans, 1999] and acetate sheet [Teng and Edirisinghe, 1998; Song *et al.*, 1999]. These are normally chosen based on the criterion that the substrate can be easily detached from the printed part for post-printing operations. The implication of the ink-substrate interaction on shrinkage, resolution and layer building has not been duly considered. Within the scope of this technology targeting at micro-engineering components through the layering of well-ordered arrays, these are certainly not areas to be overlooked.

The possibility of continuous DCIJP to metal-filled ink for thick film circuit is also yet to be explored. Potentially, this application will not only reduce the number of steps in current processing, i.e. screen printing, but also produce circuits with higher resolution. For this feasibility to be examined, suitable metal-filled ink is yet to be formulated.

Statement of the Research Problem:

As a tool intended for rapid prototyping and manufacturing of micro-engineering components, DCIJP using a continuous jet printer will have to address issues of uninterrupted deposition and dimensional accuracy. There is therefore a need to develop further a robust ink, i.e. suspension with well-controlled and reproducible behaviour, for printing. A basic understanding of the printing process, ink-substrate interaction and shrinkage on the printed part is necessary in order to exploit the technique to its best advantage for the building of micro-engineering components.

1.3 Aim and Objectives of the Research

The research work aims to contribute to the improvement of continuous DCIJP as a solid freeform fabrication method and help propel it to a viable manufacturing process for micro-engineering components of advanced ceramics and thick film circuit.

In order to achieve the aim, the objectives of the research are as follows:

(i) to enable *continuous* deposition of ceramic ink with a continuous jet printer by:

* establishing ink preparation procedure for the production of a homogenous and stable ink; and
* characterising this ink for its sedimentation behaviour, viscosity, surface tension, and electrical conductivity.

(ii) to optimise the printing parameters and investigate the effects of various printing conditions during continuous DCIJP which include printing substrate, print resolution and accelerated drying as well as ink's powder loading on the print quality and multilayer building

(iii) to study the dynamics of shrinkage of a droplet of ceramic ink

(iv) to develop silver-filled inks for circuit tracks by using sub-micrometer size particles.

1.4 Scope of Research

In the context of the aforementioned objectives, the following tasks will be carried out.

(a) Literature survey

Firstly, the term 'advanced ceramics' will be discriminated from traditional ceramics with a short summary on its potential market growth. The literature review will next outline the various fabrication methods for advanced ceramics. These include the traditional methods such as slip casting and the new and novel techniques such as sol-gel. This will be followed by a comparison of the various contemporary SFF techniques for advanced ceramics. Emphasis will be given on the past and recent works on DCIJP as well as the operating principle of various modes of jet printer. This section will conclude with a short write-up on the potential use of ink-jet printing for microcircuits and arrays.

(b) Development of ceramic ink preparation procedure

The success of continuous DCIJP is dependent on the preparation of homogeneous and stable ink and the use of the printer for layer building. This section will examine the effect of preparation procedures, such as milling and ultrasonic disruption, on the ink's sedimentation behaviour. The goal is to obtain ceramic ink with stable ink properties matching the printer's requirements and hence enables the printing to proceed continuously without interruption. The various properties of the ink such as sedimentation behaviour, viscosity, electrical conductivity and surface tension will be characterised. The ink will be tested on the printer.

(c) Effect of printing conditions on print quality and drying

The ceramic ink, prepared via the route established in the preceding work, will be deposited on different substrates and the conditions during printing will be optimised. Two types of substrates will be used - silicone release paper and acetate sheets - and the resolution of the printed dot and raster on these substrates will be correlated to their respective surface free energies. A series of overprints will be made and their drying conditions are studied with respect to accelerated drying, print resolution, printing interval and ink's powder loading.

(d) Geometrical changes in a ceramic ink droplet

The wettability and shrinkage of a droplet of ceramic ink will be studied by monitoring the evolution of droplet's contact angle, width of ink-substrate interface and droplet height during drying. The properties will be measured in-situ on two different types of substrate with surface free energies higher and lower than the ink's surface tension. The implications of these behaviours on layer building will be discussed.

(e) Dispersion and stability of silver inks

Three different types of dispersants will be employed in the formulation of silver ink. The effect of dispersant level on the sedimentation and rheological behaviours of the silver ink will be investigated.

1.5 Summary

The context of the research is established. This includes an overview of the solid freeform fabrication of advanced ceramics and the current state of research in direct ceramic ink-jet printing. In addition, a brief account of the application of direct printing of electronic circuits is also presented. The research problem is defined with the aim and objectives identified. Finally, the scope of the research necessary to realise the objectives was also determined.

Chapter 2

Literature Review

This chapter will attempt to review the DCIJP (Direct Ceramic Ink-Jet Printing) technology as a freeforming method for advanced ceramics and silver. Particular emphasis is given to the two major technologies on which DCIJP is based, i.e. colloidal processing for the preparation of suspension and freeforming technique via ink-jet printing. As a prelude to these discussions, the term 'advanced ceramics' is defined and an outline of solid freeform fabrication as a new and non-conventional manufacturing method is given alongside the traditional manufacturing methods.

2.1 Advanced Ceramics

To discriminate advanced ceramics from their traditional counterparts such as bricks, sanitary wares and household porcelain wares, many other words such as 'fine ceramics' [Saito, 1985], 'high-performance ceramics' [Shimoda, 1995], 'high technology ceramics', 'engineering ceramics' [Vincenzini, 1991] and so forth, have been introduced. Suyama and Yamaguchi [1991] had defined three features of advanced ceramics that distinguished them from their traditional counterparts:

* high-purity raw materials with controlled composition and particulate properties are used
* processing is subject to precise control of both forming and firing
* products have a well-controlled microstructure, which ensures high performance.

Because of these features, advanced ceramics have greater hardness, higher melting temperatures, greater resistance to wear and corrosion, lower thermal conductivity and lower thermal expansion than their traditional counterparts [Saito, 1985; Vincenzini, 1991]. They also possess excellent electrical properties, making them important in the production of electronic components and structural products requiring both high mechanical strength and good electrical resistance [Anon, 1996]. Advanced ceramics have inherently high electrical

resistance, but certain advanced ceramic products can be rendered electrically conductive for highly specialised applications [Anon, 1996].

The United States of America is the world leader in research and development for advanced ceramics and Japan leads the world in the processing of advanced ceramics [Smith *et al.*, 1994]. There is no unanimous classification of advanced ceramics (see Figure 2.1). The Japanese classified the advanced ceramics based on applications: functional and structural [Saito, 1985]. The former is characterised by electromagnetic, optical and biological and the latter by mechanical and thermal properties. The classification of advanced ceramics by the USA is market-driven. The more generally accepted divisions are structural ceramics, electronic ceramics, ceramic coatings and chemical processing and environmental-related ceramics [Abraham, 2000].

Materials such as silicon nitride, silicon carbide, zirconia, boron carbide, alumina and sialon, both monolithic and composite, are typical structural ceramics [Mecholsky, 1989; Schwartz, 1992]. They are used as cutting tools and wear parts for industrial applications, substitutive and re-constructive materials for medical surgery, engine components for aerospace and defence related applications [Vincenzini, 1991]. Typical properties include high hardness, low specific gravity, high-temperature mechanical strength, creep resistance, corrosion resistance, chemical inertness and biocompatiability [Schwartz, 1992]. The use of advanced ceramics allows operation at higher temperatures with reduced inertia, friction and fuel consumption and improved wear resistance [Mecholsky, 1989].

Within advanced ceramics, electronic ceramics have the most developed market. Most of the electronic ceramics utilise their functional characteristics and modern applications include insulators, substrates, capacitors, integrated circuit packages, magnetic ferrites and piezoelectric ceramics [Abraham, 2000; Swartz *et al.*, 1997a; 1997b]. Typical materials of interest include barium titanate, zinc oxide, lead zirconate, lithium niobate, aluminium nitride, zirconia and alumina [Chediak, 1996]. Important properties include relative permittivity and permeability for high-speed signal propagation, good electrical and thermal conductivity for rapid heat dissipation, thermal compatibility to metal in the case of packaging, low dielectric constant to enhance signal processing in electronic packaging [Chediak, 1996; Swartz *et al.*, 1997a]. As higher quality and consistency are increasingly

called for in industry standards, ease of fabrication for electronic ceramic component will become more important [Chediak, 1996]. A future-potential market is superconductor ceramics [Abraham, 2000].

Ceramic coating is often performed to a substrate to impart physical and mechanical properties not normally possessed by the substrate itself. Cost is significantly reduced, as the entire component does not need to be made wholly from the expensive coating material [Jethanadani, 1997]. A number of these ceramic coatings in use include zirconia, titanium nitride, titanium carbide and silicon carbide and are being applied in auto, diesel and land-based turbine engines, aircraft and aerospace engines, heat exchangers, wear parts for industrial applications and cutting tool inserts [Ferber and Tennery, 1991].

Chemical-processing and environmental-related ceramics employ the unique properties of ceramics such as controlled porosity and inertness [Abraham, 2000]. They are used as catalyst supports, membranes and filters in the chemical and process industries to reduce pollutants from automobiles as well as from hot industrial gases. For examples, filters for high-temperature gas purification, particulate filters for diesel emissions, devices where chemically resistant and permeable materials are required at high temperatures, membranes for separation processes or molecular sieves for chemical processes [Alvin, 1996; Elloit and Startin, 1997; Sepulveda, 1997]. The stability of advanced ceramics under corrosive, high-temperature, high-pressure environments offer an effective and economical alternative to pollution control technology [Alvin, 1996].

In 1996, the Freedonia Group Inc. predicted the continual growth of the electronic segment which will be dominated by integrated circuits [Anon, 1996]. Cutting tools and wear parts will continue to dominate the structural segment. Three years later, another independent analysis by Business Communications Co. [Abraham, 2000], as illustrated in Figure 2.2, estimated the size of the 1999 market for the USA advanced ceramics at $8,070 million with electronics taking 65% of the market share. This is projected to increase to $11,820 million by the year 2004, with a growth rate of 7.9%. Thus, the field of advanced ceramics is expected to continue its growth and electronic ceramics will remain to hold the major share of the market. Ceramic coatings, although initially considered as an interim solution while problems with monolithic ceramics were being overcome, claim their own value of industry

segment and are here to stay [Smith *et al.*, 1994]. In the forthcoming years, growth in advanced ceramics is expected to continue in all market segments with the following stimuli [Freiman and Onoda, 1997; Smith *et al.*, 1994]:

* the development of economical and reliable sources of relatively pure raw material
* improvement of the manufacturing processes
* realisation of the value of ceramics over conventional materials and
* commercialisation of advanced ceramic processing technologies.

In particular, new technology with the abilities to form the desired shape without sacrificing the materials' unique characteristics and without machining, will propel the growth of advanced ceramics and help promote rapid introduction of new products into the market place [Freiman and Onoda, 1997]. These new technologies for near-net shape forming, which avoid or significantly reduce machining costs, will make advanced ceramics increasingly attractive for many applications.

2.2 Processing Methods for Advanced Ceramics

Due to its high melting point, it is difficult to use the melting-casting method employed for metals and plastics to form advanced ceramic products. The high hardness of this material also makes machining of the final shape commercially prohibitive. Most of the fabrication processes for advanced ceramics generally start with powder as the precursor, then forming the powder into a green body with shape as closely as possible to the final part, followed by firing or sintering. In spite of its susceptibility to heterogeneity and non-uniform phase distribution, powder processing was considered as the most efficient method to form advanced ceramics in a landmark review by Lange [1989] 12 years ago. In this section, various methods of forming green bodies of advanced ceramics as well as densifying them to the final form will be presented. For discussion sake, those methods, which are also used to make traditional ceramics, are classified as conventional techniques (e.g. casting, moulding, and machining). The non-conventional methods are the innovative ones, which have been generated over the past decades for advanced ceramics and are not normally employed by traditional ceramics. Some of these are still under development while others are currently being employed for production. They may start with non-powder precursors (e.g. polymer or

vapour) or colloidal suspensions of particles of advanced ceramics. Another class of novel processing methods for advanced ceramics is the solid freeform fabrication method, which will be discussed separately in Section 2.3.

2.2.1 Conventional Techniques

Conventional techniques attempt to achieve the greatest degree of particle packing and a high degree of homogeneity during the forming of the green product [Reed, 1995]. In doing so, the likelihood of distortion or microstructural non-homogeneity during sintering is decreased. Careful control of the density and microstructure in the green ceramic is thus important, as large defects introduced during forming are usually not eliminated by sintering. This is especially critical for high performance ceramics and thus may restrict the options for forming [McEntire, 1991]. Examples of powder shaping methods include die pressing, slip casting, tape casting, extrusion and injection moulding. Pressing utilises a relatively dry powder and casting, a fluid suspension. Extrusion and injection moulding utilise an intermediate mixture of powder and liquid and are referred to as plastic forming techniques [Richerson, 1991].

2.2.1.1 Forming Techniques

(a) Pressing

Pressing involves mechanically compacting a dry powder. Two types of pressing are normally utilised – uniaxial pressing and cold isostatic pressing (CIP). The former is the most commonly used whereby the powder, mixed with a very small amount (1 – 2 %) of fluid and organic additives, is compacted into a rigid body by applying pressure along a single axis through upper and lower pistons. Pressing is an established forming method that has been used for decades for magnetic and dielectric ceramics, spark plugs, cutting tools, refractory sensors, ceramic tiles, porcelain, coarse-grained refractories, grinding wheels and structural clay products [Reed, 1995]. The process can be easily automated and hundreds of simple parts per minute can be produced [McEntire, 1991]. However, it is restrictive in the geometry of the part to be pressed. Pressing is not suitable for parts with thin wall, sharp edges or undercuts and holes perpendicular to the pressing axis [Kriegesmann, 1991]. Depending on the magnitude of the applied pressure, pressure distribution exists in the compact and may induce non-uniform shrinkage during sintering [Lewis, 1996].

When high quality products are required, e.g. very low-density variation, cold isostatic pressing (CIP) is used in place of the standard dry pressing. The powder is normally sealed in a rubber mould of the proper shape and immersed in a hydraulic fluid through which applied pressure is transmitted in all directions during all stages of compaction. Spark plug insulators are produced by this method [Baron and Perry, 1983]. Although CIP allows for more shape complexity, dimensional control and production rate are sacrificed [Kennard, 1991; Kriegesmann, 1991].

(b) Slip casting

Both slip and tape (Section 2.2.1.1c) castings use a fluid suspension of ceramic or metallic particles. However, tape casting is usually based upon a non-aqueous solvent as the liquid medium [Mistler, 1998] although there has been increased emphasis on the use of aqueous based tape casting system in recent years [Hotza and Creil, 1995].

In slip casting of ceramic, the liquid suspension of ceramic particles is poured into a porous plaster mould. The pores are small enough that the particles cannot enter, but large enough for the liquid to be absorbed by capillary pressure. The liquid is extracted through the pores, leaving a layer of ceramics deposited on the mould walls. The slip may be drained from the mould when the desired thickness of the compact is built up, as in drain casting. Alternately, it may remain in the mould during the whole process to achieve a solid compact, as in solid casting.

The main features of slip casting are its high solid content (> 50 vol. %) and low viscosity of 0.1 Pa s [Reed, 1995]. These allow the casting of complex shapes at a low cost. While it is used more commonly for producing sanitary ware, it is also used for forming advanced ceramics, e.g. combustor baffles, connecting ducts [Schwartz, 1992], closed-end tubes and structural refractories [Reed, 1995]. In general, it is used to produce hollow shapes with uniform thickness [Schwartz, 1992]. Its disadvantages are low production rate (due to long settling and drying time) [Reed, 1995; Schwartz, 1992], short mould life and the labour-intensive mould assembly, casting, de-moulding, trimming etc. [Schilling and Askay, 1991]. Because of its low tooling cost, slip casting may be economically viable for making prototypes and for small batch processing [Schwartz, 1992].

There are several variants of this process:

* pressure casting (where pressure is applied to the slurry),
* vacuum assisted casting (in which vacuum is applied to the outside of the mould) [Reed, 1995; Schilling and Aksay, 1991] and
* centrifugal casting (in which the spinning of the mould produces large forces) [Steinlage *et al.*, 1996].

These are used to increase the casting rate and have been investigated for forming advanced ceramics.

(c) Tape casting

Tape casting, also known as doctor-blading or knife coating, utilises a slurry of ceramic particles in a liquid as in slip casting but it has a higher content of organic binder and no porous mould is used. The slurry is cast into tapes on a moving carrier and spread to a controlled thickness with a blade. After drying, the tapes are removed from the carrier. The flat tape articles can then be punched, silk screen printed or laminated. Immensely complex shapes can be fabricated. Tape as thin as 5 μm is being reported by equipment manufacturer [DreiTrek, Inc., 1997]. The tape casting process is the best method for producing large, thin and flat ceramic or metallic parts. Such parts are virtually impossible to press, especially when the plate is to be pierced with numerous holes, and difficult to extrude [Mistler, 1998]. The main problem in tape casting is the drying process, which if not controlled properly will cause the tape to stick to the surface of the carrier.

The main application for ceramic tape casting is in the electronic industry, e.g. in the fabrication of multilayered capacitors, multilayered ceramic packages, piezoelectrics, thick- and thin-film insulators and ferrite memories [Schwartz, 1992]. New and exciting applications in recent years include the production of fuel-cell membranes, polymer based lithium-ion battery membranes, superconductor tapes and thin, 2D laminations for rapid prototyping [Mistler,1998].

(d) Extrusion

In this method, shape is formed by forcing a mixture of ceramic powder and polymeric binder under high pressure through a die orifice in an extruder. Because of the stiffness in the mixture, shape imposed by the orifice is retained after extrusion. The process can be used for fabricating elongated shapes with high aspect ratio, such as tubes and rods [Richerson, 1992]. Extrusion can be a very effective and efficient method of forming material continuously or semi-continuously with relatively simple equipment. It has been used for many years in the clay/porcelain industries and for advanced ceramics such as silicon carbide, silicon nitride and oxide materials. With this process, very complex cross-sections can be fabricated in continuous production, e.g. thin-walled honeycomb structures [Ruppel, 1991]. The disadvantage is that only shapes with constant cross-sections can be produced. Other disadvantages of extrusion lie in the drying, binder removal and firing operations which are prone to result in defects and tight process control needs to be exercised to maintain dimensional tolerances and straightness [Kriegesmann, 1991; Ruppel, 1991].

(e) Ceramic injection moulding

This forming process is the same as that for plastics. The ceramic powder is compounded with a polymeric binder and injected into a mould. Upon cooling in the mould, a rigid compact of powder bonded with polymer is formed. The binder can then be extracted and the ceramic powder compact is densified at high temperature.

Ceramic injection moulding is best suitable to manufacture small, complex shaped parts with moderate to large production quantities [Bose, 1995]. Studies have been made on advanced ceramics, e.g. alumina, zirconia, silicon nitride and silicon carbide [Edirisinghe, 1990]. It has been used to fabricate ceramic components for tool applications, heat engines, household items, medical instruments and office equipment [German and Bose, 1997]. However, debinding, which is the removal of the binder, is a key issue with this process because the time for binder removal depends on section thickness [Evans, 1994] and the upper limit on section thickness ranges from 10 – 50 mm [German and Bose, 1997]. Thus, it is not an appropriate method for large or thick parts. Defects often result from density gradient, which are brought forth from uneven filling, thickness variations, or direction change during moulding and these can induce warpage in sintering [German and Bose, 1997]. The process

also requires starting powder smaller than 20μm, which makes it uneconomical for the fabrication of large components. The cost of parts can dramatically increase due to high tooling costs.

A novel process being explored is low-pressure binderless injection moulding technique. Improved dimensional control and thus higher yield can be obtained compared to conventional ceramic injection moulding. Low-pressure moulding also allows the use of simpler, lower-cost tooling and fabrication cycle can be reduced as well because there is no binder to remove [German and Bose, 1997].

(f) Machining

The best surface finish and dimensional accuracy of ceramic parts are achieved through final machining. However, hardness of ceramic makes material removal occurs very slowly and requires expensive tooling [Kriegesmann, 1991; Schwartz, 1992]. Often a combination of a forming process such as pressing or casting plus machining is used to approach the desired shape as closely as possible. It is possible to perform machining on green ceramics of simple semi-finished geometry with good homogeneity and density distribution and high quality parts can be produced after sintering [Klocke, 1997]. This also helps to reduce expense in the very time- and cost-intensive final machining stage.

2.2.1.2 High Temperature Processing and Consolidation

Most applications for powder shaping and compaction dictate high density in the final product. This can be achieved through one of three methods [Richerson, 1992]:

* sinter to densify a low density preform (e.g. shaped by injection moulding)
* press to a high density followed by sintering, or
* simultaneously press and sinter using a full density technique.

(a) Sintering

This is the most widely used and inexpensive densification method. Complex-shaped components can be densified easily by this method if appropriate powder selection and green

forming have been accomplished. An account on the theory of sintering can be found in reference by Richerson [1992].

The densification characteristics of ceramic materials can be influenced strongly by the sintering temperature. Generally, density increases with rising temperature and sintering of advanced ceramics is performed at higher temperature than that for traditional ceramics [Kriegesmann, 1991]. However, high temperature and fine powders alone are often not sufficient to give high density, e.g. silicon nitride decomposes at temperature higher than 1500°C and yet temperature near 1500°C is still far too low for it to give dense product. In order to make the most of the inherent functions of materials, other methods, such as hot pressing, hot isostatic pressing and reaction sintering, are preferred occasionally.

(b) Hot pressing

Hot pressing involves compacting a ceramic powder under uniaxial pressure in a die at a high enough temperature that the powder can densify. With the simultaneous application of pressure and temperature, the powder can sinter more quickly at a lower temperature than if only temperature is applied. Typically, a small amount of additives is used and parts of improved properties can be produced. The parts also have higher strength and hardness due to low porosity and low grain growth [Schwartz, 1992]. However, the industrial application of hot pressing is limited due to its low productivity and expensive die maintenance cost [Reed, 1995]. It is used commercially when a sintering aid or grain growth inhibitor is not available or unacceptable and for producing specimens for research [Richerson, 1992].

(c) Hot isostatic pressing

While hot pressing is carried out with pressure along a single axis, hot isostatic pressing (HIP) uses gas pressure to obtain isostatic pressure. The pressure employed can be higher than that in conventional hot pressing because it is not restricted by the strength of the die material. This makes HIP a more powerful densification method for ceramics than hot pressing. In addition, components with a complex and well-defined shape can be produced. Unfortunately, the initial cost of the equipment is extremely high and the process itself is not economical. A combination of sintering and HIP is favourable and is used industrially to

reduce the size of closed pores in high-performance structural materials. Densification by HIP has been used for sintered advanced materials, e.g. non-oxide ceramics, oxide ceramics and composites [Kriegesmann, 1991].

(d) Reaction sintering

In reaction sintering, the sintering process involves a chemical reaction. This method is most notably used with silicon nitride (Si_3N_4) and silicon carbide [Schwartz, 1992]. In the case of Si_3N_4, a green compact of Si powder is made and then reaction-sintered in a nitrogen flow. Reaction between Si and N_2 takes place and Si_3N_4 is obtained as a final sintered product. High porosity cannot be avoided since nitrogen gas is the source of the reaction and must permeate into the interior of the compact [Kriegesmann, 1991].

2.2.2 Non-Conventional Processes

Non-conventional processes can involve solution or slurry, polymer, vapour phase or melting the powder and deposit it on a surface. The more commonly processes used for advanced ceramics are sol-gel processing, polymer-derived ceramics, vapour deposition, plasma spraying and direct casting.

2.2.2.1 Sol-Gel Processing

Sol-gel processing begins with a colloidal dispersion of particles in a liquid, which is the definition of a sol. Through subsequent chemical cross-linking, electrostatic destabilisation, evaporation or some combination thereof, the fluid sol may be transformed into a rigid gel which is a substance containing a continuous solid skeleton enclosing a continuous liquid phase. This sol-gel transition allows the solid phase to be shaped into films, fibres, microspheres or monoliths.

The most common applications of sol-gel processing are thin films and coatings being applied for the fabrication of dielectric materials, piezoelectric materials, superconductive materials and ferrites [Dislich, 1983; Yanagida *et al.*, 1996]. These are being used for protection, e.g. moisture and diffusion barriers, fracture resistance, scratch and wear

resistance, thermal and electrical insulation and corrosion resistance [Brinker and Scherer, 1990]. Film formation is accomplished through liquid film deposition methods, whereby a continuous liquid phase is forced to displace air at the substrate through a wetting process. The most commonly used methods are dip-coating and spin-coating [Klein, 1991].

The advantages of the sol-gel process are high purity, homogeneity and low-temperature processing. Some compositions that cannot be made by conventional means because of phase separation can be produced by this process [Turner, 1991]. Material use is particularly efficient in forming films with sol-gel process because of re-use of any excess material [Klein, 1991]. The main limitation of this process is the high raw material cost [Yanagida *et al.*, 1996].

2.2.2.2 Polymer-Derived Ceramics

Ceramics have been made by chemical routes employing organometallic and inorganic polymers as precursors. The precursors are converted to ceramics by pyrolysis. By controlling the pyrolysis of these polymers, a variety of products may be formed, e.g. fibres, ultrafine powders, thin films, bulk bodies, foams and open structures [Rice, 1983; Yajima, 1983]. This route of processing has been applied predominately to produce SiC and Si_3N_4 [Bao and Edirisinghe, 1998; Peuckert *et al.*, 1990]. Advantages of this processing route include lower processing temperature than that normally for sintering, the ability to control purity and a very fine-grained, high strength microstructure [Mark *et al.*, 1988].

2.2.2.3 Vapour Deposition

Vapour deposition is the condensation of an element or a compound from the vapour state on a substrate as a thin film. In chemical vapour deposition (CVD), a vapour of the source material is thermally decomposed or reacted with other gases or vapours to produce a non-volatile reaction product deposited on the substrate. CVD has been used to produce very high purity, dense coatings of a wide variety of oxide, carbide, nitride, boride and other compositions [Yanagida *et al.*, 1996]. CVD of ceramic coatings are used to reduce wear, corrosion and erosion of metal-cutting tools, turbine engine components and bearings to protect against oxidation at extreme temperature as well as to infiltrate fibrous or particulate

preforms to achieve composite structures [Schwartz, 1992]. The distinctive advantage of CVD is its low temperature synthesis, which contributes to energy conservation. It also allows the deposition of exceptionally high-purity material and the coating deposit is thick and uniform [Stinton *et al.*, 1991]. The disadvantages are the generation of toxic, corrosive and flammable by-products, high cost of the precursors and expensive process equipment and running costs [Schwartz, 1992].

Physical vapour deposition (PVD), another vapour deposition method, involves the removal of the vapour phase of a target material and deposition of it as a thin film on a substrate. PVD is normally used to deposit metals or alloys but can be modified for the deposition of ceramics. However, the technique is expensive as the deposition of oxides and nitrides by PVD requires very high temperature. Furthermore, since the compounds are not stable at very high temperature, the composition of the thin film formed is not necessary that of starting compound [Yanagaida *et al.*, 1996].

2.2.2.4 Thermal Spraying

Thermal spraying of advanced ceramic coatings find applications as thermal barriers in the aircraft industry, primarily in gas turbines and diesel engines [Jones, 1996] and as wear and corrosion resistant coatings in industrial machinery and infrastructure maintenance engineering [Herman and Sampath, 1996]. In these applications, the coatings provide wear resistance, friction reduction and corrosion/erosion resistance with derived benefits of extending component service life, increasing engine durability and reducing operating costs [Herman and Sampath, 1996; Jones, 1996]. Zirconia is a coating material with good thermal barrier properties at high temperature with coating thickness in the range of 250 - 375 μm in gas turbines and 1.5 – 6.25 mm in diesel engines [Jones, 1996; Kamo, 1991].

Some of the more important thermal spraying processes are plasma spraying, high velocity oxyfuel spraying, arc spraying and vacuum plasma spraying and are described by Jones [1996] and Herman and Sampath [1996].

2.2.2.5 Screen Printing

In screen printing, a thick paste is forced through a stencil screen, which defines the printed pattern, onto the surface. Screen printing generally produces print thickness in the range of 2 - 25μm, print patterns ranging up to about 150 x 150 mm and line widths as small as 0.25mm [Reed, 1995]. In view of this thickness it is capable of producing, it is classified as 'thick film coating' compare with thin film coating by CVD or PVD. With its low cost and development of thick film materials, the application of screen printing has been extended to fabricate temperature sensors [Tait *et al.*, 1994], solar cells [Sebastian *et al.*, 1993], solid oxide fuel cells [Labrincha *et al.*, 1993] and honeycomb structures [Anon, 1999].

2.2.2.6 Direct Casting

Direct casting of advanced ceramics is a class of methods which essentially involves the preparation of a dense and homogeneous suspension and transforms it into a stiff gel [Sigmund *et al.*, 2000]. By minimising the disturbance to the slurry during gelation, large heterogeneities and significant density variations in the final part can be reduced. The underlying principle of direct casting is the preparation of a well-dispersed suspension of high powder loading with reasonably low viscosity for mould filling. The dense suspension is prepared by colloidal processing whereby the particles are dispersed with either a physical or chemical bonding. The former is achieved mainly by manipulating inter-particle forces through changing pH, increasing salt content or addition of polymers. The latter is commonly accompanied by the formation of gels.

Most of the direct casting methods are still under development. The major problems to overcome are their low production rate and long gelling time [Sigmund *et al.*, 2000]. There are also concerns that some of the polymer systems used exhibit toxicity in the unreacted state [Janney *et al.*, 1998]. Examples of some of the direct casting method are gelcasting [Omatete *et al.*, 1991], direct coagulation casting (DCC) [Graule *et al.*, 1996] and aqueous injection moulding [Sigmund *et al.*, 2000].

2.3 Solid Freeform Fabrication

2.3.1 Rapid Prototyping

Prototyping traditionally allows a designer to check the appearance and function of a part before a significant investment in tooling is made. Rapid prototyping (RP) is thus originally defined as the 'fast production of prototype models' [Kruth, 1991] but has grown to embrace a set of manufacturing processes and information technology. These enable precise, robust and functional solid prototypes to be created quickly and directly from computer aided design (CAD) representation with little need for human intervention [Conley and Marcus, 1997]. This means greater freedom for the designers to prototype their drawings more frequently to check the assembly and function with substantial reductions in product development cost and lead times. However, the term RP no longer connotes prototype model fabrication, it is now being used directly as part of the manufacturing process for both final components and tooling manufacture [Pham and Gault, 1998]. In summary, rapid prototyping has become rapid manufacturing [Zhou, 2000].

A particular sub-class of RP techniques, solid freeform fabrication (SFF) has received substantial attention in recent years. It is also known as layered manufacturing, automated fabrication, desktop manufacturing, fast free form fabrication [Conley and Marcus, 1997]. SFF 'addresses the rapid creation of models, prototypes, patterns and limited run manufacturing' for the production of 'complex freeform solid objects directly from a computer model of an object without part-specific tooling or knowledge' [Beaman *et al.*, 1997]. The concept of manufacturing in SFF opposes that of conventional production, which creates a complex solid object by removing material from stock, shaping in a die or mould, and/or adding units together. Instead, materials are added to build up the model [Conley and Marcus, 1997]. This minimises or eliminates material waste. The technology essentially depends on an electronic database produced by CAD modelling, computed tomographic (CT) scanning, laser digitising etc. to define a tool path and the application of specific materials such as fluids, powders, wires or laminates on equipment of different physical principles from traditional manufacturing equipment [Conley and Marcus, 1997]. These characteristics make SFF suitable for fabricating geometrically complex components, eliminating tooling set up and path planning which are necessary for numerical control machining.

2.3.2 Basic SFF Processes

Many of the SFF processes are based upon layered manufacturing where material is built up layer upon layer. There are five basic layer manufacturing processes [Fuster, 1997]:

* Liquid solidification - photosensitive resins are cured by laser or UV light, e.g. Stereolithography, Solid Ground Curing
* melt deposition - molten material is deposited in layers and solidifying as it cools, e.g. Fused Deposition Modelling, Multi-Phase Jet Solidification
* powder sintering - powder layers are bonded using a laser to fuse each layer, e.g. Selective Laser Sintering
* sheet lamination - sheets (paper, foil) are cut, stacked and glued together, e.g. Laminated Object Manufacturing
* powder binding - powder layers are bonded using a binding agent usually sprayed on using ink-jet technology, e.g. Three Dimensional Printing, Direct Ceramic Ink-Jet Printing

Although the technologies of RP and SFF are not mature and still under development, the promise of maturing to a major multi-billion-dollar worldwide tooling industry seems likely [Zhou, 2000]. Conley and Marcus [1997], Kruth *et al.* [1998] and Pham and Gault [1998] provided excellent comparisons of the different RP available commercially. Qualitative comparisons of these methods for ceramics have been reviewed by Halloran [1999] and Wang and Krstic [1998]. The subsequent sections will concentrate on the applications of SFF for advanced ceramics.

2.3.3 SFF for Ceramics

SFF has been demonstrated successfully in the rapid prototyping and production for plastic parts [Pham and Gault, 1998]. The application of SFF to ceramics is motivated by a desire to take advantage of the advances in engineering ceramics (such as transformation-toughened oxide, high toughness silicon nitride and ceramic-matrix composites) [Cawley, 1997]. Despite their desirable material properties, they often incur high tooling costs and a, justifiable, concern that actual service behaviour differs from that projected from the testing stage. In addition, many powder-based processes are not necessarily conducive to the production of ceramic parts with complex internal geometry. Appropriate application of SFF

enables the designer to evaluate new ceramic materials at different testing conditions and to refine designs in the most effective way.

Among the techniques used for freeform fabrication of ceramics are: Steroelithography [Griffith and Halloran, 1996], Fused Deposition of Ceramic [Agarwala *et al.*, 1996a], Selective Laser Sintering [Subramanian and Marcus, 1995], Cer-Laminated-Object-Manufacturing [Griffin *et al.*, 1996], Computer-Aided Manufacturing of Laminated Engineering Materials [Cawley, 1997], Three-Dimensional Printing [Cima *et al.*, 1995] and Direct Ceramic Ink-Jet Printing [Edirisinghe, 1997].

2.3.3.1 Stereolithography

Stereolithography (SL) was the first SFF machine made available in the commercial market by 3D Systems in 1988 [Kruth, 1991]. This technology creates parts by polymerising ultra-violet (UV) curable resin exposed to UV radiation from a laser [Griffith and Halloran, 1996], as shown schematically in Figure 2.3, and is the most popular SFF technology being installed [Kruth *et al.*, 1998]. While most SL systems employ the building strategy outlined in Figure 2.3, significant differences in the lasers and in the re-coating and beam delivery mechanisms are found among various SL vendors [Beaman *et al.*, 1997]. Current lasers used are helium cadmium gas lasers, argon ion gas laser and more recently solid state Nd:YVO_4 lasers [Kruth *et al.*, 1998].

Prior to the creation of ceramic parts, the resin is charged with particulate [Griffith and Halloran, 1996]. For the fabrication of high-density ceramic parts, the freeform green body must have a high density with 50 – 65 vol. % of solid. The suspension, on the other hand, must have a relatively low viscosity. The three dimensional part is fabricated by successive building of layer upon layer. As the laser beam scans the liquid surface to draw the layer based on the information from a 3D computer image, the resin is cured, forming a ceramic-polymer composite. The part is built up on an elevator platform, which incrementally lowers the part into a vat (containing the liquid) by a distance of 50 - 500μm, which is equivalent to the layer thickness. As the elevator is lowered a small distance of the layer into the vat, the liquid resin coats over the last solidified layer. Re-coating and levelling a new layer of resin over the solidified surface then take place. This is necessary to ensure that the resin is at the

proper level for optimum laser focus and excess resin beyond the desired layer thickness is also removed [Pham and Gault, 1998]. Due to finite surface tension effects, small but distinct 'crease' will exist around the part perimeter at the solid-to-liquid interface and an interval before the laser drawing is allowed to eliminate these surface perturbations. Having established a quasi-planar resin surface, the system now proceeds to laser drawing. The first step is the drawing of the part border followed by hatching, which effectively is the filling in of the area within the borders drawn. The process is repeated several times until the part is built. The platform is raised and the solid polymer emerges from the vat. The cured resin is only a binder for the ceramic particles in the green body and needs to be removed by heating it to 250-500°C, followed by high temperature sintering (about 1600°C).

The process can only create solid that originates in specialised photocurable resin and this limits the choice in materials [Conley and Marcus, 1997]. To freeform high-density ceramic for the production of a dense component, the SL suspension of 50-65% of powder loading, must have sufficient low viscosity and should be at least as fluid as conventional SL resins [Griffith and Halloran, 1996]. Resin must therefore be designed carefully to control the colloidal chemistry and rheology to ensure proper flow during re-coating of the new layer at part building. Resin re-coating is a time consuming step in the SL prototype building process [Kruth *et al.*, 1998] and may create 'trapped volume' in the part, which is the excess resin that cannot be drained through the base of the part [Pham and Gault, 1998]. The presence of a trapped volume causes a build up of unwanted polymerised resin at the surface which may affect accuracy and surface finish. Although many re-coating mechanisms have been invented to eliminate this problem, e.g. scraper blade, inverted 'U', viscous retention, positive displacement pump [Kruth *et al.*, 1998], the contact between the re-coating mechanism and the liquid surface remains a problem and has to be limited. This is even more so for highly viscous ceramic suspensions where high shearing forces that may damage or destroy the part under construction should be avoided. A process in which the ceramic suspension is pre-laminated into semi-solid foils and pressed into the previous cured layers has been developed by Japanese researchers to overcome re-coating problems encountered with a scraper blade [Kruth *et al.*, 1998].

Furthermore, to yield an acceptable depth of cure, the ceramic suspension must be sufficiently transparent to the radiation. The presence of the powder particles in the

suspension induces high turbidity due to radiation scattering. This limits the penetration of the ultra-violet radiation and hence, the prototype building time. Another disadvantage associated with the high viscosity ceramic suspension is the long time needed to drain the excess resin from the complete part. SL also requires support structures to hold the various connecting parts of the product or the weak overhang parts during layer building [Kruth *et al.*, 1998]. The building of these support structures needs material and time.

2.3.3.2 Fused Deposition of Ceramics

Fused Deposition of Ceramics (FDC), as shown in Figure 2.4, was developed for the fabrication of functional ceramic parts. This technique is based on the existing Fused Deposition Modelling (FDM) technology, which was developed and commercialised by Stratasys Inc. (USA) for processing polymer and wax parts [Agarwala *et al.*, 1996a].

The starting materials for FDC are filaments of ceramic powder mixed with thermoplastic polymer or wax binder. The filaments are manufactured in ways similar to those used by the ceramic injection moulding industry. The starting materials are mixed, granulated and extruded to produce continuous lengths of flexible filaments. Sufficiently low viscosity is required of the filament, of 1.8 mm (or 0.07") nominal diameter [Agarwala *et al.*, 1996b], for it to be fed into a movable, heated nozzle where it softens just above its melting point at exit. The filament is then deposited by raster motion according to the patterns defined by the CAD model. Layer building starts by defining its boundaries followed by raster motion of the nozzle head depositing material inside these boundaries as a series of adjacent streams. Each stream is deposited on top of or next to its previously heated predecessors and then bonds by fusion to the latter upon contacting. The molten filament solidifies rapidly upon deposition by natural cooling. Layer upon layer, the filament is laid and a 3-D object resembling the model is built. The green ceramic object is then subjected to binder removal and sintering to produce a dense ceramic component [Agarwala *et al.*, 1996c].

A significant advantage of FDC is that it is not equipment intensive due to the low viscosity feedstock, which can be readily dispensed using low pressure (< 0.7 MPa or 100psi) [Beaman *et al.*, 1997]. Material is delivered on demand and the process thus does not require a large reservoir of expensive feedstock at the start and there is very little material

waste during or after production of the model [Pham and Gault, 1998]. There is also no worry of possible exposure to toxic materials or lasers. It does not need cleaning up and the materials can be changed quickly. Because the material solidifies relatively rapidly after it exits the nozzle, it is therefore possible to form short overhanging features without the need of explicit supports although in general, they are used. It is claimed that this technique is able to adjust and control layer thickness by varying the speed of the delivery head [Agarwala *et al.*, 1996c]. In one variation of FDC, which employs a dual tip mechanism, two materials - a primary material for modelling and a secondary material for producing support structure - are dispensed. The support structures are easily snapped off due to the weak bond between the model and the support structures.

However, internal defects are serious concerns of this technology with regards to the fabrication of structural ceramic components [Agarwala *et al.*, 1996a]. These defects are strength or property limiting and usually arise from debonding or poor bonding between adjacent streams or adjacent layers, or incomplete filling in the part [Agarwala *et al.*, 1996b]. Debonding and poor bonding arise either from no physical contact between adjacent streams/layers or weak interface between the streams/layers. The cause of these defects is inconsistent material flow, which can be due to variation in filament diameter, filament slippage between rollers or excessive cooling of previously deposited adjacent streams. Incomplete filling occurs as the nozzle turns around on layer building during which the actual nozzle head traces a curved tool path instead of the sharp turn defined in the CAD model. Consequently, voids can be found within the part. The use of more intelligent tool path generation software, build strategies and machine control software have helped to improve part quality and accuracy [Kruth *et al.*, 1998]. As the resolution of the process is dictated by the filament thickness, another drawback of FDC is its inferior surface finish compared with parts produced using other SFF techniques (e.g. SL) [Agarwala *et al.*, 1996a]. Subsequent finishing operations are needed for improvement of the surface [Hilmas, 1996].

FDC has been demonstrated for Si_3N_4, fused SiO_2, Al_2O_3, lead zirconium titanate (PZT) [Agarwala *et al.*, 1996c]. Prototyping investment casting positives is the major application of this technology [Agarwala *et al.*, 1996a]. A modification of FDM technology, Extrusion Freeform Fabrication, which uses two extruders to dispense dissimilar materials into a small mixing head, has been employed to prototype functionally graded material [Hilmas, 1996].

A Multiphase Jet Solidification (MJS) process, very similar to FDC, has been developed by the German Fraunhofer Institutes IFAM and IPA for the fabrication of both metal and ceramic (SiC) near-net shape parts for functional applications [Greul, 1996].

2.3.3.3 Selective Laser Sintering

Selective Laser Sintering (SLS) was originally developed at the University of Texas at Austin in 1986 and then later commercialised by DTM Corporation in 1992 [Beaman *et al.*, 1997]. EOS Corporation has also developed and marketed their own laser sintering machines [Kruth *et al.*, 1998]. In this technology, a thin layer of powdered material is spread out and levelled over the top surface of the build region as shown in Figure 2.5. A laser then selectively scans on the layer to fuse those areas defined by the geometry of the cross-section of a CAD model. The laser energy also fuses subsequent layers together. The building chamber is purged with inert gas and heated to raise the temperature of the uppermost layers of powder to nearly the fusing temperature. This reduces the additional laser energy required to heat the powder to its fusing temperature during fabrication. After each layer is deposited, an elevator platform lowers the part by the thickness of the layer and the next layer of powder is deposited. When the shape is completely built up, the finished part, buried within a cake of loose powder, is separated from the loose powder. Parts processed by SLS are porous and post processing is necessary when strength is required in the ceramic parts [Beaman *et al.*, 1997]. Conventional sintering and hot isostatic pressing are two common methods used for increasing part density.

The unused powder may be recycled and no support structure needs to be designed and built as the unfused powder remains in place as one. Changing from one material to another is straightforward and less messy than liquid based SFF techniques, given the dry solid nature of the starting material.

Compared with other SFF methods, which require the use of specific chemicals, e.g. photopolymer in SL, SLS can process materials directly without the use of a sacrificial binder [McAlea *et al.*, 1997]. The materials are thus cheaper compared with other SFF methods, e.g. SL; are non-toxic and safe and can therefore be adapted to a greater variety of materials. However, this poses a challenge in the laser sintering of high melting point

ceramics, which require a high level of laser energy that will bring forth large thermal gradients and thermal shock and hence a difficulty in forming a contiguous shape [Subramanian and Marcus, 1995]. This is partially overcome by incorporating a second phase binder of lower melting point into the ceramic powder. This second phase can be an organic binder coated on the powder, an inorganic binder (e.g. ammonium dihydrogen phosphate) [Subramanian and Marcus, 1995] or a metallic binder [McAlea *et al.*, 1997] but post SLS process is needed. The organic binder needs to be removed, which by itself is time consuming, and followed by a further sintering at high temperature. Using an inorganic binder will inevitably leave a second phase in the ceramics. In the case where a metallic binder (aluminium) is used, a post SLS process is required to fully oxidise the aluminium to alumina. The extent of conversion and hence the strength of the part is dependent upon the laser energy which, unfortunately at too high a value will induce thermal residual stresses in the part [Subramanian and Marcus, 1995].

The materials employed by the system are sensitive to the heating and laser parameters and each material requires distinct settings, which can be difficult and time-consuming to obtain [Pham and Gault, 1998]. Another drawback is that parts need a long cooling cycle in the machine before they can be removed for post processing. The recycled powders also must be sieved to get rid of globules, which will interfere with the smooth application of the next powder level.

Numerous methods have been employed to increase the powder bed density in order to increase the part (ceramic and metallic) density processed by SLS without sacrificing its freeform capability. Conventional means of improving the powder bed density include the use of spherical particulates, bimodal distributions of powder size, agglomeration of fine powder and optimising the volume fraction of combustible binder [Beaman *et al.*, 1997]. Another approach is to increase the effectiveness of the powder distribution process in SLS by the use of electrostatic field [Melvin and Beaman, 1991], magnetic field [Melvin and Beaman, 1992] or mechanical agitation [Bunnel *et al.*, 1995] of the powder and/or powder bed. On the other hand, in some applications, e.g. ceramic moulds for metal casting, porosity in the part is an important function and SLS processing of these parts allows direct fabrication.

Laser sintering of zirconium sand ($ZrSiO_4$) and silica sand (SiO_2) have been employed in industry while research with ZrSi, $ZrSiO_2$, SiC, graphite and other types of ceramics is still on going [Kruth *et al.*, 1998].

2.3.3.4 Laminated Object Manufacturing

Laminated Objected Manufacturing (LOM), as shown in Figure 2.6, was developed in 1985 and commercialised by Helisys Corp. to build components with layers of paper or plastic [Kruth, 1991]. The sheets are laser-cut according to the pattern defined by the CAD and laminated with adhesive relative to the previous layer. The laser also dices, or cubes, the excess material to help with removal of the finished component. The waste material is left in place during part building to serve as a support. The process is repeated until the component is formed.

The process was modified to fabricate ceramic components [Cawley, 1997]. Instead of paper, thin sheets, which are pre-processed from mixing ceramic powder with an appropriate binder by tape casting, roll compacting or extrusion, are used. After the thin sheets have been stacked to assemble a physical 3-D realisation of the original CAD description, the green part is removed from the platform and the waste material is decubed manually. The green LOM part is then subjected to binder removal followed by sintering. As the green parts are formed by lamination under applied pressure, one concern is the relaxation of residual stresses imparted during which delamination and bloating at binder burnout can occur. Pressure must be applied during pyrolysis to counteract this [Klostermann *et al.*, 1998].

In contrast to most SFF processes, LOM uses a subtractive method by tracing the outlines of the parts during layer fabrication [Cawley *et al.*, 1996]. This makes it potentially the fastest technology for building parts with a high ratio of volume to surface area [Pham and Gault, 1998]. Because the processing of the sheet is completely separated from component building, microstructural defects can be minimised [Cawley *et al.*, 1996]. Furthermore, any shrinkage or thickness variation during part fabrication can be accounted and compensated as the thickness of the sheet materials is known beforehand [Cawley, 1997]. It thus has the potential of yielding a highly accurate part. Another advantage of LOM is that tapes of two

or more types of material with different properties can be added to different regions, paving the way for fabricating functionally graded materials or multilayered composites with alternating compositions [Griffin *et al.*, 1996].

In LOM, the part fabricated is imbedded within a block of supporting material. This material needs to be broken into chunks before removal. Because surfaces are adhered to one another, cleaning is a manual process [Klostermann *et al.*, 1998] and much care is needed, as the scraps are as strong as the part. The amount of scrap generated is large and is non-recyclable. It is also hard to make hollow parts due to the difficulty in removing the core [Pham and Gault, 1998]. This difficulty also extends to narrow passages, internal cavities with restricted access, blind holes etc.. Another issue is that the chunks must be tiny enough to be manipulated through the small openings. The process also poses a potential hazard because the laser cuts through the material. The shear strength of the part is adversely affected by the layering of adhesion during lamination [Crump, 1991].

CerLOM, a LOM modification developed by Lone Peak Engineering Inc., has been used to combine tapes of different ceramic materials to fabricate multilayered composites with alternating composition [Griffin *et al.*, 1996]. Another LOM modification, the CAM-LEM process, was developed at Case Western Reserve University, USA [Cawley *et al.*, 1996]. This technology adopts a 'cut-then-stack' approach where the layer is cut to shape prior to placement onto the stack to be laminated. Therefore, it is possible to cut arbitrary angles by inclining the laser relative to the sheet to produce bevelled edges at the contour. This avoids 'staircasing' in the stack direction. Furthermore, layers of green and fugitive tapes can be added to the partially complete stack instead of being built onto it. The fugitive tapes are organic materials that can be burnt later. There is thus no need to remove waste material manually after assembly and hollow components can be constructed. In both of these modifications, the green part must be post-processed to remove the binder and sintered to densify the part. ZrO_2, Al_2O_3 and SiC have been investigated [Cawley, 1997; Kruth *et al.*, 1998].

Research on the use of a non-planar LOM process has also been carried out to build curved-layer part instead of only having flat layers [Klostermann *et al.*, 1998]. This concept has been implemented by alternating layers of SiC ceramic tapes and SiC fibre prepregs

(preimpregnated fibre preform) on a curved mandrel to fabricate aircraft engine components. MedLAM, a basic LOM by Lone Peak Engineering, has been used to prototype bioceramic implants with tailored porosity and these can serve as sites for bone formation and tissue regeneration [Griffin *et al.*, 1997].

2.3.3.5 Three-Dimensional Printing

The Three-Dimensional Printing (3DP) process was developed at Massachusetts Institute of Technology, USA in 1992 as a method to form green preforms for powdered metals and ceramics [Sachs *et al.*, 1992]. It has been used for many years to produce ceramic cores and shells for casting applications under the name Direct Shell Production Casting (DSPC) from Soligen Corporation [Uziel, 1997].

In 3DP, as shown in Figure 2.7, powder is being dispensed and a roller is used to spread and level the powder into a thin layer, typically 170 μm thickness. An ink-jet printhead then moves across the powder in raster motion and prints a layer of binder selectively onto the loose powder as defined by the CAD model. As the binder diffuses through the powder by capillary action, neighbouring particles are pulled together due to surface tension [Sachs *et al.*, 1993]. The layer printing process is repeated and part is built up in a bin, which is fitted with a piston to incrementally lower the part into the bin. After the part is completely printed, it is placed in a furnace to cure the binder. The excess powder is removed by immersion in a water bath. The part is then subjected to firing to sinter.

As in SLS, parts fabricated with this process do not require supports for overhanging features. The unbound powder becomes the support material. Being an ink-jet printhead technology, 3DP does not require high energy, does not involve lasers or any toxic materials and is relatively cheaper and faster [Carrion, 1997]. As the powder is deposited during part building, the process can be adapted to use a variety of powders to modify the desired pore size and shape. By using multiple printheads, additives may be deposited in a prescribed fashion to create gradients in the composition, e.g. in the fabrication of compositionally graded zirconia-toughened alumina (ZTA) ceramic multilayers [Yoo *et al.*, 1998].

The technology was initially developed to directly produce ceramic moulds for metal castings and though the final parts may be porous, it is sufficient for the intended applications. With proper placement of droplets, printed part with controlled surface texture and internal microstructure may be created. It was used to make casting mould with tailored surface texture for orthopaedic implant with bony ingrowth structures [Curodeau *et al.*, 2000]. However, this poses challenges for its applications for the fabrication of structural ceramic parts. Although the use of fine powder improved sintering of the 3DP part, its high surface area decreased the powder's flowability and therefore it became difficult to obtain layers of defect-free powder. Several methods have been implemented to produce dense ceramic parts with fine powder by intermediate isopressing or modifying the binder or powders [Cima *et al.*, 1995].

Dimensional control of the built part is determined by the accuracy of droplet placement within the plane of printing and the vertical position of the powder layer [Sachs *et al.*, 1992]. Due to the compressibility of the powder, loads applied from above cause the thin layer of powder to displace downward from its original position and therefore a loss of vertical dimensional control can occur. Layer displacements are most severe in the middle regions of powder bed, with diminishing magnitude towards the top and bottom. Using a higher packing density powder bed reduces compressibility and therefore helps to minimise layer displacement, but additional pre-processing work is necessary [Lee *et al.*, 1995]. Another drawback is inadequate surface finish due to the raster scanned by the printhead on the layers. This leads to a stair-stepping effect in the XY plane as well as in the build direction [Conley and Marcus, 1997]. Surface finish is also determined by the interaction of the binder with the powder.

Another method, Direct Ceramic Ink-Jet Printing, also employs ink-jet printing technology to produce ceramic parts [Blazdell *et al.*, 1995]. Though still in its research stage, this process displays potential to produce a wide range of fine ceramic contours with high resolution and may be used to produce miniaturise components [Edirisinghe, 1998]. Further details are given in Section 2.4.

2.3.3.6 Other SFF Methods

In addition to the above-described SFF methods, which involve solid/liquid to fabricate ceramic parts, gas precursor based techniques such as Selective Area Laser Deposition (SALD) [Birmingham *et al.*, 1995] and Selective Area Layer Deposition Vapour Infiltration (SALDVI) [Maxwell and Pegna, 1995] are being explored. In SALD, shape is built from the solid decomposition products of the gas precursor, either pyrolitically (by heat) or photolytically (by photon interaction) according to the pattern defined by the scanning laser. An example is in the forming of SiC parts where the Si powder is locally melted by the scanning laser beam in the presence of methane (CH_4) and reacts with the gas. SALDVI uses the same powder approach as in SLS and 3DP but forms the parts by infiltrating the powder by vapour. Although still in their research stage, SFFs using gas precursors look promising with their capability of producing a wide range of materials, particularly for high temperature structural materials, which are beyond current SFF processes and difficult to process by traditional methods [Conley and Marcus, 1997].

2.3.4 Challenges to SFF of Ceramics

While the applications of SFF technology to date have been significant, improvements in the technology in terms of building speed, surface finish, dimensional accuracy and material properties are needed [Kruth *et al.*, 1998]. Comparison of the various SFF techniques in terms of these four requirements has been made quantitatively for plastic products [Kruth, 1991; Ippolito *et al.*, 1995; Pham and Gault, 1998] but for ceramic parts, the basis is qualitative [Halloran, 1999; Paul and Baskaran, 1996; Wang and Krstic, 1998] as developments are recent.

Building time, which comprises of pre-processing, fabricating (layering and forming) and post-processing, remains a challenge before the techniques can be considered for industrial implementation [Sigmund *et al.*, 2000]. Difficulties are encountered in most layer-based processes to achieve accurate deposition, be it in spreading fine powder in 3DP [Cima *et al.*, 1995] or ensuring proper recoating of a new layer of viscous ceramic SL suspension [Griffith and Halloran, 1996]. This, unfortunately, often determines the success of the process [Kruth *et al.*, 1998] and dimensional accuracy of the part [Sachs *et al.*, 1992].

Surface finish is a crucial feature in SFF [Ippolito *et al.*, 1995]. The rough texture of the finished part results from the 'stair-stepping' effect and is due to the slicing of a sloped or contoured surface that is not coplanar with the x-y plane, as shown in Figure 2.8. Another contributing reason to roughness is the raster scan experienced in SLS and 3DP which results in a horizontal stairstep effect on the cross section [Conley and Marcus, 1997]. Improved texture can be obtained by reducing the laminate thickness [Paul and Baskaran, 1996] or by using secondary operation (such as grinding or polishing) [Agarwala *et al.*, 1996b], but are detrimental to production times and cost.

Most of the SFF processes for ceramics started for form and fit application, e.g. prototyping investment-casting positives, but there is an increasing effort to fabricate high-density structural ceramics that require high-density green parts. As a majority of the SFF techniques for ceramics is powder based and impregnated with polymer or wax, post-processing steps, e.g. binder burnout and sintering must be practised to remove these transitory materials followed by sintering and this is accompanied by shrinkage. The level of shrinkage is often difficult to anticipate before actually making the part and it may lead to defects and distortion. Aside of being influenced by the materials chosen and the post-processes, dimensional accuracy is also influenced by other factors such as the machine [Kruth, 1991], software algorithm [Kruth *et al.*, 1998], part building [Sachs *et al.*, 1992] and operator's skilfulness [Ippolito *et al.*, 1995]. Accuracy, as Kruth *et al.* [1998] has stressed, is the greatest challenge of SFF processes.

Another consequence of fabrication with powdered materials is porosity with the drawback of lower strength compared with solid parts. Initial results of the strength of SiC made by LOM trials was rather disappointing with strength about 50% of that expected from conventionally processed parts [Klostermann *et al.*, 1997]. SLS and 3DP, which are based on powder beds, require either infiltration or intermediate isopressing to enhance green density and ultimately, final material properties [Cima *et al.*, 1995; Beaman *et al.*, 1997]. Agarwala *et al.* [1996b] used FDC to fabricate structural ceramic components with microstructures and mechanical properties compatible to conventionally processed Si_3N_4 material.

2.4 Direct Ceramic Ink-Jet Printing

Direct Ceramic Ink-Jet Printing, DCIJP, was pioneered by Evans and Edirisinghe [Edirisinghe, 1997]. It also uses an ink-jet printhead as in 3DP to create components by multi-layer printing. However, it is distinguished from 3DP in that a ceramic-powder containing ink is dispensed directly instead of the binder. DCIJP is built upon two fundamental principles, i.e. suspension preparation by colloidal processing and freeforming by ink-jet printing. This section will review both technologies for DCIJP.

2.4.1 Ink-Jet Printing Technology

Ink-jet printing belongs to the family of non-impact printing technologies. This is a printing technique that 'takes small quantities of ink from a reservoir, converts them into droplets, and transports the droplets through the air to the printed medium (paper, transparency, beverage container etc.) by appropriate applications of physical forces' [Lloyd and Taub, 1988]. It is a technology that combines fluid dynamics, acoustics, electronics, computing and physics, to name a few. Basically, it is a computer-controlled process which enables variable data to be printed continuously at high speed [Keeling, 1981]. The main attributes of an ink-jet printer, which differentiate it from other printing techniques are [Keeling, 1981; Le, 1998]:

* high speed printing
* silent, non-impact operation
* electrically controllable by computers
* paper requires no special after-treatment
* printing on uneven or delicate surface is possible
* colour capability

The first practical construction of an ink-jet printer was demonstrated by R. G. Sweet of Stanford University in the 1960s [Kuhn and Myers, 1979]. Since then, several ink-jet printing techniques have been implemented in a wide variety of ways. A brief account of the recent development of ink-jet printing has been reviewed by Le [1998]. There are two main types of ink-jet printer: continuous (or pressurised) and drop-on-demand (DOD). Continuous ink-jet printer forms droplets continuously even when there is no printing and the droplets are selected and guided to the printed medium by electrostatic or magnetic

forces. It is normally used for high-speed printing of bar codes, sell-by dates and mailing dates. In the DOD ink-jet printer, ink droplets are formed only when required and the forces used to create and transport these droplets may be mechanical, electrostatic, magnetic or thermal. It is used mainly in home and office printing. Aside of these well-established applications, ink-jet printing technologies have also penetrated into the emerging markets of rapid prototyping and medical imaging [Carrion, 1997; Le, 1998]. Some of the novel applications of ink-jet printing, asides being found in 3DP and DCIJP, include printing of hybrid microcircuits [Teng and Vest, 1987], deposition of patterned luminescent doped-polymer films [Hebner *et al.*, 1998], printing sol-gel based inks to decorate ceramic articles [Atkinson *et al.*, 1997] and patterning ceramics [Kim and McKean, 1998].

2.4.1.1 Continuous Ink-Jet Printer

In a continuous ink-jet printer, a conducting ink is forced out of a reservoir through a 10-200 μm diameter nozzle under pressure. As it passes through the nozzle, the liquid is piezoelectrically pulsed or modulated and the stream breaks up into a continuous series of droplets so as to minimise surface area. The droplets are equally spaced from one another and of equal size. Surrounding the jet at the point where the droplets separate from the liquid stream is a charge electrode and here a voltage is applied between the charge electrode and the liquid stream. When a droplet breaks off from the stream, it also carries with it a charge proportional to the applied voltage. After leaving the charge electrode, the droplets enter into an electric field between two deflection plates which are maintained at a constant voltage potential, typically ±3kV. In this electric field, the charged droplets are deflected towards one of the plates by an amount proportional to the charge carried. Droplets that are uncharged are undeflected and collected by a gutter in order to be recycled into the ink reservoir and recirculated to the printhead. The charged droplets that are deflected continue in their flight and impinge on a substrate.

The continuous ink-jet printer can be a binary or multiple deflection system depending on the droplet deflection methodology (Figure 2.9). In a binary deflection system, the droplets are either charged or uncharged. The charged droplets are allowed to impinge directly onto the printing medium while the uncharged droplets are deflected into a gutter for recirculation. Companies such as Elmjet, Scitex and Image are developing printers in this

range [Le, 1998]. In a multiple deflection system, charged droplets are deflected to the printing medium at different levels and the uncharged droplets are returned directly to a gutter for recirculation. This approach allows a single nozzle to print a small image swath and these printers are being developed by Videojet, Diconix, Domino Amjet and Linx [Le, 1998].

Theory of Operation

(a) Droplet formation process

After the jet emerges from the nozzle, it decays and breaks up into droplets. This decay is caused by the existence of surface tension, which forces the jet to assume the shape of minimum surface area [Rayleigh, 1882]. It occurs whether or not any additional forces act upon the jet. These disturbances tend to be random and consequently, the droplet formation frequency and the distance from the nozzle where droplets first occur also vary randomly. This is unstable for a printer in which each droplet formed is individually addressed to assure that it will reach the exact pre-determined point on the substrate being printed. By perturbing the jet periodically with a slight excitation (modulation) at a fixed frequency approximately equal to the spontaneous droplet formation rate, the droplet formation process is synchronised with the forced vibration and therefore produces ink droplets of uniform mass. This excitation may be applied by various means, the most common of which is mechanical via the use of a piezoelectric device attached or built into the printhead. Rayleigh [1882] was the first to treat this droplet formation theoretically for a non-viscous liquid jet and he deduced that the wavelength of the fastest growing frequency λ_{opt} occurs when $\lambda_{opt} = 4.51 d_j$ (where d_j is the diameter of the jet). Weber [1939] included viscosity in the calculation of the same problem and arrived at a result very similar to that of Rayleigh. Most ink-jet printers are designed to operate at a frequency near to λ_{opt}. Given the relationship between the jet velocity (v) and the frequency of the modulation (f) to be

$$v = f\lambda \qquad (2.1)$$

there can be significant variations between v and f for a fixed wavelength $\lambda_{opt.}$ Incorrect modulation will introduce satellites, which are small droplets formed between the main (or parent) droplets. Satellites are undesirable as they can contaminate the printhead or cause misplaced print marks [Pimbley and Lee, 1977].

(b) Droplet charging

At the locality where the jet breaks up into discrete droplets is a charge electrode which surrounds it. When the droplet breaks off from the jet, charge is trapped on the droplet. The charge Q on a droplet for a given charging voltage V is then given by Equation 2.2 [Keeling, 1981].

$$Q = \frac{2\pi\ \varepsilon_o\ V\ \lambda}{\ln\left(\frac{4d_c}{\pi\ d_j}\right)} \qquad (2.2)$$

Where d_c is the width of the slot in the charge electrode

d_j is the diameter of the jet and

ε_o is the permittivity of free space.

The voltage of the electrode is limited to a few hundred volts. Too high a voltage will cause the droplet to explode if the repulsion between charged droplets exceeds the surface tension of the liquid [Lloyd and Taub, 1988]. The maximum charge Q_{max} (in coulombs) is given by Equation 2.3.

$$Q_{max} = \sqrt{64\ \pi^2\ \varepsilon_o^2\ r^3\ \gamma} \qquad (2.3)$$

where r is the droplet radius and

γ is the surface tension of the ink.

(c) Deflection

The charged droplet continues its flight path and enters into the deflection field. The amount of deflection for a single droplet is [Keeling, 1981]:

$$x = \frac{QEZ_d^2}{2mv^2}\left(\frac{2Z_g + Z_d}{Z_d}\right) \qquad (2.4)$$

Where E is the deflection field strength

m is the droplet mass

Q is the droplet charge

v is the droplet velocity in the direction of the jet

Z_d is the length of the deflector plates and

Z_g is the distance between the bottom of the deflector plates and the substrate.

This is a simplified equation as in actual printing a number of droplets are deflected and being in close proximity to one another, also experiences a repulsion force from the neighbouring charges and an aerodynamic drag as it travels in air [Fillmore *et al.*, 1977]. However, it is clear from this equation that deflection increases when the deflector plate to substrate distance is increased.

2.4.1.2 Drop-On-Demand Ink-Jet Printer

The drop-on-demand (DOD), or impulse, ink-jet system is the most common jet printing method in recent years. It was developed to circumvent some of the limitations of continuous jet printing technology, e.g. start-up and shut down requirements, complex charging, need for ink re-circulation etc. and is a system well known for simplicity [Lee *et al.*, 1984]. There are four major types of DOD printers, categorised according to their droplet formation process: piezoelectric, thermal, electrostatic and acoustic ink-jet, of which the first two methods are most common at present [Le, 1998].

(a) Piezoelectric ink-jet DOD printer

In a piezoelectric DOD ink-jet method (Figure 2.10), part of the chamber consists of a piezoelectric element, which in most cases is a piezoceramic. When excited by an electrical signal, the piezoceramic material is deformed and this causes a sudden change in the ink pressure in the chamber and a pressure wave, which propagates towards the nozzle, is generated. By overcoming the viscous pressure loss at the nozzle and the surface tension in the ink meniscus, an ink droplet is formed at the nozzle. The pressure must also be sufficient to expel the droplet towards a recording medium. Droplets are ejected only when needed for printing. Thus, no ink re-circulation or high pressure source for the ink is necessary. Conceptually it requires less hardware than a continuous ink-jet printer [Lee *et al.*, 1984].

(b) Thermal ink-jet DOD printer

Though not the first ink-jet method implemented in a DOD printer, the thermal ink-jet is the most successful method on the market today. The thermal ink-jet printer normally uses a disposable ink-jet printhead, which contains all the elements necessary to produce a print. It is comprised of a liquid ink supply, several nozzles and their associated droplet formation

systems. Figure 2.11 shows the droplet formation process in a thermal ink-jet printer. A droplet of ink is formed when electrical heat is transferred from the surface of the heater to the water-based ink. In a very short duration, the ink is superheated to the critical temperature required for bubble nucleation. A bubble of water vapour is formed and instantaneously expands to force the ink out of the nozzle. Once all the heat stored in the ink is used, the bubble begins to collapse and the ink droplet breaks off concurrently and is transferred onto the substrate to be printed. Capillary forces cause the ink chamber to refill with ink and the process is ready to begin again. The dimensional stability, accuracy and uniformity of the orifice are known to have great effects on jet performance such as droplet frequency, volume and velocity [Le, 1998]. The mass and velocity of the droplet are also a function of the geometrical parameters of the printhead and the physical properties of the ink [Lloyd and Taub, 1988].

In general, DOD systems use nozzle openings ranging from 40 – 100 μm and for thermal DOD, an upper limit of droplet rate of 12 kHz has been reported [Le, 1998]. Compared with the continuous ink-jet method, the DOD principle is less useful for printing on curved surfaces or where the ink droplet must traverse a long distance.

2.4.1.3 Ink

It is obvious that the ink used is of crucial importance to the functioning and reliability of jet printing and the quality of the printed image.

(a) Types of ink

In general, aqueous- or water-based inks are used in office ink-jet printers whereas solvent-based inks are used in industrial marking or coating applications [Le, 1998]. For the latter, printing normally requires to be done on a non-porous substrate such as plastic, metal or glass. Because no absorption or penetration occurs, the printed image relies on quick evaporation of the ink solvent for fixation onto the substrate [Hudd, 1999].

The idea of ultra-violet (UV) curable ink for jet systems has been considered and is driven by a need to produce durable and sharp images on non-absorbent substrates such as metal, glass and plastic. Furthermore, UV curable ink also has the advantage of almost

instantaneous transformation from the fluid phase to a solid cross-link phase [Hargreaves, 1999]. However, many factors, such as printhead capability, photo-initiator and low toxicity monomer and market needs have hindered the progress of UV curable ink-jet development [Le, 1998].

Ideally, the liquid ink must be converted to a solid structure as quickly as possible within the restraints of the printing process itself. The ink may be dried by absorption, oxidation, evaporation, chemical (where a reaction occurs) or radiation (e.g. induced by UV radiation, infra-red, microwave) [Leach and Pierce, 1999].

(b) Ink properties

For consistent droplet formation, inks must possess a careful balance of rheology, surface tension and electrical conductivity, in the case of a continuous jet printer.

The viscosity range may vary with machine type but ideally the flow should be Newtonian. A value of 1 – 3 mPa s is normally chosen for continuous jet printer and this is lower than for a DOD printer. DOD printers require a stable viscosity during long periods of use but this requirement is less critical for continuous jet printers [Marsh, 1988]. For this reason, a number of DOD printers incorporate thermostatically controlled nozzles as viscosity varies with temperature. For a low viscosity liquid, a variety of viscometers are available for measuring its viscosity, e.g. Ostwald U-tube, cone and plate and concentric cylinder viscometers [Shaw, 1996].

Surface tension is critical both to the formation and maintenance of discrete droplets. Water at 72 mN m^{-1} would provide the optimum surface tension but this value decreases when blended with dyes, resins and additives [Marsh, 1988]. Solvent-based inks for continuous jet printers have even lower surface tension. The more commonly used methods for measuring surface tension are the ring method (du Noüy ring method), the Wilhelmy plate method, the drop-volume and drop-weight methods and the pendant drop profile method [Shaw, 1996]. In addition, the spreading of the ink droplets over the printing substrate also needs to be considered. If the ink has a lower surface tension than the surface free energy of the substrate, the ink will spread across and wet the surface. It is said to have a lower contact

angle. If it forms globules, it is said to have a high contact angle. By drawing a tangent to the liquid surface at the point of three-phase contact, contact angle is measured. Contact angle can be measured for an equilibrium, advancing or receding droplet. The angle may be obtained by projecting an enlarged image of the droplet onto a screen and measuring the angle with a protractor [Rance, 1982]. Alternatively, the tilting plate method in which a slab of solid is dipped into the liquid and is rotated until the liquid surface appears perfectly flat right up to the solid surface can be used [Shaw, 1996].

Electrical conductivity, the reciprocal of electrical resistance, is an important property in the case of continuous jet printers, which use an electrical field to deflect droplets. The ink droplet has to be fully charged in the duration of the charging pulse so that it can be deflected and deposited at the pre-determined position on the printing substrate. Usually the value is at least 0.1 S m^{-1} [Hudd, 1999]. Polar solvents such as water can yield high conductivity but when printing is made on non-absorbent material and/or a faster drying rate is required, organic solvent, such as ethanol or methyl ethyl ketone is used. These solvents normally produce less conductive inks than water and it is common to add soluble salts to improve electrical conductivity [Lloyd and Taub, 1988].

As the nozzles are small, e.g. in the range of 10-220 μm, it is important that particles, which clog the nozzle, are removed at upstream. The ink should not dry in the nozzle when the printer is not in operation [Buehner *et al.*, 1977]. Some of the key design parameters for the printer/ink are summarised in Tables 2.1 and 2.2.

Table 2.1 Typical design parameters for a continuous jet printer.

Parameters (units)	Typical Range
Nozzle diameter (μm)	10 – 220
Operating frequency (kHz)	17 – 1000
Charging voltage (V)	100 –300
Deflection voltage (V)	1000 –5000
Ink pressure (kPa)	0.5 – 24
Jet velocity (m s^{-1})	10 – 50
Ink viscosity (mPa s)	1 – 10
Ink surface tension (mN m^{-1})	25 – 70
Ink conductivity (S m^{-1})	> 0.1
Particle size (μm)	< 1

Table 2.2 Typical parameters for a drop-on-demand jet printer.

Parameters (units)	Typical Range
Nozzle diameter (μm)	40-100
Droplet volume (picoliters)	50-500
Operating frequency (kHz)	3-25
Droplet velocity (m s^{-1})	3-15
Resolution (dots per m)	4000 -9500

2.4.2 Colloidal Processing of Ceramics

A colloidal dispersion is defined as a system in which particles of colloidal size (1 - 1000 nm) of any nature (solid, liquid or gas) are dispersed in a continuous phase of a different composition or phase. In this particle range, the particles are sufficiently small (≤ 1 μm) not to be affected by gravitational force but large enough (> 1 nm) to show marked deviation from the properties of a true solution [Shaw, 1996]. In this range, the interactions between the particles are dominated by short range forces such as van der Waals attraction and surface force. Colloidal processing of ceramics normally involves the preparation of a well-dispersed suspension of solid particles with reasonably low viscosity to facilitate the mould-filling process. Lange [1989] proposed the use of colloidal methodology for powder processing by manipulating and controlling the inter-particle forces. A stable dispersion was first prepared to eliminate heterogeneities usually caused by powder agglomerations. Milling, sedimentation and/or filtration processes can be used for this. This results in a weakly flocculated system with the desired plasticity for forming and minimised mass segregation during storage and handling prior to consolidation.

2.4.2.1 Components of Dispersion

The colloidal dispersion normally comprises of the ceramic powder, solvent, dispersant or surfactant, binder, plasticiser and other additives. Each component is carefully selected and accurately controlled to give the ink the desired properties and to ensure its compatibility with others. Zirconia powder is chosen for discussion as it was used in this research.

(a) Zirconia

Zirconia is an oxide described by the formula, ZrO_2 and is a white powder in its processed form. It is mainly produced from zircon sand ($ZrSiO_4$) by melting the latter in an electric arc furnace. ZrO_2 has an extremely high melting point of about 2680°C, a high density (between 5680 to 6270 kg/m^3) and was originally used as a refractory material.

ZrO_2 exhibits three well-defined crystal structures: monoclinic, tetragonal and cubic. Its use would be limited because of its peculiar transformation, which proceeds as follows:

$$\text{Monoclinic} \xrightarrow{1170^\circ C} \text{Tetragonal} \xrightarrow{2370^\circ C} \text{Cubic}$$

The monoclinic phase is stable up to 1170°C where it transforms to tetragonal phase, which is stable up to 2370°C. From this point onwards, the cubic phase exists but up to 2680°C. The monoclinic-tetragonal transformation is accompanied by a volume change of 3-5%. Without modification, cracks can occur during its usage, rendering application of pure ZrO_2 not feasible. The addition of cubic oxides: CaO, MgO, CeO_2 or Y_2O_3, is known to avoid the deleterious volume expansion which takes place as the tetragonal to monoclinic phase change occurs and maintains the cubic structure even at low temperatures. This is called 'stabilised zirconia'. If the stabilising oxide present is less than that required for complete stabilisation, the resultant ceramic is a combination of cubic and tetragonal and/or monoclinic phases. This is known as a partially stabilised ZrO_2, better known by its acronym, PSZ. The retention of tetragonal phase, which is the toughening agent, offers great potential for improved strength and toughness [Lange and Claussen, 1984].

The raw material used in this study is Y_2O_3-PSZ. The addition of yttria to zirconia extends the range of the tetragonal phase field and lowers the temperature of tetragonal-monoclinic transformation. It is possible to obtain sintered body with a uniform fine grain texture and density close to the theoretical density with this powder. This allows the fabrication of a dense zirconia polycrystalline ceramic consisting of nearly 100% tetragonal phase (TZP). It is suitable as a ceramic material [Scott, 1975].

PSZ is attracting interest because of its wide range of properties such as high melting point, high refractive index, chemical inertness, high strength and toughness and excellent wear

resistance. Increasingly it is replacing conventional material, typically metal, with significant advantages. Examples of PSZ applications can be found in Table 2.3. Its conductivity has also been recognised and is used as a good solid electrolyte in high temperature solid oxide fuel cell and oxygen sensor [Saito, 1985; Li *et al.*, 1999].

Table 2.3 Examples of applications of partially stabilised zirconia [Skidmore, 1998].

Structural ceramics	Pump components, bearings, seals, valves, various industrial parts, e.g. optical fibre connectors
Bioceramics	Body implants - hip joints, bone replacements, dental implants
Low wear ceramics	Grinding media, mill linings, engine components - cams, valves, piston crowns/liners, thread guides, printheads
Forming dies	Copper extrusion and wire drawing
Cutting applications	Blades, scissors, shears, cutting tools
Coatings	Thermal barrier, plasma spray
Gemstones	ZrO_2 single crystal - synthetic diamonds can be made in various colours
Glass	Camera lenses/measuring instruments/use in glass fibres
Jewellery	ZrO_2 in various colours

(b) Solvent

Solvents are necessary both to impart the fluidity and as a vehicle for the dissolution and uniform distribution of all additives and the ceramic particles. The desired properties of a solvent are:

* ability to dissolve other additives, e.g. the dispersants, binders and plasticisers
* chemical inertness to the ceramic powder
* low viscosity at high powder loading
* high evaporation rate
* safety, i.e. non-toxic and non-flammability
* low cost

Solvents used for ceramic processing are either polar or non-polar and can be aqueous or non-aqueous. This characteristic will dictate the type of stabilisation mechanism dominant in the dispersion (to be discussed later). The advantages and disadvantages of both aqueous based and organic based inks were discussed by Morneo [1992].

(c) Dispersant

Sometimes also called deflocculant, wetting agent or surfactant, a dispersant helps to distribute the powder homogeneously in the solvent. As a deflocculant, it promotes deflocculation and stability; as a wetting agent, it enables effective total wetting of the solid by the solvent. In addition, it may alter the rheological property of the solvent-solid system and acts as a plasticiser and/or lubricant. The dispersant keeps the powder in a stable dispersed state by different stabilisation mechanisms (Section 2.4.2.3).

Dispersants for ceramic processing are broadly divided into two groups - inorganic and organic. Each can be divided further into four categories [McHale, 1991; Shanefield, 1995]:

(i) Anionic - they are most common in ceramic processing and include common soaps; usually acidic and may either be corrosive or interfere with binder performance. The negatively charged part of the anionic dispersant adsorbs onto the ceramic particle and charges it. They then electrostatically repel each other and make a fairly stable colloidal suspension.

(ii) Cationic - they are not commonly used and are often toxic; generally basic and act to neutralise acidic additives or impurities and are thus used as corrosion inhibitors. Instead of the negatively charged, the positively charged ions of the dispersant are adsorbed onto the ceramic particles.

(iii) Zwitterionic - they have two functional groups and include many naturally occurring substances, such as lecithin and triglycerides.

(iv) Non-ionic - being non-ionic, they tend not to interfere with other necessary functions of the systems and this makes them valuable in processing. They may exhibit ionic character in certain pH ranges. As they cannot impart an electrostatic charge on ceramic particles, they only work as dispersants by steric hindrance (to be discussed later). In an aqueous system, this is not strong enough to overcome the competing tendency of hydrogen bonding to form agglomerates.

Mikeska and Cannon [1984] suggested the following considerations in selecting a suitable dispersant:

* consider only those dispersants that are readily soluble in the binder/solvent system
* determine the appropriate dispersant type (anionic, cationic or non-ionic) which maximises surface adsorption
* determine which dispersant yields minimum viscosity at a high solid loading. Test only solvent/dispersant systems because binder viscosity characteristics could mask dispersant properties
* observe which dispersant has minimum settling volume, either gravitational or centrifugal
* conduct further compatibility tests of the best dispersant in conjunction with the binder.

It is not always easy to predict the quantity and configuration of a given dispersant adsorbed to a given particle surface [Horn, 1990]. There is a certain range of concentration over which a monolayer of dispersant is adsorbed on the particle surface such that its molecule is oriented perpendicular to the surface and provides the required coverage to promote stabilisation. Below this range, there is less coverage with the possibility of dispersant molecules lying parallel to the surface. On the other hand, at a higher concentration, it is possible for a second monolayer adsorbed on the first, generally in the opposite direction. This neutralises the effect of the first layer and the particles will be likely to agglomerate [Pashley and Israelachvili, 1981].

(d) Binder

Binder provides strength to the green part for handling and storage. After the solvent has evaporated, the binder remains in the green part and forms a strong, adhesive bridge. The desirable characteristics of the binder are [Reed, 1995; Shanefield, 1995]:

* easy burnout without leaving residues
* compatibility with other additives in the suspension
* good strength and toughness
* low cost

* effective at low concentration

Binders used in processing ceramics are usually molecular binders, which provide wide flexibility in modifying rheological behaviour. They can be organic or inorganic. The former is more often used as they introduce little inorganic impurity when decomposed under oxidising conditions. Inorganic molecular binders are used when the inorganic component is compatible with the particle composition [Reed, 1995]. Because binder strongly affects the rheology of the liquid phase, the suitable amount to be added is usually determined experimentally [Hozta and Creil, 1995].

(e) Plasticiser

Plasticisers toughen the binder. They are organic substances with a lower molecular weight compared with the binders. They usually have a chemical structure similar to that of the binder and can penetrate in between the binder molecules and lubricate them, allowing them to slide against each other and take up strain without actually cracking. Without the plasticiser, and even with three times as much a binder, the green body usually is too brittle, particularly when fine powders are used [Shanefield, 1995]. There is an optimum value of binder/plasticiser concentration which corresponds to a low porosity [Hotza and Creil, 1995]. Further addition results in increased inter-particle distances and decreased green density.

2.4.2.2 Dispersion Mechanisms

Preparation of the suspension essentially involves dispersing the powder in a liquid. Bell and Crowl [1973] described the process as the 'incorporation of a dry powder into a liquid medium in such a way that the individual particles of the powder become separated from one another, or form small clusters, evenly distributed throughout the entire liquid medium'. Parfitt and Barnes [1992] had sub-divided the dispersion process of powder in liquid into four stages:

* incorporation of powder
* wetting
* breaking up particle clusters to form colloidal particles

* colloidal stabilisation

These stages may overlap with one another in practice. Essentially they involves inter-particle forces to be overcome before each of these can be accomplished.

The dispersion process starts with a fine powder of a relatively large specific area and this tends to agglomerate. In a powder are particles and agglomerates. According to BS5600 [1981], a 'powder' is an assembly of particles usually less than 1 mm in size. A 'particle' is a unit of powder that cannot be readily subdivided by the usual separation process such as sieving, milling, ultrasonic action or other moderately strong stirring method. An 'agglomerate' comprises of several particles adhering together. These terms are further illustrated in Figure 2.12. Various inter-particle forces, which are responsible for the formation of agglomerates, exist in a 'dry' powder. They are van der Waals forces, electrostatic forces, bonding due to moisture and gravitational forces [Bossel *et al.*, 1975; Harnby, 1992]. They must be overcome before the powder can be incorporated in the liquid where powder-air and powder-powder interfaces are replaced by powder-liquid interfaces.

Wetting refers to the spreading of a liquid over a solid surface whereby the adsorbed air and other contaminants on the particle surface are being replaced. The use of a surface active agent is known to assist the wetting of liquid over the powder surface. However, the entire surface of each particle must be available for wetting and this requires the breaking down of the agglomerates. This is usually achieved mechanically by either shear or impact but the strongly bonded agglomerates may not be disrupted.

2.4.2.3 Inter-Particle Force and Stability of Dispersion

The breakdown of agglomerates is usually a dynamic process in which re-agglomeration (or flocculation) is constantly in competition with de-agglomeration (or deflocculation) as the attractive van der Waals forces are ever omnipresent in the dispersion [Shaw, 1996]. The inter-particle force can be controlled so that the colloidal suspension is prepared in the dispersed, weakly flocculated or strongly flocculated states [Lewis, 2000]. The dominating inter-particle forces in most ceramic colloidal systems are the van der Waals, electrostatic and steric forces. With the exception of van der Waals force, they can be manipulated by a surface-active agent [Lange, 1989]. By further controlling the properties of the suspension,

the desired rheological behaviour can be tailored for the application. However, these require an understanding of the theory and characteristics of the inter-particle forces. The theory of inter-particle forces is relatively established and is discussed by Horn [1990] but much work is still in progress in the direct measurement of the inter-particle forces in ceramic systems [Sigmund *et al.*, 2000].

Van der Waals force is always attractive and electrodynamic in origin as it results from the interactions between oscillating or rotating dipoles within the interacting media. Its interaction is of varying importance depending on the system. The Hamaker constant is a conventional and convenient way of assessing the interaction although the Lifshitz theory is able to predict accurately if complete optical data for the material of interest is available [Horn, 1990]. To create a stable suspension, a repulsion needs to be introduced to overcome the van der Waals attraction forces between the ceramic powder in the colloidal suspension [Sigmund *et al.*, 2000]. Stabilising mechanisms in a colloidal suspension are achieved by creating an electrostatic double layer at the solid-liquid interface or by adsorbing polymer or surfactant on the particle surfaces (Section 2.4.2.1c). The third type of stabilisation mechanism is known as electrosteric stabilisation, which is a combination of a pure electrostatic repulsion and a steric force.

The first mode of stabilising mechanism, electrostatic stabilisation, is normally found in suspensions of ceramic powder in a polar liquid, such as water. Ions can be attracted to or dissociated from the liquid to the particle surface, forming a diffuse layer of charges adjacent to the particle. The surface charge and the diffuse layer of opposite charge constitute an electrical double layer. The strength of this electrostatic force, which is repulsive in nature, decays exponentially with distance from particle surfaces. It also depends on the surface potential induced on the interacting colloidal particles and the dielectric property of the intervening medium [Shaw, 1996]. Complete analysis of the interaction between two charged particles in a polar media is quite complicated and normally analytical approximations or numerical solutions are used [Lewis, 2000]. The well known DLVO (Derjaguin-Landau-Verwey-Overbeek) theory, which combines the interactions between van der Waals and electrostatic forces, is used successfully to predict the stability of ceramic in polar medium.

Compared with electrostatic stabilisation, steric stabilisation is more commonly used to create a colloidally stable suspension although it is not always possible to predict which type of force dominates under a set of circumstances [Horn, 1990]. It has several distinct advantages over electrostatic stabilisation such as insensitivity to the presence of a high electrolyte level, equal efficacy at both high and low solid contents as well as in aqueous and in non-aqueous dispersion media [Heusch and Reizlein, 1987]. It is developed by macromolecules, which attached themselves to the surface of the particles. This protective sheath of polymer shields the influence of van der Waals forces between the particles and prevents them from attracting to one another. Many factors determine the adsorption of the polymers onto the ceramic particle, e.g. solvent quality, molecular architecture, number of anchoring groups and active surface site density [Napper, 1983]. Steric stabilisation is also influenced by factors such as temperature, pressure and solvent composition [Shaw, 1996]. The state of a sterically stabilised system can be changed by manipulating the thickness of the adsorbed layer, the affinity of the polymer to the surface and the solvency of the polymer in the medium [Sigmund *et al.*, 2000]. When the solvency is reduced, the dispersion often shows sharp transitions from long-term stability to rapid flocculation.

2.4.2.4 Assessment of Dispersion

Because the properties of the printed parts and hence the sintered parts are dependent upon the state of dispersion, the ability to characterise the state of dispersion helps to control the process or the product. Most investigators assess the dispersion stability of concentrated suspensions of ceramic qualitatively by estimating the extent of flocculation.

The two most common methods for measuring flocculation rates, and hence dispersion stability, are based on particle counting and the use of optical techniques, i.e. measurements of turbidity or scattering light. Unfortunately, these normally apply to dilute suspensions containing 1% or less of dispersed phase [Shaw, 1996]. Some of the particle counting, e.g. Coulter counter or gravitational and centrifugal sedimenting equipment cannot be used with non-aqueous media. Methods involving photo- or electromicrography of dried films are of limited use as artefacts may be introduced by the sample preparation techniques [Shaw, 1996]. Electron microscopy, being an optical method, has the advantage of not disturbing the system and can yield useful information on the floc structure. In addition, rheology,

adsorption, settling rate and sediment volume methods were found to be related to the state of the dispersion [Bell and Crowl, 1973; Chou and Lee, 1989].

(a) Rheology

Rheology is the measurement of changes in flow behaviour in response to an applied stress or strain. In ceramic industry, rheological study is used to help in the design and optimisation of the forming procedures so that uniform and dense green bodies can be achieved. For colloidal suspensions with particles < 1 μm, the range and magnitude of the inter-particle forces have a profound influence on the suspension structure and hence the rheological behaviour. Therefore, the flow behaviour can provide insight to its state of dispersion [Bell and Crowl, 1973; Shaw, 1996]. It is a function of the viscosity of the dispersion medium, particle concentration, particle size and shape, particle interaction and particle-dispersion medium interaction [Shaw, 1996]. A minimised viscosity is an indication of efficient dispersion of the ceramic particles in the organic vehicle [Moloney *et al.*, 1995]. Pseudoplastic flow is common in colloidal systems with asymmetric particles and particle aggregates. In a deflocculated dispersion containing pigment or other powders at a high volume concentration, the flow generally displays a dilatant behaviour. Many colloidal systems also exhibit plasticity and a certain minimum shear stress must be sufficiently applied before flow can commence due to the rigidity imparted by a continuous structural network [Bell and Crowl, 1973].

(b) Sedimentation

Apart from rheology, sedimentation behaviour is another test applied to study the behaviour of dispersion. It is often performed in a cylinder to follow the evolution of particle agglomeration by monitoring the descent of particles and rise of sediment from the bottom under the influence of gravity until the sediment is constant [Chartier *et al.*, 1996; Teng *et al.*, 1997]. Information concerning the extent of particle flocculation can be elucidated as the nature of the settling phenomena depends on size, shape, density and distribution of particle as well as particle interaction and degree of flocculation [Bell and Crowl, 1973; Tiller and Khatib, 1984]. Thus, the state of particle agglomeration in a suspension may be inferred from the sediment volume. When flocculation has occurred, the flocculates may effectively

behave as single large particles and settle at a considerably faster rate. Consequently, a flocculated dispersion will settle considerably more than a deflocculated system. The sediment volume is loosely packed whereas that of a deflocculated system is compact but small. In a partly flocculated dispersion as shown in Figure 2.13b, a suspension layer of variable composition will form on top of the sediment. A clear layer of liquid above the settling layers will increase in volume as time progresses. In a completely deflocculated system as shown in Figure 2.13c, a layer of sediment is first formed. On top of this, a layer of variable composition with no clearly defined boundary appears. These layers descend with time. Above it cloudy liquid is present and still contains finer particles which will eventually settle over a long period [Bell and Crowl, 1973].

(c) Adsorption

For dispersion stabilised by steric stabilisation, the degree of stability is related to how firmly the stabilising agent is 'held' to the ceramic particles. If the adsorbed molecules are free to move about on the surface, redistribution of the solvated layers will result in lower repulsion energy and hence re-agglomeration of the flocs may occur. Surface adsorption can lead to pronounced physical changes to the solution with the effect on surface tension being particularly prominent [Porter, 1994]. Therefore, the surface tension at the interface can be measured as a function of the amount of dispersant adsorbed over the particle surface, and hence can be used as a tool for assessing the stability of the system. Other methods of determining the concentration of the stabilising agent adsorbed on the particle involve chemical or radiochemical analysis, calorimetry and refractive index [Shaw, 1996]. An alternate method is pyrolysis of the supernatant solution and determination of the weight loss due to the dispersant [Richards, 1989; Teng *et al.*, 1997].

Adsorption is diffusion controlled and the smaller molecules at the surface, which are first adsorbed, may be displaced subsequently by larger molecules. It is also important to ensure that the dispersant is available in sufficient quantity from the beginning, since displacement may be very slow. Where multicomponents are used, the order of addition is important due to competitive adsorption onto the particle surface [Cannon *et al.*, 1986].

2.4.3 Processing Fundamentals

In Direct Ceramic Ink-Jet Printing (DCIJP), as shown in Figure 2.14, a ceramic suspension is passed through a printer nozzle. Layer upon layer, the ink is deposited according to the information provided by a computer model until the part is built. The green ceramic part is then subjected to conventional binder removal and sintering to produce dense ceramic component.

2.4.3.1 Ink and its Preparation

A variety of ceramic inks, in term of the type of ceramic powder being deposited or the solvent system used, has been printed via DCIJP. Miniature components were built from ceramic inks of titania [Kim and McKean, 1998; Xiang *et al.*, 1997], ZrO_2 [Mott *et al.*, 1999; Song *et al.*, 1999; Wright and Evans, 1999], lead zirconate titanate (PZT) [Windle and Derby, 1999] and alumina [Reis *et al.*, 1999] using different printers. Also, two or more different ceramic inks were mixed during printing to construct a one-dimensional functionally graded component of ZrO_2/Al_2O_3 [Mott and Evans, 1999].

Most of the inks were non-aqueous [Mott and Evans, 1999; Song *et al.*, 1999]. There are only two known instances employing aqueous based inks [Slade and Evans, 1998; Windle and Derby, 1999] but this has not been pursued further. The slow drying rate of water is a major reason for this [Slade and Evans, 1998]. In most cases, aside of a commercial dispersant, at least another polymeric component was used to modify the flow behaviour of the ink. The incorporation of wax in the ink of high powder loading lowers the ink's viscosity [Reis *et al.*, 1999]. Successful trials using preceramic polymer in jet printing SiC has also been demonstrated [Mott and Evans, 2001]. Although it was recognised that the sedimentation behaviour, viscosity, surface tension and electrical conductivity of the ceramic ink are crucial quality control parameters for the success of the process [Edirisinghe, 1977], little information could be elucidated except from the early work by Teng [1997].

A high liquid content is normally employed in the ink. The level of powder loading in the ink will be discussed in conjunction with the printer as this is partly dictated by the type of printer used.

In practice, the preparation of ceramic ink is modified from the standard procedure for ceramic suspension, which generally follows two stages. During the first stage, a mill product or slurry containing solvent, dispersant and powder is prepared during which the agglomerates are broken down and the dispersant is coated over the powder surface. Other additives (e.g. the binder and plasticiser) are then added at the second stage of mixing and homogenisation [Mott and Evans, 1999]. Ultrasonic agitation (ultrasonic bath as well as high power ultrasonic probe) can also be used to produce the dispersion [Blazdell and Kuroda, 2000; Song *et al.*, 1999; Teng and Edirsinghe, 1998]. Pressure waves are induced during ultrasonic treatment and these generate cavities with the development of bubbles that collapse and release energy for de-agglomerating of flocs. This method of dispersion is effective and fast for dispersing ceramic powders in suspensions. For instance, 180 s of ultrasonic treatment was equivalent to one hour of ball-milling [Jorge *et al.*, 1990] and large flocs were defloculated and possibly broken down into particles with the initial size distribution [Higashitani *et al.*, 1993]. At a given frequency, deflocculation is a function of the ultrasonic power and treatment duration [Higashitani *et al.*, 1993] as well as temperature [Jorge *et al.*, 1990]. However, beyond a certain power threshold, ultrasonic disruption may cause coagulation instead of dispersion [Higashitani *et al.*, 1993]. Several methods can be used to estimate the actual amount of ultrasonic power input into the dispersion and the most common is calorimetry [Kimura *et al.*, 1996; Mason *et al.*, 1992]. The use of a high shear mixer, e.g. twin roll mill, followed by ultrasonic treatment was found to enhance homogeneity and stability in the dispersion [Song *et al.*, 1999].

The order of adding the components is critical as the viscosity of the suspension as well as the strength and density of the green and sintered parts are affected by the addition sequence [Cannon *et al.*, 1986]. This could possibly arise from two causes. Firstly, some reactions may occur between the dispersant and the other components, which affect the adsorption behaviour of the dispersant on the powder surface. Secondly, since adsorption is a competitive and slow process, the organic components that are added first must be desorbed from the powder surface before the dispersant can be adsorbed on it. The effectiveness of the dispersant is decreased when it is prevented from adsorbing on the surface of the powder.

After dispersion where the agglomerates are broken down, the ink mixture is left undisturbed at sedimentation during which the strong agglomerates (formed because of flocculation) settle and are then removed [Mott *et al.*, 1999; Song *et al.*, 1999]. The remaining suspension constitutes the printing ink. Prior to printing, the ink is filtered to further remove any flocs not eliminated during sedimentation as they may block the printer nozzle [Mott *et al.*, 1999; Song *et al*, 1999] and cause agglomerate-related defects in the final microstructures [Edirisinghe, 1997].

2.4.3.2 Freeforming by Jet Printing

Various types of commercially available jet printer have been used successfully for DCIJP with or without modification. These includes a Biodot continuous jet printer [Blazdell *et al.*, 1995; Song *et al.*, 1999; Teng and Edirisinghe, 1998], a Domino continuous jet printer [Blazdell and Kuroda, 2000], an IBM four-nozzle colorjet DOD printer [Mott *et al.*, 1999; Xiang *et al.*, 1997], a HP thermal jet printer [Slade and Evans, 1998] and an Epson Stylus colour ink-jet printer [Windle and Derby, 1999]. Other variants include an electromagnetic jet printer constructed to facilitate easy cleaning [Wright and Evans, 1999] and a 3D ink-jet plotting system modified from a prototyping machine (ModelMaker 6PRO, Sanders Prototype Inc.) [Reis *et al.*, 1999, Seerden *et al.*, 1999].

As can be seen, most of the developments in DCIJP concentrate on the use of commercially available continuous and DOD jet printers. The advantages of both the continuous and DOD jet printers were outlined in Section 2.4.1. In addition, because it is possible to install more than one nozzle, different ceramic inks can be held in these printers for fabrication of ceramic composites, graded microstructures, microcircuits and micro-enginneered cavities [Edirisinghe, 1997]. This was demonstrated with the construction of a one-dimensional ZrO_2/Al_2O_3 functionally graded material [Mott and Evans, 1999]. The need of supports for cavities and overhang features, which is a problem faced by most SFF methods, can be overcome with the use of fugitive carbon ink deposited simultaneously with the ceramic ink [Mott *et al.*, 1999]. The features of the continuous and DOD jet printers for DCIJP are compared in Table 2.4 [Edirisinghe, 1998].

Table 2.4 A comparison of the continuous and drop-on-demand jet printers for DCIJP [Edirisinghe, 1998].

Continuous Ink-Jet Printer	Drop-On-Demand Ink-Jet Printer
Pressurised ink supply	Non-pressurised ink supply
In-line filtration	No in-line filtration
Conductive ink	Non-conductive ink
Higher droplet formation rate	Lower droplet formation rate
Higher deposition rate of ceramic	Lower deposition rate of ceramic

With respect to their applications to DCIJP, the continuous jet printer has the advantage of its superior printing speed and can be printed at a printhead-to-paper distance as much as 25 to 50 mm. However, re-circulation of the ink in the printer may pose a problem to the reliability of ink properties. Furthermore, the capital cost of a continuous jet printer is higher than a DOD printer.

The main limitation of DCIJP is the high liquid content in the ink, which inevitably slows down the forming rate because of the long drying time required before the next layer is printed. Although suspensions of up to 30 vol. % ceramic ink has been prepared, successful printings were reported mostly with suspension of 2 - 10 vol. % ceramics. The quest for a higher powder loading in the ink entails much more considerations beyond ink stability. The properties of the ink must also conform to the specifications of the printer used (Tables 2.1 and 2.2) and a typical commercial jet printer normally demands a low viscosity ink. Reis *et al.* [1999] claimed success in printing a 30 vol. % ceramic ink but this is made by depositing a hot melt with an ink-jet printer specifically manufactured for prototyping and incorporation of waxes in the ink formulation.

To date, the maximum thickness of the ceramic feature (green part) produced is 2.5 mm printed from 1700 layers using a continuous jet printer and a 4.4 vol. % ZrO_2 printing ink [Song *et al.*, 1999]. A total of 1440 layers has been printed with a DOD printer using a 10 vol. % ZrO_2 ink [Slade and Evans, 1998]. However, for the former, printing was intermittent and far from 'continuous'; whereas for the latter, it is not known if the 10 vol. % refer to the powder content in the *printing* ink or the formulation. Another investigation by Mott *et al.* [1999] produced a ZrO_2 feature of maximum thickness 0.45 mm after printing a 2.5 vol. %

ink and depositing 1200 layers with a DOD printer. Clearly, the present state of DCIJP restricts it to small and thin components. Although there is no mention of discontinuous printing in most investigations, there is an element of doubt if the printing process can go on continuously without interruptions for long period as blockage of the nozzle by ink is a common problem faced in printers, in particular the continuous jet printers. Another problem associated with long period of printing is that the properties of the ink may change and lead to instability in printing process. Continuous printing has to be investigated more to enable the printing of thicker components, paving the way for mass production.

Ripples on the top surface, which are attributed to the droplet drying kinetics, has been consistently observed in most printed parts [Mott *et al.*, 1999; Song *et al.*, 1999; Xiang *et al.*, 1997]. Other reported printing defects included undefined boundaries, 'faded' prints [Windle and Derby, 1999], pockets and layer position inaccuracies in the vertical direction [Slade and Evans, 1998; Song *et al.*, 1999]. The causes of most of these defects can be the image quality, feeding of the ink and ink properties, in particular drying rate. When a slow drying rate is used, Slade and Evans [1998] observed improved smoothness in the top surface. As a SFF process, layer position accuracy in the vertical direction in DCIJP is a concern as the boundaries of the printed parts are not constrained by a mould. Therefore, precise placement of each droplet is important. This is a function of the printer operating conditions and the ink properties. Because of evaporation, the properties of the ink changes after printing on a continuous jet printer (Table 2.5).

Table 2.5 Ink properties before and after printing for 18000 s [Teng and Edirisinghe, 1998].

Ink Properties	Before Printing	After Printing
Electrical conductivity, S m^{-1}	0.338	0.403
Viscosity, mPa s	1.11	1.50
Surface tension, mN m^{-1}	24.5	25.9
Solid loading, vol. %.	2.4	2.6

Resolution of the printed features is primarily limited by the shape and size of the deposited droplets and spacing between them. This can be attributed to the device used and the substrate on which print is made [Mott *et al*, 1999; Xiang *et al.*, 1997]. The first layer has to

be printed on a substrate for handling and ashless filter paper [Windle and Derby, 1999], silicone release paper [Mott and Evans, 1999] and acetate sheet [Song *et al.*, 1999; Teng and Edirisinghe, 1998] have been used in previous works. These choices are based largely on the criterion that the substrate can be easily detached from the printed part in order to carry out post-printing operations. The use of different substrates have contributed to the production of a series of irregular but continuous features on an acetate sheet [Xiang *et al.*, 1997] and an orderly array of pillars on silicone release paper [Mott *et al.*, 1999]. However the spreading of the ink droplet on different substrates, the evaporation of the liquid and the accompanying shrinkage have not yet been duly considered in DCIJP.

In their investigations of the evaporation of a liquid droplet on a smooth surface, Shannahan and Bourges [1994] showed that the droplet experienced three stages. In the first stage, the width of the droplet at the liquid-solid interface remains constant while the contact angle and droplet height decrease. In the second stage, the width and height decrease concomitantly while maintaining a constant contact angle. In the last stage, all three parameters decrease sporadically as the droplet volume diminishes to zero. In another study, the contact angle was found to decrease and the width of the liquid-solid interface remains constant [Birdi and Vu, 1993]. If the droplet is a colloidal suspension, the shape changes during drying are more complicated due to the accumulation of particles near the solid-liquid-vapour interface [Parisee and Allain 1996; 1997]. Furthermore, with shrinkage normally accompanying drying, the different drying kinetics mentioned above will affect the shape and spacing of a series of droplets deposited near to one another in DCIJP. As this technology is targeting micro-engineering components, these are certainly not areas to be overlooked.

The evaporation of a liquid droplet on a solid surface has been investigated in several instances and various models for the kinetics of drying have been proposed. Many factors affect the behaviour of a droplet deposited on a horizontal, non-porous substrate, e.g. the wetting characteristics of the substrate [Birdi and Vu, 1993; Lau and Burns, 1973], atmospheric conditions [Erbil, 1999; Ray *et al.*, 1988], temperature [Chandra *et al.*, 1996], the presence of surfactant [Chandra *et al.*, 1996] and the size of dispersed particles in the droplet [Maenosono *et al.*, 1999].

2.4.3.3 Post-Printing Processes

The printed parts, after drying, are heat treated or fired in a furnace to develop the desired microstructure and properties. There are three stages in the firing process:

(i) pyrolysis, which is performed prior to sintering, to burnout organic components

(ii) sintering and

(iii) cooling, which may include thermal and chemical annealing.

The two main variables for binder removal are debinding atmosphere and heating rate. In the case of ZrO_2, the green parts have been pyrolysed in air to remove the binder [Slade and Evans, 1998]. They were then densified by heating at 0.083°C s^{-1} to 1450°C and held at this temperature for 7.2 x 10^3 s. A uniform microstructure resulted from this procedure [Song *et al.*, 1999; Wright and Evans, 1999]. Although removal of organic additives often posed problems in most powder forming processes, e.g. ceramic injection moulding [German and Bose, 1997], none was reported in DCIJP. The small thickness of the green (printed) parts is the reason for this and the binder and plasticiser can be removed rapidly without much difficulty. Parts with aspect ratio as high as 90 were also printed with minimal distortion at sintering [Song *et al.*, 1999] and pyrolysis and sintering did not change the shape of the components produced by printing [Mott *et al.*, 1999]. There has been no report of internal defects in the sintered DCIJP parts, indicating good adherence of the printed layers.

2.4.4 Potential Application for Conductive Circuitry

In recent years, there has been a drive to achieve higher densities in electronic circuit packaging and assembly [Wang *et al.*, 1994]. With the advancement of surface mount technology (SMT), this has led to miniaturisation of circuit boards and cards. Increasingly, more manufacturers are turning to surface mount packages which permit fine conductive traces with narrow spacing between them and higher device populations on the circuit boards [Sclater, 1999]. SMT construction is crucial in the manufacture of many of the new electronic products such as notebook and palmtop computers, cellular telephones, pagers, CD players and handheld GPS receivers. A small, high density circuit board made possible by SMT also permits higher speed and greater reliability in many electronic products that are not enclosed in handheld or pocket cases, such as desktop computers, stereo components, VCRs, television sets and test instruments.

(a) Advantages of direct printing

The conductive trace on the printed circuit boards (PC boards or PCB; also known as printed-wiring boards, PWB) is conventionally formed by etching away of a layer of copper foil from the insulating substrate or plating a thick film of conductive metal on a chemically prepared insulating substrate [Walig, 1988]. Potentially, DCIJP can be adapted for liquid metal ink dispensed from a jet printer to print circuitry. The advantages of ink-jet technology for forming ceramic parts are applicable to metal ink fabrication too. With this technology, images can be transferred rapidly from the initial design stage to prototype and any improvement to the design can be made easily. There is also more flexibility during manufacturing as it is a data driven and computer controlled operation and additive material approach [Hayes *et al.*, 1999]. At the same time, a higher degree of automation than a conventional manufacturing technique for PCB is allowed with better repeatability and reliability. The low temperature during printing also minimises any unwanted reactions during processing. With direct printing, many of the processing steps can be eliminated with savings in device and process materials. Like the recently developed conductive lithographic film, this purely additive process can avoid the expensive and potentially polluting photo-resist and etching process [Ramsey *et al.*, 1997].

The advantages of jet printing metal inks for electronic manufacturing have long been recognised. Recent applications include metallisation of hybrid microcircuits [Teng and Vest, 1987], solar cells [Teng and Vest, 1988; Teng *et al.*, 1990], superconducting circuits [Glowacki, 2000] and large area electronic structures [Cheong *et al.*, 2000]. They are also used in the printing of solder and flux for microelectronic packages [Hayes *et al.*, 1998] and flat panel display [Hayes *et al.*, 1999]. The use of ink-jet printers in microelectronic manufacturing was also reported recently where solder bumps of 24 μm in size and having a line width of 25 μm wide have been made with a 100% yield [Hayes *et al.*, 1999].

(b) Ink properties

The conductor conventionally used in electronics often contains a precious metal and is expensive. The more common metals are Au, Pd, Pt and Ag, or binary or ternary alloy combinations of these metals. Most metals used as conductors are not utilised in their pure state. Of these, Ag and its solid mixture offer substantial cost benefits over Au alloys, pure

Pd, or Pd/Pt alloys and are an important class of thick film conductors [Wang *et al.*, 1994]. Silver thick films are used extensively for making electrical contacts in silicon solar cells, hybrid circuits and other devices owing to their excellent electrical properties.

As in freeforming ceramic parts by jet printing, critical to the development of jet printing circuit tracking using Ag is the formulation of an ink with good printing characteristics. The properties of the ink such as viscosity, conductivity, surface tension and powder content, will affect the deposition. The ink must also conform to the printer specifications and display stability throughout the printing process. The principle of handling the ceramic ink is also applicable here, i.e. de-agglomeration and homogenisation of the powders and preparation of a stabilised colloidal suspension. In addition, great care is to be exercised during handling of the raw material, as the powder is susceptible to oxidation and explosion in air. Of particular concern to conductive circuitry is its low resistivity. This is related to the current carrying capacity of the track and it reduces with decrease in the width of the conductor. After firing, the conductor on a finished PCB should exhibit good current-carrying capability and this is affected by the materials and processes used to form the conductors [Rust, 1995].

Further requirements of the ink may be derived from thick film conductor for screen printing. The thick film conductor generally comprises of the followings to produce a screen-printable paste [Wang *et al.*, 1994]:

* a metal or metal alloy to provide conductivity and joinability
* an inorganic additive, usually a glass or oxide to promote adhesion to the substrate
* an organic-based vehicle
* dispersants and
* other additives.

The criteria for a good thick film conductor, according to Vest [1986], are :

* high electrical conductivity
* high migration resistance
* compatibility with other components and other thick film deposits in the circuit
* ease of producing solder or wire interconnection bonds that have good electrical and mechanical integrity
* good adhesion to the ceramic substrate when printed and fired

* good line definition and able to fire in air at 1000°C or less.

These properties are controlled by several parameters, including constituents of the paste, physical characteristics of the metal and additive powder, paste rheology, overall processing procedures and oxidation of the metal [Wang *et al.*, 1994]. Furthermore, the type of surfactant on Ag powders and surface area of the powders also affect the screen printability of the conducting Ag pastes [Lin and Wang, 1996].

(c) Conductive lithographic printing

Lithography, or offset lithography, is a printing process used widely in the printing of newspaper and packaging of folding cartons, labels and metal decorating. Recently, the process has been adopted as a means of printing Ag-based conductive inks for circuit tracks.

Standard lithography is planographic, i.e. the image and non-image areas are in the same plane. The printing image carrier is chemically treated to ensure that the ink adheres to some areas and not others. On areas where the printed image is dark, water is repelled but oil-based ink is allowed to adhere to, whereas the non-image areas are water accepting. During printing, as shown in Figure 2.15, the plate first comes into contact with a damping roller. Water forms a film to cover the non-image area but contracts into tiny droplets on the image area. When the plate next passes through the inked roller, areas that are covered by the water film (the non-image areas) will repel the ink but water droplets on the image area will be pushed aside and covered with ink. The inked image on the plate does not print onto the paper substrate but 'offsets' onto a rubber blanket, hence the name offset lithography. The image is normally affixed on the substrate by evaporation and/or oxidation. A detail of the process has been described by Birkenshaw [1999].

The standard lithographic printing machine can deposit layer thicknesses of the order of 3 μm with the advantages of high speed, good dimensional control and low cost per sheet [Ramsey *et al.*, 1997]. With a Ag based conductive ink, circuit of 100 μm line width and 0.3 Ω^{-2} sheet resistance has been reported [Gilbert *et al.*, 1999]. Since the conductive lithography method is adapting to the standard lithographic machine, the electrically conductive ink should be printable and a compatible substrate must be prepared [Ramsey *et*

al., 1997]. Clearly the usual laminated, insulating substrate material for PCB is not suitable for the lithography method as it will cause damage to the substrate and the printed ink when fed into the roller nip [Gilbert *et al.*, 1999]. There is also a need to prepare a plate to transfer the image of the circuitry layout onto it for printing. This adds to the cost and time of the operation and also restricts conductive lithography to production stage.

2.5 Summary

The various manufacturing methods for advanced ceramics, in particularly Direct Ceramic Ink-Jet Printing (DCIJP), are surveyed. As in most solid freeform fabrication (SFF) methods, DCIJP creates the component by depositing layer upon layer. However, it distinguishes from most SFF methods with the use of two fundamental technologies, which are the colloidal processing of ceramics and freeforming using an ink-jet printer. With the former, improved material properties can be obtained as problems associated with powder heterogeneity are eliminated during the ink preparation stage. With the latter, ceramic components of intricate geometry can be fabricated and control over local composition is feasible. Both of these open pathways for DCIJP to be applied in the forming of micro-engineering components. Potentially, this method can be adapted to deposit liquid metal ink to print conductive circuitry. However, the technique is still in its early stages of development and more research needs to be done especially in making it a more efficient method. So far, the ability of this process to print continuously over long period has not yet been demonstrated in the continuous jet printer. This restricts its application to thin components. For it to be a viable solid freeform fabrication method for micro-engineering components, areas such as shrinkage at printing, ink-substrate interaction, drying time etc. need to be examined.

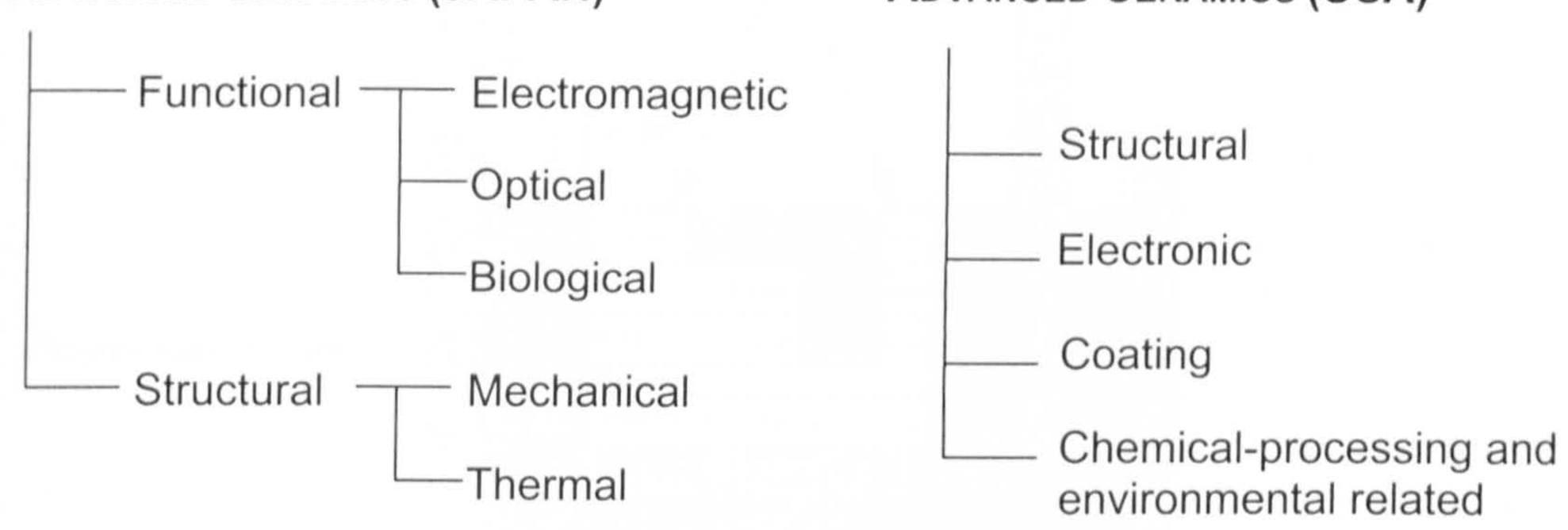

Figure 2.1 Classifications of advanced ceramics in Japan and USA [Abraham, 2000; Saito, 1985].

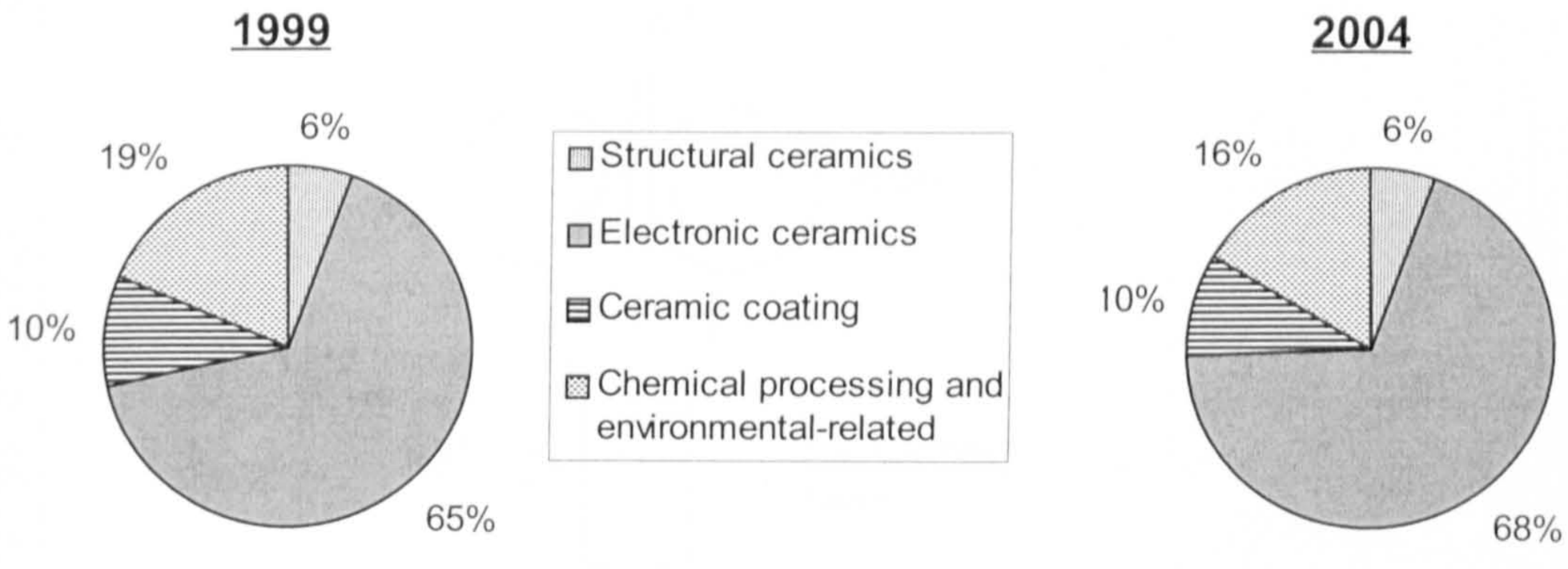

Figure 2.2 Summary charts showing shares of the USA advanced ceramic market segments for 1999 and projected shares for 2004 [Abraham, 2000].

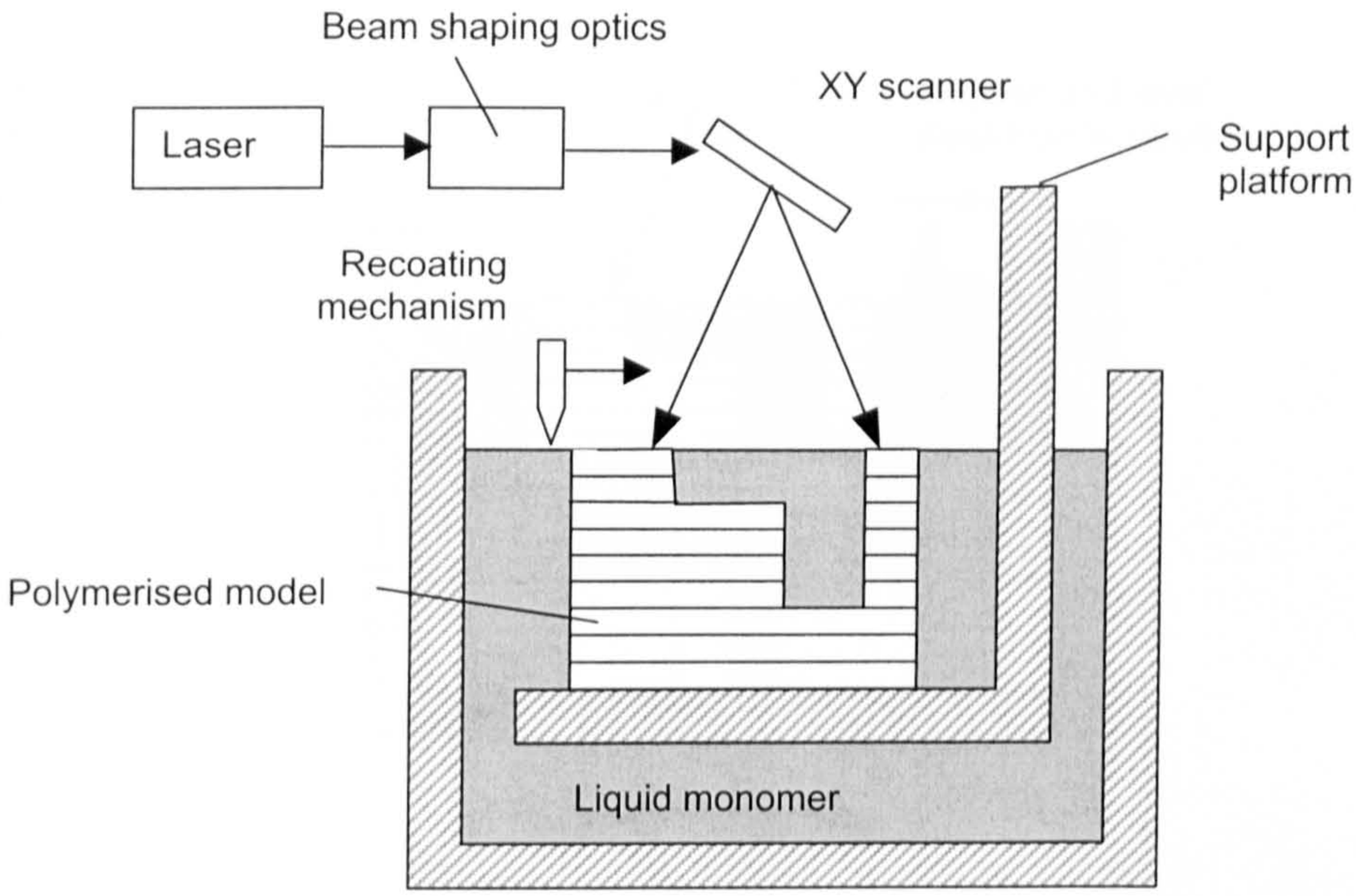

Figure 2.3 Schematic of 3D Systems stereolithography apparatus [Griffith and Halloran, 1996].

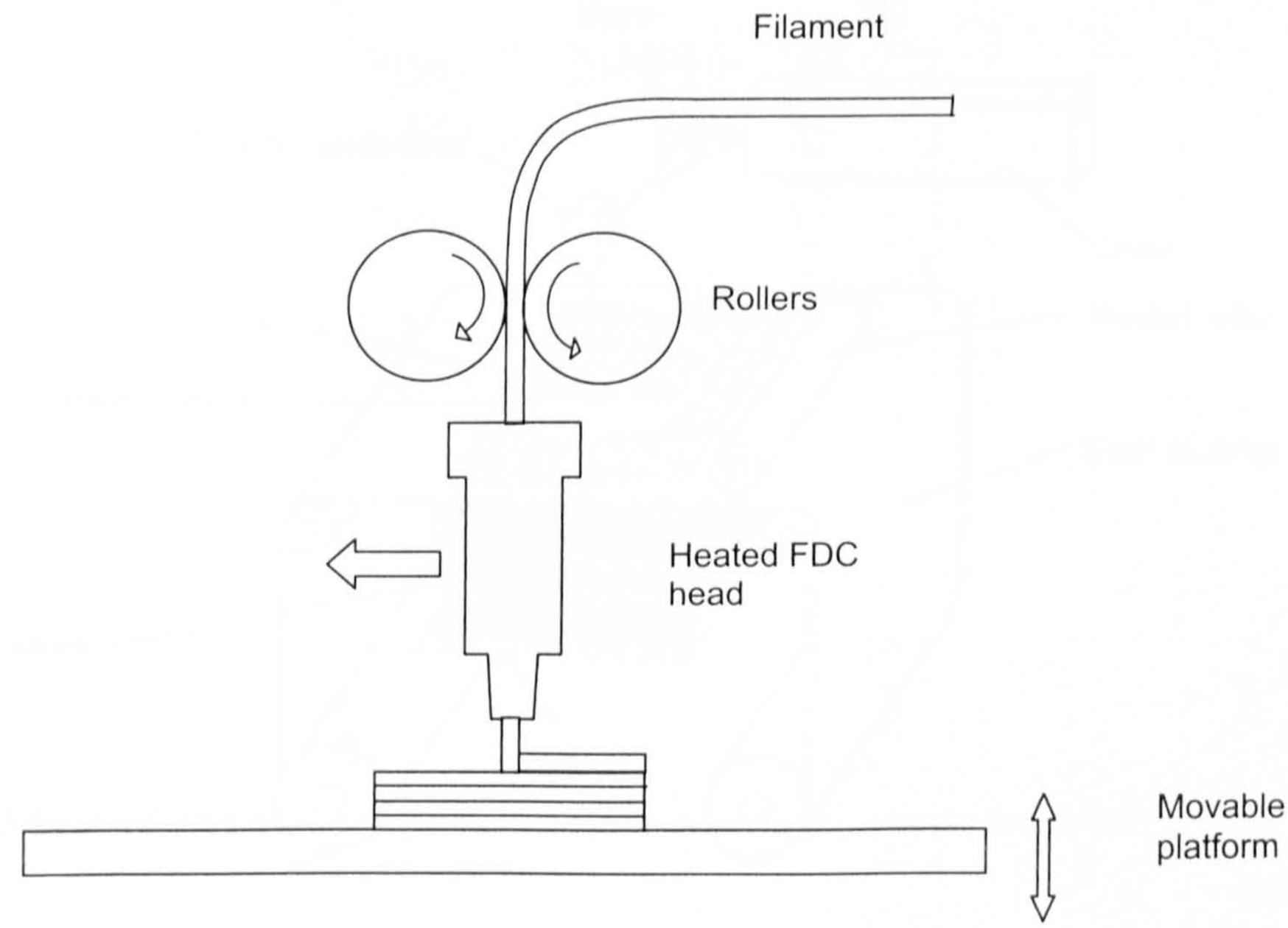

Figure 2.4 Schematic of Fused Deposition of Ceramics (FDC) apparatus [Conley and Marcus, 1997].

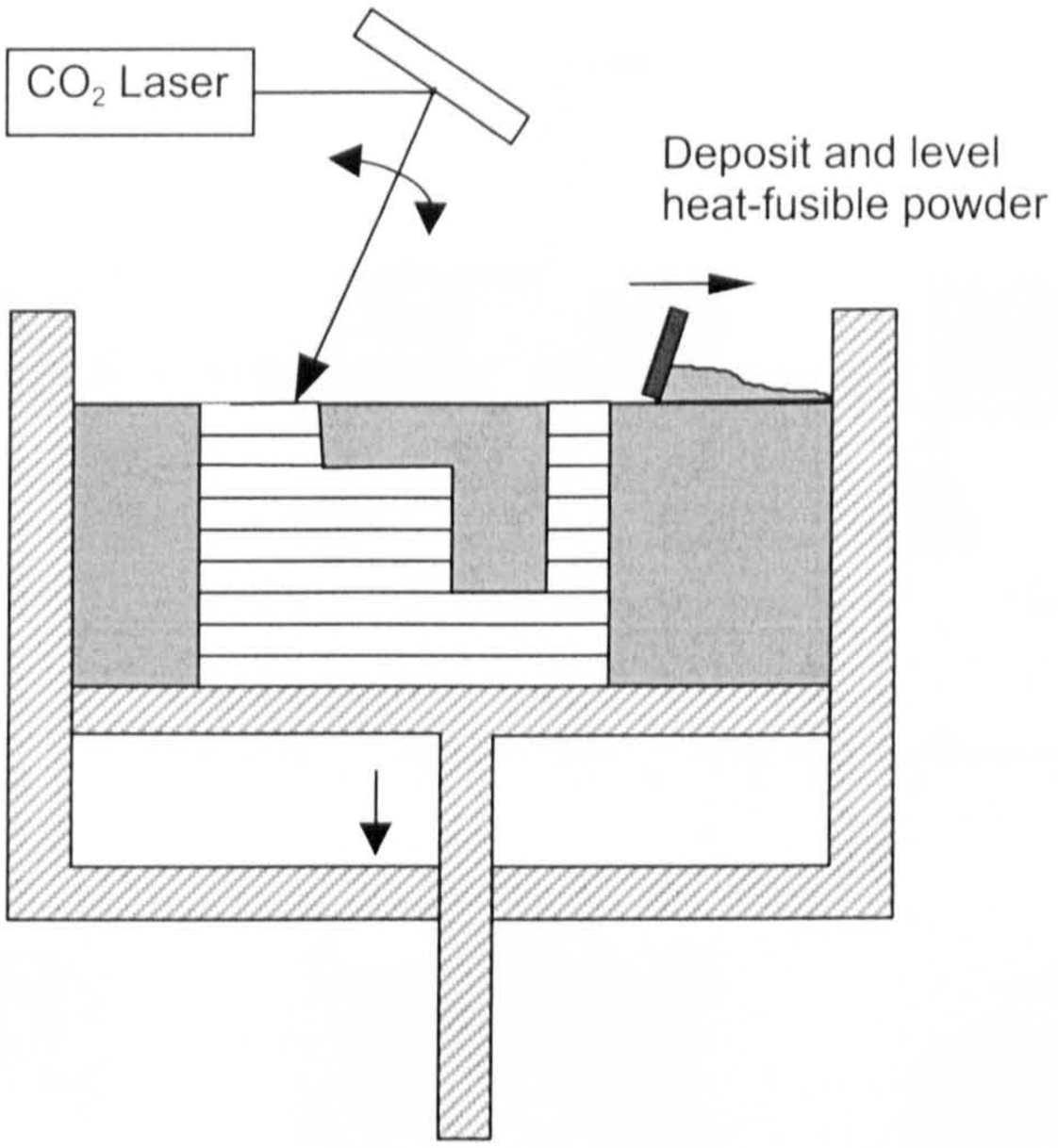

Figure 2.5 A schematic drawing of the Selective Laser Sintering process [Beaman *et al.*, 1997].

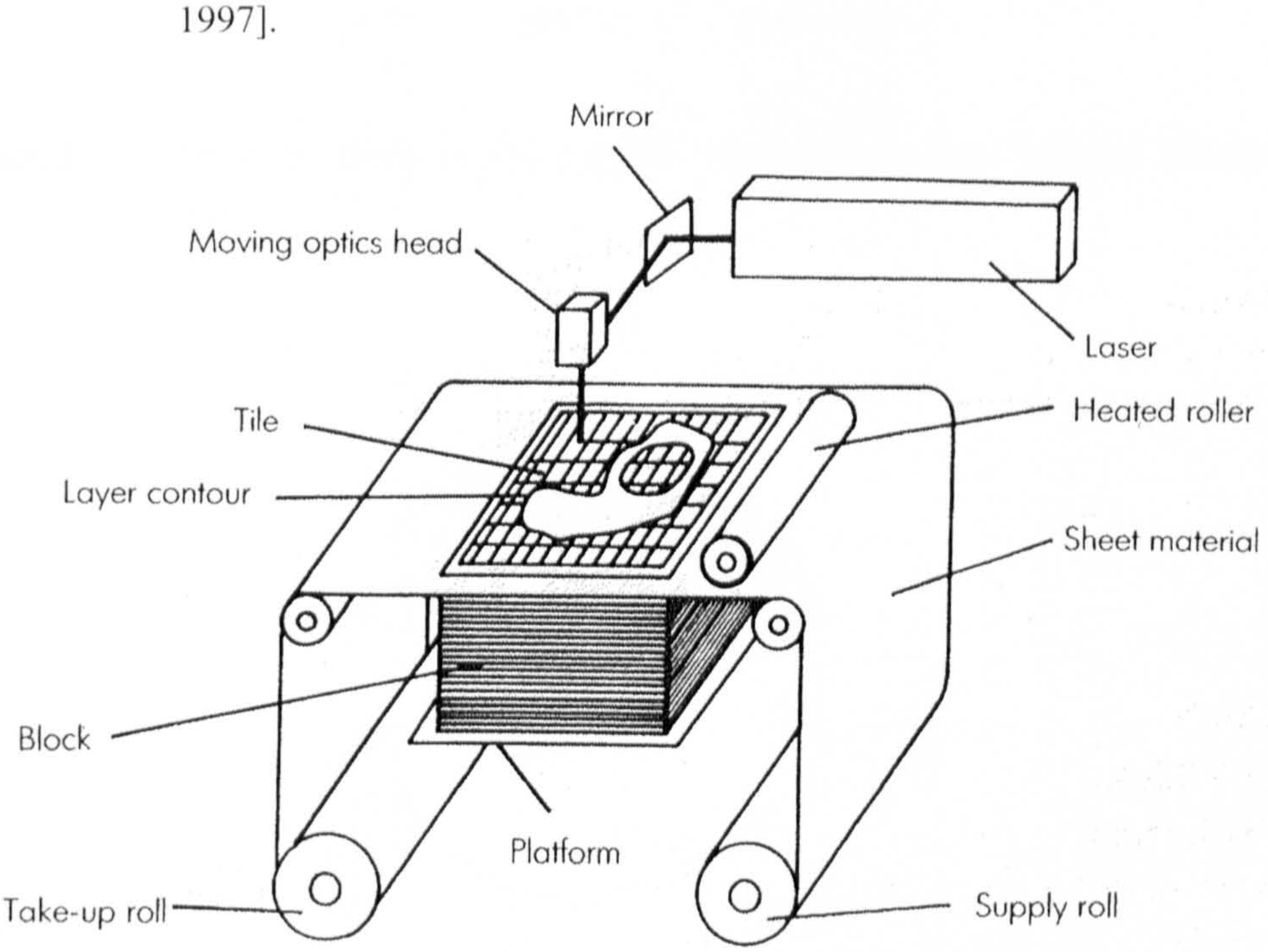

Figure 2.6 A schematic drawing of the Laminated Object Manufacturing process [Conley and Marcus, 1997].

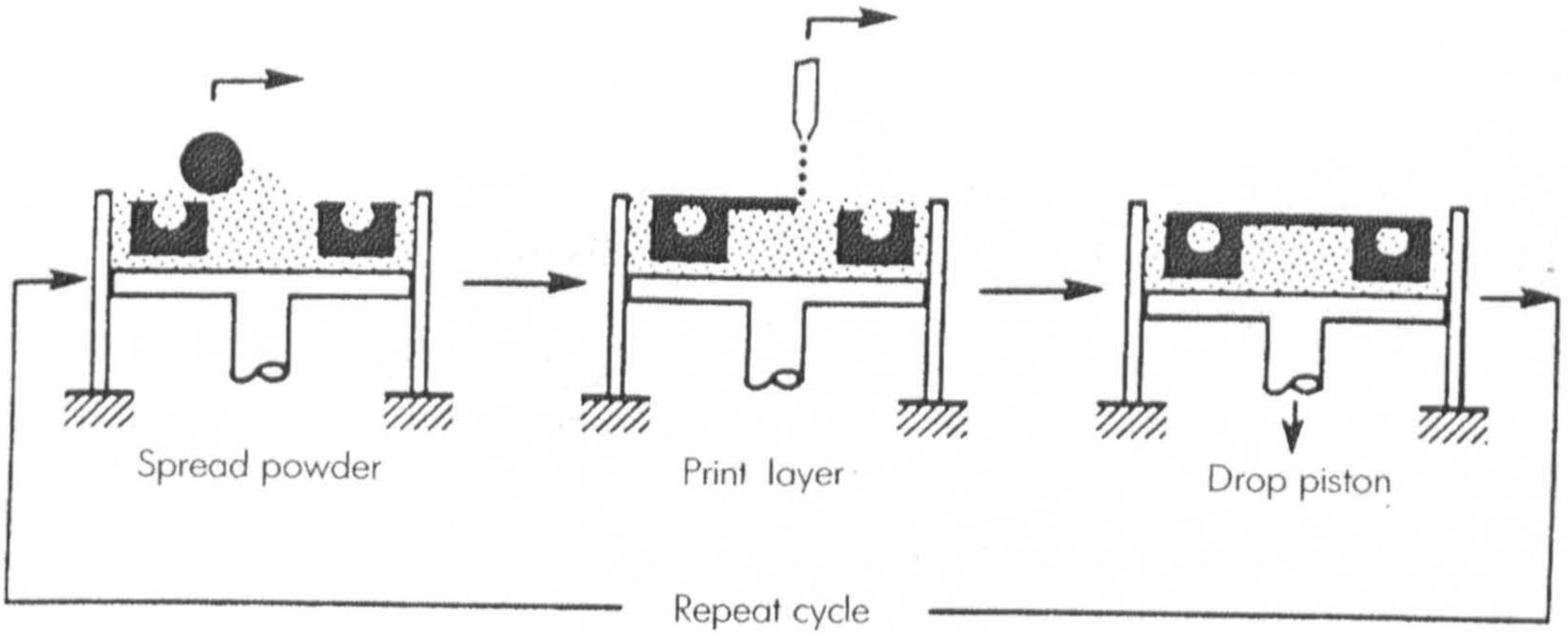

Figure 2.7 Diagram showing forming by Three-Dimensional Printing [Sachs *et al.*, 1992].

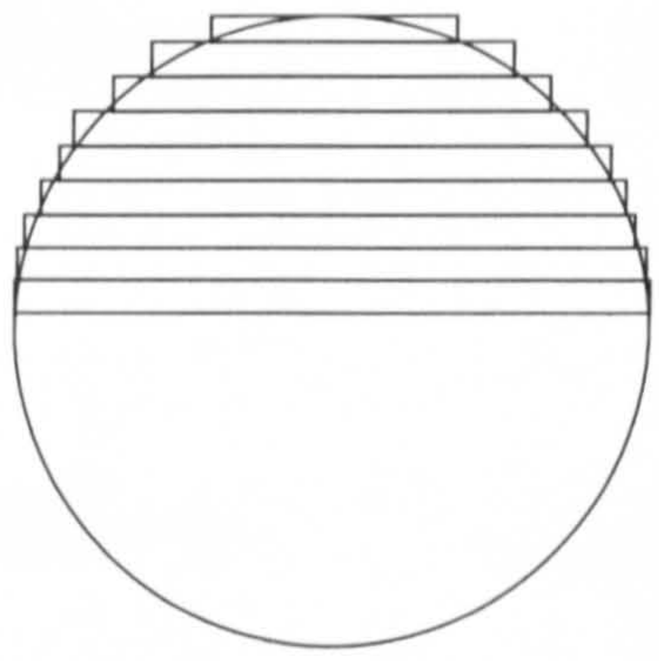

Figure 2.8 Schematic illustration of the stair-stepping effect in the build direction during SFF layer formation.

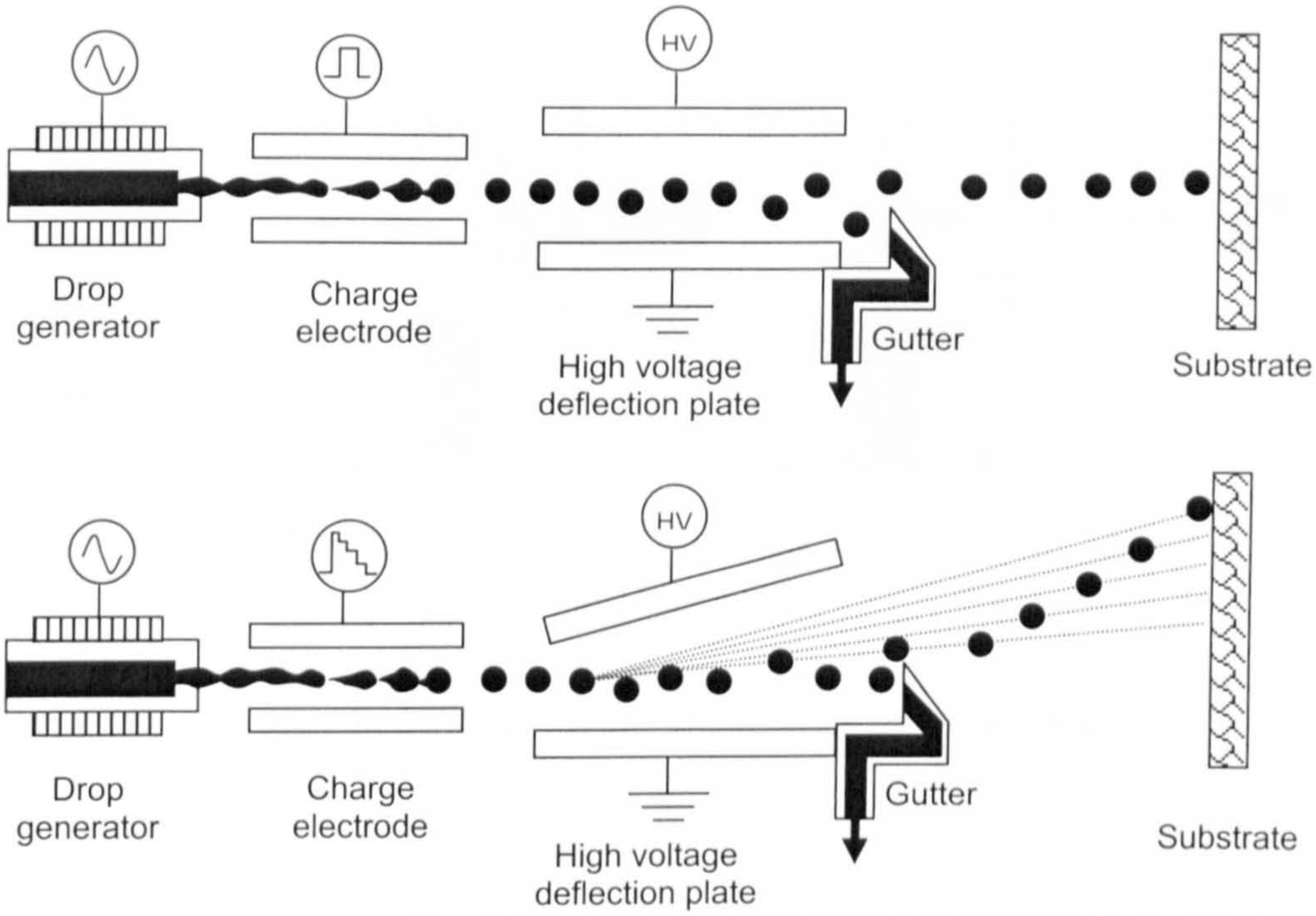

Figure 2.9 Continuous ink-jet printer: (a) a binary deflection system and (b) a multiple deflection system [Le, 1998].

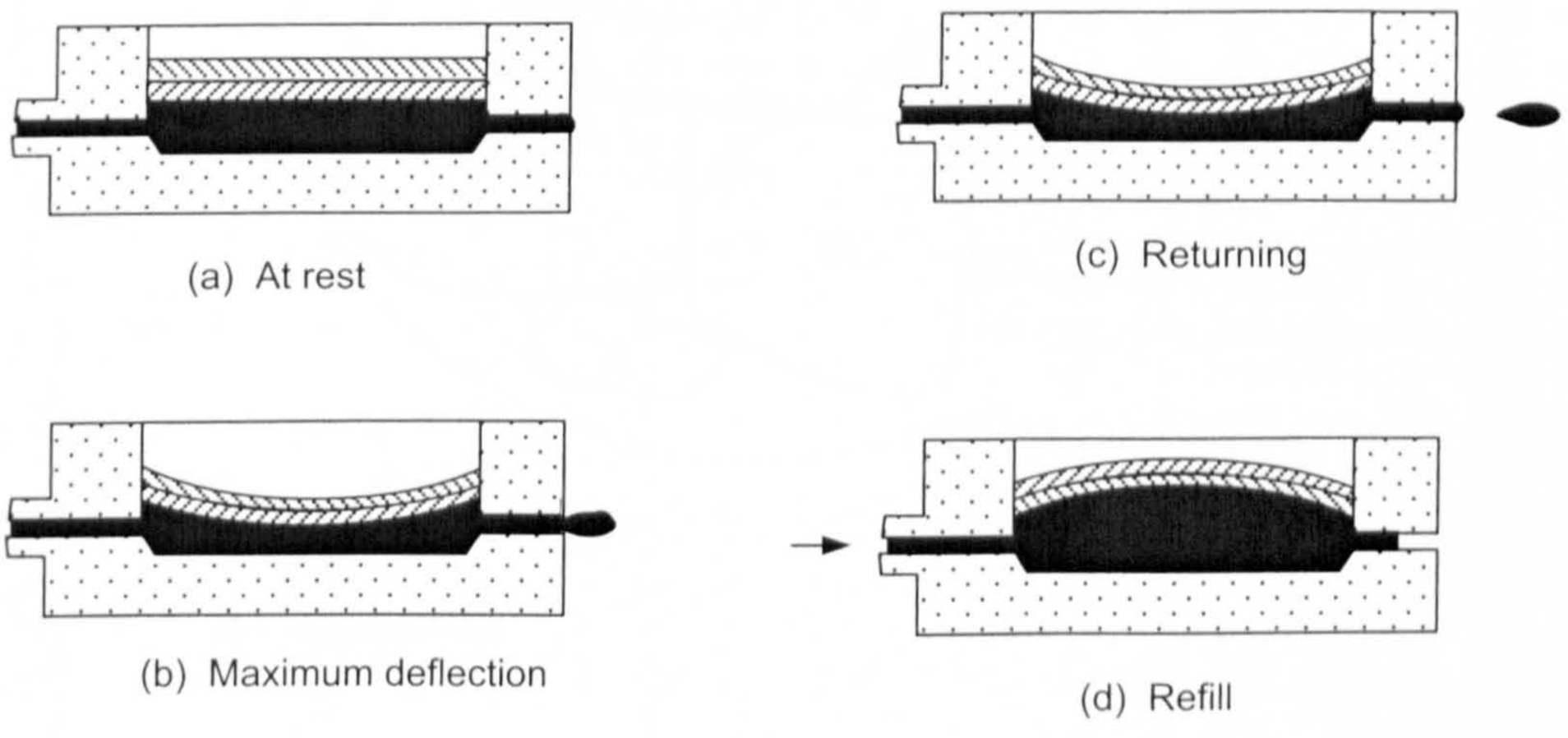

Figure 2.10 Droplet formation in a piezoelectric drop-on-demand ink-jet printer [Lloyd and Taub, 1988].

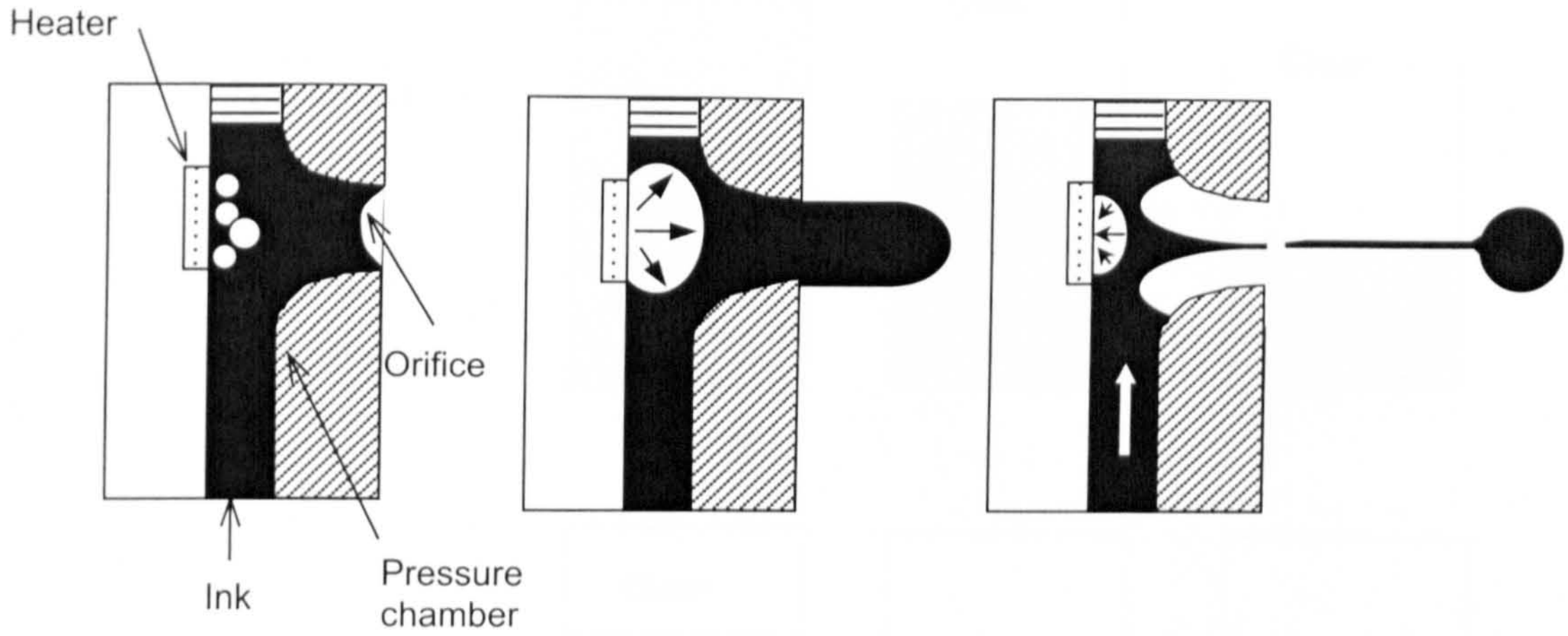

Figure 2.11 Droplet formation process in a thermal ink-jet printer [Le, 1998].

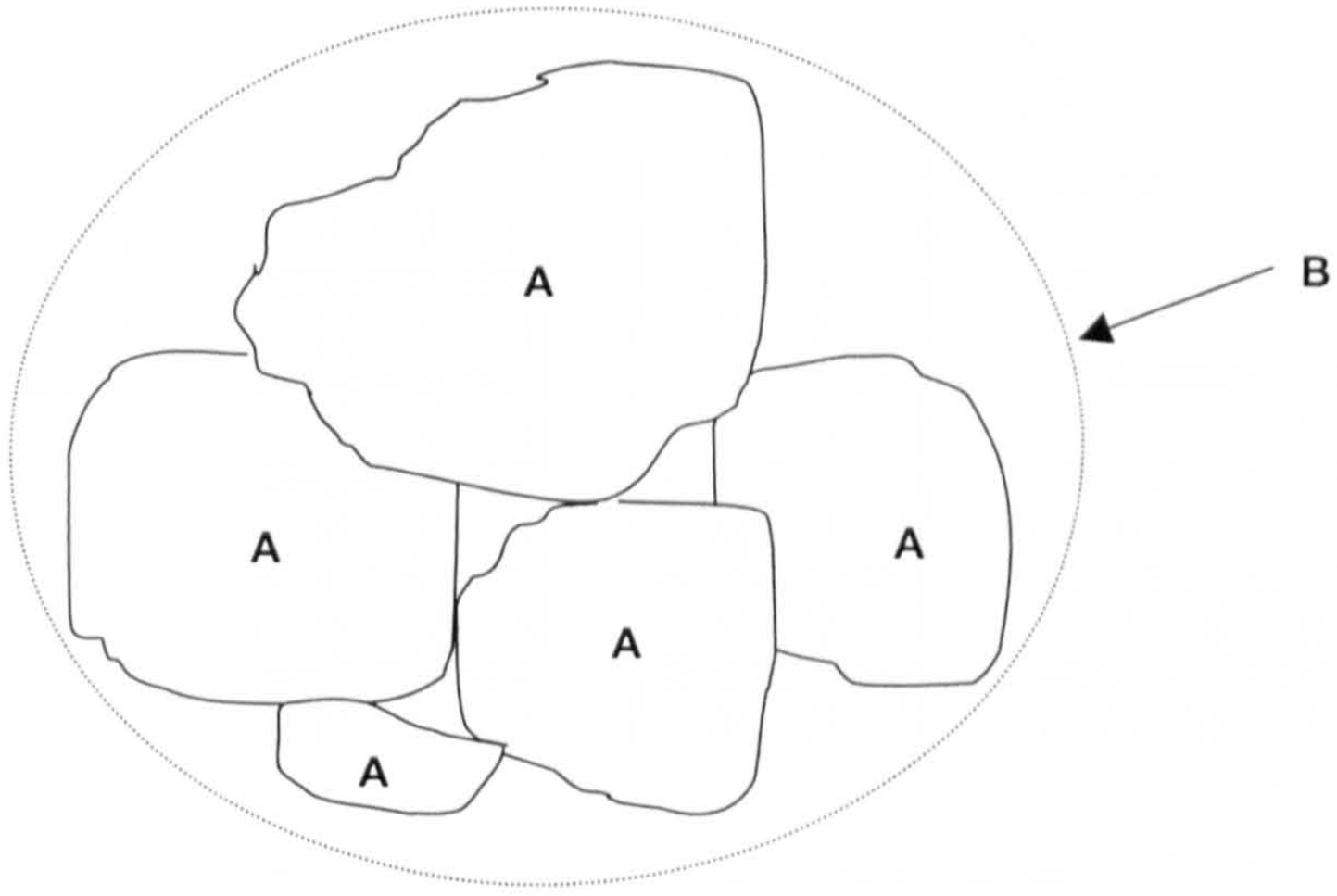

A = Particle

B = Agglomerate

Figure 2.12 An agglomerate [BS5600, 1981].

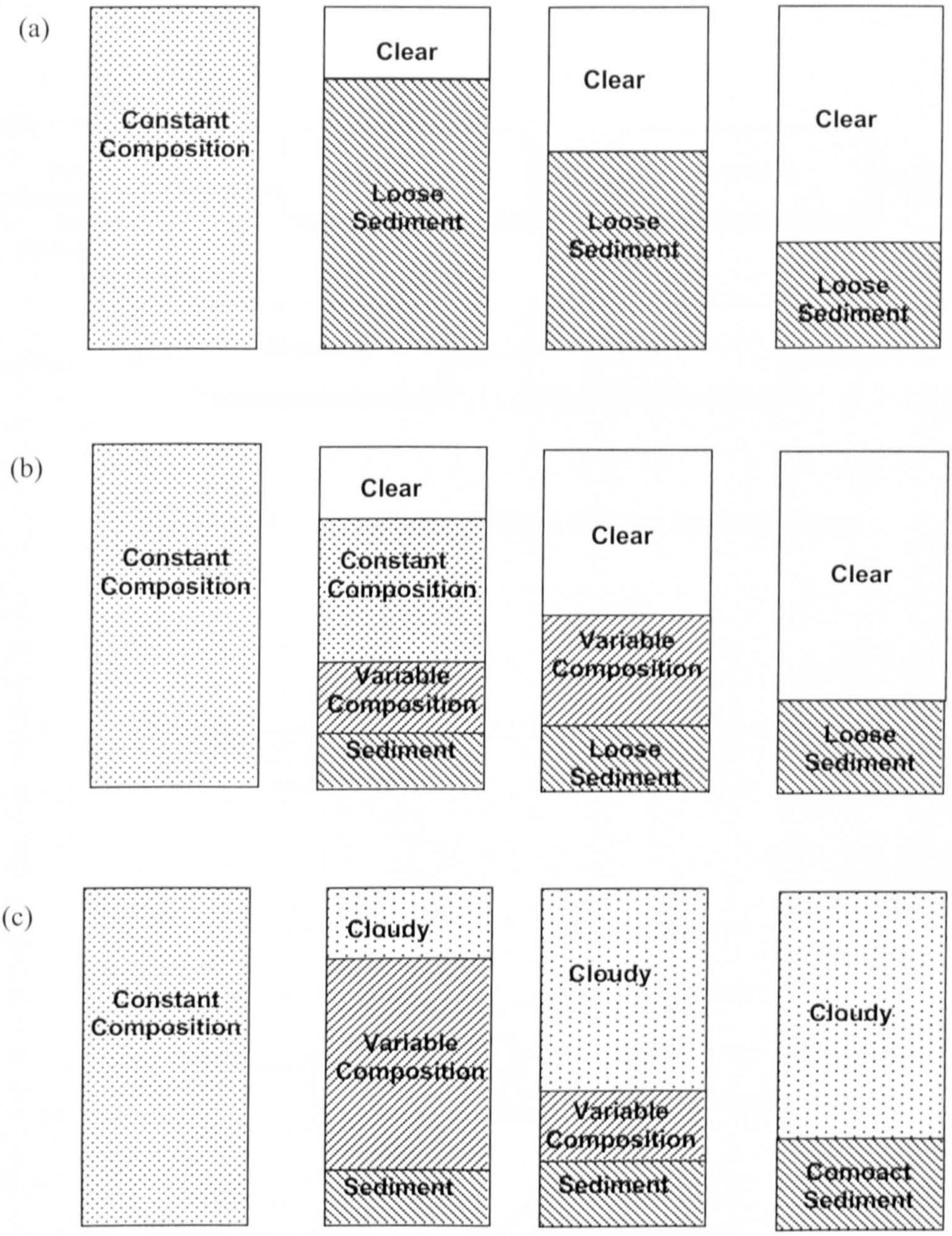

Figure 2.13 Sedimentation behaviours of concentrated dispersion which is (a) flocculated, (b) partly flocculated and (c) deflocculated [Bell and Crowl, 1973].

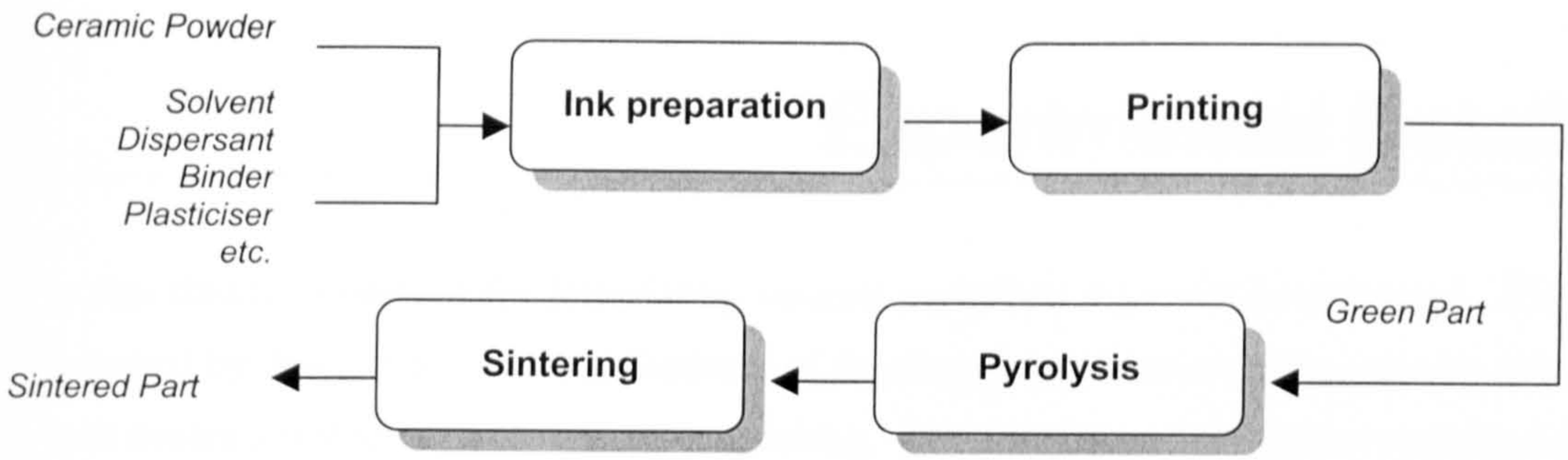

Figure 2.14 The scheme of Direct Ceramic Ink-Jet Printing.

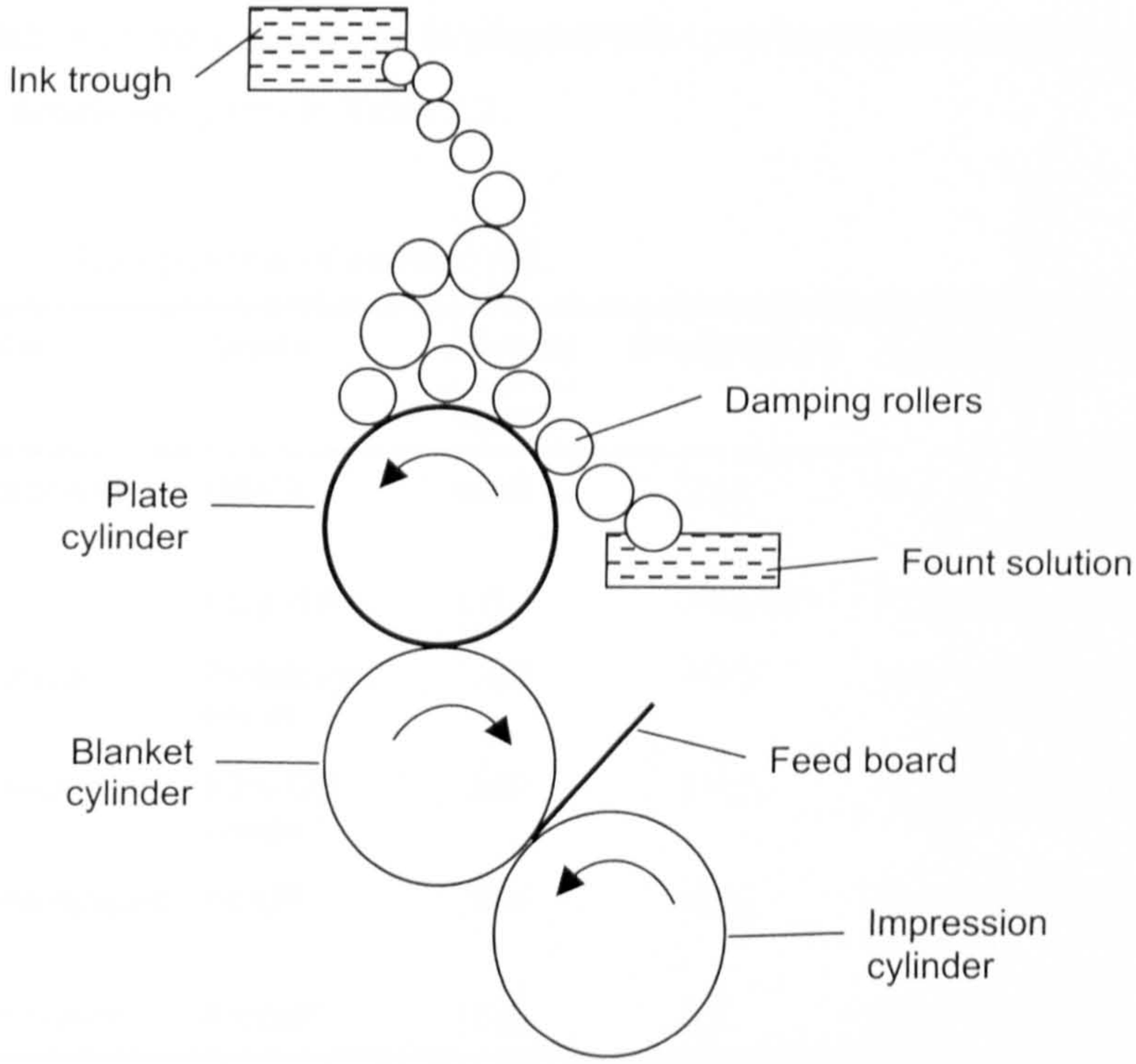

Figure 2.15 Single-colour rotary offset machine for lithographic printing [Birkenshaw, 1999].

Chapter 3

Experimental Details

In this chapter, materials for formulating ceramic and silver inks will be presented. This is followed by descriptions of the procedures of developing and characterising ceramic ink for both evaluation study and continuous jet printing. The printing process is then examined and the different conditions studied are detailed. The results and discussions of the work conducted here can be found in Chapters 4-7.

3.1 Materials

3.1.1 Ceramic Ink

The formulation of the ceramic ink is adopted from previous work carried out by Song *et al.* [1999]. Its details are given in Table 3.1.

Table 3.1 Components of ceramic ink.

Constituent	Grade	Density	Designation	Manufacturer/Supplier
		kg m^{-3}		
Partially stabilised zirconia	HSY3	6000	ZrO_2	Daiichi Kigenso Kagaku Kogyo Co. Ltd., Osaka, Japan
Zephrym [1]	PD3315	1100	PD3315	Uniqema, Cleveland, UK
Polyvinylbutyral	Pioloform BN18	1100	PVB	Wacker Chemicals, Burghausen, Germany
Dibutyl sebacate	93% GC Grade	940	DBS	Fisher Scientific, Leicestershire, UK
Industrial methylated spirit	74 OP	790	IMS	Fisher Scientific, Leicestershire, UK
Ammonium nitrate	AnalaR	1730	AN	BDH Chemicals Ltd., Poole, UK

Note: [1] Zephrym PD3315 was previously known as Atsurf 3315 and Arlatone 3315.

The zirconia (ZrO_2) powder was doped by the supplier with 5.4 wt. % yttria. Its average particle size (d_{50}) and specific surface area are 0.41 μm and 7 m^2 g^{-1}, respectively [Daiichi Kigenso Kagaku Kogyo, 1998].

The powder was dispersed in industrial methylated spirit (IMS) with the aid of Zephrym PD3315, a dark red-brown liquid. This is a commercially available polymeric dispersant, which provides dispersion through steric stabilisation [ICI Surfactants, 1997]. Zephrym PD3315 is a solution of anionic surfactants in a mixture of water and propylene glycol. In addition, polyvinylbutyral (PVB) was incorporated into the ink as a binder. A plasticiser, dibutyl sebacate, was also included to reduce the viscosity of the ink. Lastly, ammonium nitrate (NH_4NO_3) was added as an electrolyte to improve the electrical conductivity of the ink so that it can be deflected in the electrical field during printing.

3.1.2 Silver Ink

The silver (Ag) powder used is Silver NanoPowder #562 and is supplied by NanoPowders Industries, Kfar-Saba, Israel. This is an ultrafine powder used for conductive coatings, conductive inks and thick conductive pastes. The Ag purity in the powder is 99.73% (by weight); the average particle size and specific surface area are 1.6 μm (d_{50}) and 3.62 m^2 g^{-1}, respectively [NanoPowders Industries, 2000].

Three different types of dispersants (Table 3.2) were used to disperse the Ag powder in IMS. All the dispersants were supplied by Uniqema (Everberg, Belgium) and are soluble in IMS. Zephrym PD7000 is a polyoxyalkylene amine derivative based surfactant whereas the Atphos' are phosphate esters-based. The later were recommended by the manufacturer for dispersing metallic powder in ethanol-based solvent.

Table 3.2 Dispersants used for dispersing Ag powder in IMS.

Dispersants	Density
	kg m^{-3}
Zephrym PD7000	1020
Atphos 3202	1097
Atphos 3205E	1097

3.2 Preparing Small Batch of Ceramic Ink

Three series of ceramic ink containing 5 vol. % of ZrO_2 were prepared for ink development study. In the first series (Group I), three sets of inks C, U and EU with compositions listed in Tables 3.3 were prepared. Ink C was prepared as a reference ink and it did not contain any electrolyte nor was it subjected to any ultrasonic disruption. Inks U and EU were identical to ink C except that they were dispersed using ultrasonic disruption. Ink EU also contained NH_4NO_3 to improve its electrical conductivity.

Table 3.3 Composition of Group I inks.

Constituents	Ink C	Ink U	Ink EU	Quantity
	Vol. %	Vol. %	Vol. %	
ZrO_2	5.0	5.0	5.0	60.0g
PD3315	1.4	1.4	1.3	3.0 g
PVB	1.8	1.8	1.8	4.0 g
DBS	1.8	1.8	1.8	3.3 g
IMS	90.0	90.0	89.5	180 ml
NH_4NO_3	-	-	0.6	2.2g

The preparation procedure for the Group I inks is schematically shown in Figure 3.1. The dispersant was first dissolved in a small quantity of solvent. Powder was then stirred gradually into the mixture until there was no visible sign of the dried powder. The mixture was left standing for 5.40×10^4 s (15 hours) and the binder and plasticiser were then added to produce a viscous paste. The paste was further homogenised in a twin roll mill (Section 3.2.1a) and the resultant mill product was left to dry at ~ 21°C for 8.64×10^4 s (1 day). The same batch of mill products was used to prepare inks C, U and EU and correct amount was added to sufficient amount of solvent, as shown in Table 3.3, to make up 5 vol. % of ZrO_2 ink. The mixtures were then left on rotating rollers (Denley Spiralmix 5) at 50 rpm for at least 7.20×10^4 s (20 hours).

Ink C was obtained at the end of the above mixing. Ink U was obtained by subjecting the mixture to ultrasonic disruption (Section 3.2.2). Ink EU was prepared in a similar way as ink U except that the IMS was pre-dissolved with NH_4NO_3 before it was used to dilute the mill product. Immediately after the inks were prepared, their sedimentation behaviours were studied for 2.59×10^6 s or 30 days (Section 3.4.1).

Group II inks were prepared to compare the effectiveness of twin roll milling to triple roll milling. The resultant mill products were used to produce inks 2R and 3R, respectively, with compositions and preparation procedures similar to ink EU. Same quantity of ceramic-polymer blend was processed using the twin and triple roll mills. Before the inks were prepared, the non-ceramic content in the mill product was determined by loss-on-ignition (Section 3.4.7).

The third series of ink, Group III, was prepared at different powder to binder, plasticiser and dispersant ratio of 50:50 (ink P1), 60:40 (ink P2) and 70:30 (ink P3) with compositions shown in Table 3.4. All the three inks were prepared in the same way as ink 3R and about the same quantity of materials between 170 - 180 g (excluding NH_4NO_3) was used during milling. Furthermore, the non-ceramic content in the mill product was also determined by loss-on-ignition test.

Table 3.4 Composition of Group III inks. The quantity (Qty) refers to the amount used in preparing the suspension for ultrasonic disruption.

Constituents	Ink P1		Ink P2		Ink P3	
	Vol. %	Qty	Vol. %	Qty	Vol. %	Qty
ZrO_2	5.0	60.0 g	5.0	60.0 g	5.0	60.0 g
PD3315	1.3	3.0 g	1.4	3.0 g	1.4	3.0 g
PVB	1.8	4.0 g	1.0	2.2 g	0.4	0.9 g
DBS	1.8	3.3 g	1.0	1.9 g	0.4	0.7 g
IMS	89.5	180 ml	91.0	183 ml	92.3	186 ml
NH_4NO_3	0.6	2.2 g	0.6	2.2 g	0.6	2.2 g

3.2.1 Dispersive Mixing by Roll Milling

(a) Twin roll mill

Milling was performed on a twin roll mill (Lescuyer Ltd., France) with chrome-plated rolls (length = 0.432 m and diameter = 0.152 m) at ~ 21°C for about 900 s (15 minutes). At the beginning of mixing, the nip was set to a minimum and adjusted during milling so that only a small rolling bank of material always remained at the entry region to the nip, i.e. on top of the rolls. As the solvent was evaporating during mixing, a continuous film gradually formed on the roll. The nip gap was then set to 0.24 mm. To assist lateral mixing in the matrix,

cutting and folding were performed on the film during milling. The friction ratio, i.e. ratio of the peripheral velocities of the front and back rolls, was maintained at 0.8 with the front roll rotating at a slower speed of 0.167 m s^{-1}.

(b) Triple roll mill

The triple roll mill (Cox Machines Ltd., Bristol, UK) has roll dimensions 0.4 m (length) by 0.15 m (diameter). All the three rolls are chrome-plated and the feed-to-exit roll speeds were 0.21, 0.60 and 1.53 m s^{-1}. The two nips between the rolls were set at a constant width of 25 μm. Milling was performed at room temperature (~ 21°C) for 720 – 900 s (12 - 15 minutes). During milling, the material in process became increasingly dried as solvent was evaporating. Mist of IMS was sprayed on the rolls to moisturise the material and kept the milling process continue.

3.2.2 Homogenisation by Ultrasonic Disruption

A volume of about 180 - 190 ml of liquid mixture was subjected to ultrasonic disruption over a period of 960 s in preparing inks from Group I, II and III. The mixture was contained in a 200 ml capacity Pyrex glass beaker of height 120 mm and internal diameter 60.9 mm (liquid height ~ 90 mm). The beaker was immersed in an ice-water bath to prevent the mixture from overheating during ultrasonic disruption. A Branson Sonifier 250 ultrasonic disrupter (Branson Ultrasonic Corporation, Danbury, USA), which is an assembly of transducer plus horn, was immersed in the liquid mixture with the horn tip placed 40 mm beneath its surface. The horn is a 130 mm long uniform cylinder of 12.5 mm diameter. Electrical energy is supplied from a 20 kHz generator source to the transducer, which converts it to mechanical energy in the form of longitudinal vibrations. This motion is transmitted to the horn tip from which the energy is radiated. The mixture was treated using a 'continuous pulse mode', i.e. continuous sonication.

The amount of energy being dissipated in the ink was estimated by calorimetric method [Mason *et al.*, 1992]. A mercury-in-bulb thermometer was placed in the liquid mixture midway between the horn and the beaker wall during sonication and the temperature was

recorded against time at 30-s interval. The power dissipated, P_{diss} in the ink was calculated to be 48 W by Equation 3.1.

$$P_{diss} = m\ C_p \left(\frac{dT}{dt}\right)_0 \qquad (3.1)$$

Where C_p is the specific heat capacity of the solvent (in J kg^{-1} K^{-1})

m is the mass of the liquid (in kg)

T is the temperature of ink (in °C)

t is time (in s)

$(dT/dt)_0$ is temperature rise at $t = 0$ obtained by curve-fitting the data to a polynomial in t.

3.3 Preparation of Ceramic Ink for Continuous Printing

A minimum amount of 8.8 x 10^{-4} m^3 (or 880 ml) of ink is required to fill the ink reservoir of the printer before printing could proceed. It is essential that the ink is free of agglomerates, which may clog the piping and nozzle and lead to a halt in printing. The procedure for preparing the ceramic ink for printing is schematically shown in Figure 3.2. It is similar to that for small batches of ink for evaluation and development (Figure 3.1) except for the additional steps at downstream. The composition of ink for printing is shown in Table 3.5. The concentration of NH_4NO_3 used was 0.8 g per 100 ml of IMS instead of 1.2 g per 100 ml of solvent.

Table 3.5 Nominal composition of the ink used for continuous printing.

Components	Composition
	Vol. %
ZrO_2	5.0
PD3315	1.4
PVB	1.8
DBS	1.8
IMS	89.6
NH_4NO_3	0.4

3.3.1 Ultrasonic Disruption

The liquid mixture was first prepared by mixing the mill product in IMS, which was pre-dissolved with NH_4NO_3, on the roller mixer. It was then transferred to an 800 ml Pyrex glass beaker, which was immersed in an ice water bath. Two batches of ink, each of 540 ml (liquid height in beaker = 90 mm), were subjected to ultrasonic disruption with the Branson Sonifier 250 ultrasonic disruptor using 'continuous pulse mode' for 1.50×10^3 s (25 minutes) at 75 W. During this period, the horn tip was positioned at 20, 50 and 70 mm beneath the liquid surface for 480, 540 and 480 s, respectively. The ink was stirred manually at each change over of position.

3.3.2 Sedimentation and Filtration

After ultrasonic disruption, the ink was left to settle under gravity in a sealed container during which the flocculated agglomerates descended to the bottom of the container as sediment. The ink suspension, which resided on top of the sediment, was separated out from the sediment. Smaller agglomerates in the ink (suspension) were further removed by filtering. The size of the agglomerates was estimated by filtering in steps with the followings:

(i) syringe filter, 40 μm (Polydisc, Fisher Scientific, Leicestershire, UK)

(ii) syringe filter, 25 μm (Polydisc, Fisher Scientific, Leicestershire, UK)

(iii) filter funnel, 20-25 μm (Whatman FilterCup 70 disposal filter funnel, Fisher Scientific, Leicestershire, UK) and

(iv) filter funnel, 8-10μm (Whatman FilterCup 70 disposal filter funnel, Fisher Scientific, Leicestershire, UK).

The first two steps were performed by manual injection while the last two were assisted with a suction pump at 0.1 MPa. Steps (i) - (iii) proceeded with ease but the filtering process came to a standstill at step (iv) due to blockage in the filter. With a crude estimation of the average agglomerate size, the filtration system as shown in Figure 3.3 was set up. A micropump (Micropump Inc., Vancouver, USA) was used to dispense the ink through a Polycap filter capsule (Arbor Technologies Inc., Ann Arbor, USA) from a reservoir of sonicated ink that had its sediment removed. The suction pressure, which was used to drive the ink through the filter, was controlled by a power supply source (Thurlby Thandar

Instruments, Cambridgeshire, UK). The ink was filtered in two stages through filter media rated at 10 and 5 μm with filtering rates at 1.41×10^{-2} and 3.60×10^{-3} $m^3 s^{-1}$, respectively.

3.3.3 Evaluation of Ink Preparation Procedure for Printing

The sonicated inks were subjected to different conditions of sedimentation and filtration given in Table 3.6. This is to find out the best combination of sedimentation time and filtration to yield stable ink for continuous printing. These inks were allowed to circulate in the printer for 1.73×10^5 (2 days) or as long as it could. During this process, the time of flight, TOF (Section 3.5), and the ink pressure were monitored constantly by the printer control. A consistent TOF and ink pressure displayed during the printer operation was an indication of stable ink.

Table 3.6 Different preparation routes for printing ink.

Route	Sedimentation duration / s	Filtration
1	0	No
2	8.64×10^4	No
3	8.64×10^4	10 μm
4	8.64×10^4	10 μm then 5 μm filter medium
5	1.73×10^5	10 μm then 5 μm filter medium

3.4 Ink Characterisation

3.4.1 Sedimentation

Gravitational sedimentation test was employed to determine the extent of particle flocculation by monitoring the evolution of the volumes of sediment, suspension and cloudy/clear liquid. This was carried out over a period of 2.59×10^6 s (30 days) for ZrO_2 ink and 8.64×10^5 s (10 days) for Ag ink. The test was performed immediately after the ink was subjected to ultrasonic disruption. Five samples of ZrO_2 ink or three samples of Ag ink of 10 ml were extracted and transferred to Pyrex test tubes, which were pre-calibrated to an accuracy of ±0.1 ml. The test tubes were stoppered, sealed and left undisturbed to settle throughout the period of study. The evolution of the volumes of the sediment, suspension

and cloudy/clear liquid was measured at regular interval of 3600 s (1 hour) during the first eight hour of study and thereafter every 8.64 x 10^4 s (24 hours). A light was shone on the ZrO_2 sample to help discern the boundary between different zones.

3.4.2 Density

The density of the ink was measured according to BS733: Part 2: 1987 with a Type 3: capillary-stoppered pyknometer flask (Gay-Lussac) of 25 ml nominal capacity. The flask was cleaned, dried and weighed to the nearest 0.0001g with an electronic precision weighing balance. It was subsequently filled with deionised water and brought to 20°C in a water bath. The apparent mass of the content was determined. The flask was then emptied, cleaned, dried and filled with the test sample. It was also sealed to prevent the ink from evaporating and placed in the same water bath. The apparent mass of the sample was determined and its density at 20°C was calculated with Equations 3.2 and 3.3 [BS733: Part 2: 1987]. Three samples were measured to obtain the average density of the ZrO_2 ink.

$$\rho = \frac{m_t - m_0}{V_c} + A \qquad (3.2)$$

$$V_c = m_c - m_o \qquad (3.3)$$

where ρ is the density of the sample at 20°C (in g/ml)

A is the buoyancy correction

m_c is the apparent mass of the pyknometer in air when filled with water at 20°C (in g)

m_o is the apparent mass of the pyknometer in air when measured empty (in g)

m_t is the apparent mass of the pyknometer in air when filled with the sample at 20°C (in g), and

V_c is the volume of the water contained at 20°C (in ml).

3.4.3 Viscosity

A Haake RheoStress 150 rotational rheometer (Haake GmbH, Karlsruhe, Germany) was used to determine the viscosity of the inks. This is a controlled stress rotational rheometer but it can be used under controlled rate application. When it operates at controlled rate, the lowest measurement limit of viscosity is 2 mPa s [Haake, 1998].

A C35/2 cone and plate sensor system (cone diameter = 35 mm, cone angle = 2°) was used for viscosity measurements in this research. Measurements were made in a temperature-controlled room at 20°C. During measurement, correct amount of ink sample was first dispensed on the plate and the cone was then moved to the gap position set at 0.105mm. Any excess liquid effusing out of the plate was wiped off carefully. In addition, the temperature of the plate was controlled by a circulator (Haake B3 Circulator) maintained at 20°C. The viscosity of the ZrO_2 ink was measured at a constant shear rate of 1000 s^{-1} applied for 60 s. Three samples were tested and their average value is reported. The viscosity of the Ag ink was measured at constant shear rates of 100, 500 and 1000 s^{-1}, with each applied for 30 s. Similarly, three samples were measured.

The application of the instrument to test low viscosity liquids was further verified by test solution isopropanol (AnalaR Propan-2-ol, Merck, Leicestershire, UK) and this can be found in Appendix B.

3.4.4 Electrical Conductivity

The conductivity of the ZrO_2 ink was measured by a hand-held unit of Conmet 1 HI98305 Conductivity Meter (Hanna Instruments, Padova, Italy). Before use, the meter was calibrated with a standard solution of KCl (Calibration solution HI7031, Hanna Instruments, Padova, Italty) of conductivity value 0.1278 S m^{-1} at 20°C. The ink sample was first immersed in a constant temperature bath at 20°C for a minimum of 1.80×10^3 s. The meter probe was then inserted into the ink. It was then stirred gently to remove air bubbles trapped inside the probe shield and reading was taken when stabilised. Three samples were measured and their average is presented.

3.4.5 Surface Tension

The surface tension of the ZrO_2 ink was measured by two different instruments.

(a) Ring method

The Krüss K10 surface tensiometer (Krüss GmbH, Hamburg, Germany), also known as du Noüy ring method (Figure 3.4), was used to measure the surface tension of the ink. It has a

platinum ring of mean radius (R) 9.545mm and the radius of the wire (r) is 0.185mm. This method determines the amount of force (f) required to detach the ring from the surface of the ZrO_2 ink. Before measurement, the ring and the measuring vessel were cleaned, and rinsed thoroughly with distilled water and ethanol. The ring was further heated in a flame to remove any contaminants. During measurement, the ring was suspended horizontally, dipped into the ZrO_2 ink and slowly removed. The equipment measured the force necessary to pull the wetted circumference of the ring through the ink and displayed the corresponding surface tension value. Prior to measurements, the accuracy of the equipment was verified with distilled water of surface tension 72.8 mN m^{-1} [West *et al.*, 1985].

The value recorded by the equipment is the uncorrected surface tension and needs to be multiplied by a correcting factor F [ASTM D1331-89]. The true surface tension $\gamma_{l,ink}$ is calculated from Equation 3.4 [Harkins and Jordan, 1930]:

$$\gamma_{l,ink} = \frac{f}{4\ \pi\ R}\ F\left(R/r\ ,\ R^3/V\right) \qquad (3.4)$$

where F is a function of the contour of the liquid surface in the neighbourhood of the ring at the instant of breakaway, i.e. it is a function of $(R/r,\ R^3/V)$, and

V is the maximum volume of liquid elevated above the free surface of the liquid.

Five samples were measured and their surface tension values were corrected using Equation 3.4. The average value is reported (see Appendix C).

(b) Plate method

This method is also named after its inventor, Wilhelmy. It is based on the measurement of force like the ring method; but unlike the ring method, it does not require hydrostatic corrections [Adamson and Gast, 1997]. The test probe used is a rectangular glass plate as shown in Figure 3.5. It was suspended vertically from a torsion balance (White Electrical Instrument Co. Ltd., Worcestershire, UK). The wetted length (L_b) and the surface tension $\gamma_{l,ink}$ (in mN m^{-1}) are calculated from Equations 3.5 and 3.6:

$$L_b = 2\,l + 2\,b \qquad (3.5)$$

$$W_{total} = W_{plate} + \gamma_{l,ink}\,L_b \qquad (3.6)$$

Where l, b are the length and depth of the Wilhelmy plate, respectively

W_{plate} is the weight of the plate in air (in N) and

W_{total} is the weight of the plate in ZrO_2 ink (in N).

The plate and the measuring vessel were prepared in the same way as described previously in the ring method. The balance consists of two scales, a dial scale, which reads off the surface tension value, and a vernier scale, which indicates the position of the plate. The balance was first levelled and calibrated with a known weight. Next, the plate was suspended vertically from the balance and the dial reading on the balance was adjusted to zero to compensate for the mass of the plate. The bottom edge of the plate was then brought into contact with the ZrO_2 ink and was thereby wetted. The vessel was lowered slowly. At the same time, the balance reading was offset carefully so that the plate remained constantly in its zero position at the vernier scale. When the plate detached from the ZrO_2 ink, the dial reading was noted. A total of five measurements were made and the average value is presented. The accuracy of this instrument was also verified with distilled water.

3.4.6 Microscopy

Scanning electron microscope (SEM) was used to characterise the mill product, ink and the droplet relics deposited by ink-jet printing. Both a Cambridge 360 Stereogun SEM and a Toshiba JEOL 6300 SEM were used. These units were fitted with Energy Dispersive X-ray (EDX) for elemental analysis. The specimen was either gold (for microstructure examination) or carbon (for elemental analysis) sputtered prior to SEM examination. For the latter, dot mapping was used to detect the presence of Zr in the droplet relics. A line scan mode was further performed on the relics across its diameter to examine the distribution of Zr.

The prints made by ink-jet printing were also examined with an Olympus BX60 optical microscopy linked up to an image analysis software.

3.4.7 Loss-on-Ignition

The amount of ZrO_2 powder in the ink was estimated by loss-on-ignition. At least three samples, each ~ 6 ml of mass m_1, were contained in dried, clean porcelain crucibles in a

furnace. Initially, the amount of solvent in the ink was determined by heating the samples in air at 2°C min^{-1} to 90°C and holding at this temperature for 1.44 x 10^4 s (4 hours). At this temperature, the solvent would be burnt off but it is too low for the decomposition of other additives. Thus, the amount of material lost (m_2) was equivalent to the mass of the solvent. The samples were then heated at 5°C min^{-1} to 600°C and held for 3.60 x 10^3 s (1 hour) to burn off the remaining additives. The residual mass (m_3) at the end of this was determined and this was equivalent to the mass of ceramic. All the masses were measured with a 4-decimal place precision weighing balance. The vol. % of ZrO_2 in the ink ϕ, was estimated by Equation 3.7, assuming all the processing additives were distributed uniformly in the solvent.

$$\phi = \frac{V_{ZrO_2}}{V_{ZrO_2} + V_{IMS} + V_{Polymer} + V_{AN}} \qquad (3.7)$$

V_i is the volume of the i^{th} constituent in the ink (in m^3) where:

$$V_{ZrO_2} = \frac{m_3}{\rho_{ZrO_2}}$$

$$V_{IMS} = \frac{m_2}{\rho_{IMS}}$$

$$V_{AN} = V_{IMS} \frac{x}{\rho_{AN}} \; ; \qquad m_{AN} = V_{IMS} \text{ x } x$$

$$V_{Polymer} = \frac{m_1 - m_2 - m_3 - m_{AN}}{\rho_{Polymer}} \; ; \rho_{polymer} = \frac{m_{PD3315} + m_{PVB} + m_{DBS}}{\left(\frac{m}{\rho}\right)_{PD3315} + \left(\frac{m}{\rho}\right)_{PVB} + \left(\frac{m}{\rho}\right)_{DBS}}$$

m_1 is the mass of the ink sample (in kg)

m_2 is the mass of the solvent in the sample (in kg)

m_3 is the mass of the ceramic in the sample (in kg)

m_{AN} is the mass of NH_4NO_3 in the sample (in kg) and

x is the concentration of NH_4NO_3 (in kg) in 1 m^3 of IMS

$\rho_{polymer}$ is the density of polymer comprising of the PD3315, PVB and DBS and is computed at formulation.

3.5 Continuous Printing of Ceramic Ink

3.5.1 Operating Principle of Printer

The printer system, as shown in Figure 3.6, was supplied by Linx Printing Technologies Plc., Cambridgeshire, UK for the printing of ethanol-based ink. It consists of a Linx 6200S continuous printer, an ink dispensing system, a MIDI printhead and a table over which the printhead is mounted. The table was designed by Biodot Ltd. (Diddington, Cambridgeshire, UK).

(a) Linx 6200S continuous printer

This is the control unit of the system. It contains all the electronics to drive the ink system and the printhead and this is done via the keyboard interface. Software for generating patterns is also installed in it.

(b) Ink dispensing system

The ink dispensing system is a separate stainless steel enclosure that comprises mainly of a solvent tank, an ink tank, a 40μm pre-pump filter, a pump and motor, a 10μm main ink filter and a manifold assembly. Both the ink and solvent tanks have a capacity of 1.44×10^{-3} m^3 each and the minimum level of operation is 8.8×10^{-4} m^3. The filters will remove any foreign debris from the ink before it reaches the manifold and the printhead. The manifold assembly regulates the distribution of the ink and solvent. There is a pressure transducer installed near the manifold to monitor the ink pressure. When the ink pressure exceeds the set reference pressure, the control system recognises this as the ink viscosity has become too high and solvent may be added automatically to the ink.

(c) Printhead

The conducting ink is forced out of a reservoir through a 62μm diameter nozzle in the printhead (Figure 3.7) under pressure. As it passes through the nozzle, it is piezoelectrically pulsed or modulated and the stream breaks up into a continuous series of droplets to minimise surface area. The droplets are equally spaced from one another and of equal size. Surrounding the jet at the point where the break-up occurred is a charge electrode maintained at a voltage of 0 – 255V. Each droplet is given an electrostatic charge, which is retained by

the droplet throughout its flight to the printing substrate. At the base of the electrode is a light emitting diode (LED), which is strobed at the same frequency as the modulation signal. Thus, the jet appears to be stationary and the details of droplet formation can be observed.

The charged droplets continue their flight paths through a pair of deflection plates maintained at 3-4 kV. The Linx printhead incorporates 'guard droplets' between the charged droplets to reduce their interactive effect in flight. The guard droplets are not printed, but enter the gutter where they are re-circulated. Within the deflection plates, the droplets are deflected according to the magnitude of charge. As the droplets are deflected, the printing substrate is driven horizontally relative to the printhead, which remained stationary, and the droplets are deposited on appropriate positions to form the desired character or pattern. The character or pattern is made up of rasters and each raster is a column of dots and/or spaces printed at 90° to the movement of the substrate.

The printhead has a time of flight (TOF) sensor, which is located near the gutter, to measure the velocity of the jet by timing the flight of the droplets between two fixed points. There is also a phase sensor to provide a feedback signal indicating if the droplets have been adequately and correctly charged so as to synchronise the charging pulse with the droplet generation frequency. This routine is called phasing. Both parameters (TOF and phase position) are monitored at regular intervals. Adjustments are made within the electronics of the printer to ensure that optimum TOF and phase positions are maintained to produce consistent print quality.

(d) Table

The table is built with a movable platform on which the printing substrate was placed. In addition, a photocell and a shaft encoder are installed in it to ensure that printing is triggered at the same position and same rate during overprinting.

3.5.2 Setting Up the Printer

Polymeric ink, which contained only the binder (PVB) and NH_4NO_3 in IMS, was used as test solution to set up the printer.

(a) Preparation of test solution

A viscosity of 3 - 4 mPa s and electrical conductivity of 0.1 S m^{-1} (both at 20°C) are required for printing. Thus, different amounts of PVB and NH_4NO_3 were used to arrive at a solution with these properties.

The first series of polymeric ink contained no NH_4NO_3. The wt. % of PVB (as a percentage of the weight of the solvent) was varied at 2, 3, 4, 5 and 8. Their viscosities were measured with flow cup at 20°C by Linx Printing Technologies Plc.. In addition, another series of polymeric inks at 4 wt % of PVB was prepared with different concentrations of NH_4NO_3 at 0.3g (PE1), 0.6 g (PE2) and 1.2g (PE3) for every 100 ml of the solvent. The electrical conductivity of the inks was measured with a Jenway Conductivity Meter 4200, which has been calibrated at 21°C. The inks were printed on acetate sheets.

(b) Printhead set up

The charged droplet was deflected in the electrical field within the printhead. As it emerged out of the printhead, it continued its flight towards the printing substrate. As shown in Figure 3.8a, the amount of deflection in the Y-direction increases when the printhead to substrate distance (D) is increased. Thus, there exists a distance between the base of the printhead and the printing substrate (D) where the dimension of the print in the Y-direction (l_y) is undistorted. To determine this optimum distance, a matrix of 32 rasters was made at various settings of D = 4, 5, 7, 8, 10 and 12 mm. Each raster comprised of 32 dots in the y-direction. At different D, five prints were made and their dimensions in the X and Y directions, l_x and l_y, respectively, were measured with a project comparator (Ceast S.P.A., Torion, Italy) at 10x magnification. At the optimum setting, the measured dimensions l_x and l_y should be equal.

3.5.3 Printing Conditions

(a) Test patterns for printing

Four sets of test patterns were used. Test pattern 1 involves printing of alphanumeric characters. Test pattern 2, as shown in Figure 3.9, is a matrix of 89 rasters. Each of these rasters comprises of 32 dots, various combinations of dots and spaces, or 32 spaces. Test

pattern 3 (Figure 3.10) is a rectangle of 64 x 32 dots. Test pattern 4 (Figure 3.11) is a set of four rectangles and square with configurations given in Table 3.7. The print resolution for test pattern 4 is the same in all cases, 3543 and 3660 dots per m in X- and Y-directions, respectively.

Table 3.7 Configurations of test pattern 4.

Test Pattern	Number of rasters in X-direction	Number of dots in each raster in Y-direction	Area, X by Y mm x mm
4a	64	32	18 x 8.5
4b	32	16	9 x 4.5
4c	16	8	4.5 x 2.2
4d	8	8	2.2 x 2.2

(b) Effect of modulation frequency

The modulation frequency was varied from 10 to 120 kHz in step of 10kHz and test pattern 1 was printed on substrate S2 (Table 3.8) to estimate the optimum modulation frequency. As the frequency was changed, the phenomenon of jet break-up was observed visually in the charge electrode with the help of the LED. The quality of the prints was also assessed.

Table 3.8 Substrates used for printing.

Identification	Trade name and type	Supplier
S1	Xerox: Acetate sheet for photocopier and laser printing	Xerox (UK) Ltd., Uxbridge, UK
S2	Smart: Acetate sheet for photocopier and laser printing	OfficeSmart, Twickenham, UK
S3	Silicone release paper	Sterling-Lohja, Glossop, UK
S4	Niceday: Acetate sheet for photocopier	Guilbert UK Ltd., Horsham, UK
S5	Niceday: Write-on acetate sheet	Guilbert UK Ltd., Horsham, UK
S6	Niceday: Acetate sheet for laser printing	Guilbert UK Ltd., Horsham, UK
S7	Stabilo: Acetate sheet for photocopier	Stabilo Ltd., Berkshire, UK
S8	Stabilo: Acetate sheet for ink-jet printing	Stabilo Ltd., Berkshire, UK
S9	Punchline: Write-on acetate sheet	John Heath & Co. Ltd., Birmingham, UK

(c) Substrate-ink interaction in single layer print

The substrate-to-printhead distance and modulation frequency were set at their optimum values and nine different substrates, listed in Table 3.8, were used for printing single layer of test pattern 2. These substrates are being used for a diversity of applications in printing and their surface free energies were estimated (Section 3.5.4). The quality of the resultant prints was assessed by examining single printed dot and the interaction between overlapping dots under an optical microscope. The presence and distribution of Zr within the single printed dot was also investigated (Section 3.4.6).

(d) Multi-layer printing

Test pattern 3 was overprinted on substrate S2 at different print area resolutions in X- and Y-directions given in Table 3.9. The substrate-to-printhead distance and modulation frequency were also set at their optimum values. During printing, the layers were dried with cool air (at 24°C) from a dryer placed 120 mm from the print. The print interval was maintained at 15 s during printing.

Table 3.9 Overprinting of test pattern 3 with varying print resolution.

Print resolution, X by Y		No. of layers
dot per m^2	dot per $inch^2$ *	
3543 x 3660	90 x 93	100
2638 x 3660	67 x 93	100
1930 x 3660	49 x 93	100
1969 x 1930	50 x 49	100 and 495

Note: * 1 dpi = 39.37 dot per m.

(e) Drying condition

Overprinting was performed with test pattern 4 on substrate S2 to study the effect of drying using ZrO_2 inks of 1.5 and 2.5 vol. %. The same print resolutions of 3543 and 3660 dot per m in X- and Y-directions, respectively, were employed for all printings. During printing, the layers were dried by increasing the evaporation rate of the solvent through flowing streams of cool or hot air, or increasing the temperature of substrate. The first two modes of assisted drying were attained by a dual function dryer operating at 70 and 250 W and allowing the

draught current to blow over and not directly on the printed parts. The third mode of assisted drying was achieved by shining a 100W light bulb directly onto the substrate during printing.

Five sets of experiments, which are given in Table 3.10, were conducted. In natural drying, the overprinted parts were dried without any externally enforced factor. For each set of experiment, the followings were varied:

(i) the interval between overprinting: 15, 30 and 60 s, and

(ii) print area - with test patterns 4a, 4b, 4c and 4d (Section 3.5.3a).

Five samples were printed and the number of layers that can be printed before the occurrence of defects was visually examined.

Table 3.10 Drying experiments conducted under different conditions.

Experiment Set	Assisted Drying	Heated substrate	ZrO_2 Loading (Vol. %)	Remark
I	No	No	1.5%	Dried under natural convection
II	Cool air	No	1.5%	-
III	Hot air	No	1.5%	-
IV	No	Yes	1.5%	-
V	No	No	2.5%	Dried under natural convection

3.5.4 Characterisation of Printing Substrates

(a) Surface free energy

The surface free energy (γ_{sv}) of the substrates listed in Table 3.8 was estimated by the Owens and Wendt's approach [1969] given in Equation 3.8.

$$\gamma_l \left(\cos\theta + 1\right) = 2 \left(\gamma_l^d \ \gamma_{sv}^d\right)^{1/2} + 2\left(\gamma_l^{nd} \ \gamma_{sv}^{nd}\right)^{1/2} \qquad (3.8)$$

where γ_l is the surface tension of the liquid in equilibrium with the vapour of the liquid (in mN m^{-1})

γ_l^d and γ_l^{nd} are the dispersive and non-dispersive components, respectively, of γ_l (in mN m^{-1})

γ_{sv}^{d} and γ_{sv}^{nd} are the dispersive and non-dispersive components, respectively, of γ_{sv} (in mN m^{-1}) and

θ is the average contact angle formed by the liquid on the substrate.

Using contact angles and surface tension components of standard liquids, γ_{sv} of the substrate can be calculated. Two standard liquids were used. They were purified water (Merck, Dorset, UK) and di-iodomethane (99% purity, Sigma-Aldrich Company Ltd., Dorset, UK). By solving a system of equations for water and di-iodomethane, the square roots of γ_{sv}^{d} and γ_{sv}^{nd} are obtained and γ_{sv} is then equal to $\gamma_{sv}^{d} + \gamma_{sv}^{nd}$.

Contact angles were measured with a FTA Dynamic Contact Angle Analyser (First Ten Angstroms, Portsmouth, USA), which uses video to capture the image of a droplet for analysis. No pre-treatment was applied to the substrates but new, clean sheets of the materials were stored in a closed container before use. Sample of S3 (silicone release paper) was secured and mounted on a flat support with adhesive tape during measurement. No mounting was necessary for the acetate sheets, which did not pose any problems of remaining flat on the measuring platform. The evenness of the supporting platform was also confirmed with a level spirit. Prior to measurements, angle measurement was checked with a 90° standard.

Measurements were made at 21°C and droplets of 5µl and 10µl of water and di-iodomethane solution, respectively, were dispensed from syringe on the untreated substrates. The reason for using a greater droplet-volume for di-iodomethane was for better resolution in contact angle measurement.

A live image of each droplet was captured on video and transferred to a continuous frame grabber which is capable of digitising full RS-170 (NTSC) frames at VGA resolution. Contact angle measurements were made about 10 s after the droplet had landed on the substrate to allow for droplet relaxation while minimising liquid evaporation. Five sets of measurements were made for each liquid-substrate combination and the image of the droplet was stored for analysis. Both the left (θ_l) and right (θ_r) contact angles of the droplet, as shown in Figure 3.12, were measured to obtain the average contact angle.

The measured γ_{sv}'s of the substrates were compared with the surface tension of the ink ($\gamma_{l,ink}$). Where $\gamma_{sv} < \gamma_{l,ink}$, it was categorised as a Type I substrate and where $\gamma_{sv} > \gamma_{l,ink}$, Type II.

(b) Swelling Test

Substrates S2 and S3 were submerged in a container of industrial methylated spirit for 250 s during which any thickness changes were examined every 5 s under an optical microscope.

(c) Mass loss during drying

The mass loss of ZrO_2 ink droplets on substrates S2 and S3 was measured at 21°C in air under natural convection by weighing with an electronic precision balance. Unloaded substrates of the same cross section area (10 mm x 10 mm) were used and their masses were first monitored every 15 s over a period of 600 and 900 s, for Type I and II substrates, respectively. Subsequently, an ink droplet was deposited on each substrate and the mass changes were recorded over the same period. The same procedure was repeated twice for each substrate type. The mass changes of the ink droplet on the substrate, as a percentage of the initial mass are presented with appropriate correction made for the mass changes of the unloaded substrate due to equipment drift.

(c) Wettability

The changes in geometry of ZrO_2 ink droplet deposited on substrates S2 and S3 were studied at 21°C in air under natural convection with the FTA Dynamic Contact Angle Analyser. Images of the droplet were captured and analysed by the image analysis program associated with the instrument. The program assumes a spherical fit on the droplet to calculate the average contact angle (θ), the width of the base of the droplet (W) and the height of the droplet (H), as illustrated in Figure 3.12. Again, angle measurement was checked with a 90° standard prior to measurement. In addition, magnification was calibrated against an object of known dimension. The substrates were mounted in the manner as described previously.

A droplet of ZrO_2 ink was dispensed from a plastic syringe fitted with a disposable blunt-end stainless steel needle of 174 μm internal diameter. The syringe was secured vertically on a

stage fitted with a stepper motor, which meters the dispensing rate. Pumping was proceeded at a slow rate of 1 μl/s to form a pendant droplet at the needle tip (Figure 3.13a). The platform was raised slightly and slowly until the substrate just touched the bottom of the droplet (Figure 3.13b) and then lowered slowly to detach the droplet from the needle. For substrate S2, data were taken after the droplets were detached completely from the needle. For droplets deposited on substrate S3, data were taken 2.5 s after they were detached completely from the needle. This time period was necessary to allow the droplets to stabilise. At the same time, the pump was reversed to prevent any dripping of the ink onto the droplet. Adequate lighting was used to enhance the contrast at the edge of the droplet. A sequence of images of the droplet drying on substrates S2 and S3 were captured on video over periods of 200 s and 300 s, respectively. About 20 frames of image were captured before the detachment of the droplet. After that, images were captured at 0.5 s per frame and 1.2 s per frame, for substrates S2 and S3, respectively, with a period multiplier of 1.05. Only data collected after complete detachment of the droplet were analysed. Each experiment was repeated twice on each substrate.

3.6 Debinding and Sintering of Ceramic Printed Parts

The printed parts were embedded in alumina powder (Grade LG20, Alcan Chemicals, UK) and pyrolysed in a muffle tube furnace flowing with oxygen-free nitrogen gas to remove the binder. The heating schedule is given in Table 3.11. The debound part was then sintered in air by heating at 5 °C min^{-1} to 1400°C and held at this temperature for 7.20 x 10^3 s (2 hours).

Table 3.11 Debinding schedule.

Step	Heating rate	Temperature	Dwell Time
	°C min^{-1}	°C	s
1	2.0	70	1.80 x 10^3
2	0.1	90	1.80 x 10^4
3	0.1	150	1.80 x 10^4
4	0.3	210	7.20 x 10^3
5	0.3	350	1.80 x 10^4
6	0.3	400	3.60 x 10^3

3.7 Development of Silver Ink

Dispersants listed in Table 3.2 were used to prepare 2 and 5 vol. % of Ag in industrial methylated spirit (IMS). The amount of dispersant to Ag ratio was varied from 0.5, 1.5, 2.5 and 5 for each dispersant-Ag loading combination given in Table 3.12. The dispersant was first dispersed by ultrasonic disruption in 60 ml of IMS for 120 s at 28 W in a 100 ml Pyrex beaker. The Ag powder was then stirred into the mixture and ultrasonic disruption was carried out for another 360 s at 39 W. During mixing, the beaker was kept in the ice-water bath. The sedimentation behaviour of the inks was studied as described in Section 3.4.1 for 8.64×10^5 s (10 days). Samples were taken at time = 0 s, 2.59×10^5 s (3rd day), 5.18×10^5 s (6th day) and 7.78×10^5 s (9th day). Their viscosity at 100, 500 and 1000 s^{-1} was measured as described in Section 3.4.3b.

Table 3.12 Series of silver inks prepared using different dispersants.

Dispersant	Ag Vol. Loading	Dispersant / Ag weight ratio
	%	%
Atphos 3202	2	0.5, 1.5, 2.5, 5
Atphos 3202	5	0.5, 1.5, 2.5, 5
Atphos 3205E	5	0.5, 1.5, 2.5, 5
Zephrym 7000	2	0.5, 1.5, 2.5, 5

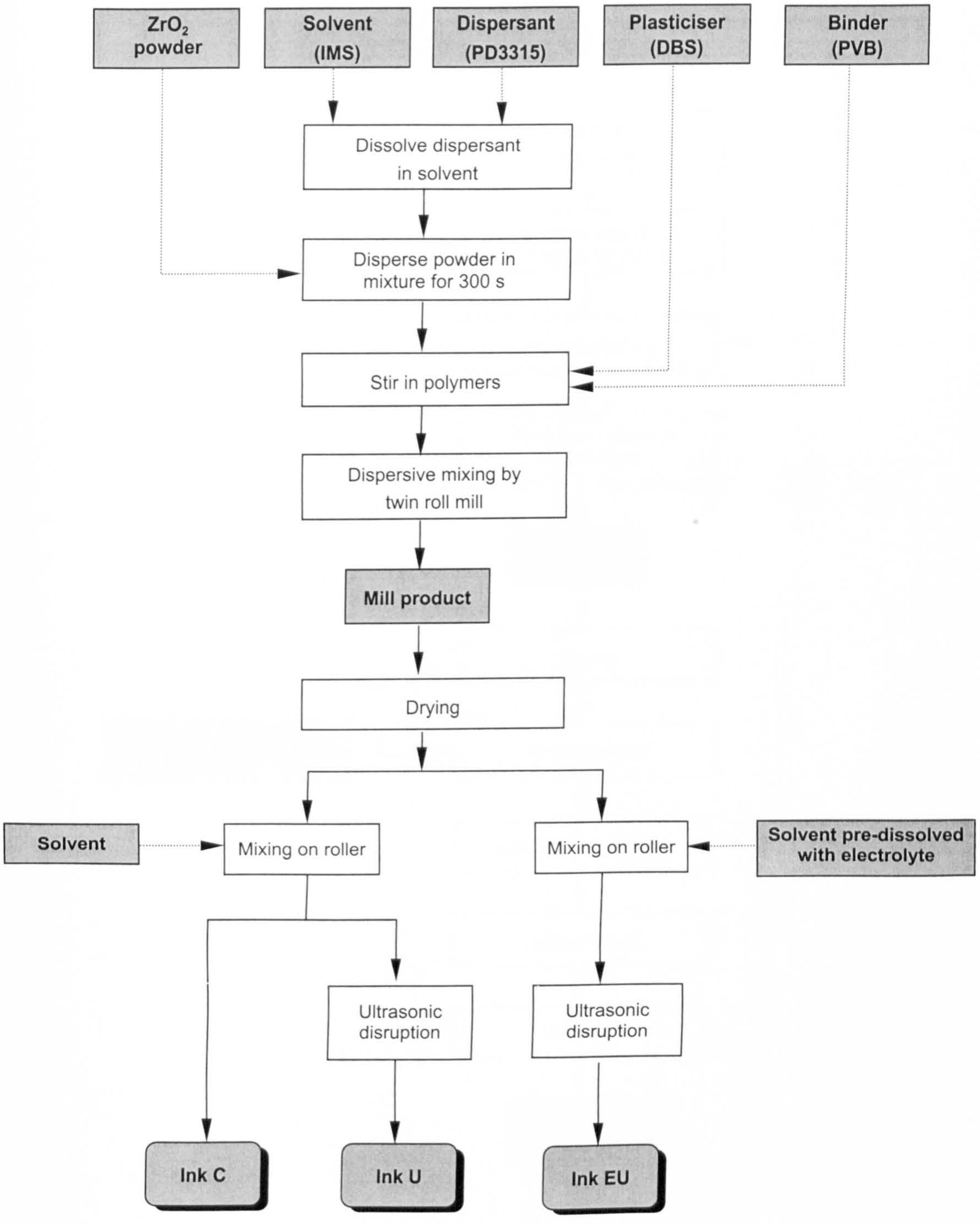

Figure 3.1 Preparation procedures for inks C, U and EU.

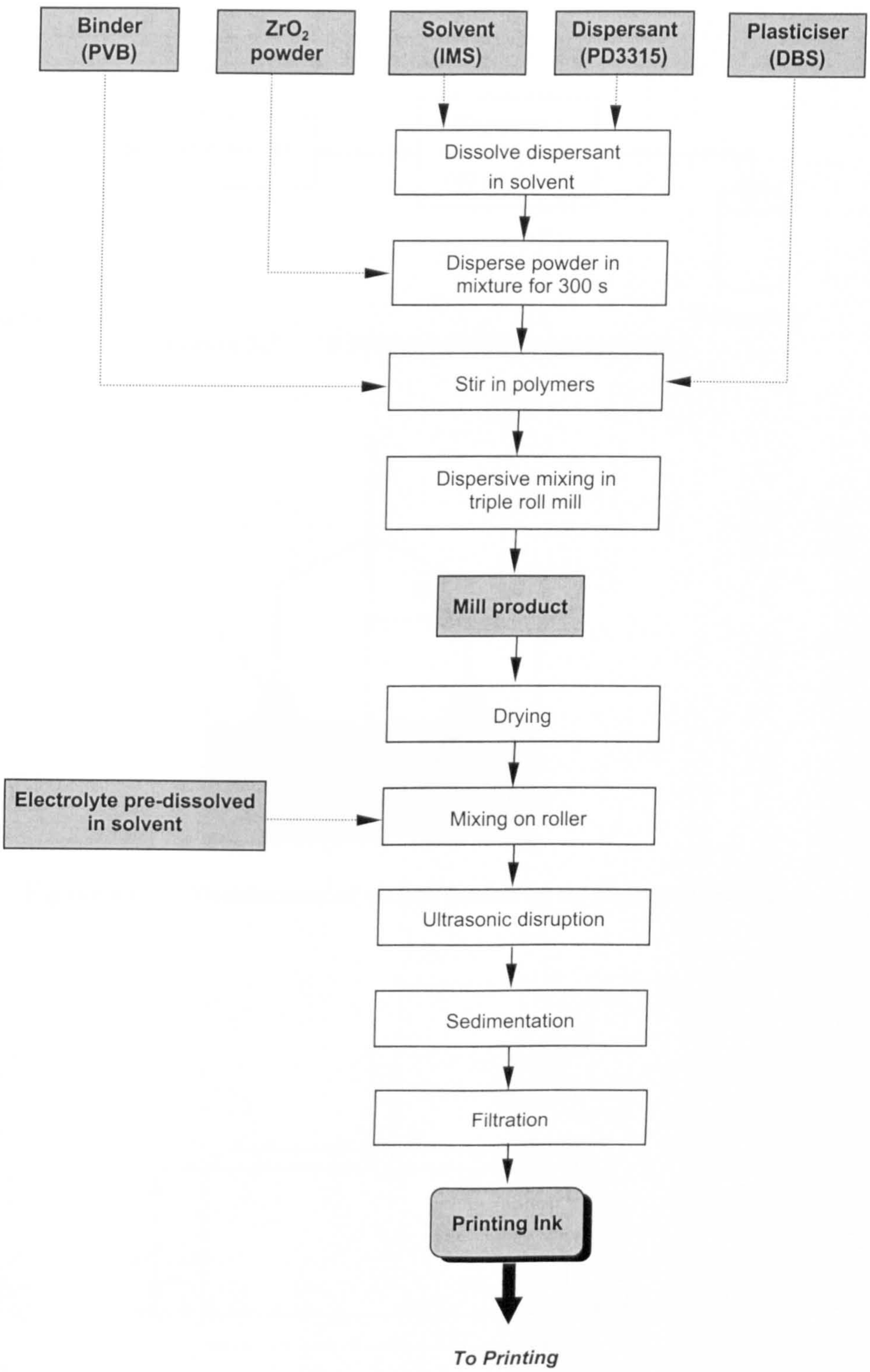

Figure 3.2 Preparation route of ceramic ink for printing.

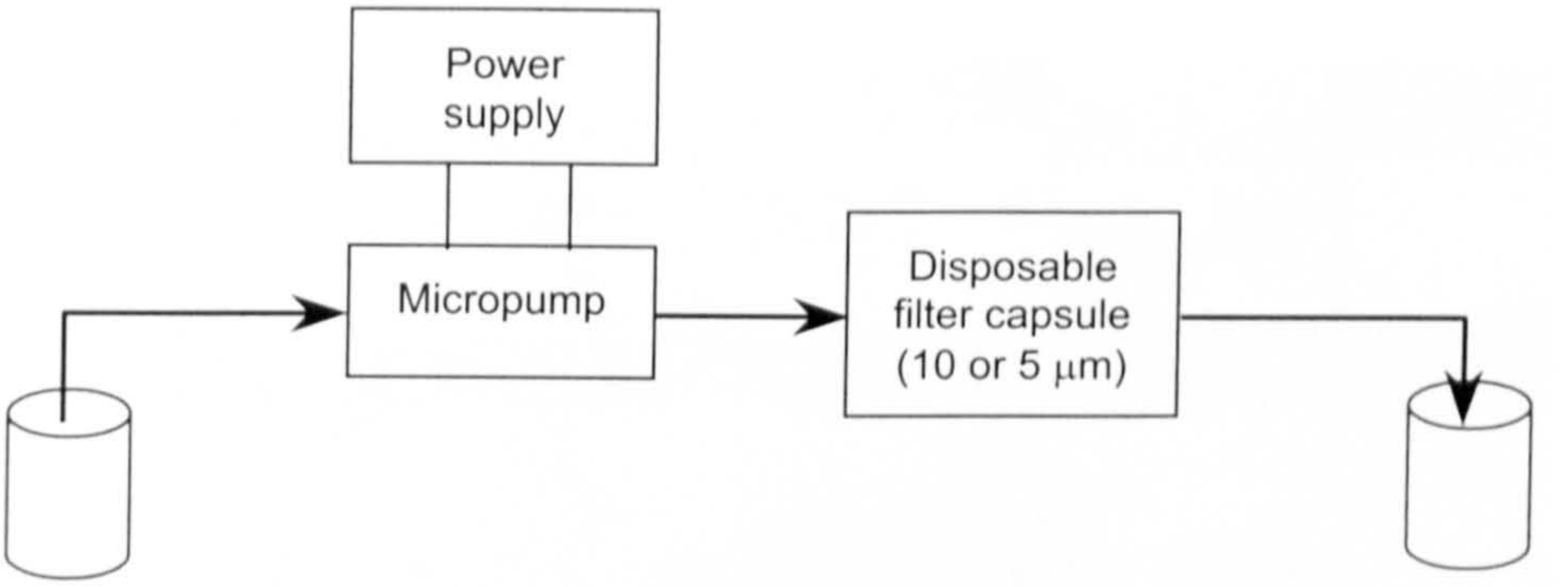

Figure 3.3 Filtration setup with micropump.

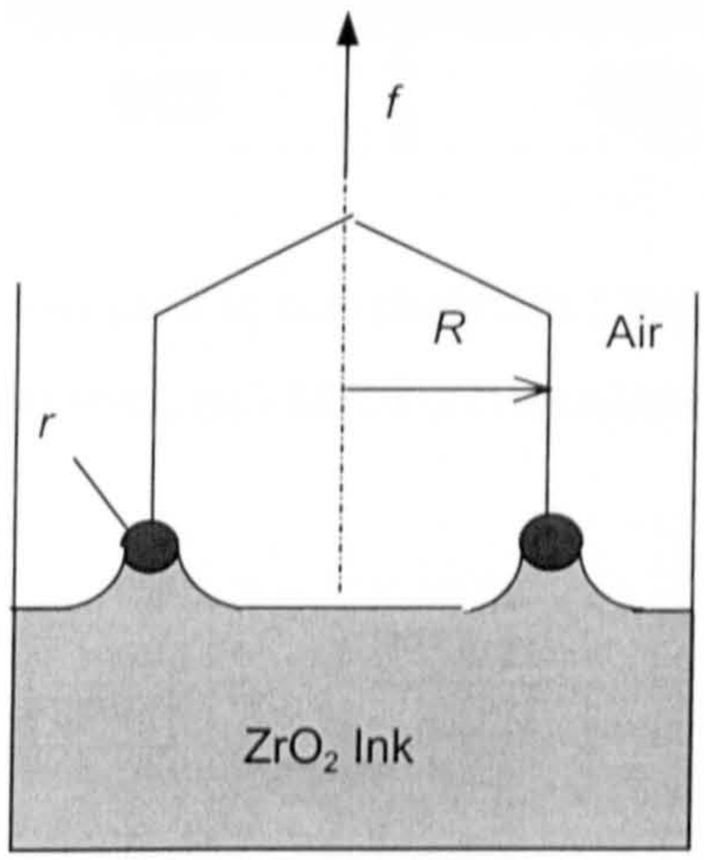

Figure 3.4 Measurement of surface tension by du Noüy ring method.

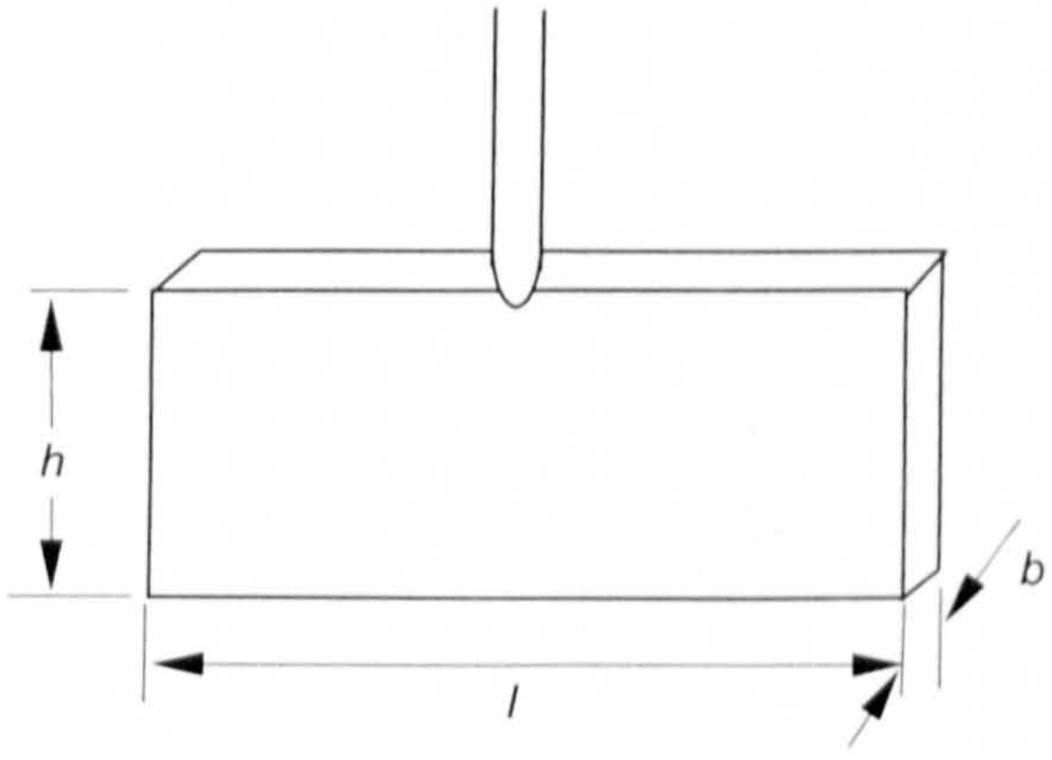

Figure 3.5 Geometry of the Wilhelmy plate.

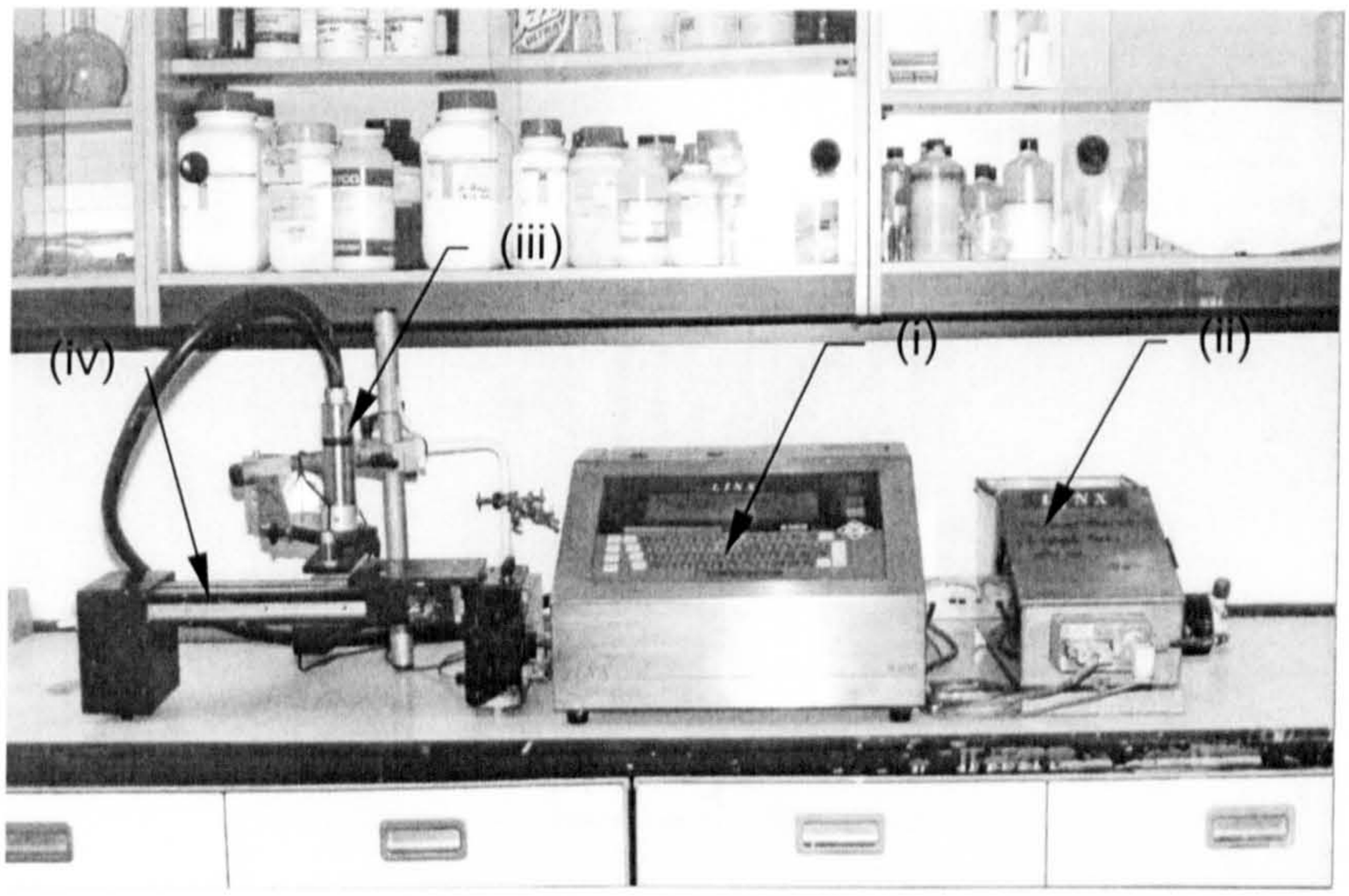

Figure 3.6 Printer system used in this study: (i) Linx 6200S continuous printer, (ii) ink dispensing system, (iii) MIDI printhead and (iv) table.

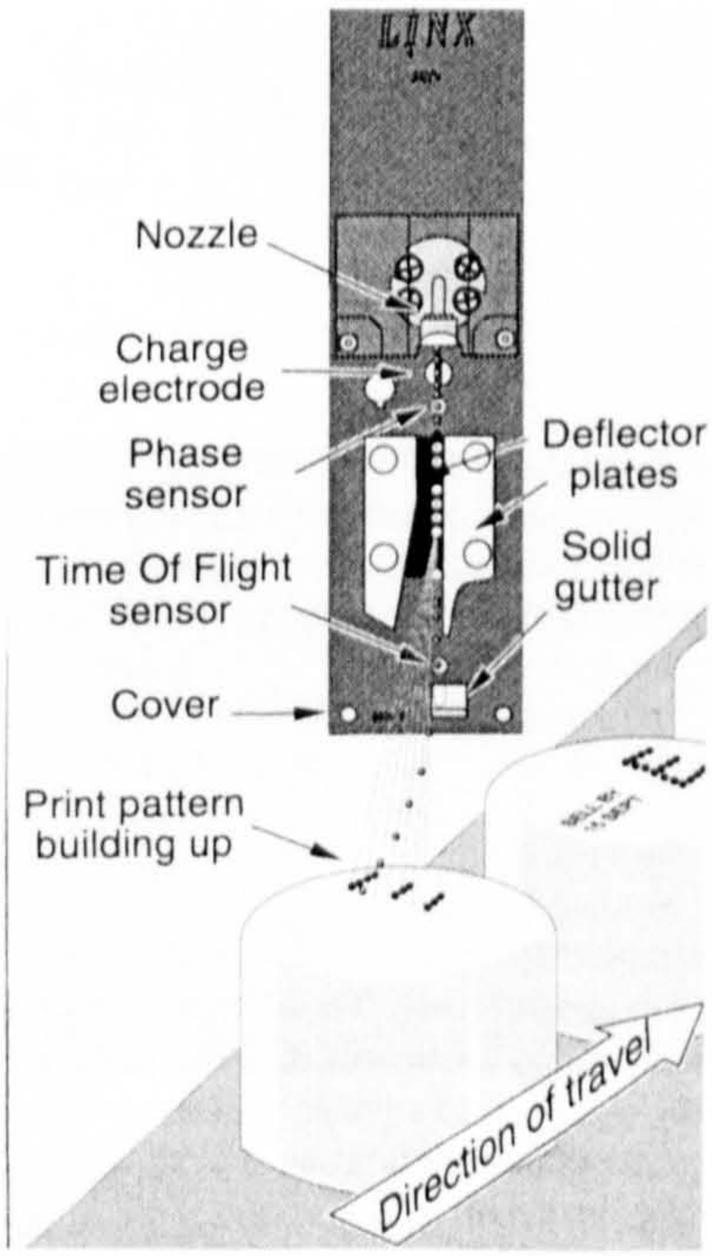

Figure 3.7 Linx MIDI printhead.

(a)

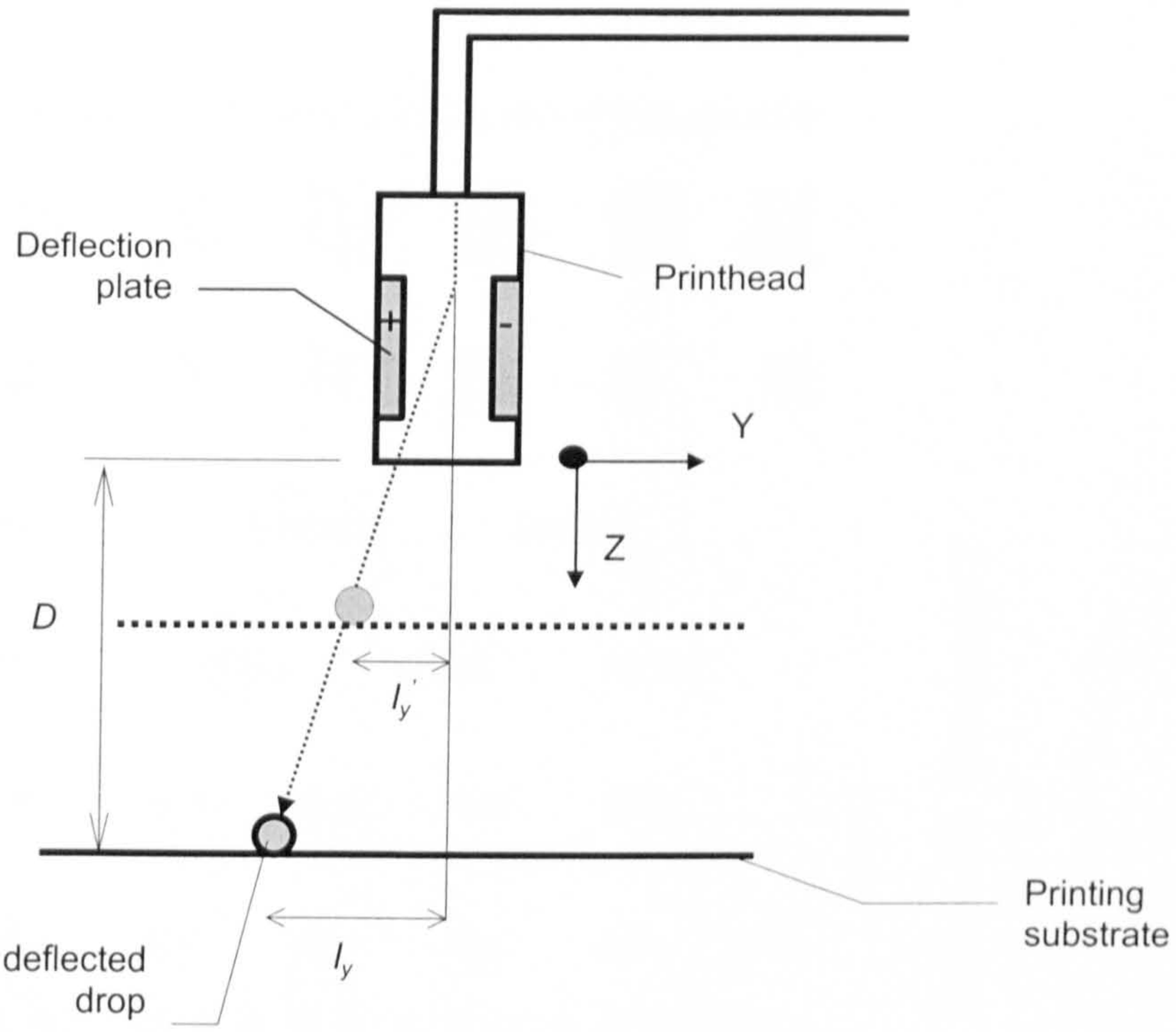

(b)

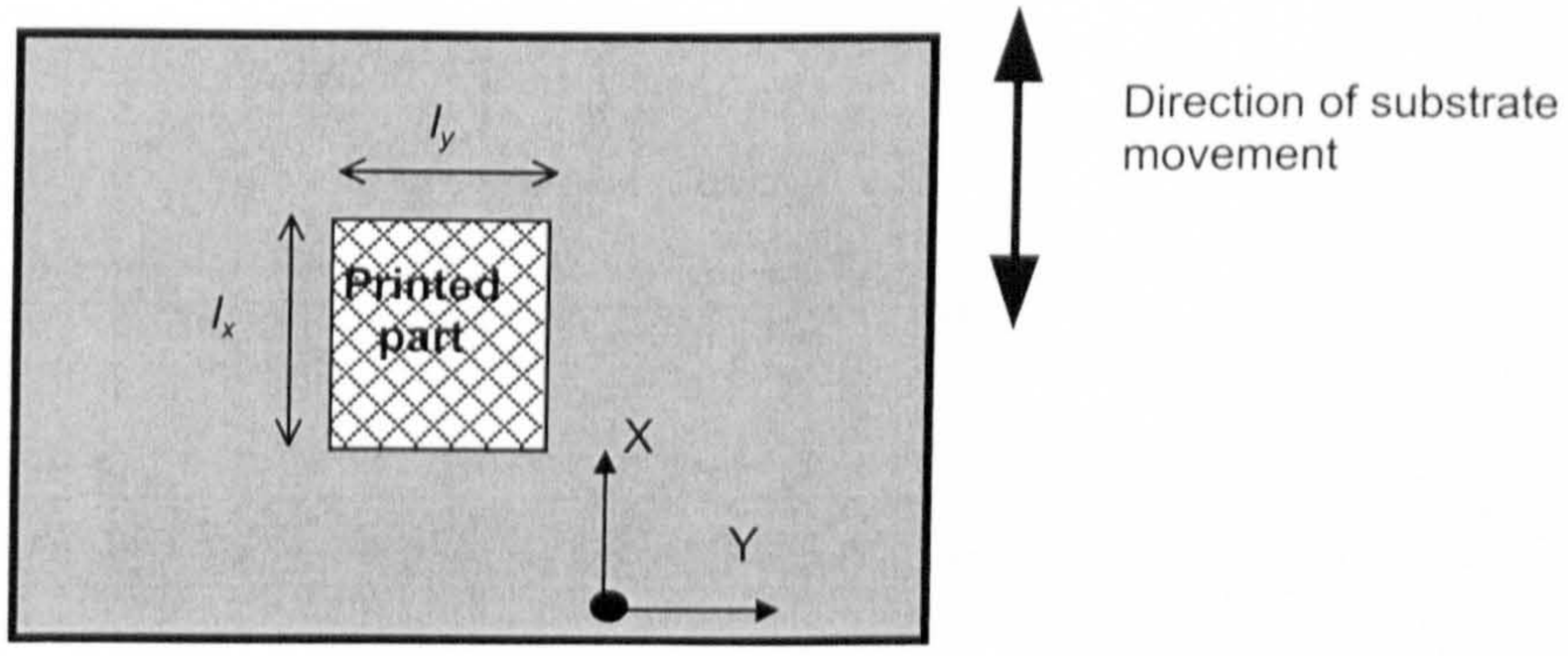

Figure 3.8 Setting up the printhead: (a) side view and (b) top view.

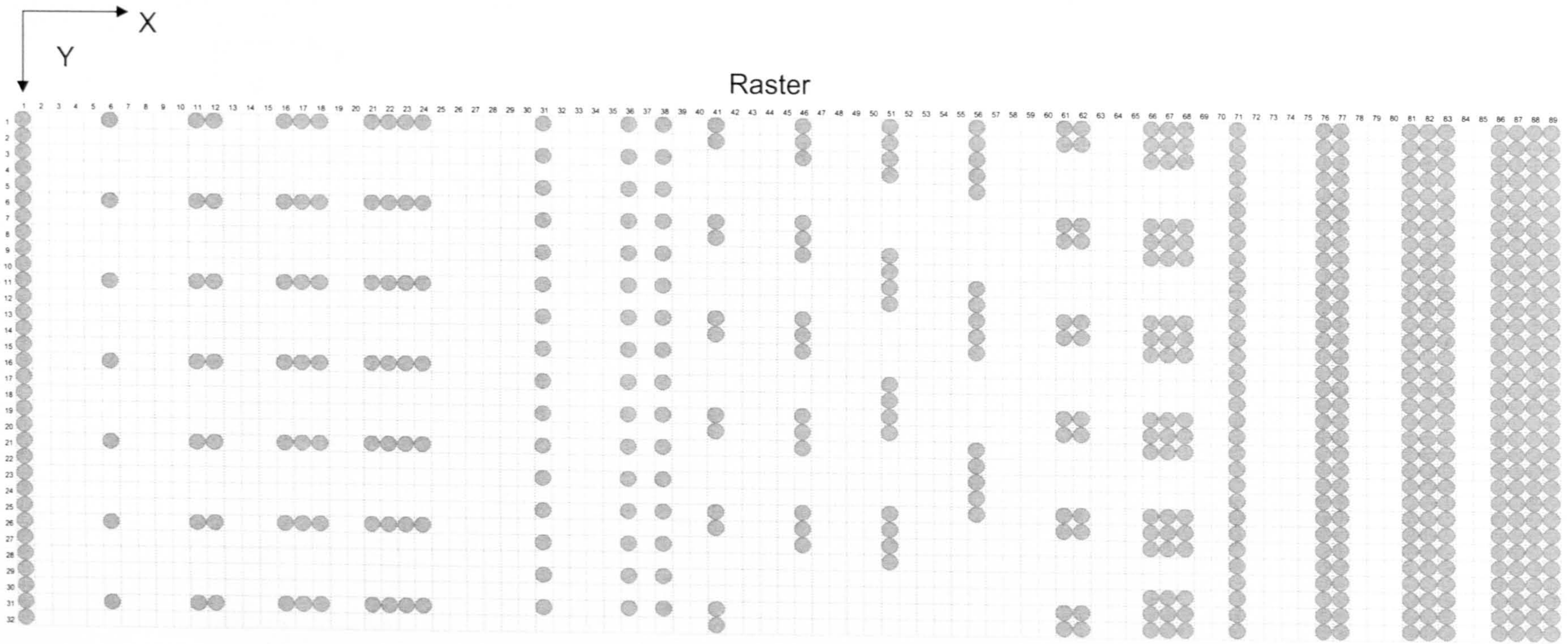

Figure 3.9 Test pattern 2

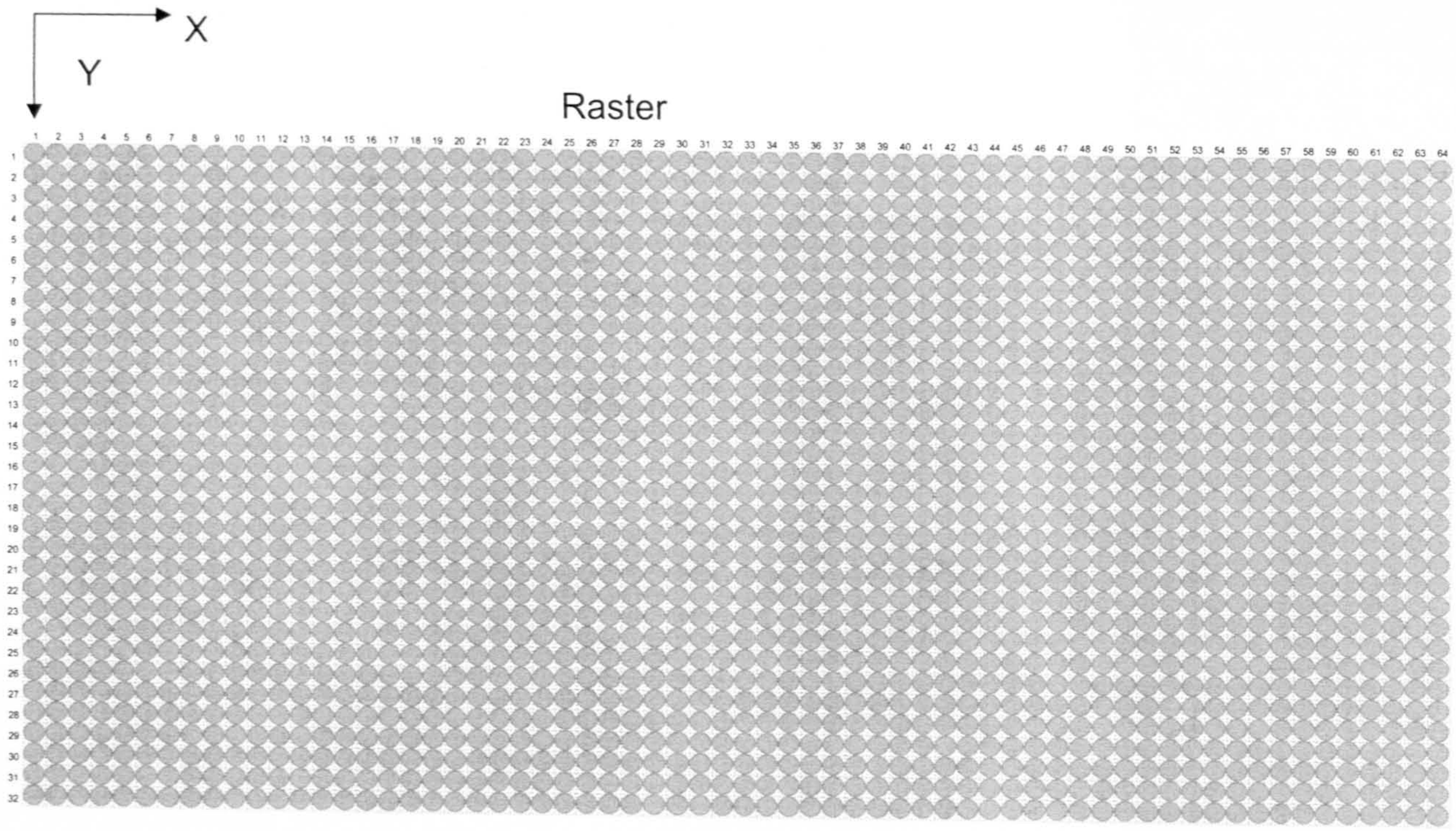

Figure 3.10 Test pattern 3

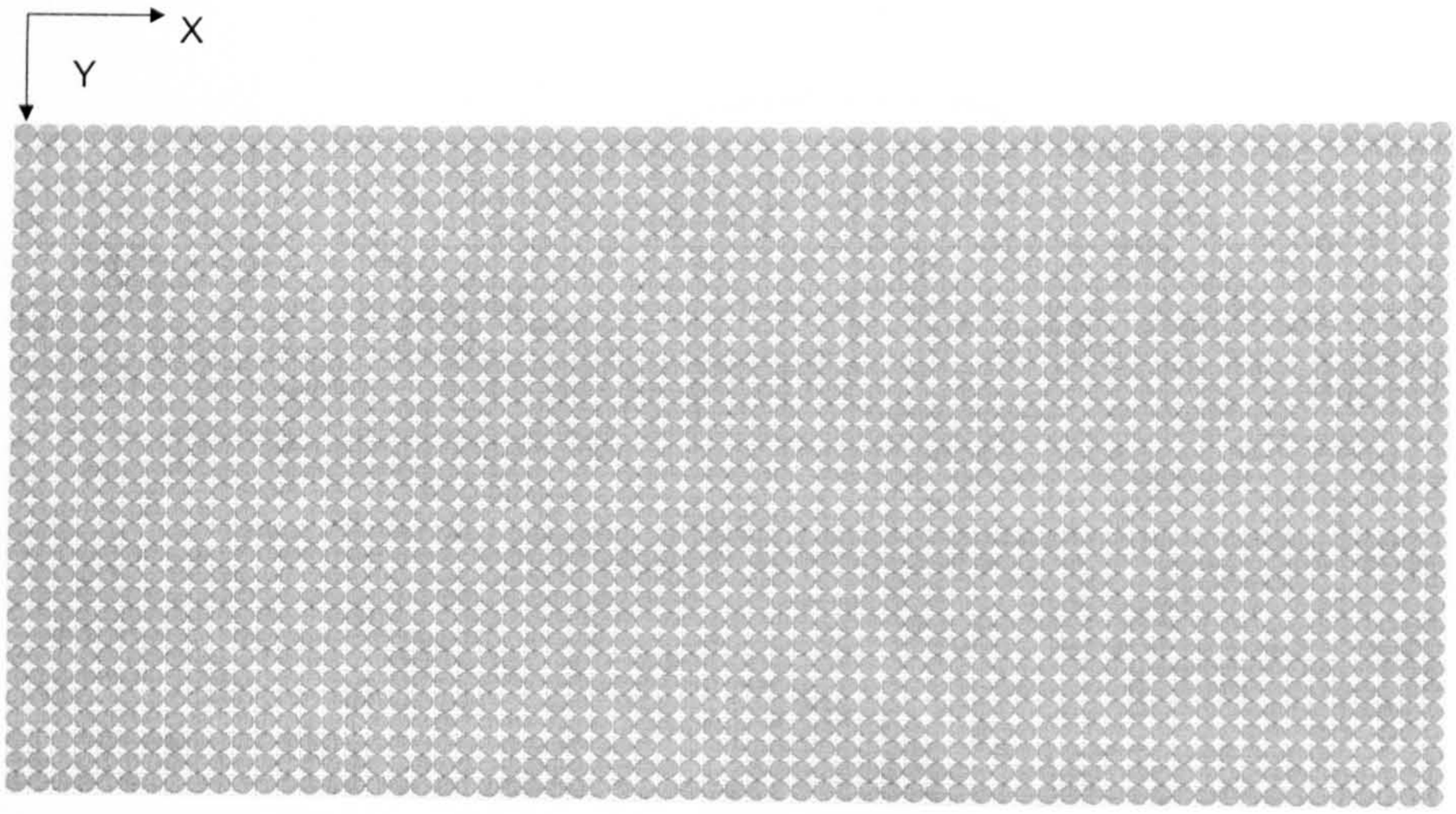

Test pattern 4a

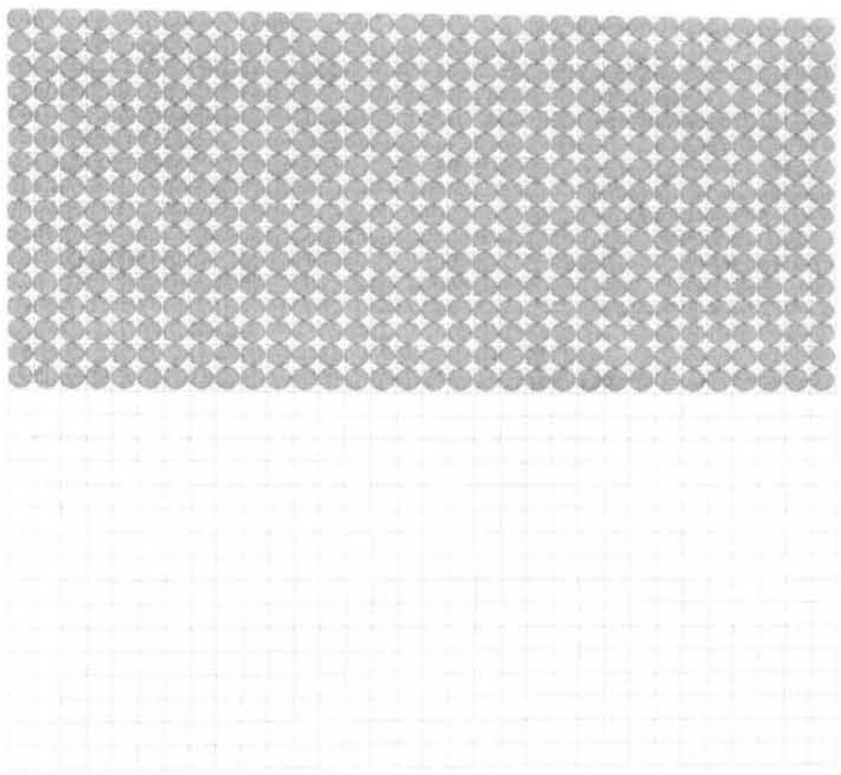

Test pattern 4b

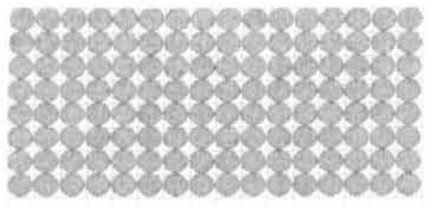

Test pattern 4c

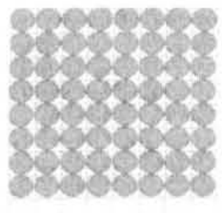

Test pattern 4d

Figure 3.11 Test pattern 4

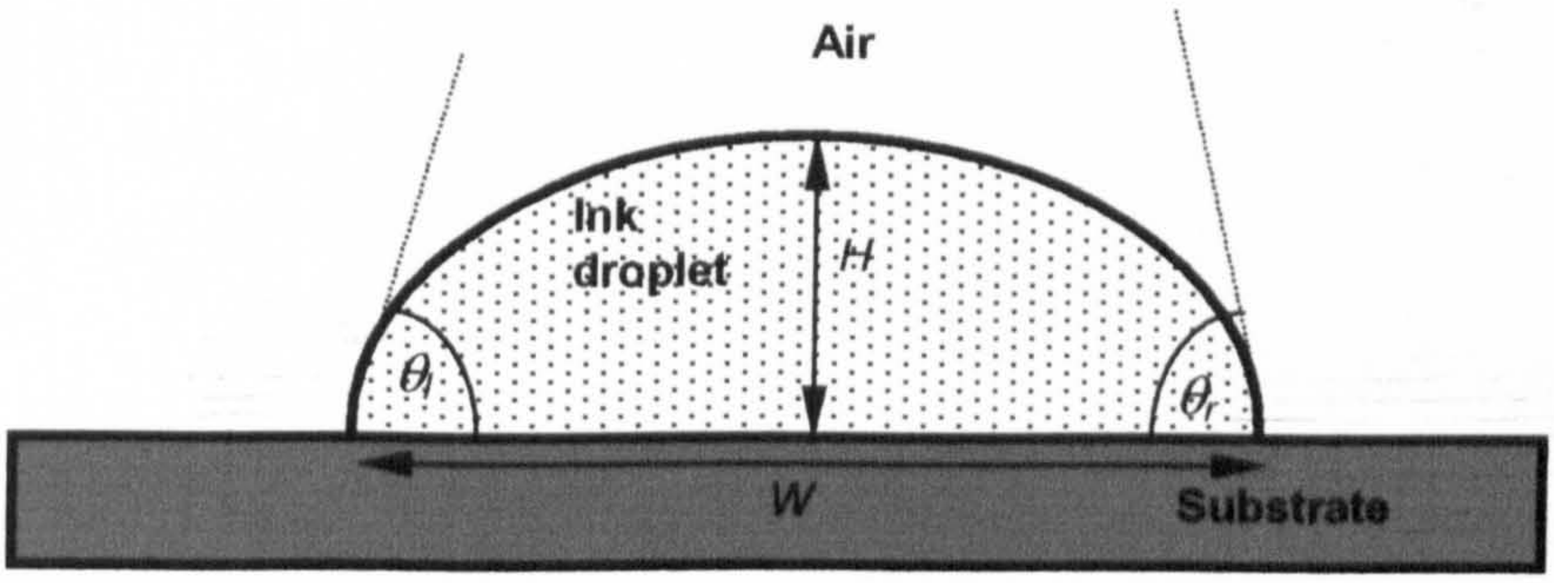

Figure 3.12 Contact angle (θ), base (W) and height (H) of a sessile droplet on substrate.

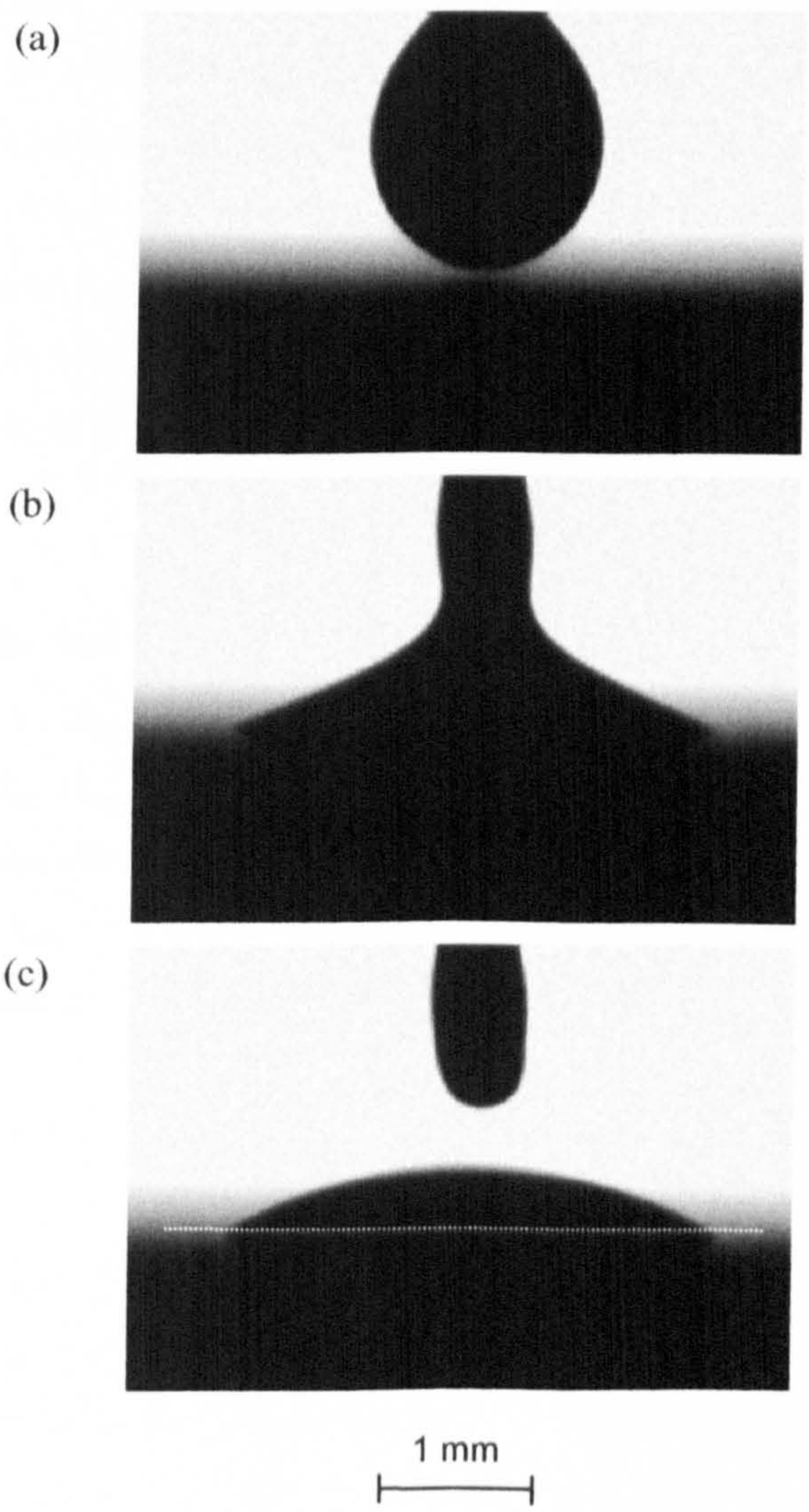

Figure 3.13 Illustration showing droplet deposition procedure: (a) pendant droplet, (b) detaching droplet and (c) detached droplet. The dotted line indicates baseline.

Chapter

4

Development of Ink Preparation Procedure

An important obstacle to overcome is to be able to print the ceramic ink continuously without interruption. This requires a homogenous and stable ink. In this chapter, test solutions were first used to set up the printer and establish the working ranges of viscosity and electrical conductivity. Next, different mixing equipment was employed to process the ceramic-polymer blend and the sedimentation behaviours of the inks were investigated. These were followed by using various preparation routes to produce stable ink, which could be circulated continuously in the printer. The properties of this ink were also measured at different stages during preparation.

4.1 Test Solution

A viscosity of 3 - 4 mPa s and electrical conductivity of 0.1 S m^{-1} (both at 20°C) are required for printing [Williams, 1998]. Thus, different amounts of polyvinylbutyral (PVB) and NH_4NO_3 were dissolved in industrial methylated spirit (IMS) to arrive at a solution with these properties. The first series of polymeric ink contained only PVB whereas the second series contained both PVB and NH_4NO_3.

4.1.1 Characteristics

(a) Viscosity

The amount of PVB in the first series of polymeric ink was varied at 2, 3, 4, 5 and 8 wt. % and their viscosities are shown in Figure 4.1. From the figure, the suitable level of PVB in the polymeric ink to be used on printer is 4 wt. %. At this concentration, the viscosity of the ink was within the range of 3 - 4 mPa s recommended by the printer manufacturer.

(b) Electrical conductivity

The variation in electrical conductivity of the 4 wt. % polymeric ink at different NH_4NO_3 concentrations (inks PE1, PE2 and PE3 in Section 3.5.2a) is shown in Figure 4.2. The relationship can be fitted into a linear one with

$$S = 0.165\,x + 0.026$$

Where S is the electrical conductivity (in S m^{-1})

x is the amount of electrolyte (g) in 100 ml of IMS and $0.3 \leq x \leq 1.2$.

Song and his co-workers used 1.2 g of NH_4NO_3 per 100 ml of IMS in their ceramic ink [Song *et al.*, 1999]. However, it is desirable to reduce the amount of additives in the ink in order to yield a higher ceramic/additive ratio in the green part. This is especially so for the NH_4NO_3, which has a high density of 1730 kg m^{-3}. In Sections 4.2 - 4.4 of this chapter, the ceramic inks being evaluated contained 1.2 g of NH_4NO_3 per 100 ml of IMS. However, in Section 4.5 and chapters 5 and 6, which involved inks for printing, the amount of NH_4NO_3 used in the inks was 0.8 g per 100 ml of IMS.

4.1.2 Printing Test Solutions of Different Electrical Conductivity Values

Test pattern 1, which was made up of alphanumeric characters, was printed using inks PE1, PE2 and PE3. Inks PE1 and PE3 had electric conductivity values lower and higher, respectively, than the range that was recommended by the printer manufacturer (~ 0.1 S m^{-1}) [Williams, 1998] whereas ink PE2 had its value within the range. Results of the printings are discussed in the following.

For printing to occur, the jet emerged from the nozzle must be broken up into droplets. In the case of the low conductivity ink (PE1), although droplets were formed at the charge electrode, successive prints lacked consistent quality. In a low conductivity ink, the charge induced on the droplet is lower and thus a lower λ (Equation 2.2). At a constant modulation frequency, this produced a low droplet velocity (Equation 2.1) or a high value of time of flight, TOF, which is the time required for a droplet to travel between two fixed points. Changing printing conditions such as pressure setting and modulation frequency did not help to lower the TOF. This is because the printer control interpreted a high TOF value as an indication of high viscosity, even though the real cause was due to low electrical

conductivity. In this instance, the printer control instructed the pump to increase pressure in order to reduce TOF. When this failed, it added solvent to dilute the ink, which lowered the electrical conductivity of the ink. Likewise, a high electrical conductivity in ink PE3 (~ 0.23 S m^{-1}) also resulted in unstable printing conditions with great fluctuation in the TOF values. Although the jet was broken down into droplets, no printing was possible.

In the printing of ink PE2, the TOF value was also monitored during successive printings over a period of 1.80 x 10^3 s (or 30 min). Its deviation from the calibrated value at 18500 was within ±40%, a condition necessary for continuous printing [Linx, 1996]. Prints with good resolution were produced.

4.1.3 Optimum Printhead-to-Substrate Distance

The average dimensions of the printed part, which comprised of a matrix of 32 rasters, at different printhead-to-substrate distance (D) were calculated from five prints and given in Table 4.1. As each raster was made up of 32 dots, the print should be undistorted at the optimum D, i.e. $l_x = l_y$, where l_x and l_y are the dimensions of the print in the X and Y-directions, respectively. From the table, the optimum value for D is 7.0 mm.

Table 4.1 Average dimensions of printed parts.

D / mm	l_x / mm	l_y / mm
4	10.0	9.0
5	9.9	9.5
7	10.0	10.0
8	10.1	10.4
10	10.0	10.6
12	9.9	11.0

4.2 Effects of Electrolyte Addition and Ultrasonic Disruption

Group I inks, which comprised of C, U and EU, were formulated to study the effects of ultrasonic disruption and electrolyte addition on the ink's sedimentation behaviour (Section 3.2). Ink C was used as the reference ink, which contained no electrolyte and was not

subjected to ultrasonic disruption. Both inks U and EU were subjected to ultrasonic disruption. Ink EU also contained electrolyte, NH_4NO_3.

4.2.1 Sedimentation

Three zones, as shown in Figure 4.3, were observed in the sedimentation experiment carried out with inks C, U and EU. There was a layer of cloudy liquid at the top, followed by a suspension, which seemed to get more concentrated with increasing depth, and a layer of sediment at the bottom. All the three inks underwent similar sedimentation behaviour. As the inks were left to settle, the sediment was increasing. At the same time, the suspension-cloudy liquid interface was moving downwards. Consequently, there was a continual expansion of the cloudy liquid and a concomitant contraction of the suspension. The variations in volumes of the cloudy liquid, suspension and sediment for inks C, U and EU are shown in Figures 4.4 – 4.6.

For ink C, the sediment increased rapidly within the first 8.64×10^4 s (24 hour), but levelled off subsequently. Concurrently, its suspension-cloudy liquid interface descended at a fast rate but slowed down after 8.64×10^4 s, as shown in Figure 4.7, which compares the movement of the suspension-cloudy liquid interfaces of inks C, U and EU over the first 6.05×10^5 s of the sedimentation study. This slowing down was probably caused by vibration waves moving up through the suspension volume as the powder in the sediment hit the bottom of the test tube [Tiller and Khatib, 1984]. The rapid sedimentation during the first 8.64×10^4 s (24 hour) indicates rapid flocculation in ink C as soon as the study commenced. However, both the cloudy liquid of inks U and EU only became discernible from the suspension after 2.88×10^4 s.

The interface between the sediment and suspension was discernible for all the three inks but no sharp demarcation existed between the cloudy liquid and the suspension. To help to discern the second demarcation, a bright light was shone behind the test tubes when readings were taken. The degree of clarity diminished from inks U, EU to C, in the said order. This accounts for a larger variation of ±0.4 ml for the five samples of ink C (Figure 4.4) compared to ±0.1 ml for ink U and ±0.2 ml for ink EU (Figures 4.5 and 4.6, respectively).

Figure 4.8 compares the volumes of the sediment and the suspension of inks C, U and EU after 8.64×10^4 s. For the period between 8.64×10^4 s to 1.73×10^6 s, the suspension was contracting at an average rate of 2×10^{-6}, 1.4×10^{-6} and 1.6×10^{-6} ml s^{-1} for inks C, U and EU, respectively. From 1.73×10^6 s onwards, the suspensions of the three inks were reducing at approximately the same rate (2×10^{-6} ml s^{-1}). For the sediments, between 8.64×10^4 s to 8.64×10^5 s, they were increasing slowly for the three inks. The same increment of 0.4 ml was experienced during this period compared to 1.2, 0.9 and 1.2 ml, which were achieved within the first 8.64×10^4 s for inks C, U and EU, respectively, upon the commencement of sedimentation. From 8.64×10^5 s onwards, the sediments remained at a fairly constant level. The final volumes of the sediment at 2.59×10^6 s are tabulated in Table 4.2, with ink U yielding the lowest sediment volume throughout the period of study. The inks were also re-dispersed at this stage but was difficult to do so for ink U. However, ink C could be easily re-dispersed with gentle stirring while ink EU needed more vigorous stirring.

Table 4.2 Final sediment volumes at 2.59×10^6 s.

Ink	Sediment volume
	ml
C	1.8
U	1.6
EU	1.8

4.2.2 Effectiveness of Ultrasonic Disruption

(a) In relation to sedimentation behaviour

It is important that the ZrO_2 powder be well dispersed in the solvent as this influences strongly the viscosity of the ink and hence its flow through the printer nozzle. The ink should also be free from agglomerations and resist flocculation when dispensed at the nozzle. Otherwise, density variation will exist in the printed parts [Edirisinghe, 1997]. In the colloidal ink, several binding forces between the powders have to be overcome in order to achieve an acceptable deagglomerated state. The two major forces are: (i) van der Waals interaction and (ii) binding forces due to wetting liquid [Bossel *et al.*, 1995]. The forces can be overcome by chemical and/or mechanical means so that there are good wetting of solid powders by the liquid, breakdown of agglomerates and stabilisation of the suspension to

prevent re-agglomeration. The use of twin roll milling followed by ultrasonic treatment was found to be effective in achieving a homogenous mixture for direct ceramic ink-jet printing [Song *et al.*, 1999].

The effect of ultrasonic disruption was most significant during the first 8.64 x 10^4 s after ink preparation. As discussed before, compared to ink C, the cloudy liquid and the sediment in ink U only started to become discernible after 2.88 x 10^4 s (Figure 4.7). Furthermore, the suspension of ink U was contracting at a slower rate. The sediment volume was also lower; indicating that ink U was less flocculated than ink C. At 2.59 x 10^6 s, the final sediment volume of ink U was 11% lesser than that of ink C (Table 4.2).

(b) In relation to the state of dispersion

Figure 4.9 shows the micrographs of inks C, U and EU at the beginning of sedimentation study. An open structure of flocculates, consisting of loosely bounded clusters of particles and agglomerates, was present in ink C (Figure 4.9a). In contrast, uniform-sized particles of ~ 0.5 μm prevailed in ink U (Figure 4.9b). These particles were thus able to pack themselves more effectively when settled to the bottom of the test tube (Figure 4.10a), hence yielding a dense sediment, which was difficult to disperse by manual stirring. On the other hand, the loose and "networked" structure in ink C enhanced sedimentation, giving rise to a fast settling rate. When settled to the bottom of the test tube, the agglomerates bridged readily, giving loose sediment of larger volume, which was easier to disperse (Figure 4.10b).

4.2.3 Effect of Electrolyte Addition

(a) In relation to sedimentation behaviour

As in ink U, sediment in ink EU only became discernible after 7.20 x 10^3 s and the suspension-cloudy liquid interface was arrested for at least 2.88 x 10^4 s after sedimentation had commenced. After that, there was a rapid increase in sediment and downward movement of the interface (Figure 4.7). Throughout the period of study, the sediment volume of ink EU was always greater than that of ink U. There was thus greater flocculation in ink EU.

(b) In relation to state of dispersion

Figure 4.9c shows the micrograph of a relic of a droplet of ink EU taken at the beginning of the sedimentation study. The average size of particles is ~ 0.5 μm, which is the same as that of ink U. The particles formed agglomerates, which clustered with one another and yielded a more opened structure with less edge to edge contacts than ink U. The clusters of agglomerates inevitably accelerated sedimentation. On reaching the bottom of the test tube, they packed in a more compact manner than ink C but in a less orderly pattern than ink U. This explained the ease of re-dispersing ink EU than ink C but less so when compared with ink U.

4.3 Effectiveness of Twin and Triple Roll Millings

Inks 2R and 3R, which were prepared from mill products processed by twin and triple roll millings, respectively, were subjected to identical conditions of ultrasonic disruption. Loss-on-ignition tests and SEM were performed on the mill products to compare their homogeneity. In addition, the sedimentation behaviours of inks 2R and 3R were compared.

4.3.1 Loss-on-Ignition

Results of the loss-on-ignition test of the two mill products are given in Table 4.3. Both mixing routes produced ceramic-polymer blends with the same ZrO_2 content of 53.1 vol. %, which is higher than the expected value of 50 vol. %. The products can be considered as homogenous since the maximum variation in ZrO_2 was within ±0.1 vol. %.

Table 4.3 Content of ZrO_2 in the mill products from which inks 2R and 3R were made.

Sample	ZrO_2 CONTENT IN MILL PRODUCT			
	Ink 2R		Ink 3R	
	Wt. %	Vol. %	Wt. %	Vol. %
1	86.63	53.1	86.61	53.0
2	86.61	53.1	86.56	52.9
3	86.62	53.0	86.60	53.0
4	86.61	53.0	86.67	53.2
5	86.63	53.1	86.70	53.2
Average	86.62	53.1	86.63	53.1
Variation	0.01	0.1	0.06	0.1

4.3.2 State of Dispersion

Figure 4.11 shows the micrographs of the mill products processed by twin and triple roll millings. Both micrographs show that millings had yielded particles of approximately the same size, in the range of 0.5 - 1 μm. These particles joined with one another to form a continuous matrix.

4.3.3 Sedimentation

The sedimentation results of inks prepared from mill products processed using the twin (ink 2R) and triple (ink 3R) roll mills are shown in Figure 4.12. Both inks underwent similar stages described in section 4.2.1 where three zones were observed.

Although the loss-on-ignition test and micrographs from SEM did not reveal any significant distinction between the two types of mill product, their inks displayed different sedimentation results. Firstly, the sediment of ink 2R was always larger than that of ink 3R throughout the study, indicating greater flocculation in the former. At 2.59 $x10^6$ s (30th day), the average volumes of sediment in inks 2R and 3R were 1.8 and 1.5 ml, respectively. Thus, there was a 17% reduction in sediment volume if the triple roll mill was used to produce the ceramic-polymer blend. Secondly, the interface of suspension-cloudy liquid was descending at a faster rate for ink 2R than 3R. The average contracting rates of the suspension volume during the period 8.64×10^4 - 2.59×10^6 s were 1.8×10^{-6} ml s^{-1} and 1.2×10^{-6} ml s^{-1} for inks 2R and 3R, respectively.

The lesser flocculation experienced in ink 3R could be attributed to a higher fraction of broken particles in the mill product due to a greater shear rate at milling arose from the smaller gap between the rolls and the higher differential surface speeds of the rolls. According to Manas-Zloczower [1991], who calculated the theoretical fraction of broken particles of carbon-black elastomer in an intensive mixer (e.g. roll mill), these factors will result in higher agglomerate breakdown. Hence, more agglomerates were expected to exist within the mill product used for making ink 2R. They also tended to cause a more opened structure in the sediment volume. This explains the larger sediment volume in ink 2R.

4.4 Effect of Increasing Powder/Polymer Ratio in Ink

Group III inks were made with volumetric ratio of powder to polymer (dispersant, polyvinylbutyral and dibutyl sebacate) at 50:50 (ink P1), 60:40 (ink P2) and 70:30 (ink P3). Their mill products were processed by triple roll milling, from which the inks were prepared.

4.4.1 Loss-on-Ignition

Table 4.4 lists the amount of ceramic in the mill products for inks P1, P2 and P3. The average volumetric loadings of ZrO_2 in the mill products were 53.1%, 66.2% and 76.6% for inks P1, P2 and P3, respectively. As before, processing by triple roll milling caused some losses of polymer and the mill products thus contained a higher content of ceramic. Overall, homogeneity in the samples was good, with maximum variations of 0.06, 0.21 and 0.19 wt. % or 0.1, 0.6 and 0.7 vol. % for mill products of inks P1, P2 and P3, respectively. The variation in the mill product of ink P1 was at least three times (in wt. %) or six times (in vol. %) lesser than those for inks P2 and P3. This is because a higher ratio of polymer in the composition helped to distribute the powder evenly within the matrix.

Table 4.4 Ceramic contents in mill products of inks P1, P2 and P3 as determined by loss-on-ignition.

Sample	ZrO_2 CONTENT IN MILL PRODUCT					
	Ink P1		Ink P2		Ink P3	
	Wt. %	Vol. %	Wt. %	Vol. %	Wt. %	Vol. %
1	86.61	53.0	91.67	66.0	95.04	77.5
2	86.56	52.9	91.84	66.5	94.70	76.2
3	86.60	53.0	91.91	66.7	94.70	76.2
4	86.67	53.2	91.81	66.4	94.61	75.9
5	86.70	53.2	91.39	65.2	94.95	77.1
Average	86.63	53.1	91.72	66.2	94.80	76.6
Variation	0.06	0.1	0.21	0.6	0.19	0.7

4.4.2 State of Dispersion

Figure 4.13 shows the micrographs of the mill product of inks P1, P2 and P3. All the three micrographs revealed that triple roll mill had effectively broken down the agglomerates and distributed the particles in the matrix. The average particle size in the mill products is in the

range of 0.5 - 1 μm.

4.4.3 Sedimentation

The sedimentation results of inks P1, P2 and P3 over a period of 2.59 x 10^6 s (30 days) are given in Figure 4.14. These inks underwent similar stages as previously described in section 4.2.1. For the period 8.64 x 10^4 - 2.59 x 10^6 s, the suspension-cloudy liquid interface was descending at a constant rate for all the three inks. The suspension volumes were contracting at an average rate of 1.2 x 10^{-6}, 2.4 x 10^{-6} and 2.2 x 10^{-6} ml s^{-1} for inks P1, P2 and P3, respectively. Ink P1 thus had the largest volume of suspension throughout the period of study. It also had the smallest sediment volume and there was thus lesser flocculation. The average volume of sediment at 2.59 x 10^6 s amounted to 1.5, 1.6 and 1.6 ml for inks P1, P2 and P3, respectively.

4.5 Ink for Continuous Printing

4.5.1 Requirements

The ink with nominal composition given in Table 3.5 was subjected to printing. Before printing could commence, it is a prerogative that the jet passing through the nozzle must be broken up into a series of droplets. This phenomenon is complex and is dependent on the properties of ink. To ensure that printing is continuous and the production of consistent prints, the properties of the ink (such as viscosity and electrical conductivity) should be maintained throughout the process. Although the printer system is installed with a pump, which circulates the ink constantly, this circulation is unable to keep the ceramic ink in its original dispersed state, i.e. as when it was subjected to ultrasonic disruption (ink U). Attempts to print it via route 1 (Table 4.5) were unsuccessful as the jet failed to break up into droplets at the nozzle. Another possible reason could be due to high viscosity of ink U (see 4.5.2). By subjecting the ink to 8.64 x 10^4 s of sedimentation (route 2) and followed by filtration using a 10 μm filter (route 3), inks US1 and US1F1 were able to break up into droplets but this could not be sustained for more than 3.00 x 10^3 s. With an additional filtration step using a 5 μm filter (route 4), the jet was able to break up into droplets. Printing was made possible for ~ 5.40 x 10^3 s before the printer aborted its operation automatically due to the large variation in TOF. By further subjecting the ink to an

additional 8.64 x 10^4 s of sedimentation (route 5), the ink was able to circulate within the printer continuously for at least 1.73 x 10^5 s. The prints produced were also consistent.

Table 4.5 Evaluation of different printing routes.

Route	Ink	Sedimentation duration	Minimum filter size	Length of continuous circulation in printer
		s	μm	s
1	U	0	-	-
2	US1	8.64 x 10^4	-	3.00 x 10^3 [a]
3	US1F1	8.64 x 10^4	10	3.00 x 10^3 [a]
4	US1F2	8.64 x 10^4	5	5.40 x 10^3
5	US2F2	1.73 x 10^5	5	1.73 x 10^5 [b]

Note: [a] - the printer shut down automatically after it failed to sustain droplet break-up
[b] - the value is the minimum time

4.5.2 Evaluation of Characteristics of Printing Ink

The ZrO_2 content, density, viscosity, electrical conductivity and surface tension of the ink at various stages of the ink preparation were evaluated and are shown in Figure 4.15.

(i) ZrO_2 content (W_c):

The wt. % of ceramic in the ink, W_c, at different stages was estimated by loss-on-ignition test. There was a continual decrease in the ceramic content as ink preparation proceeded. The sharp drops occurred from inks U to US1 and from inks US1F2 to US2F2, during which the ink was settling and the sediment was accumulating. The reduction in W_c between inks U and US1 amounted to 4 wt. % whereas that between U and US2F2 was 12 wt. %. With about 1 - 2 wt. % of ZrO_2 powders 'lost' at each filtration (inks US1F1 and US1F2), the amount of loss resulted from 1.73 x 10^5 s of sedimentation, was estimated to be 9 wt. %. From the sedimentation results of ink 3R in Figure 4.12, the rate of increase in the sediment volume was 2.2 x 10^{-6} ml s^{-1} at 8.64 x 10^4 s, but this retarded to 1.1 x 10^{-6} ml s^{-1} at 1.73 x 10^5 s. Thus, the ink was still unstable at 8.64 x 10^4 s and this explains one of the reasons why it was difficult to sustain a break-up jet in the electrode for ink US1. Although the ink was still settling at 1.73 x 10^5 s, it did so at a slower rate. The continuous circulation by the pump within the printer system was sufficient to keep the ink from settling and hence maintaining its properties from large variation.

The vol. % of ceramic in the ink was estimated and given in Table 4.6. US1 was processed in similar way as the ink used by Song *et al.* [1999] except that a triple roll mill was used in place of a twin roll mill. Although this ink was able to pass through the printer and generate drop break up, the latter could not be sustained for more than 3.00 x 10^3 s because it was 'unstable'. In attempting to print these inks (US1, US1F1 and US1F2), the printer had to be shut down and restarted if printing over long period was required.

Table 4.6 Estimated powder loading (in vol. %) of inks at different stages of the ink preparation.

Sample	Estimated Powder Loading of Inks				
	U	US1	US1F1	US1F2	US2F2
	Vol. %	Vol. %	Vol. %	Vol. %	Vol. %
1	5.1	4.2	4.0	3.6	2.5
2	5.1	4.3	3.9	3.6	2.5
3	5.1	4.2	3.8	3.7	2.5
Average	5.1	4.2	3.9	3.6	2.5

(ii) Density, ρ

The density of the ink at various stages of the ink preparation was measured at 20°C. The density curve (Figure 4.15b) followed closely the trend of W_c (Figure 4.15a). Notably drops were also observed after the ink had been subjected to sedimentation periods of 8.64 x 10^4 s (ink US1) and 1.73 x 10^5 s (ink US2F2) where substantial loss of ceramic content occurred.

(iii) Viscosity, η

The viscosity of the ink, η was measured at 20°C and shear rate 1000 s^{-1}. The drop in viscosity (Figure 4.15c) also occurred after the ink had been subjected to sedimentation periods of 8.64 x 10^4 s (ink US1) and 1.73 x 10^5 s (ink US2F2). These also corresponded to changes observed in W_c (Figure 4.15a). Although inks US1, US1F2 had viscosity values within the specification recommended by the manufacturer, they could not be printed continuously.

(iv) Electrical conductivity, S

The electrical conductivity S of the ink was also determined at 20°C. About the same value of S (~ 0.126 S m^{-1}) was obtained at different stages of the ink preparation. This indicates that the electrolyte was dissolved homogeneously in the solvent during ink preparation. Any losses of solvent through evaporation or separation of the salt from the solvent was negligible.

(v) Surface tension, γ

The surface tension values, measured at 20°C, remained at a constant value of about 24 mN m^{-1} for the various inks. As in the case of S, γ was not affected by sedimentation and filtration.

4.6 Summary and Conclusions

A test solution containing polyvinylbutyral and NH_4NO_3 in industrial methylated spirit was used to establish suitable working ranges of viscosity and electrical conductivity for the printer. Three series of ceramic inks of ~ 5 vol. % ZrO_2 were also prepared under different conditions, where the effectiveness of different mixing processes (ultrasonic disruption, milling by twin or triple roll) and the effect of additives (electrolyte addition and polymer content) were studied by monitoring sedimentation over 2.59×10^6 s (30 days).

(i) Ultrasonic disruption was an effective way to disperse the ink homogeneously and breaking down agglomerates in mill products. The ink produced did not flocculate for at least 2.88×10^4 s after subjected to ultrasonic disruption. In addition, it had a smaller final sediment volume and a larger suspension of volume at the end of the study. Without ultrasonic disruption, the ink prepared from mill product flocculated immediately when sedimentation commenced.

(ii) The addition of NH_4NO_3 as an electrolyte in the ink reduced the effect of ultrasonic disruption. The length of time for which the ink remained deflocculated was reduced to 7.20×10^3 s. Consequently, a larger sediment volume and smaller suspension volume were resulted compared with the ink prepared without NH_4NO_3.

(iii) Both twin and triple roll millings have yielded homogenous mill products for ceramic ink-jet printing with a maximum variation of ±0.1 vol. % ZrO_2. Although the loss-on-ignition and micrographs by SEM did not show significant difference between the products by the two methods, the sedimentation results of the inks were different. Ink prepared from mill product made by triple roll mill had a smaller sediment volume and larger suspension volume and thus less flocculated. The final sediment volume at 2.59×10^6 s was 17% lower than that of ink prepared from twin roll milling.

(iv) Increasing the volumetric ratio of ZrO_2 to polymer (dispersant, polyvinylbutyral and dibutyl sebacate) from 50:50 to 60:40 or 70:30 was found to increase flocculation in the ink.

Printing of the ceramic ink was carried out without interruption of any kind. This was made possible by the use of stable ink obtained by 1.73×10^5 s of sedimentation and filtration with a 10 μm and then a 5 μm filters. The properties of the ink at various stage of the preparation procedure (between ultrasonic disruption and before printing) were evaluated. The electrical conductivity and surface tension were unaffected by sedimentation and filtration. However, the density and viscosity reduced drastically after sedimentation. The reduction was attributed to losses of ceramic content. The powder loading of the printable ink was 2.5 vol. % ZrO_2 (or equivalent to 37.6 vol. % ZrO_2 in green printed part).

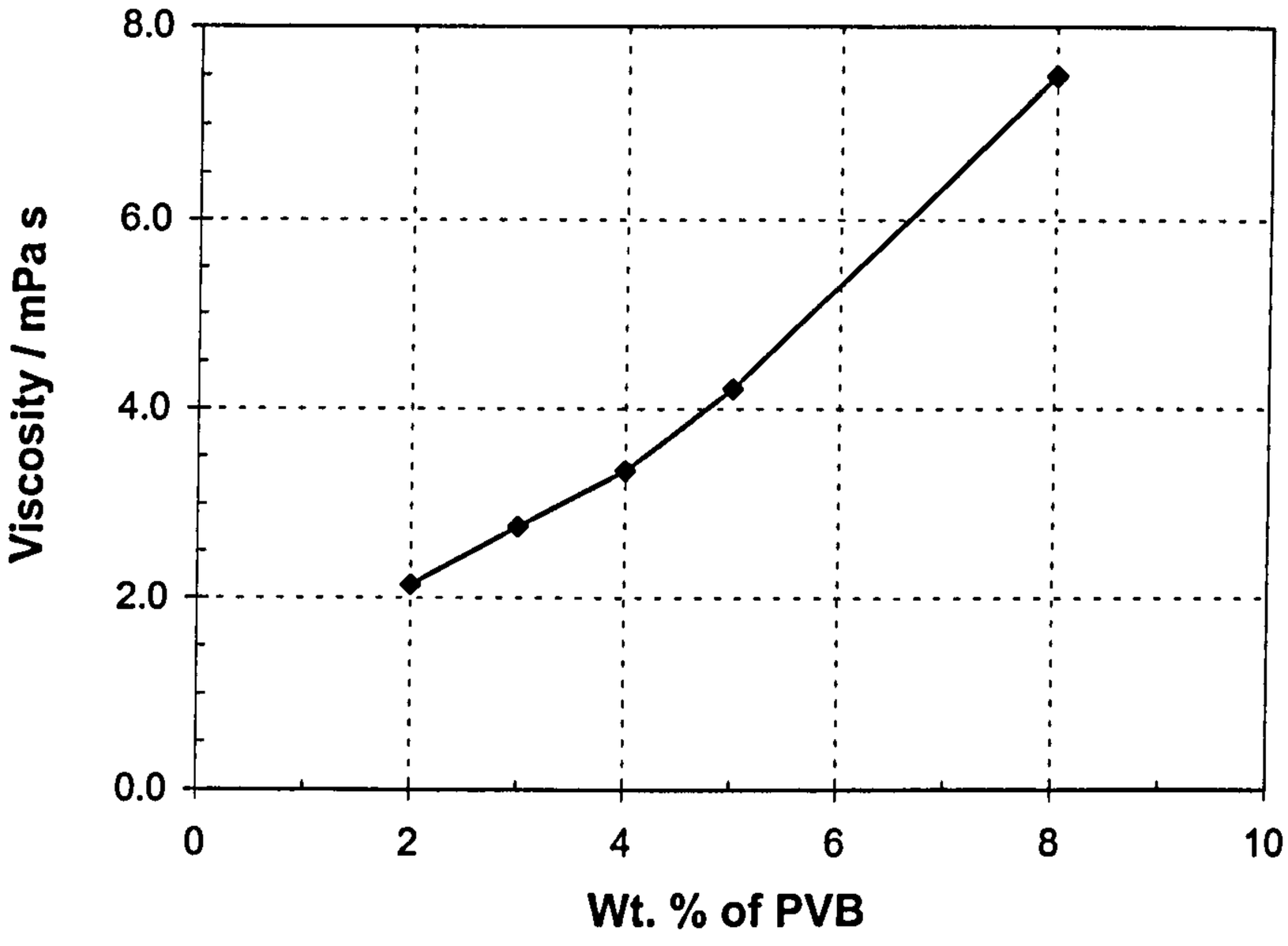

Figure 4.1 Viscosity of unfilled polymeric ink at different PVB content, 20°C.

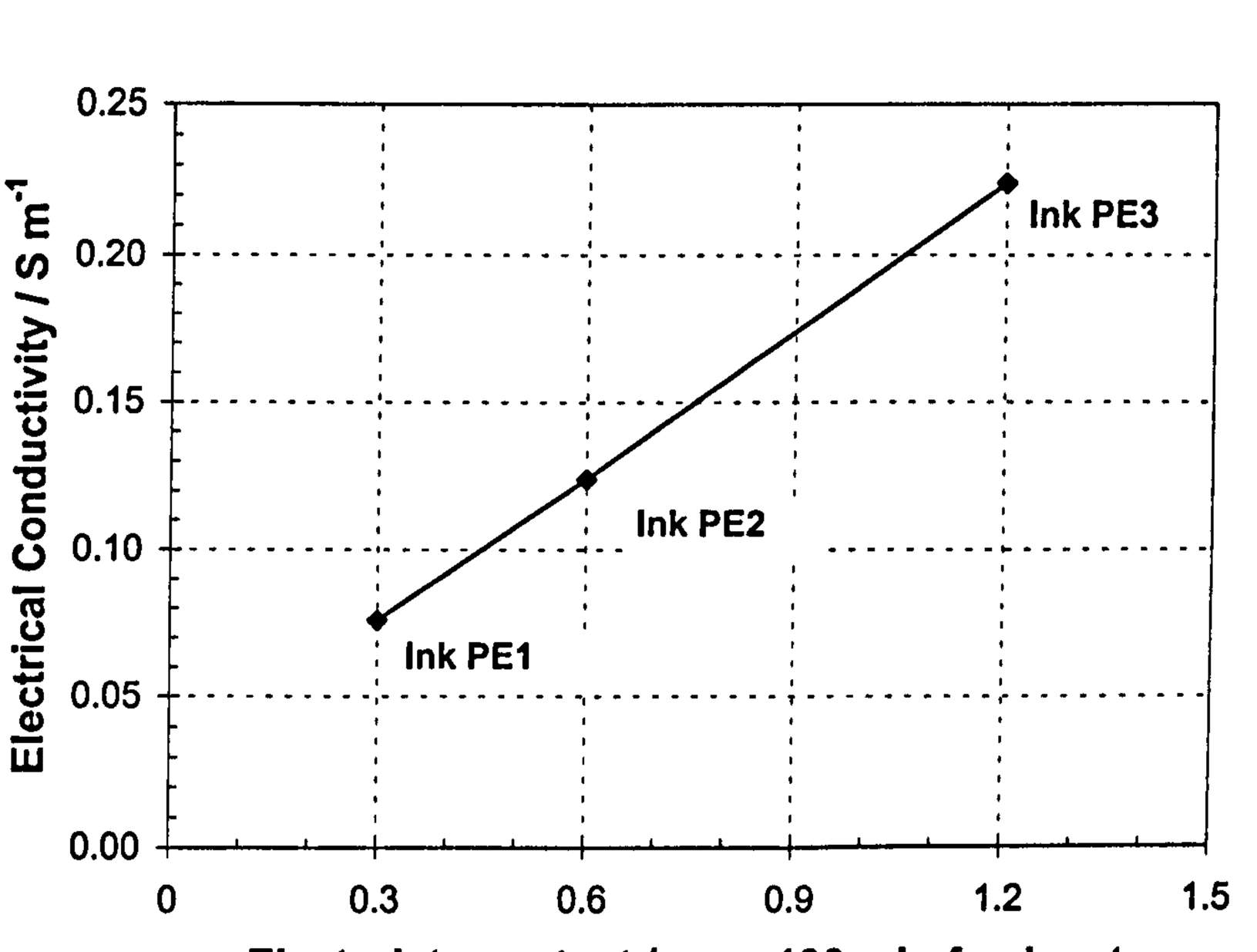

Figure 4.2 Electrical conductivity of polymeric ink (contained 4 wt. % of PVB) at different electrolyte concentrations, 21°C.

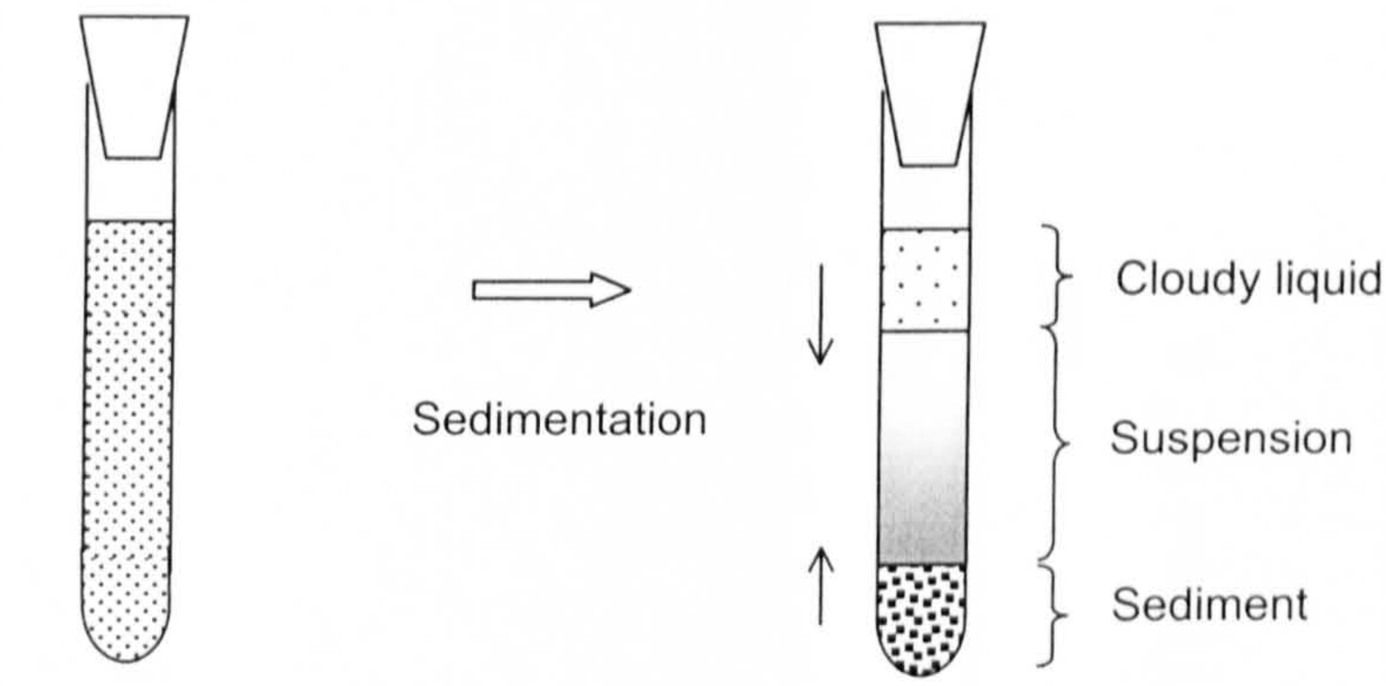

Figure 4.3 Sedimentation behaviour of inks C, U and EU.

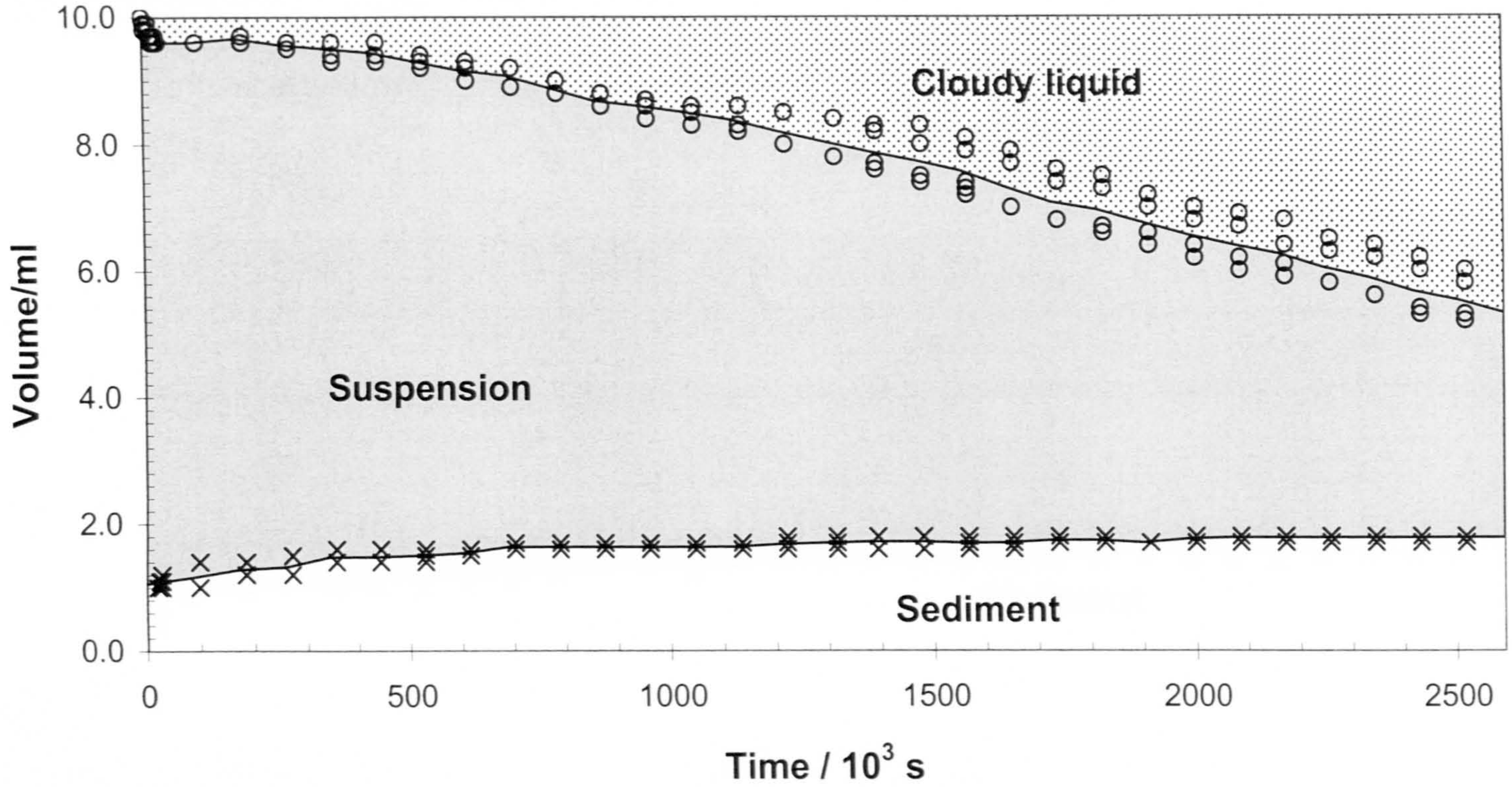

Figure 4.4 Variation in volumes of cloudy liquid, suspension and sediment in ink C as a function of time.

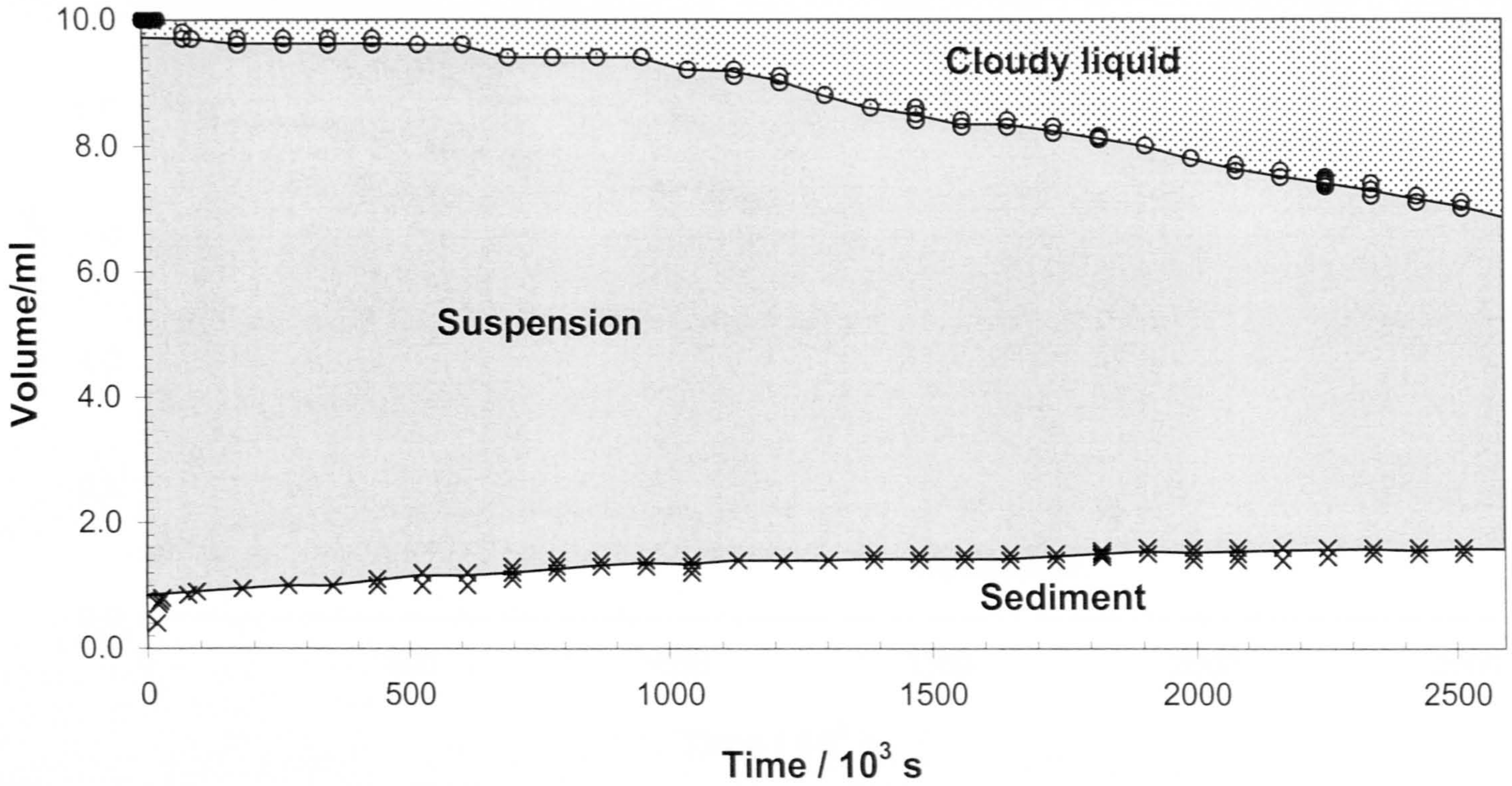

Figure 4.5 Variation in volumes of cloudy liquid, suspension and sediment in ink U as a function of time.

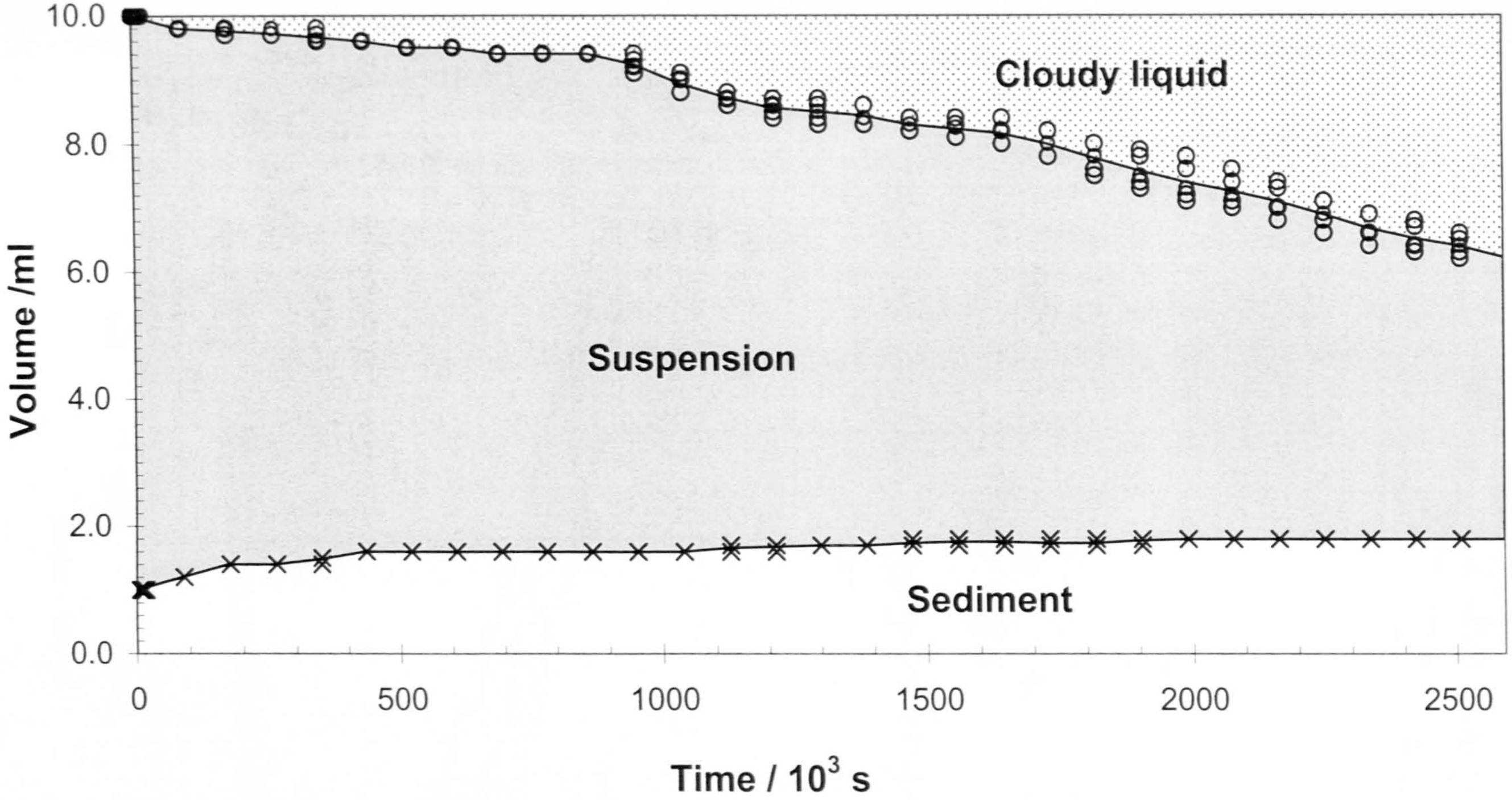

Figure 4.6 Variation in volumes of cloudy liquid, suspension and sediment of ink EU as a function of time.

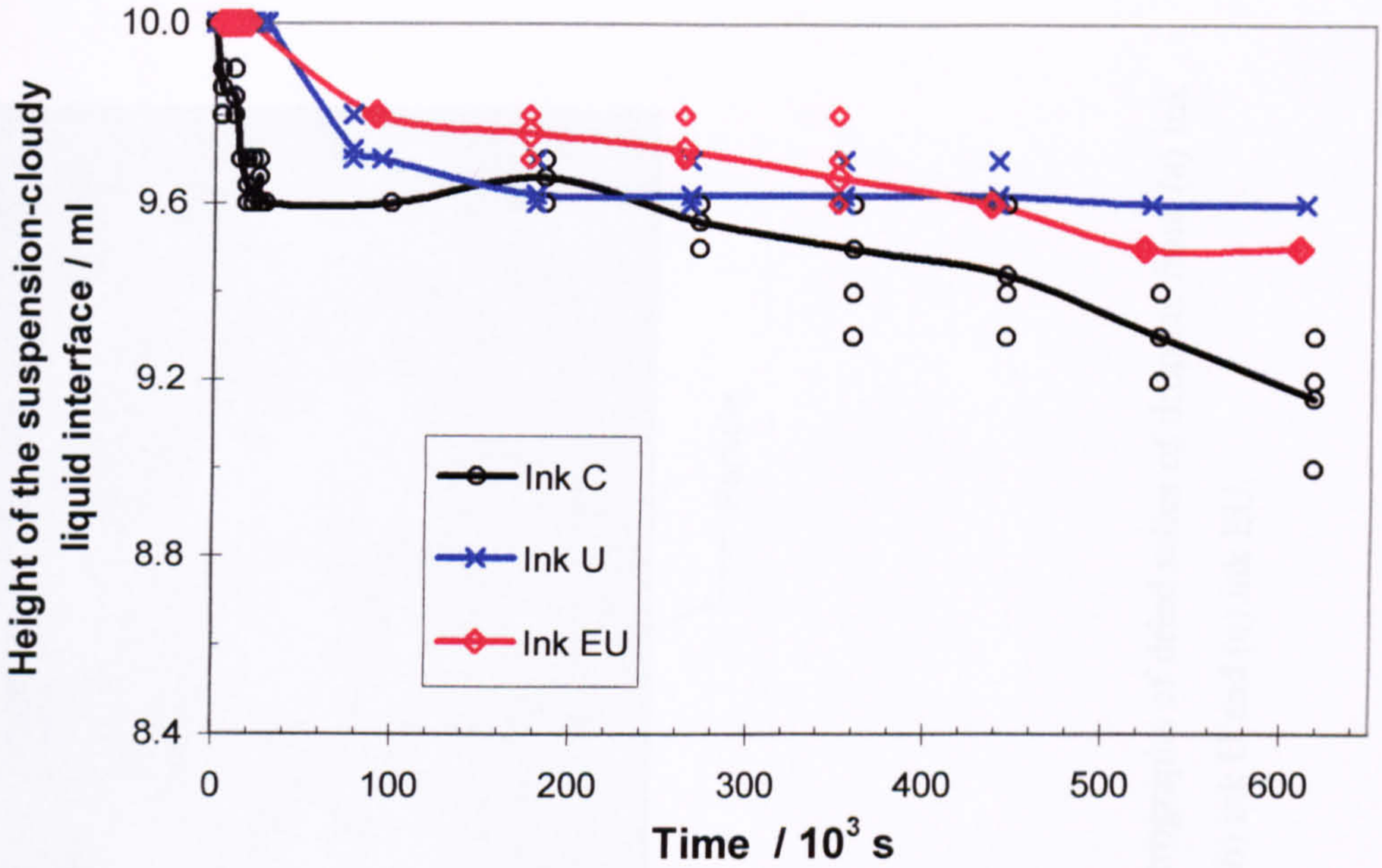

Figure 4.7 Comparison of the height of suspension-cloudy liquid interface in the first 6.05×10^5 s (7 days) of study.

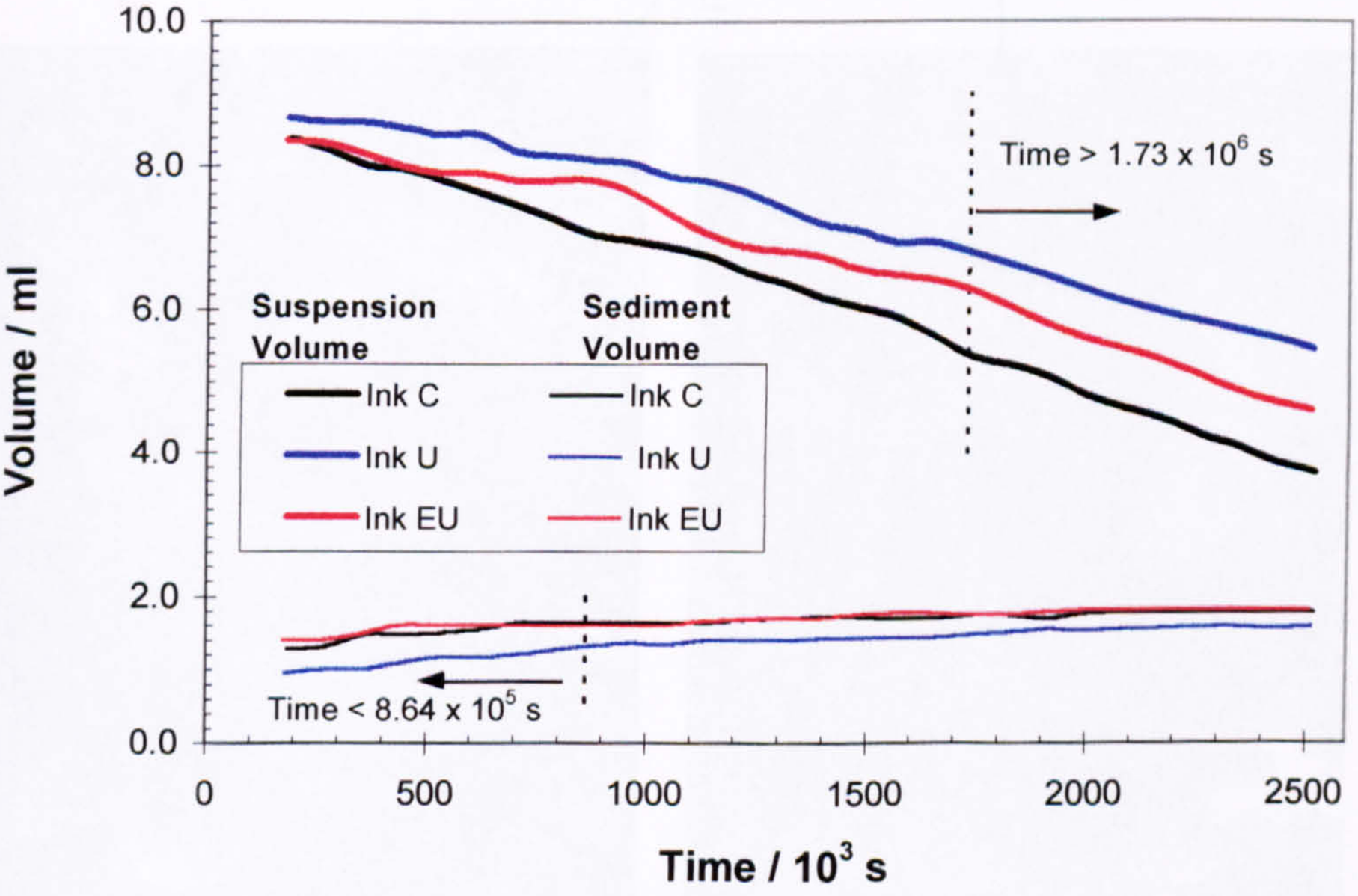

Figure 4.8 Comparisons of variation in suspension and sediment volumes for inks C, U and EU.

(a)

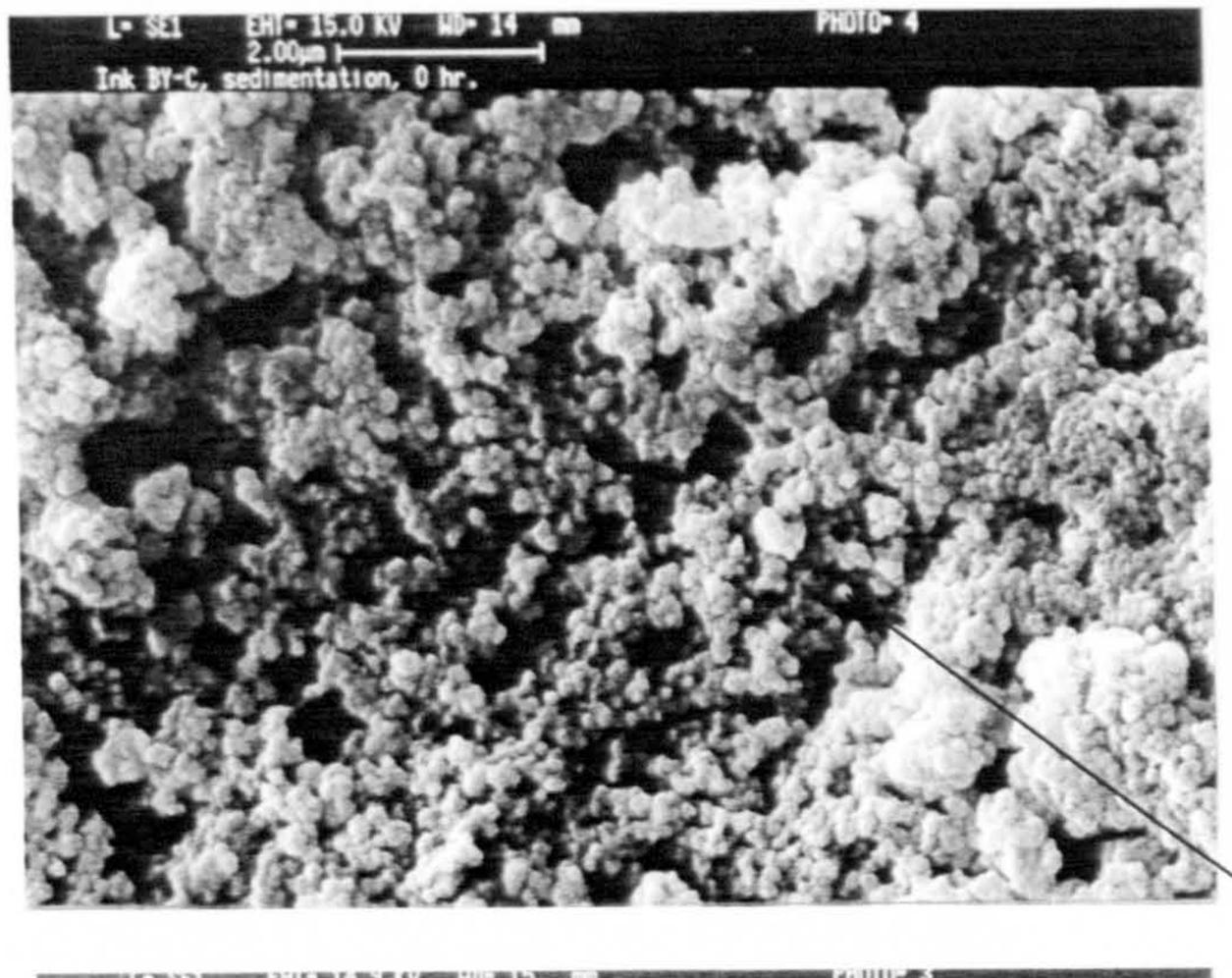

(b)

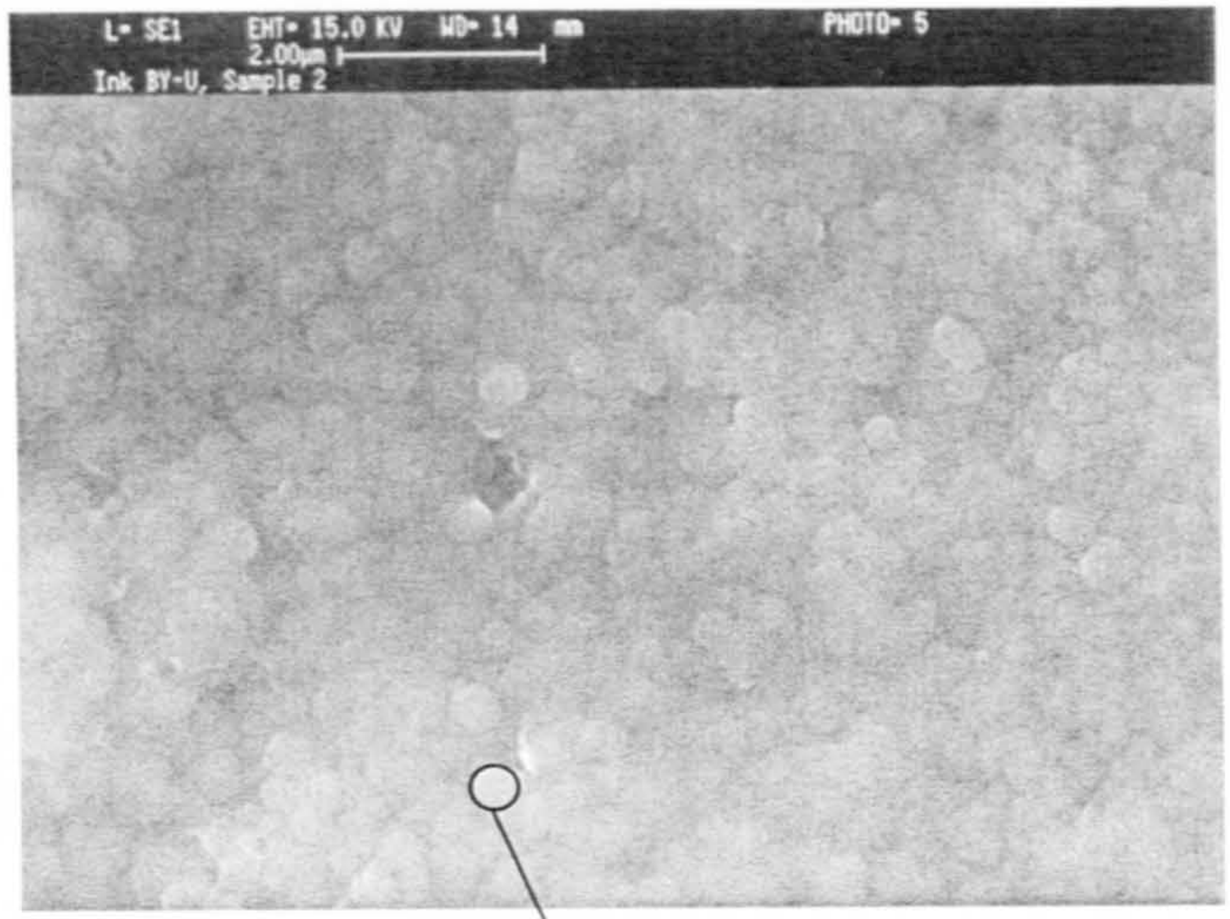

Particle

Particle

(c)

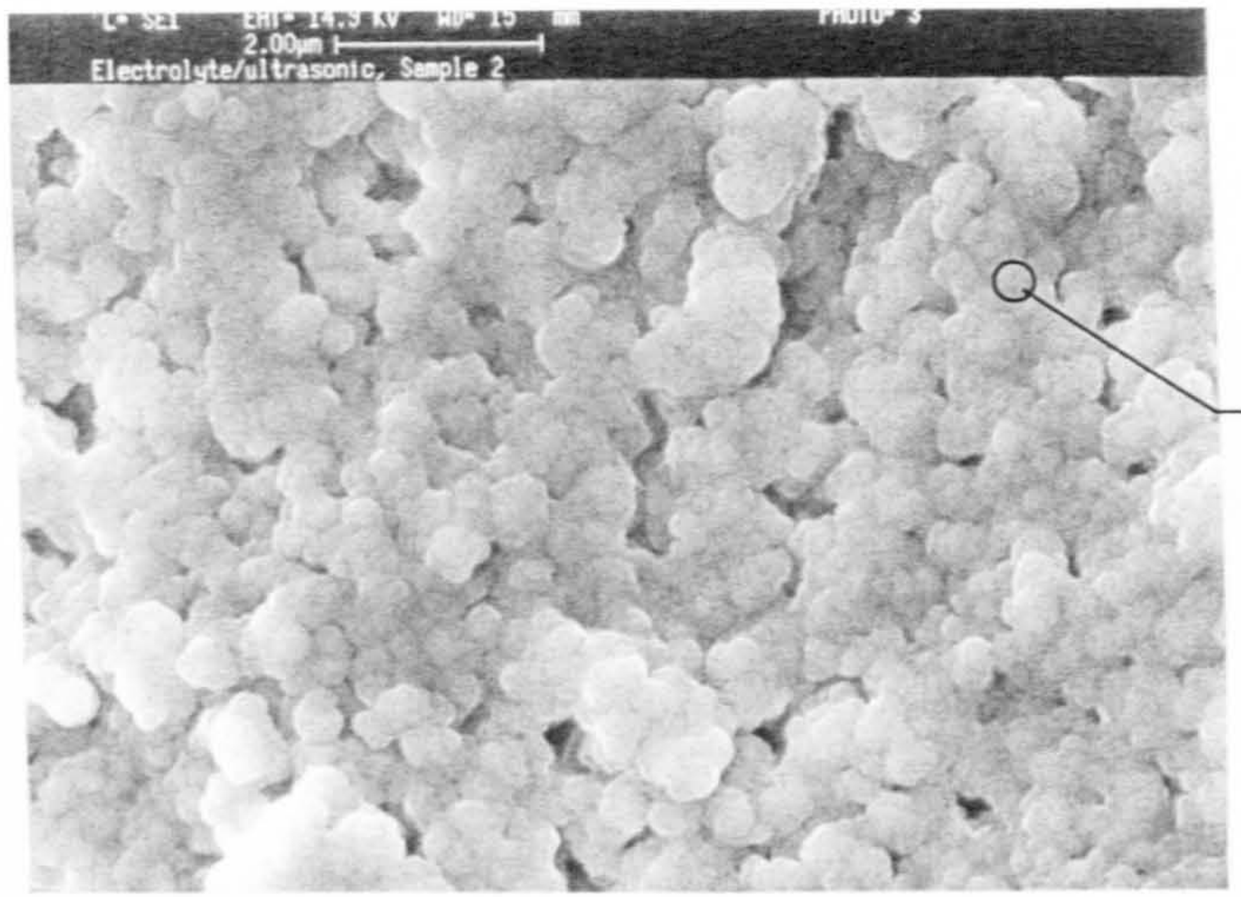

Particle

Figure 4.9 Micrographs of dried relics of droplets from (a) ink C, (b) ink U and (c) ink EU.

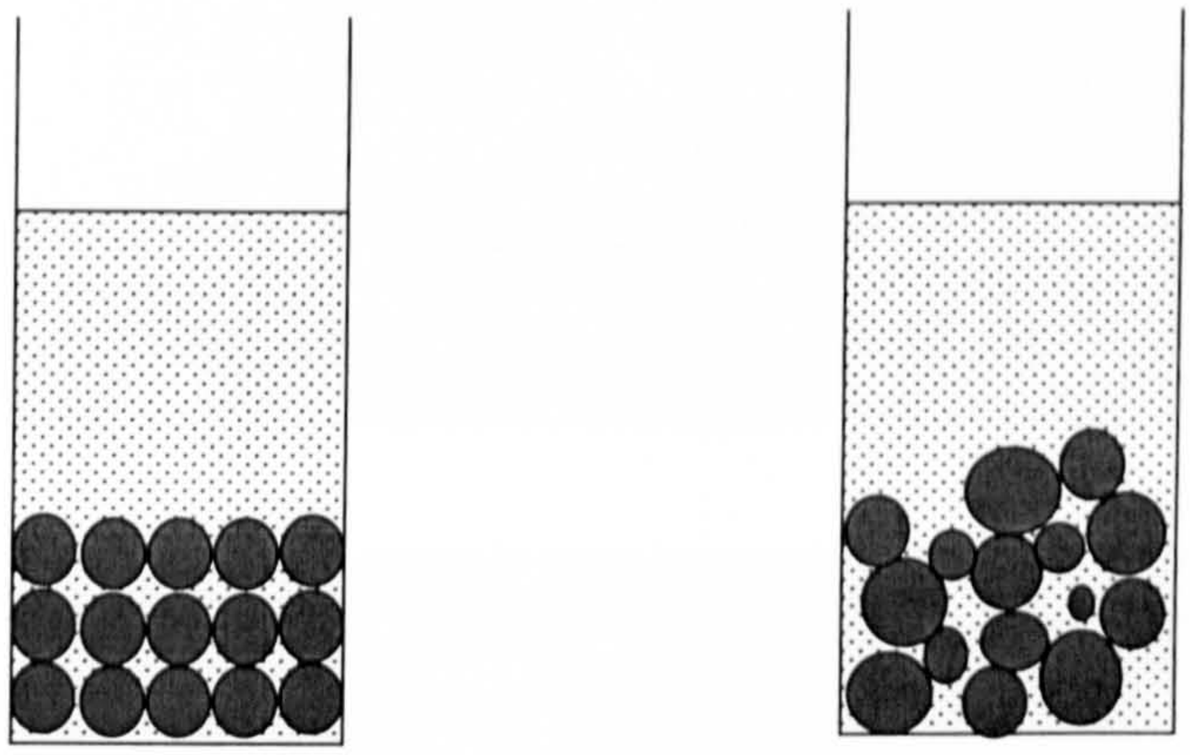

Figure 4.10 Schematic representation of packing of sediment at the bottom of the test tube (a) particles of uniform size and (b) agglomerates.

(a)

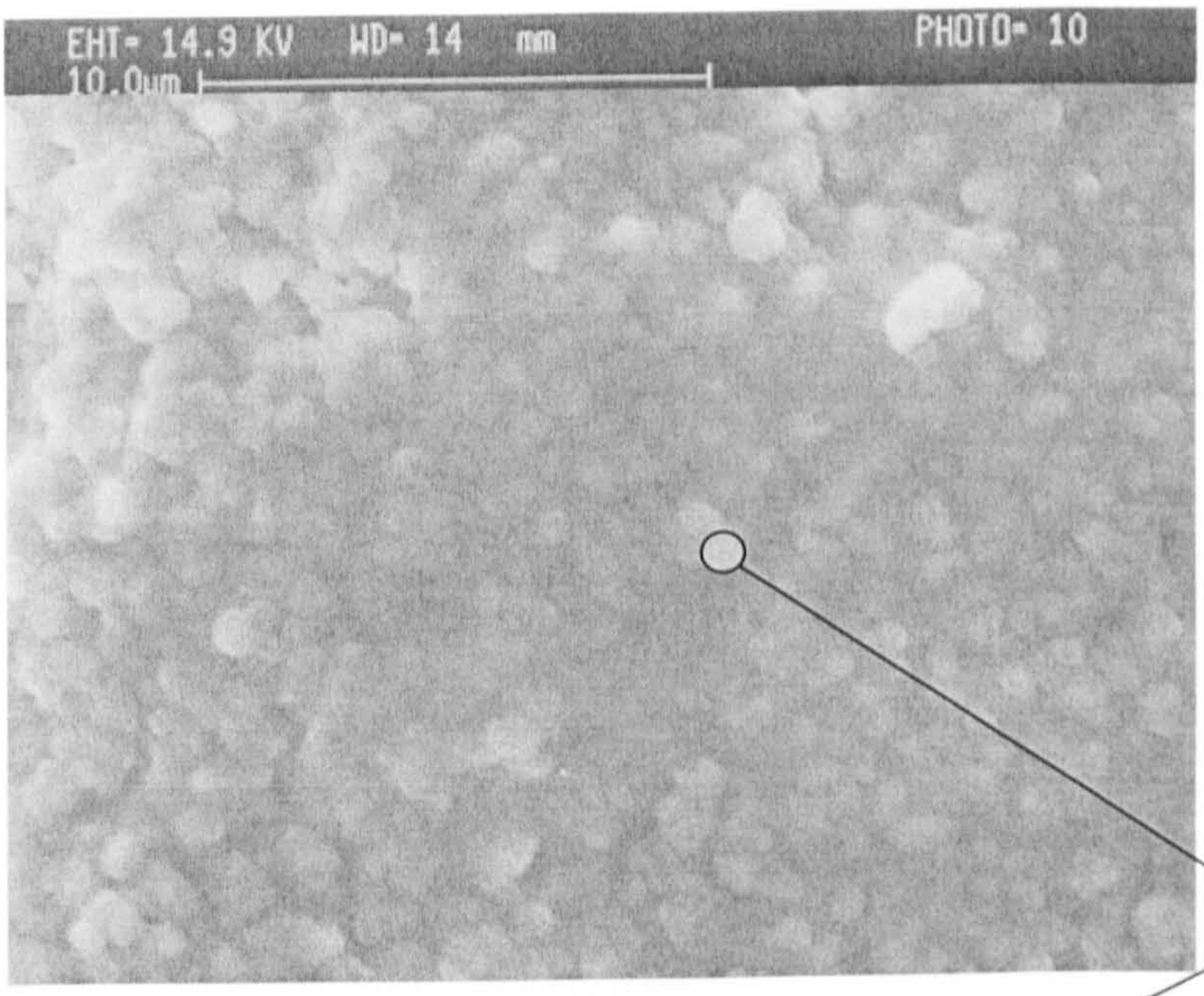

(b)

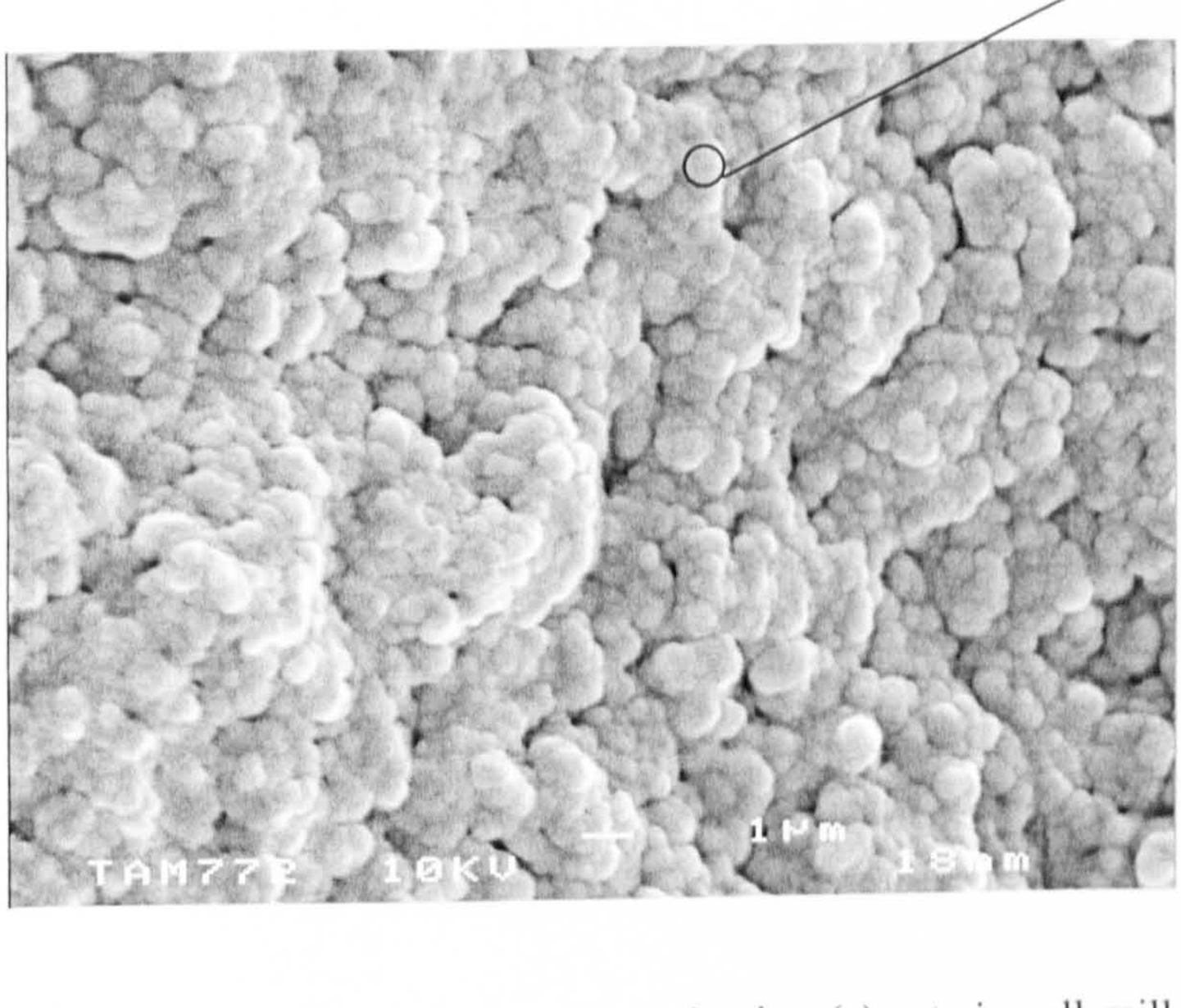

Figure 4.11 Micrographs of mill products processed using (a) a twin roll mill (ink 2R) and (b) a triple roll mill (ink 3R).

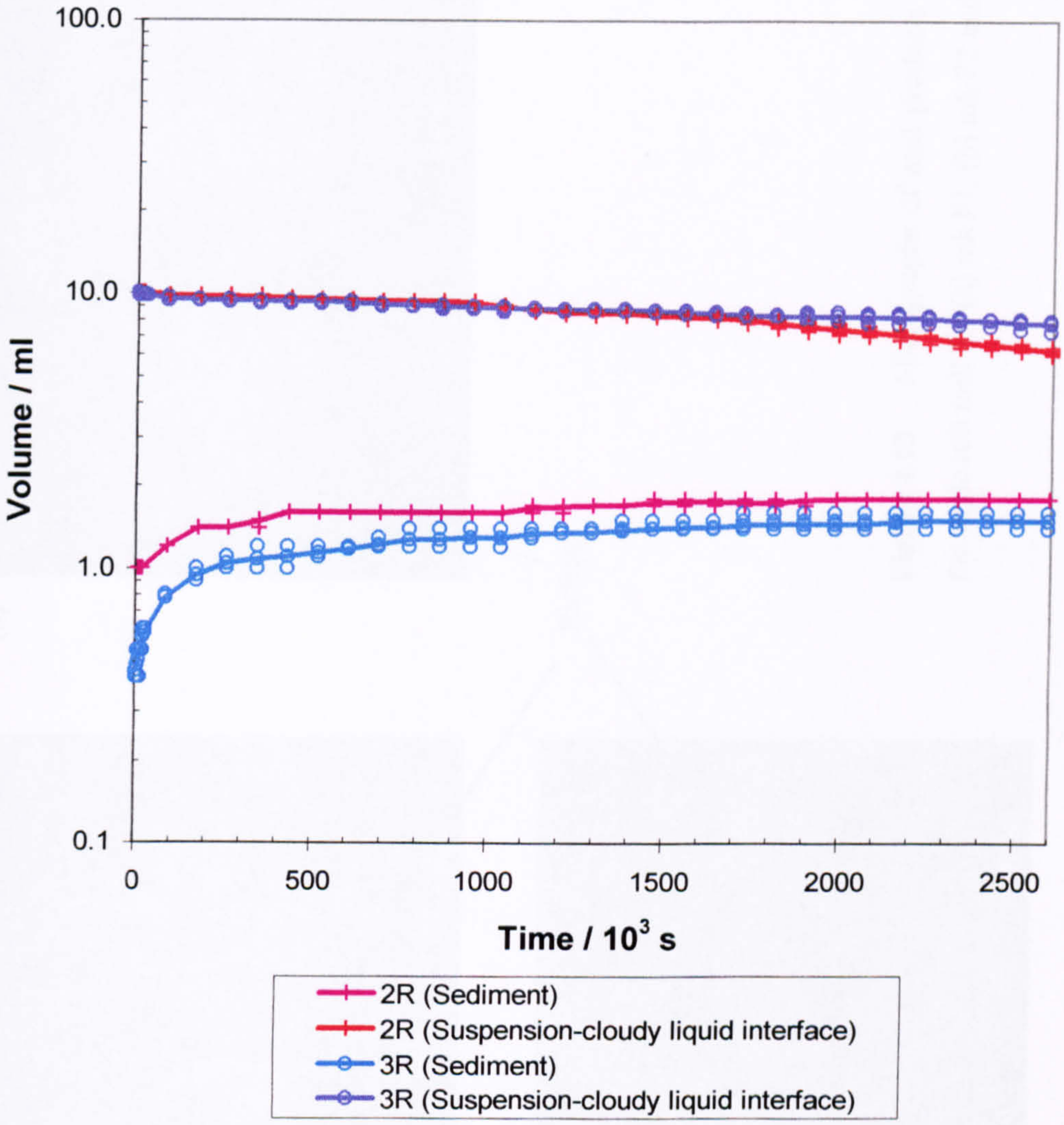

Figure 4.12 Variation in supension-cloudy liquid interterace and sediment volume of inks 2R and 3R.

(a)

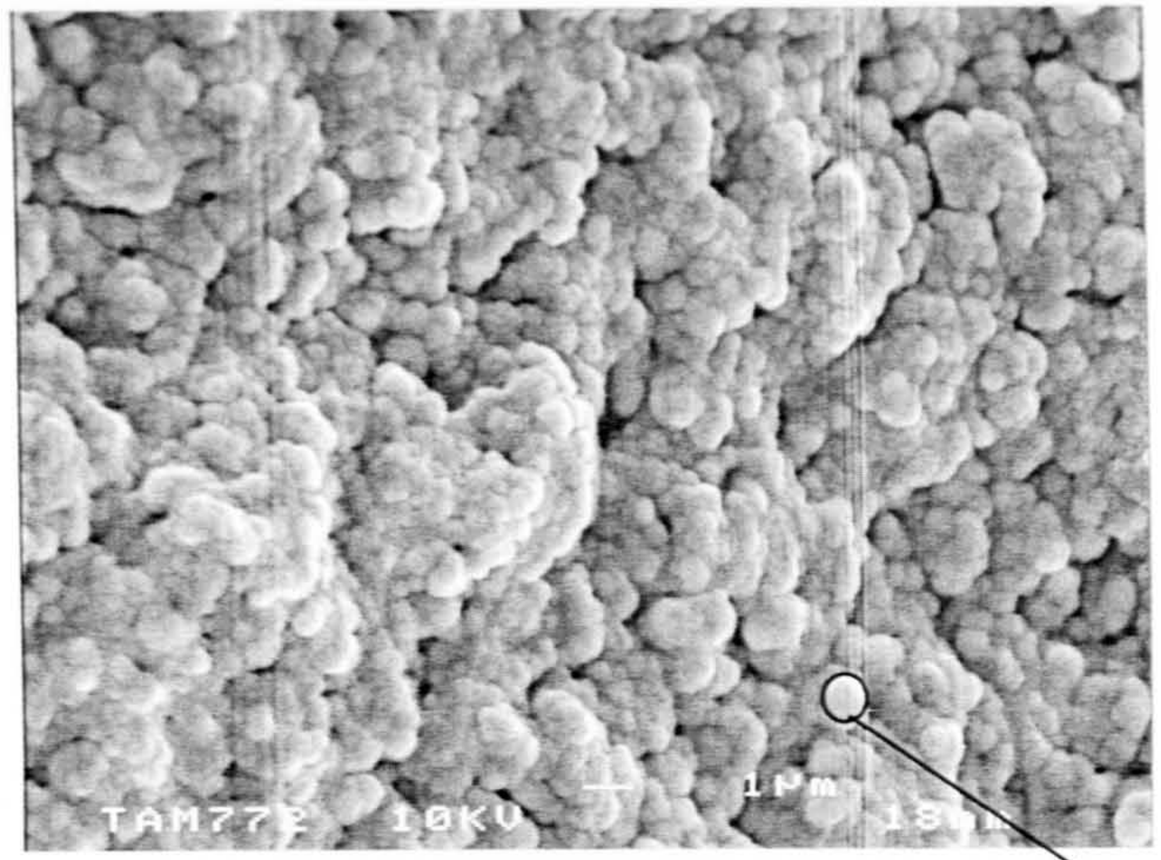

(b)

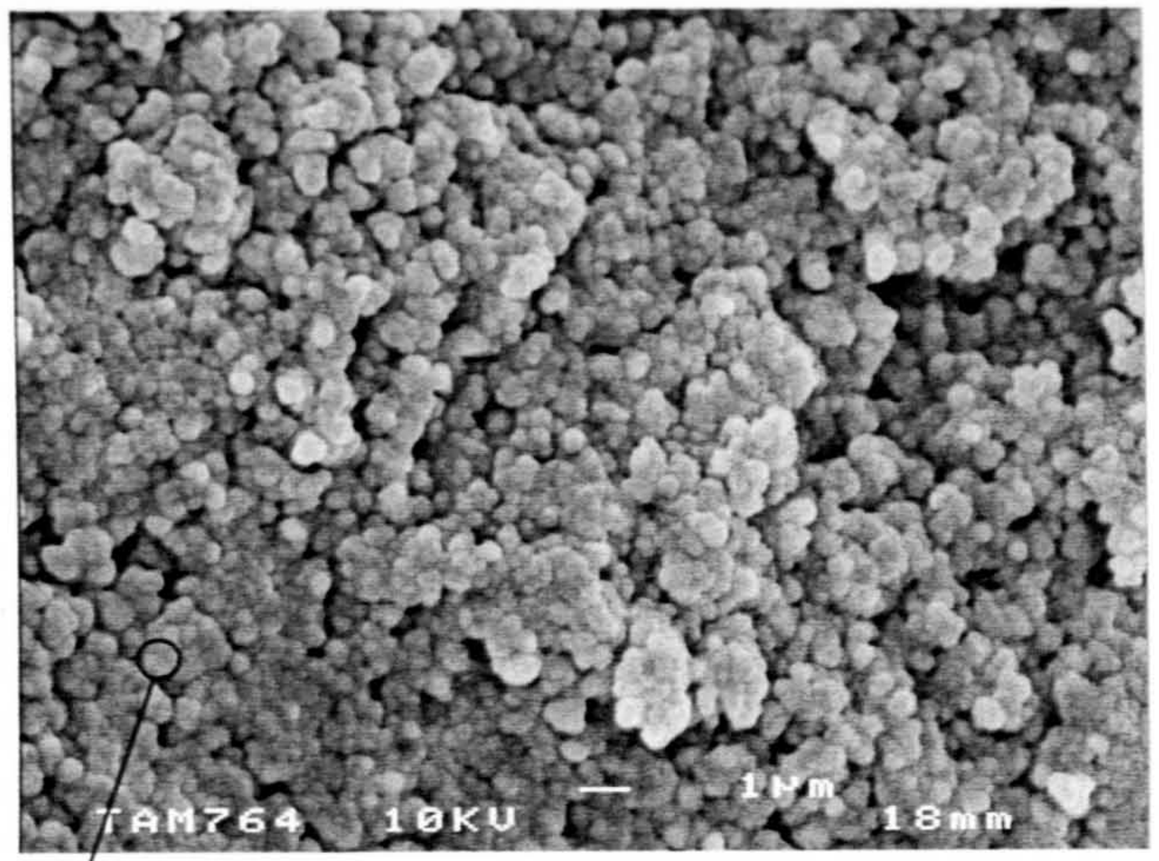

(c)

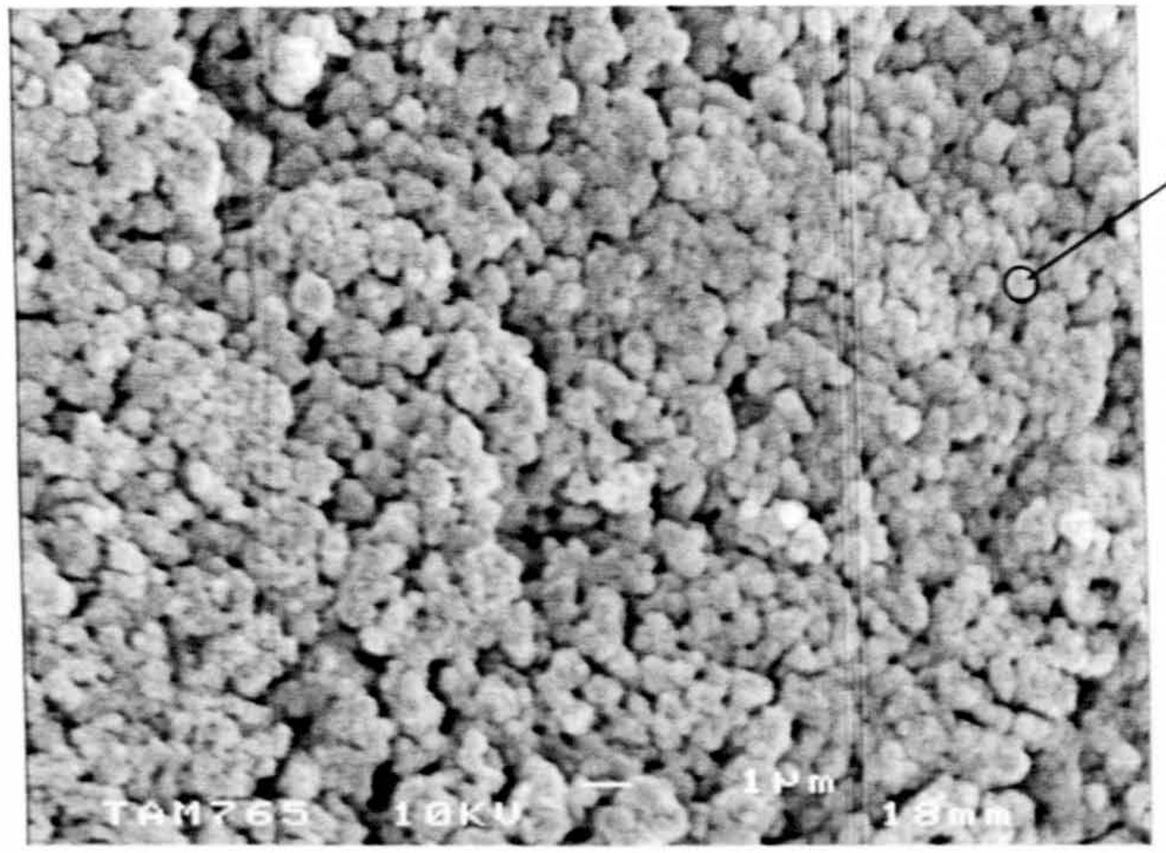

Particle

Particle

Figure 4.13 Micrographs of mill products processed using the triple roll mill for (a) ink P1, (b) ink P2 and (c) ink P3.

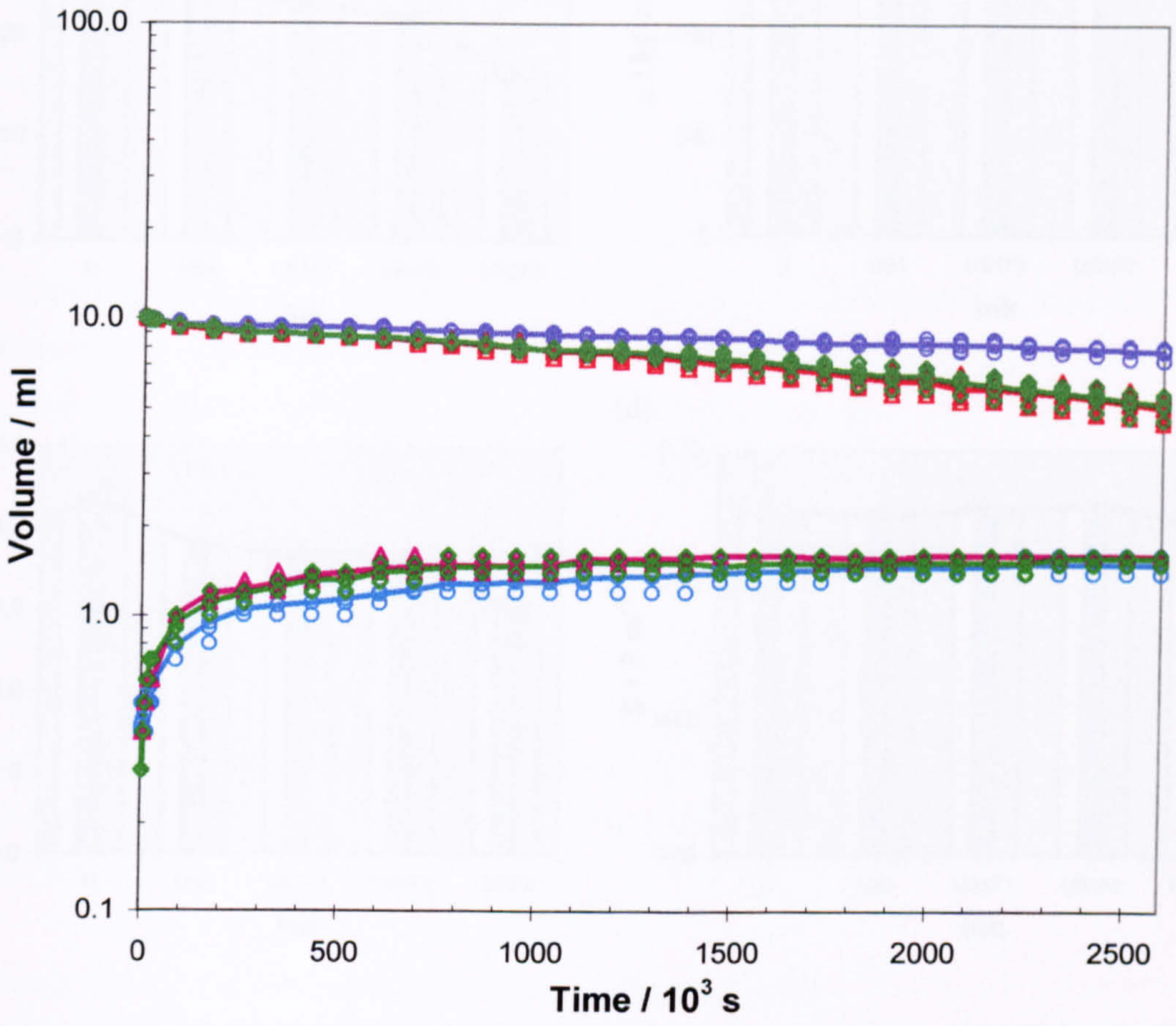

Figure 4.14 Variation in suspension-cloudy liquid interface and sediment volume of inks P1, P2 and P3.

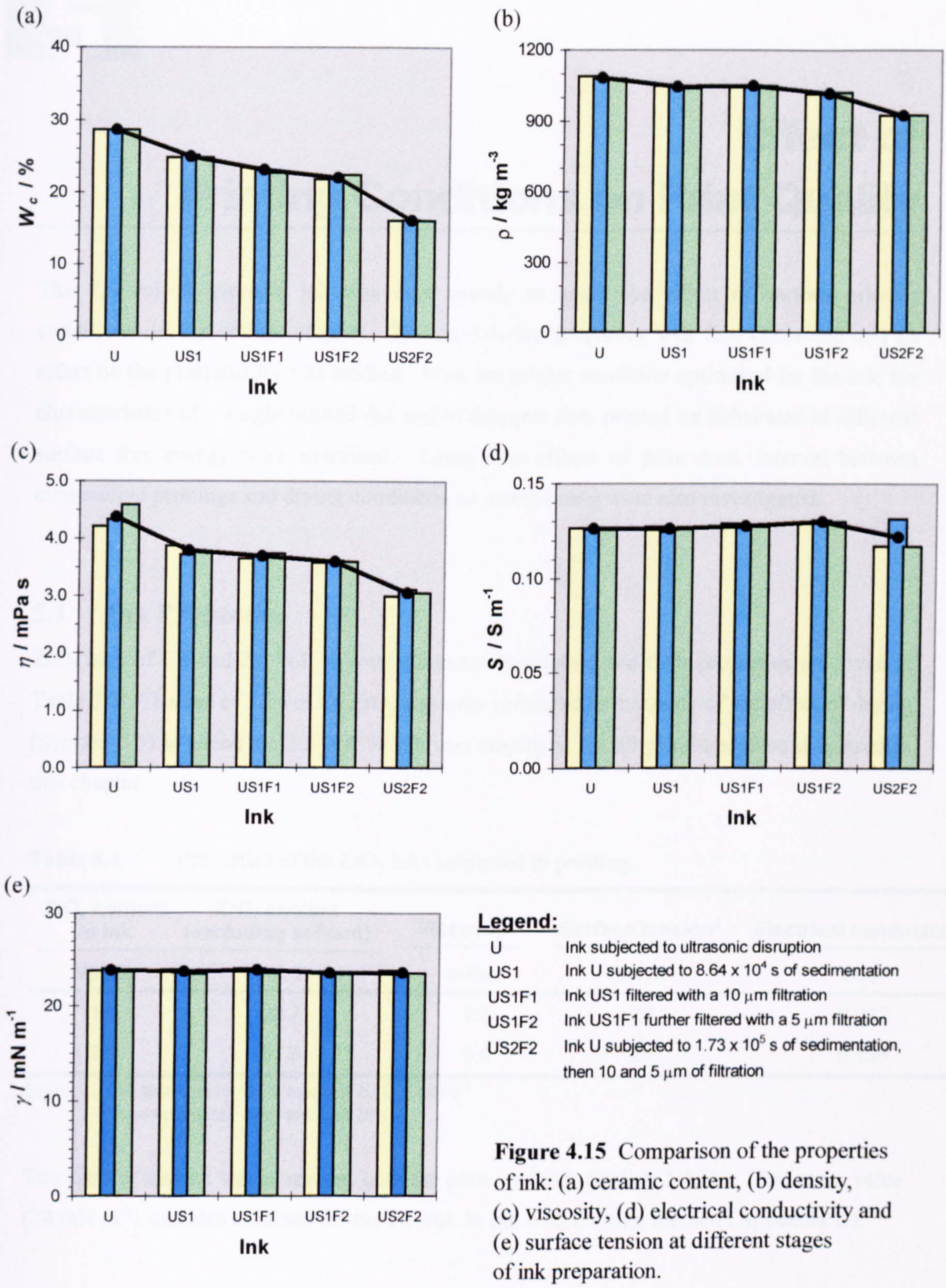

Figure 4.15 Comparison of the properties of ink: (a) ceramic content, (b) density, (c) viscosity, (d) electrical conductivity and (e) surface tension at different stages of ink preparation.

Chapter

5

Effect of Printing Conditions on Print Quality

The 2.5 vol. % zirconia ink was used mainly to study the effect of various printing conditions on the quality of print. The modulation frequency was first optimised and its effect on the print quality was studied. With the printer condition optimised for the ink, the characteristics of a single printed dot and overlapped dots printed on substrates of different surface free energy were examined. Lastly, the effects of print area, interval between consecutive printings and drying conditions on overprinting were also investigated.

5.1 Ink Properties

ZrO_2 inks of 1.5 and 2.5 vol. % were subjected to printing and their properties are given in Table 5.1. The use of 1.5 vol. % ZrO_2 was only restricted to the study of the effect of drying (Section 5.5) whereas the 2.5 vol. % ink was employed for all printings to be discussed in this chapter.

Table 5.1 Properties of the ZrO_2 inks subjected to printing.

ZrO_2 content in ink	ZrO_2 content (excluding solvent)	Viscosity[1]	Surface tension[2]	Electrical conductivity[2]
Vol. %	Vol. %	mPa s	mN m^{-1}	S m^{-1}
1.5	28.7	2.5	23	0.082
2.5	37.6	3.0	24	0.138

Note: [1] Measurements were made at 20°C, 1000 s^{-1}.
[2] Measurements were made at 20°C.

The surface tension was measured with the plate method (Section 3.4.5b). The same value (24 mN m^{-1}) was also obtained for the 2.5 vol. % ink with the ring method (Appendix C).

5.2 Effect of Modulation Frequency

As the ZrO_2 ink passes through the nozzle in the printer, it is piezoelectrically modulated and the jet breaks up into a series of droplets. Here, the modulation frequency was varied from 10 to 120 kHz in steps of 10 kHz and the jet break-up phenomena was observed. At the same time, test pattern 1, which was a set of alphanumeric characters, was printed on substrate S2 at each modulation frequency.

5.2.1 Jet Break-up

At 10 kHz modulation frequency, the jet emerged from the nozzle almost as a continuous stream that started to break up only at the exit of the charge electrode. As the jet modulation frequency was increased to 70 kHz, the break-up point gradually shifted away from the exit towards the centre of the electrode, i.e. there was a decrease in jet break-up length. Consequently, more droplets were formed within the electrode. The droplets also appeared to be pear-shaped and symmetrical. Satellite droplets were seen trailing behind the parent droplets (Figure 5.1a) but these disappeared when the modulation frequency was increased. At 70 kHz, the droplets detached from the continuous jet at the centre of the electrode as shown in Figure 5.1b. On the other hand, when the jet was over-modulated beyond this frequency, no significant change in the jet break-up length was observed. Instead, the break-up point remained almost at the same position, i.e. around the mid-point of the electrode. The shape of the detached droplets also started to deviate from the pear-shape and appeared elongated and clustered in groups of two or three droplets (Figure 5.1c). At such high frequencies, the droplets were generated too close to one other. The orientation may be due to the droplets seeking to repel one another since they are charged at the same polarity.

5.2.2 Print Quality

The effect of increased modulation frequency on print quality is shown in Figure 5.2. At low modulation frequency (e.g. 20 kHz), all the droplets were printed but incorrectly placed. The result was compressed characters with additional 'print-marks' at the top. These errors might be due to the presence of satellite droplets, which were being detached from the main droplets in the charge electrode. They may merge with the preceding or trailing droplet during their flights through the air [Lloyd and Taub, 1988]. If the satellites merge with the preceding parent droplets, which are charged at the same time (hence, at the same level), coalescence does not seem to have any detrimental effect on the droplet trajectory. If the

satellites merge with the trailing droplets, which are charged at a different time, the charge-to-mass ratio of the resultant droplet is affected and this contributes to dot placement errors on the substrate. Satellite droplets are therefore detrimental to print quality and should be avoided in all cases.

As the frequency was increased, the print quality also improved until an optimum was achieved at 60 and 70 kHz. Clear prints with well-defined boundaries were produced, indicating that the droplets were placed correctly. A consistent time of flight (TOF) of 18500 was also observed during printing at these frequencies. This was pre-calibrated at 18500 (equivalent to 2.06 ms at 70 kHz) by the manufacturer. On the other hand, a high TOF (>> 18500) was observed at low frequency, such as 20 kHz.

Further increase in the modulation frequency beyond the optimum value of 70 kHz degraded the print quality rapidly with the droplets printed in the wrong positions (Figure 5.2). At such a high frequency, droplets were generated close to one another. Consequently, the electrostatic repulsive force between them might contribute to the scattering of droplets at printing. At high modulation frequency (90 - 120 kHz), the TOF value was fluctuating and noted to be lower than 18500.

5.3 Effect of Substrate's Surface Free Energy

Single layer of test pattern 2 (Figure 3.9) was printed on substrates S1 - S9 (Table 3.8) and the printed features were compared. Prior to that, the surface free energies of the substrates were estimated from the contact angle (θ) of di-iodomethane and water on them.

5.3.1 Substrate's Characteristics

The calibration result of the FTA Dynamic Contact Angle Analyser with a 90.0° sapphire ball gave an average angle of 89.7±0.5° for five repeated measurements. The surface free energy of the substrate (γ_{sv}) as well as its dispersive and non-dispersive components (γ_{sv}^{d} *and* γ_{sv}^{nd}, respectively) was calculated using Owens-Wendt's approach as outlined in Equation 3.8 and compared with the surface tension of the ink ($\gamma_{l,ink}$). These values are given in Table 5.2 alongside with θ. The variations for five measurements of θ were within ±2° for di-iodomethane and ±4° for water.

Table 5.2. Mean value of θ of di-iodomethane and water on substrates S1 - S9 and the surface free energy components of these substrates. γ_l^d, γ_l^{nd} and γ_l of the standard liquids used in the calculations were 50.8, 0, 50.8 mN m^{-1} (for di-iodomethane), 21.8 51.0 and 72.8 mN m^{-1} (for water), respectively [Goods, 1992].

Substrate	θ of di-iodomethane on substrate	θ of water on substrate	γ_{sv}^d	γ_{sv}^{nd}	γ_{sv}	$\gamma_{sv}^d / \gamma_{sv}$	$\gamma_{sv} / \gamma_{l,ink}$	Type
	Degree	Degree	mN m^{-1}	mN m^{-1}	mN m^{-1}			
S1	45	12	37	38	75	0.5	3.1	II
S2	40	83	39	3	42	0.9	1.8	II
S3	78	104	19	1	20	1.0	0.8	I
S4	27	76	45	4	49	0.9	2.0	II
S5	26	76	46	3	49	0.9	2.0	II
S6	40	18	40	34	74	0.5	3.1	II
S7	28	74	45	4	49	0.9	2.0	II
S8	34	76	43	4	47	0.9	2.0	II
S9	25	75	46	4	50	0.9	2.1	II

Where $\gamma_{sv} / \gamma_{l,ink} < 1$, the substrate is classified as a Type I substrate and where $\gamma_{sv} / \gamma_{l,ink} > 1$, a Type II substrate. S3 is a Type I substrate. Of the eight Type II substrates, two of them have their γ_{sv}^{nd} values comparable to their γ_{sv}^{d}, i.e. $\gamma_{sv}^{d} / \gamma_{sv} \sim 0.5$ for substrates S1 and S6. In contrast, the rest of the Type II substrates have $\gamma_{sv}^{nd} << \gamma_{sv}^{d}$ or $\gamma_{sv}^{d} / \gamma_{sv} \sim 1$. The fact that $\gamma_{sv}^{d} / \gamma_{sv} \sim 1$ for substrates S2, S4, S5, S7, S8 and S9 (Type II) indicates that the interaction at the ink-substrate interface was predominantly dispersive. On the other hand, for S1 and S4, the ink-substrate interface is not purely dispersive.

5.3.2 Printing of Single Layers

The substrate was placed 7 mm (section 4.1.3) vertically below the printhead and the average speed of the platform, on which the substrate was placed, was 65 mm/s. The velocity of the jet, V_J, is 22.3 m/s [Williams, 2000] and the radius of the droplet, r_d, is given by Equation 5.1 [Schredier *et al.*, 1967]:

$$r_d = \left(\frac{3 \quad a^2 \quad V_J}{4 \quad f} \right)^{1/3} \qquad (5.1)$$

where a is the radius of the jet, which can be approximated to the radius of the nozzle (31 μm) and
f is the optimum modulation frequency of the jet (70 kHz).

The radius of the modulated droplet was calculated to be 61 μm with Equation 5.1 and was about twice the radius of the nozzle. Assuming it to be spherical, the droplet volume is therefore 9.6×10^{-13} m^3.

(a) Single printed dot

The shape and size of a single printed dot in raster 6 (Figure 3.9) on substrates S1 - S9 is shown in Figure 5.3. When the ink droplets were printed on a Type I substrate (S3) of $\gamma_{sv}^{d} / \gamma_{l,ink} < 1$, globular dots formed. Generally, the dots were placed at the right positions but their shape was irregular. On the other hand, when printed on a Type II substrate, the ink droplet spread and wetted the surface. Within the raster, the printed dots were circular and uniform in size. However, the size of the dot and its outline were dependent on the ratio $\gamma_{sv}^{d} / \gamma_{sv}$.

The size ratio of the printed dot to the ink droplet was also studied (Table 5.3). In most cases, there appeared to be a correlation between R_d / r_d and $\gamma_{sv}^d / \gamma_{sv}$ of the substrate, where R_d is the radius of the printed dot and r_d is the radius of the droplet given in Equation 5.1. If $\gamma_{sv}^d / \gamma_{sv} \sim 1$, a bigger dot spread with $R_d / r_d > 10$ occurred and rays could be seen 'fingering' out of the dot. An exception is S2, which has $\gamma_{sv}^d / \gamma_{sv} \sim 1$ but no substantial spreading was observed. This might be related to the proprietary coating present on this type of acetate sheet. A closer examination of the single printed dot will be discussed in section 5.3.3.

Table 5.3 Size ratio of printed dot (R_d) to droplet (r_d) for substrates S1 - S9. In the case of S3, R_d / r_d was not calculated as the printed dots varied appreciably in size.

Substrate	Type	$\gamma_{sv}^d / \gamma_{sv}$	R_d / r_d
S1	II	0.5	8.5
S2	II	0.9	7.2
S3	I	0.9	-
S4	II	0.9	11.1
S5	II	0.9	11.5
S6	II	0.5	6.9
S7	II	0.9	12.5
S8	II	0.9	12.5
S9	II	0.9	12.6

(b) Overlapping dot

Certain degree of overlapping was purposely allowed during printing of test pattern 2 (Figure 3.9) to investigate the effect of dot-to-dot overlapping. Different combinations of printed dots overlapping in horizontal, vertical and both directions were examined. Results are discussed below.

Type I substrate

Figures 5.4b, c and d show a series of dots printed in close proximity to one another on substrate S3. Figure 5.4b is the printed pattern of rasters 36 and 38 in test pattern 2 with a raster of space (raster 37) between them; and a space between every dot within the raster. Figure 5.4c was the printed pattern of raster 71, which is made up of 32 dots. Figure 5.4d

was printed from rasters 76 and 77, both of which also comprises of 32 dots. They are compared with a single printed dot on the same substrate in Figure 5.4a. In rasters 36 and 38 (Figure 5.4b), the high contact angle of the single printed dots kept them separated from their neighbours, as originally intended. The size of the individual dot (~ 100 μm) was similar to the single printed dot in Figure 5.4a. When the dots were printed close to one another, as in raster 71 (Figure 5.4c), they merged. Instead of forming a continuous line as designed or a series of 32 individual dots, only 16 dots resulted. The individual 'single' printed dot showed in Figure 5.4c was larger than that in Figure 5.4a and was formed by two neighbouring dots coalesced with each other. The neighbouring dots merged due to close proximity. However, the high contact angle of the ink droplet on the substrate kept the coalesced dots (from two printed dots) from merging with other coalesced drops nearby. When the distance between the individual dots in rasters 76 and 77 was further reduced, the two factors, i.e. distance between neighbouring dots and contact angle, competed with each other and resulted in a disarray pattern. Further reduction in the dot-to-dot distance (in both X and Y directions) resulted in pools of ink on the substrate at printing. The movement of the substrate during printing could also contribute to coalescence.

Type II substrate

Where there was substantial spreading when the ink droplet impinged on a substrate (S4, S5, S7, S8 and S9), the printed dot merged with its neighbouring dots printed close to it and resulted in a larger elliptical dot. Obviously, this will have an effect on the minimum resolution, and hence the detail, that can be attained with continuous ink-jet printing on these substrates. On the other hand, where the spreading was limited (on S1, S2 and S6), the individual dots retained their positions. Figure 5.5 is an illustration of a series of printed dots overlapping in the X direction for these two categories of Type II substrate. The dots overlapping in the Y direction are not shown as they displayed similar features to the X direction.

The edge definition of raster 71, which comprises of 32 dots, was also examined (Figure 5.6). Acetate substrates S4, S5, S7, S8 and S9, which induced substantial spreading in printing, generated stripes that were thick at the middle and thin at the ends. However, for

substrates that caused limited spreading (S1, S2 and S6), thin stripe of uniform thickness was printed.

The contour of the edge also corresponds to the outline of the single printed dot (Figure 5.3). Where a circular dot of well-defined outline was produced on the substrate, the edge of the stripe printed was also well defined. Powder migration to the dot periphery, which will be later discussed, became more obvious when the dots were printed close to one other in a raster.

(c) Implications on layer building

For Type I substrate with $\gamma_{sv} < \gamma_{l,ink}$, the high contact angle of the printed dot prevented the printing of a continuous feature with the printer used. However, this can be overcome with software algorithm and appropriate hardware attachment made to the printer table (as discussed in Section 5.3.3). With a smaller size of the printed dot (~ 150 μm), details in a CAD model can be reproduced faithfully on this substrate. Compared to the Type I substrate, the individual printed dot on a Type II substrate was bigger, circular and uniform in size. Although it is possible to produce a continuous feature from the coalescence of individual dots printed on it, the resolution was inferior compared to that on the Type I substrate. This is especially so for those substrates which induced greater spreading (such as S4, S5, S7, S8 and S9). In addition, another problem with the Type II substrate was the phenomenon of powder migration, which seemed to worsen when the printed dots overlapped. Its implication on multi-layer printing will be examined in Section 5.4.

5.3.3 Powder Migration during Drying

In Figure 5.3, the ZrO_2 powder appeared to migrate to the periphery of the dot when the ink was printed on all the Type II substrates (S1-S2, S4-S9). Figure 5.7 is an enlarged view of a printed dot on substrate S2. The outermost ring (region I) is translucent and comprised mainly of binder and plasticiser. Circumvented by this ring are three regions of varying concentrations of ZrO_2. The darker region II has the highest concentration of ZrO_2 while the lighter regions III and IV have lower ZrO_2 concentrations. Scanning electron microscopy (Figure 5.8) further reveals that the dense ring (region II) was formed by multiple layers of

powder building upon one another whereas regions III and IV were comprised of much fewer layers of powder.

The dot mapping of Zr and line scan of Zr in Figures 5.9b and c, respectively, confirmed that there was a high concentration of Zr (or ZrO_2) at the outermost region. The centre portion was almost devoid of powder, thus giving rise to a 'ring' appearance. A similar dense band of particles at the edge of the wetted area has also been observed during drying of colloidal suspension droplets [Deegan *et al.*, 1997; Denkov *et al.*, 1992; Parisee and Allain, 1996]. Deegan *et al.* [1997] found that contact line pinning and evaporation are two sufficient conditions for the formation of this 'ring'. The 'ring' formed because the contact line, between the droplet perimeter and the substrate, cannot move. Therefore, when evaporation removed the solvent around the contact line, liquid rapidly moved outwards to it compensating for the evaporation loss. As it did so, it carried the dispersed powder to the edge.

Dot mapping and line scan for Zr were also performed on a single dot printed on the Type I substrate (S3), as shown in Figure 5.10. No powder migration was observed and in contrast to what was observed in the Type II substrate, there was almost a uniform coverage of Zr (or ZrO_2) powder over the dot surface (Figure 5.10c). Set aside the problem of coalescence with neighbouring dots when printed close to one another, this substrate would be considered a better option for part building in Direct Ceramic Ink-Jet Printing (DCIJP) using the continuous printer.

The problem of coalescence can be overcome by first printing a layer of dots sufficiently isolated from one another. This is then overlaid with a second layer, which is offset from the first so that its dots are interspersed between those of the first layer [Mott *et al.*, 1999], as shown in Figure 5.11. Because of the limited spreading on this type of substrate and hence a lower area coverage per dot, it is foreseeable that a longer time will be required for drying. The printing algorithm for Type I substrate can be realised with appropriate hardware and numerical control attachments made to the printer table. However, this was not tested in this research due to financial constraint.

5.4 Multi-layer Printing

The fabrication of small engineering components by DCIJP is achieved by printing layer upon layer. The quality of the appearance of the overprint is affected by the fundamental element, which is the single layer. Each layer is made up of an array of single printed dots and as evidenced from discussion of the preceding section, its characteristics will be affected by substrate-ink interaction and dot-to-dot overlapping. Here, influence of the configuration within a single layer on multi-layer printing on one of the Type II substrates will be examined. It was not possible to build multi-layered parts on Type I substrate. The reasons were discussed previously.

Test pattern 3 (Figure 3.10) was printed on substrate S2 with different print resolutions in the X and Y directions, as given in Table 5.4. The substrate-to-printhead distance was maintained at 7 mm and the modulation frequency was set at the optimum value of 70 kHz.

Table 5.4 Overprinting with different print resolutions.

Print resolution, X x Y		Figure No.	No. of layers
dots per m^2	dots per $inch^2$ *		
3543 x 3660	90 x 93	5.13	100 and 301
2638 x 3660	67 x 93	5.14	100
1930 x 3660	49 x 93	5.15	100
1969 x 1930	50 x 49	5.16	100 and 495

Note : * 1 dpi = 39.37 dots per m.

Test pattern 3 was first printed at resolution 3543 x 3660 dots per m^2 under three different cooling conditions, firstly, natural convection, secondly, forced convection with cool air directed at the print and thirdly, forced convection with cool air flowing across the print (Figure 5.12). The temperature of the cool air, measured at 120 mm from the exit of the dryer, was 24°C. The use of the second type of drying has resulted in the formation of agglomerates of about 50 μm in size with space interspersed in between. There was no significant difference between the first and third types of drying.

5.4.1 Pockets and Ridges

Subsequently, overprinting was performed with a forced convection of cool air flowing over the printed part with 15 s between consecutive printings. Patches, as shown in Figure 5.13b started to appear after eight layers of overprinting. As printing continued, these patches built up continuously as 'ridges' enmeshed in one another in both horizontal and vertical directions (Figure 5.13c).

Figures 5.14 and 5.15 show the effect of increasing the distance between adjacent rasters where the print resolution in the X-direction was reduced by 25% and 45%, respectively. By allowing the same degree of dot-to-dot overlapping within the same raster (Y-direction) but increasingly isolating the adjacent rasters (X-direction), ridges in the horizontal direction were largely prevented. Eventually, only the vertical ridges remained and they were equally spaced from one another (Figure 5.15). When the print resolution in the Y-direction was reduced by 47%, all the printed dots in the same layer were isolated from one another (Figure 5.16a). An array of orderly pockets, as shown in Figure 5.16b, also started to appear. These pockets were quite consistent in size and distributed uniformly throughout the printed area. They continued to deepen as overprinting continued, as shown in Figure 5.16c.

The enmeshed ridges, vertical ridges and pockets were caused by powder migration within the printed dots and dot overlapping (or increased print resolution). Upon impingement on the substrate, the geometrical constraint imposed by the pinned contact line of the printed dot caused the powder to migrate to its perimeter. The same episode was repeated when the next layer of dots was printed precisely on the same positions over their predecessors. The condition was further complicated by insufficient drying. The undried layer provided a soft bed on which the incoming droplet impinged upon and created the deepened pockets observed in Figure 5.16c. The overprint, after having dried overnight, was examined under an optical microscope (Figure 5.17a). Round pockets fitting to the profile of a droplet can be seen. In addition, the surface of the overprint was overlaid with a skin, possibly resulting from the differential cooling rate between the interior and exterior of the part. As more layers were built, the depth of the pockets started to reduce. This can be seen in Figure 5.17b of a 1000 layers printed part. There was also a layer of skin on the top of the printed part and voids were visible between this layer and that underneath it. The surface of the printed part, as seen in Figure 5.17b, was also far from smooth.

The orderly array of pockets that was observed in the overprint (Figure 5.16c) also indicates that dots were placed consistently at the same positions during layer building. This was possible because the properties of the ink remained reasonably constant and stable throughout printing of 495 layers over 7.43×10^3 s. The ink did not cause blockage to the printer nozzle at any stage during printing of 495 and 1000 layers. Printing was only terminated due to operator fatigue. Figure 5.18 shows the printer nozzle before use and after 1800 layers of printing.

5.4.2 Spattering

Tiny dots were found spattered around the printed patterns, e.g. in Figure 5.14b. These dots, as shown in Figure 5.19, were of various sizes but smaller than the printed dots in Figure 5.3. They were not satellite droplets as, in the first place, these were not observed at the charge electrode. Spattering occurred when the incoming raster overlapped on the preceding raster, which had not dried completely, at printing [Buehner *et al.*, 1997]. It was more severe when the dot-to-dot overlapping in adjacent rasters was greater. When the dots were completely isolated from one another as in Figure 5.16, spattering was absent.

5.4.3 Non-vertical Walls

Non-vertical walls can also be seen at the first and last rasters of the overprint in Figure 5.13c. They were caused by the decreasing printhead-to-substrate distance (Z_d) as more layers were printed. As Z_d decreased, the dots in the same layer were printed closer to one another. Therefore, the top-most layer has a smaller width (in the X direction) than the bottom-most layer. This could be eradicated with appropriate hardware attachments to adjust Z_d as a function of the number of layers printed. The walls appeared to be smooth with no 'stair-stepping' effect which has been observed in other solid freeform fabrication process such as fused deposition modelling, laminated object manufacturing, selective laser sintering and stereolithography [Paul and Baskaran, 1996].

5.5 Effect of Drying

The results of the effect of different drying conditions listed in Table 3.10 are discussed in this section. Overprints covering areas (A) of 2.2 mm x 2.2 mm, 4.5 mm x 2.2 mm, 9.0 mm x 4.5 mm and 18.0 mm x 8.5 mm were produced at intervals (t_{print}) of 15, 30, 60 s between consecutive printings under each drying condition. These conditions were natural convection (Experiment I), forced convection of cool air from a dryer functioning at 70 W (Experiment II), forced convection of hot air from the same dryer at 250 W (Experiment III) and heated substrate (Experiment IV). An additional Experiment V was also conducted under natural convection with a 2.5 vol. % ink. Experiments I to IV were carried out by printing a 1.5 vol. % ZrO_2 ink. For every experiment, five samples were printed for each set of A and t_{print}. The same print resolutions of 3543 and 3660 dot per m in X- and Y-directions, respectively, were employed for all printings. A maximum of 30 layers was printed.

5.5.1 Defects

In the case of a larger area print (A = 9.0 x 4.5 and 18.0 x 8.5 mm^2), immediately after a layer was printed, an elliptical cooling front initiated from the boundary of the print area and shrank towards its centre as drying progressed. The sample in Figure 5.20a was obtained by printing over undried layers at t_{print} = 5 s. The cooling front can be seen 'frozen' within it. When t_{print} was increased beyond 5 s, the cooling front closed up eventually during drying. With more layers being overprinted, white stripe (indicated by L in Figure 5.20b) became apparent. The stripe appeared white as it contained a high content of ZrO_2 powder, which was swept along with the front. This was similar to the early appearance of the ridges observed in Figure 5.13. These stripes were either vertical or horizontal depending on the drying conditions and A.

Depending on the drying conditions, the white stripes can be continuous or discontinuous. Figure 5.21 shows the white stripes appearing on two overprints of A = 18.0 x 8.5 mm^2 and dried with forced convection (Experiment II) or printed on a heated substrate (Experiment IV). These are compared with the overprint in Figure 5.20b, which has the same area but was dried under natural convection. There is only a single, thick, white stripe located at the centre of the overprint. When assisted drying was used, i.e. by forced convection or

increased substrate temperature, more stripes were produced. This situation was more so with a heated substrate, which yielded discontinuous lines running across one another. A higher powder content was present at the intersection points of these stripes, giving rise to a more intense white colour.

The numbers of layer (N) that can be printed before the defect (white stripes) became visible macroscopically was noted for each of the five samples. The values of N for Experiments I, II, III and IV were shown in Figures 5.22, 5.23, 5.24 and 5.25 for A = 2.2 x 2.2, 4.5 x 2.2, 9 x 4.5 and 18 x 8.5 mm^2, respectively.

5.5.2 Area of Print

As mentioned earlier, for the prints with larger A, the cooling front was moving towards the interior. However, this was moving outwards to the boundary in prints of small A (2.2 x 2.2 mm^2) and hence the powder was accumulated at the boundary.

Comparing Figures 5.22 to 5.25, for each drying condition, the smaller A was, the more layers can be printed without the occurrence of defects. At A = 2.2 x 2.2 mm^2, the area showed no defects after overprinting with 29 layers under natural convection. The size and/or the square configuration of the 2.2 x 2.2 mm^2 had allowed effective drying without producing defects within the part. As A increased, the curves describing N as a function of the different drying conditions slowly 'flattened'. At A = 2.2 x 2.2 mm^2 (Figure 5.22), the relationship is a concave curve but this 'flattened' when A = 18 x 8.5 mm^2 (Figure 5.25). The occurrence of defects was thus less sensitive to the type of drying conditions when A was large. However, as A became smaller, the influence of the type of drying on N was increasingly more important. If it is necessary to employ assisted drying, the suitable type to be chosen will depend on A.

5.5.3 Assisted Drying

Figures 5.22 - 5.24, in which A = 2.2 x 2.2, 4.5 x 2.2 and 9 x 8.5 mm^2, show that more layers could be printed before defects became visible (i.e. greater N) by not using any type of assisted drying. That is, a larger N was attained when natural convection was employed at

printing. The next suitable way to reduce surface defects was to use force convection of cool air. These figures also show that the drying conditions, which removed solvent at a faster rate (through hot air or heated substrate), produced thinner defect-free part than when a slower rate (e.g. cool air) was used. Although the use of assisted drying (by forced draught of hot air and heated substrate) increased solvent evaporation, it also caused the early appearance of defects. The defect was described previously. In this study, the requirements of efficient drying and surface quality of the parts were in competition with one another.

5.5.4 Powder Loading

Figure 5.26 shows the number of layers printable (N) for different area (A) using the 1.5 and 2.5 vol. % of ZrO_2 ink at t_{print} = 15, 30 and 60 s. As discussed before, N decreased with increasing A. The variation of N with t_{print} was not significant as A, except for larger A (18 x 8.5 mm^2) in the case of the 1.5 vol. % ink. However, the effect of t_{print} became more significant in the case of the 2.5 vol. % ink and generally, more layers could be printed at greater t_{print}. Furthermore, the use of 2.5 vol. % also reduced N. Although a faster drying rate was expected in a higher powder loading ink due to a lower solvent content, there would be a greater build-up of ZrO_2 at the defect lines and hence its early detection. The influences of print area size and printing interval on surface quality became more significant with a higher powder loading ink.

5.6 Debinding and Sintering

Figure 5.27a shows a component of 0.6 mm in thickness built by printing 1800 layers of 2.5 vol. % ZrO_2 ink on substrate S2 at print resolution of 3543 by 3660 dots per m^2 in the X- and Y-directions. The overprinting was performed at 15 s interval and dried with a forced convection of cool air. After printing, the component was dried in a fume cupboard for 3.60 x 10^4 s (10 hours). The green part was then debound and sintered according to the schedules described in Section 3.6. Figure 5.27b shows the sintered part with significant improvement in surface quality. The shape of the printed part was also retained during debinding and sintering. The total amount of shrinkage from green to sintered states were 17%, 29% and 18% in height, width and thickness, respectively.

5.7 Summary and Conclusions

A 2.5 vol. % zirconia ink was printed directly with the Linx continuous printer to evaluate the effect of printing conditions on print quality. A lower than the optimum modulation frequency for printing brought about a longer break-up length in the jet to form droplets and produce undesirable satellite droplets. On the other hand, too high a value produced elongated droplets. In either case, the print quality was bad. The optimum modulation frequency was approximately 70 kHz and printing under these conditions produced pear-shaped, symmetrical droplets and consistent droplet placements. The ink displayed stability during printing and 1800 layers were printed without any process control problems, in particular, blockage of nozzle.

Nine printing substrates with surface free energies both lower and higher than the surface tension of the ink have been evaluated. The former (Type I) induced little ink spreading and it was not possible to print continuous features with the present printer. There was greater spreading in the latter (Type II) and this allowed continuous features to be printed. Zirconia powder was also found to migrate to the dot periphery for the Type II substrate and was responsible for the enmeshed ridges and pockets observed in multiple layer printing.

The conditions of drying under different modes of accelerated drying, increased printing interval, extent of print area and different powder loading were examined by printing multi-layers on a Type II substrate. It was found that the requirement of efficient drying was in competition with the surface quality of the part. The employment of accelerated drying caused the early appearance of defects and produced thinner defect-free part. The influence of the type of drying was more significant when the extent of print area was smaller.

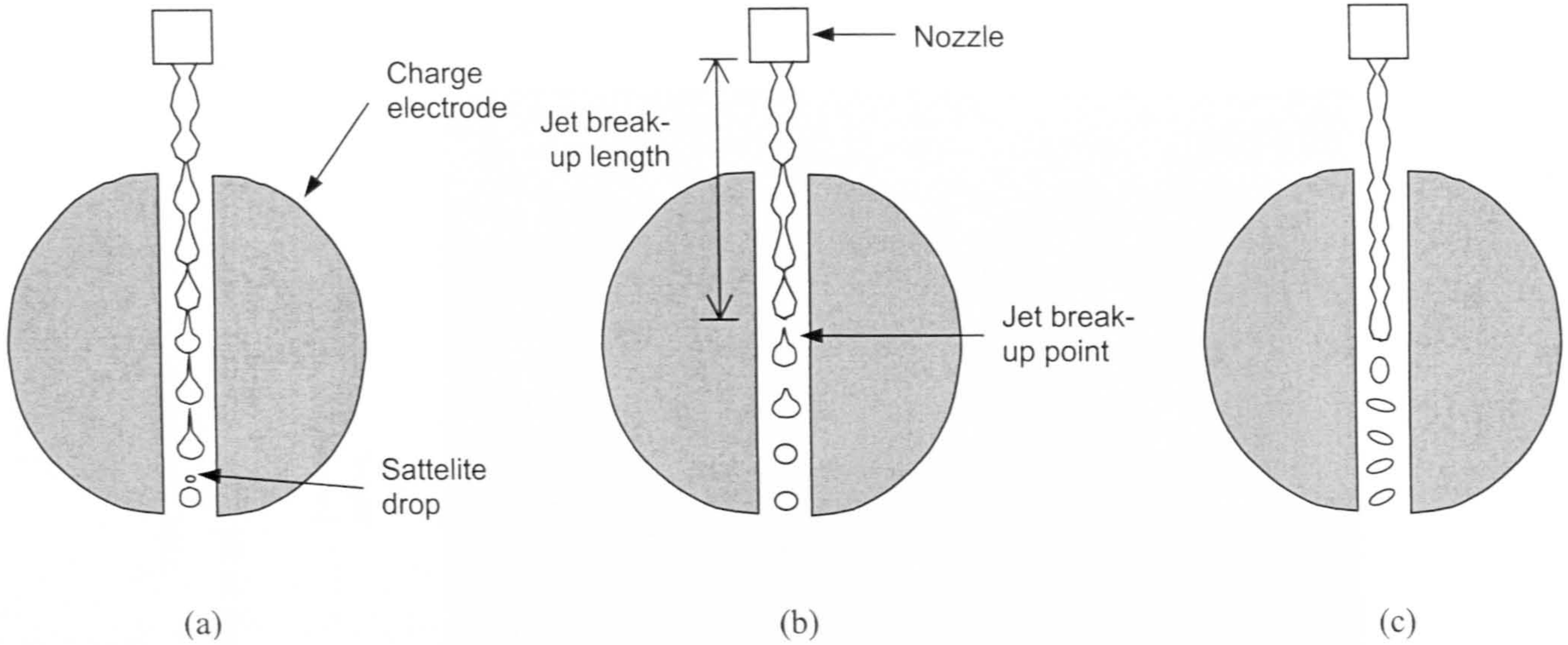

(a) (b) (c)

Figure 5.1 Jet break-up phenomena observed at different modulation frequencies: (a) under-modulated jet, (b) correctly modulated jet, and (c) over-modulated jet.

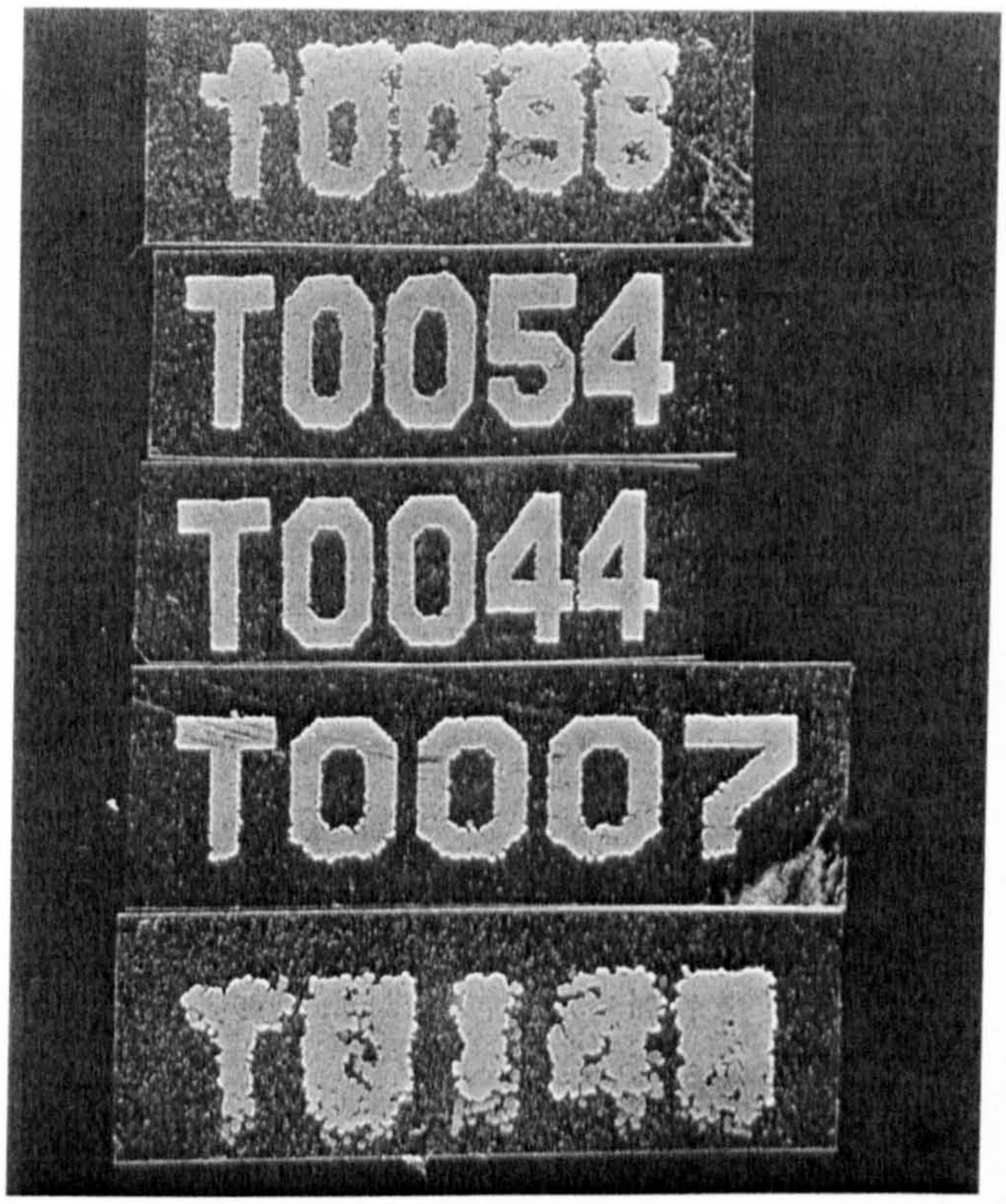

Figure 5.2 Test pattern 1 printed on substrate S2 at modulation frequencies (from top to bottom) of 20, 60, 70, 80 and 110 kHz.

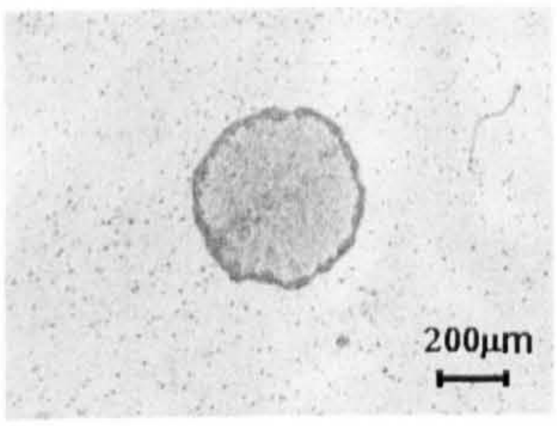

S1

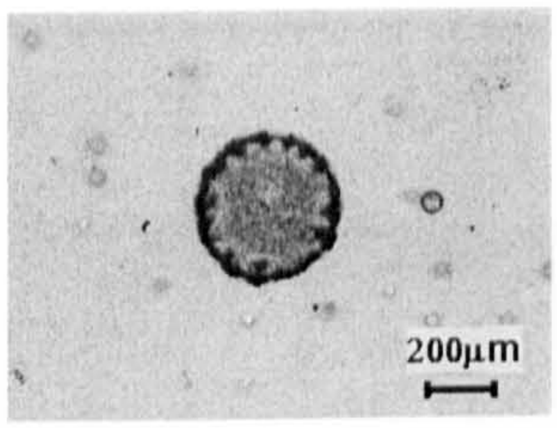

S2

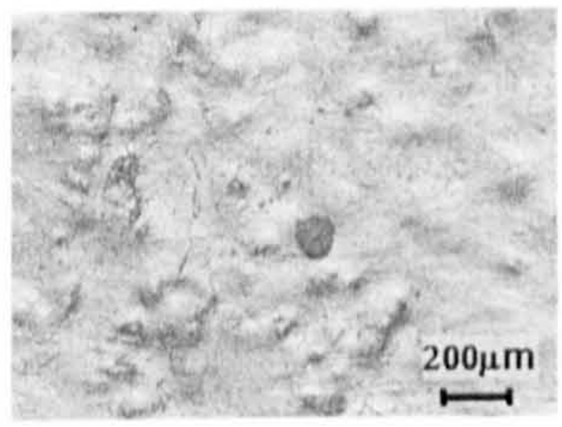

S3

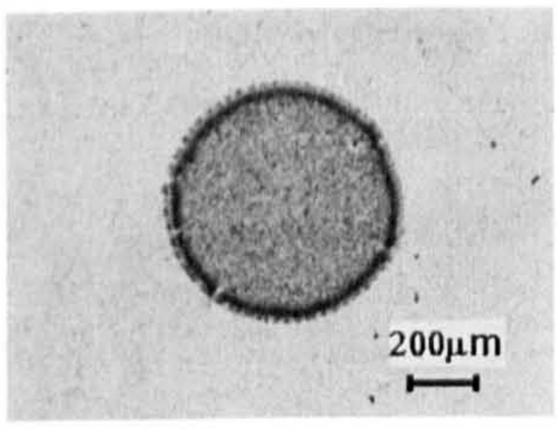

S4

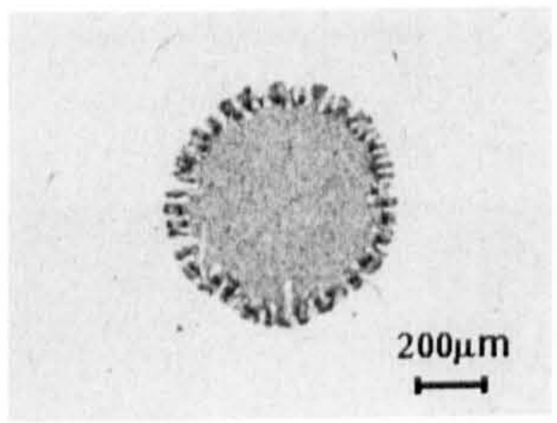

S5

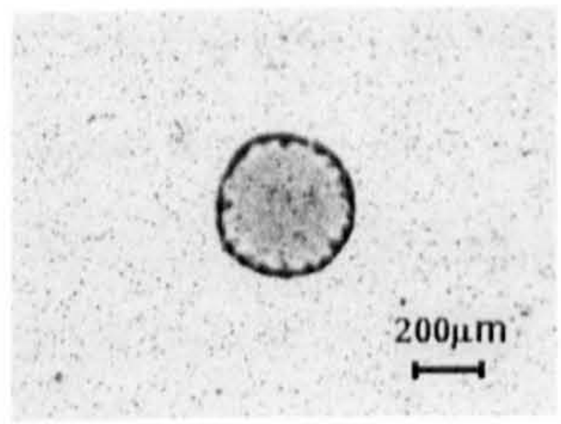

S6

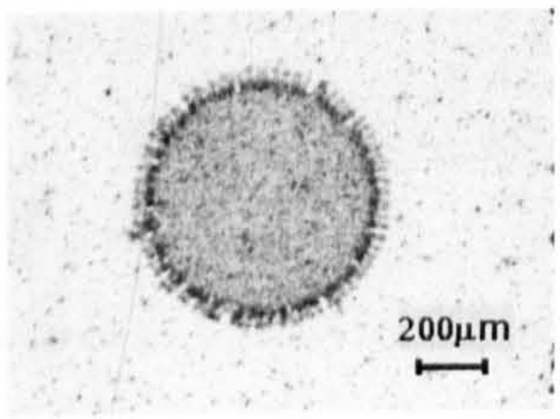

S7

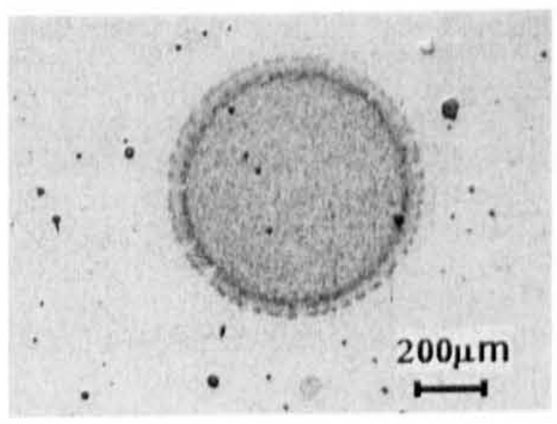

S8

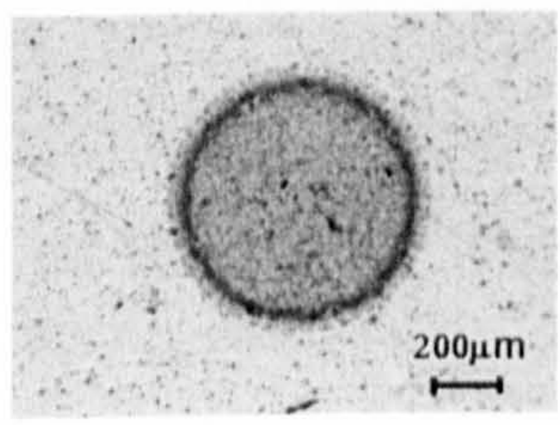

S9

Figure 5.3 Appearance of a single printed dot on substrates S1 - S9.

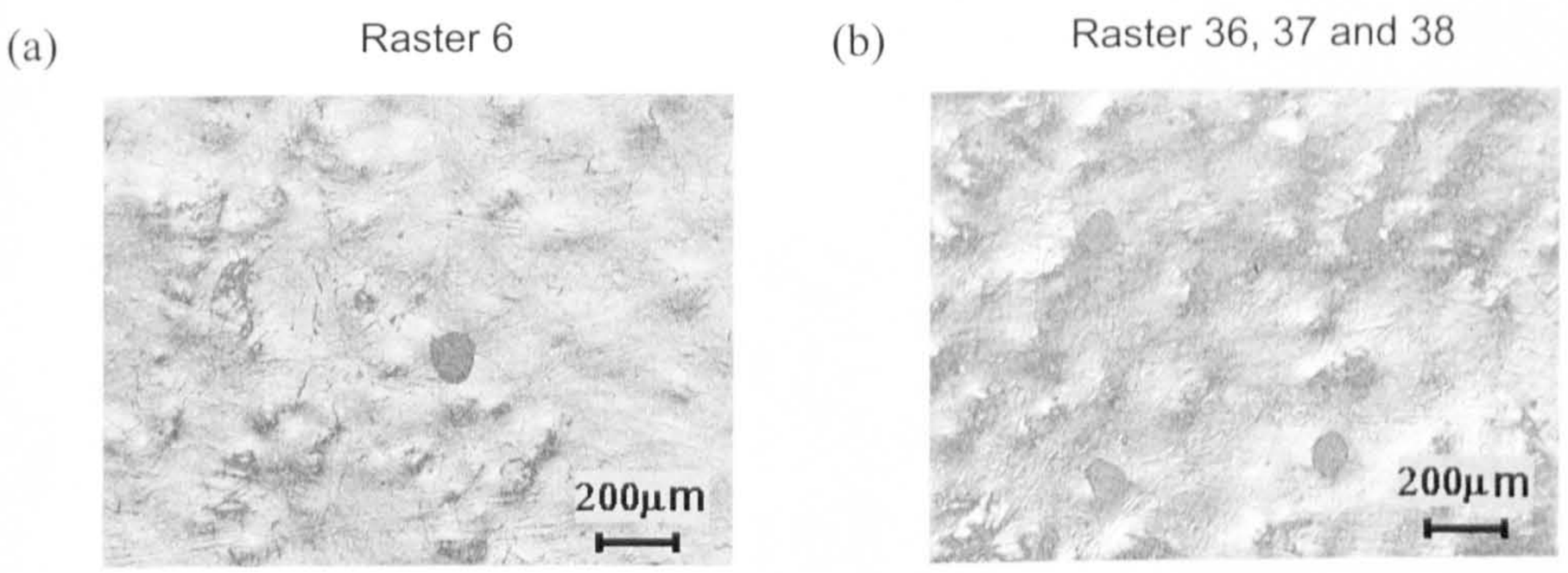

Figure 5.4 Printed features on a Type I substrate (S3): (a) single printed dot, (b) 2 x 2 dots, (c) a continuous raster and (d) 2 neighbouring rasters.

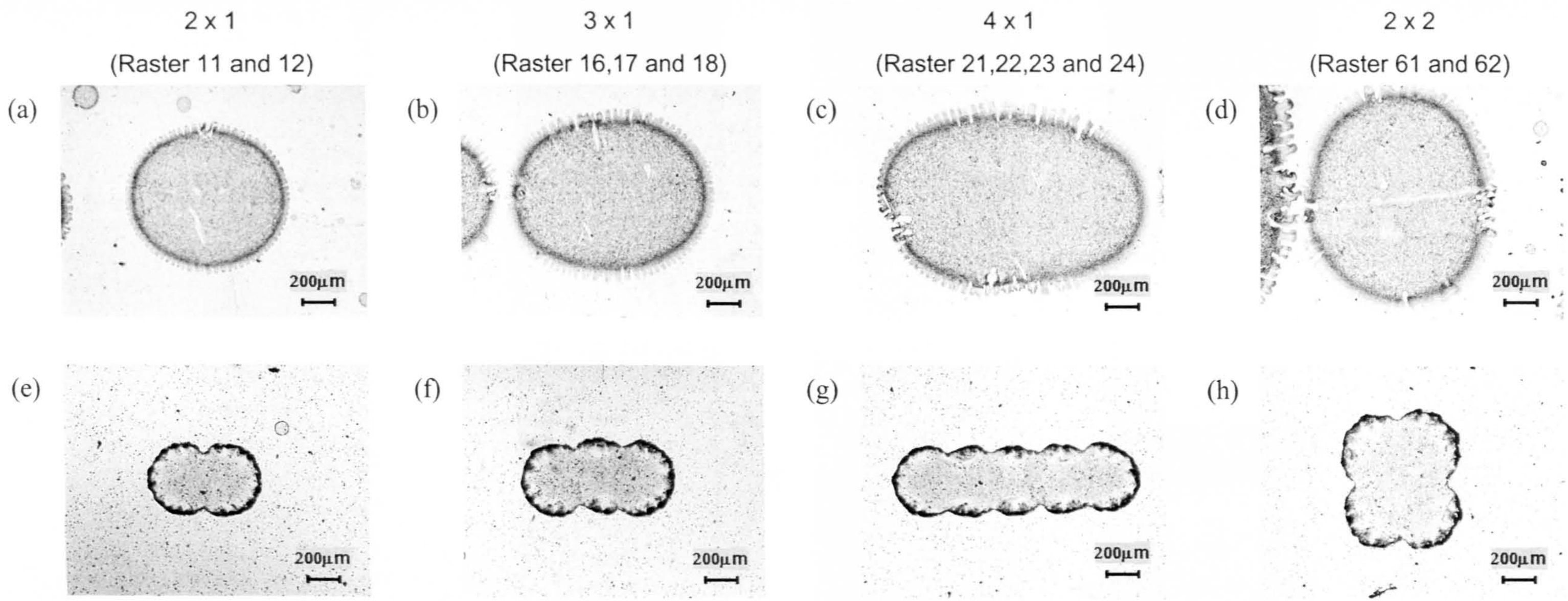

Figure 5.5 Dot-to-dot overlapping patterns (X x Y directions) for Type II substrates with different extents of spreading: (a-d) substantial spreading (S4, S5, S7, S8 and S9) and (e-h) limited spreading (S1, S2 and S6).

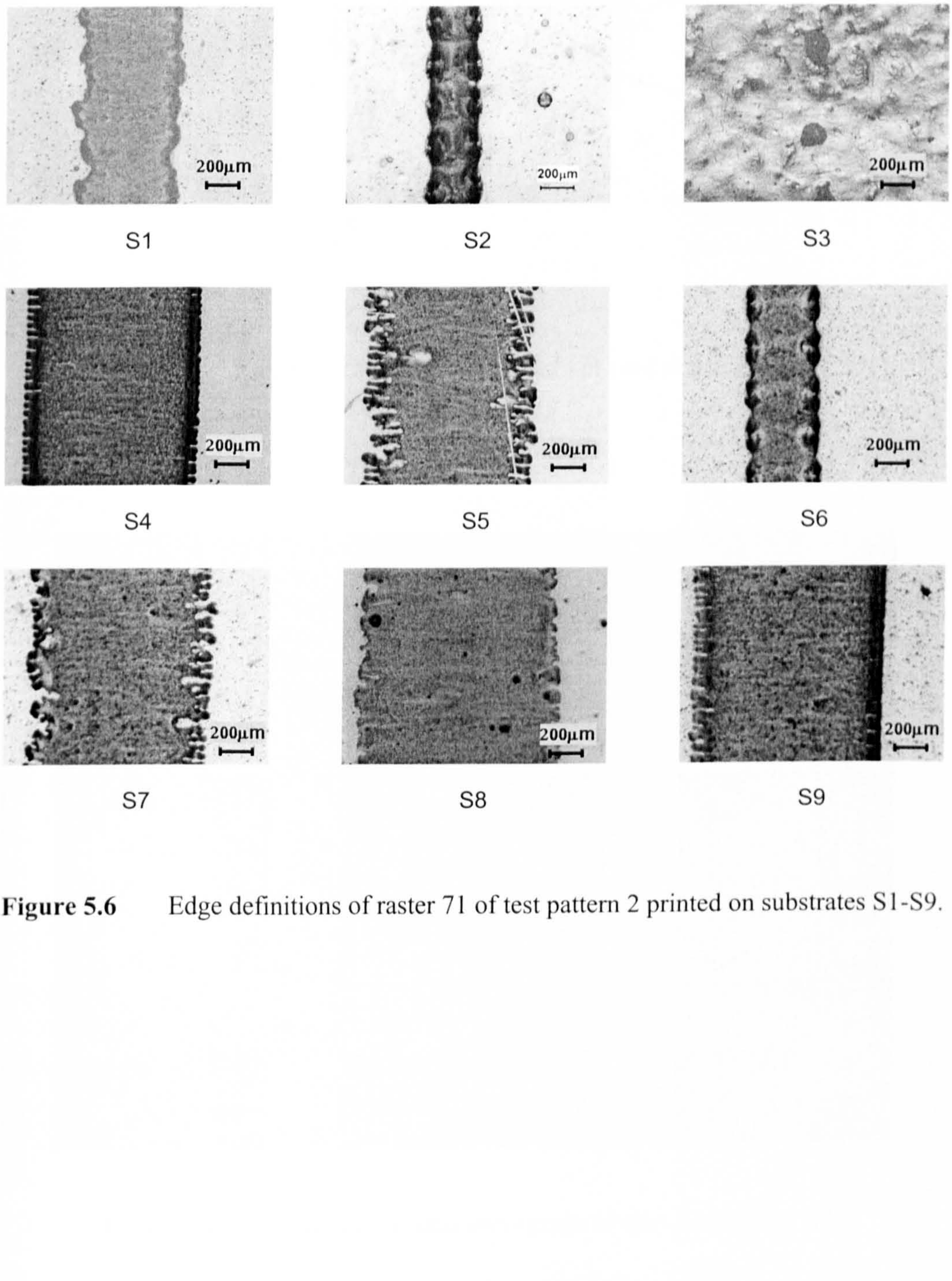

Figure 5.6 Edge definitions of raster 71 of test pattern 2 printed on substrates S1-S9.

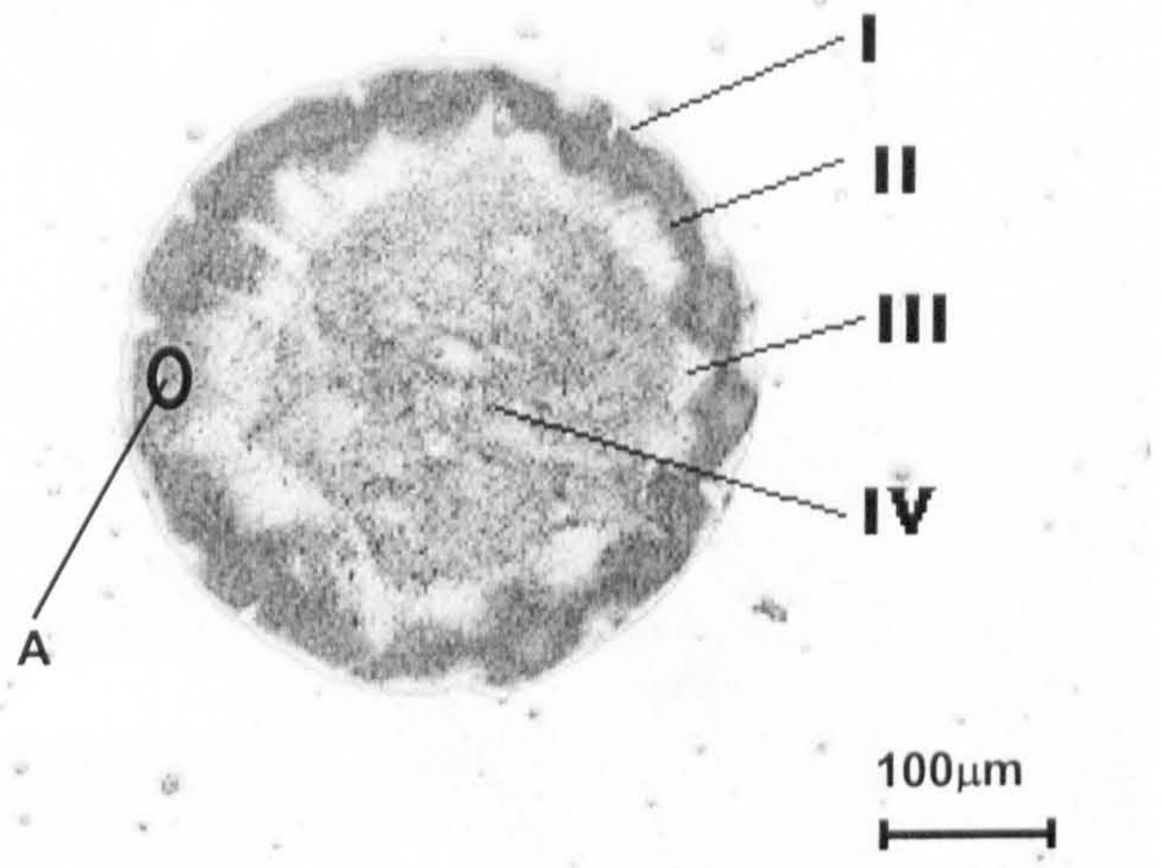

Figure 5.7 Optical micrograph of a single printed dot on substrate S2.

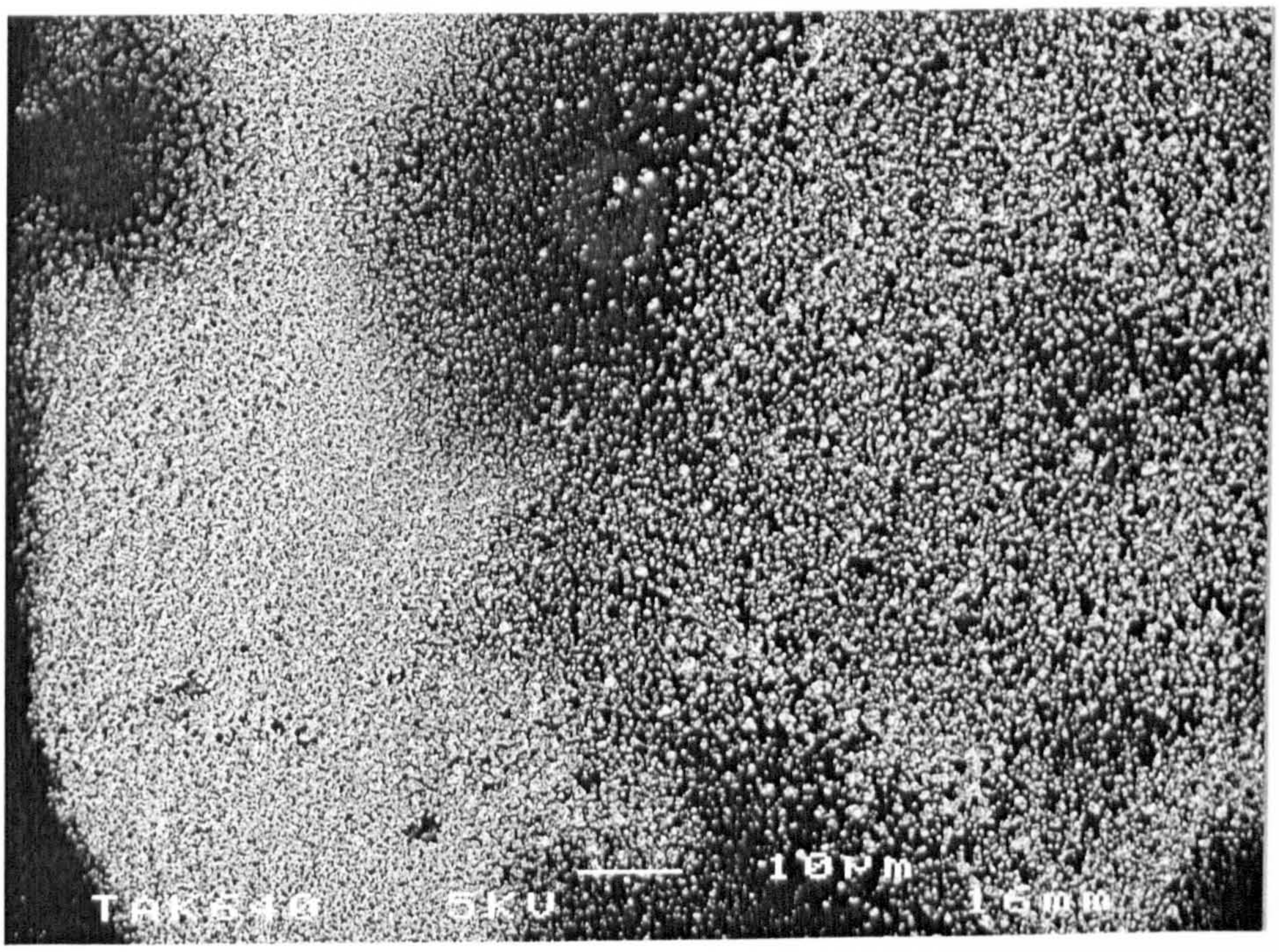

Figure 5.8 Scanning electron micrograph of spot A in Figure 5.7.

(a)

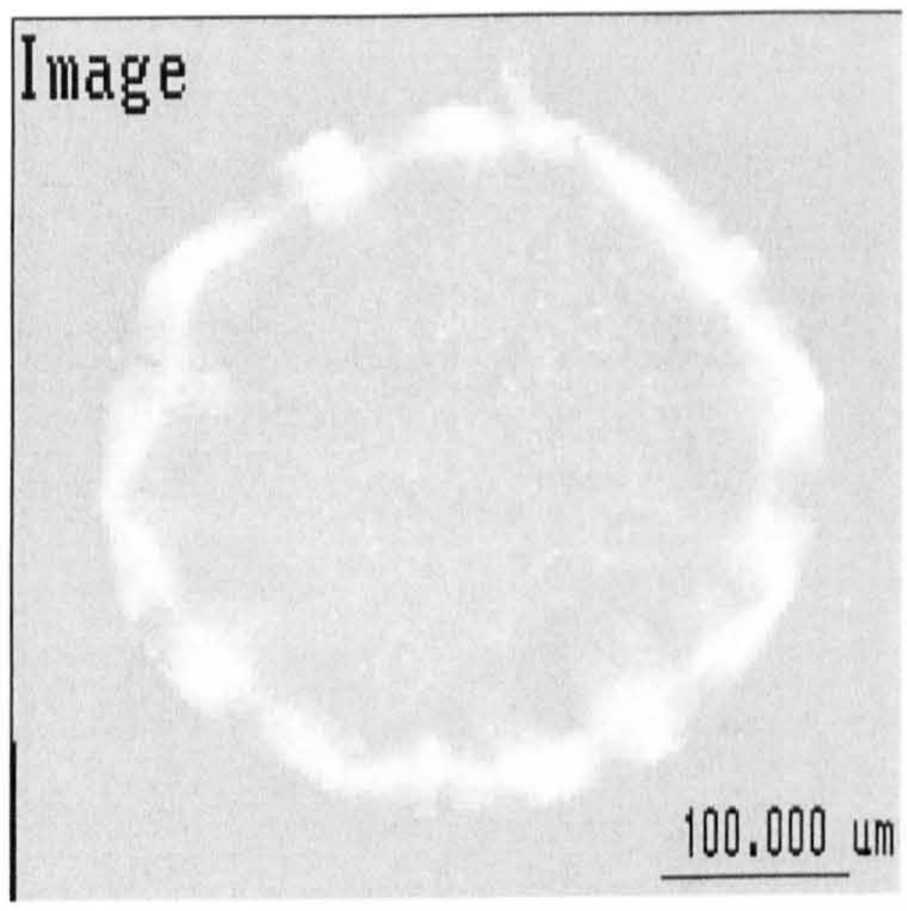

(b)

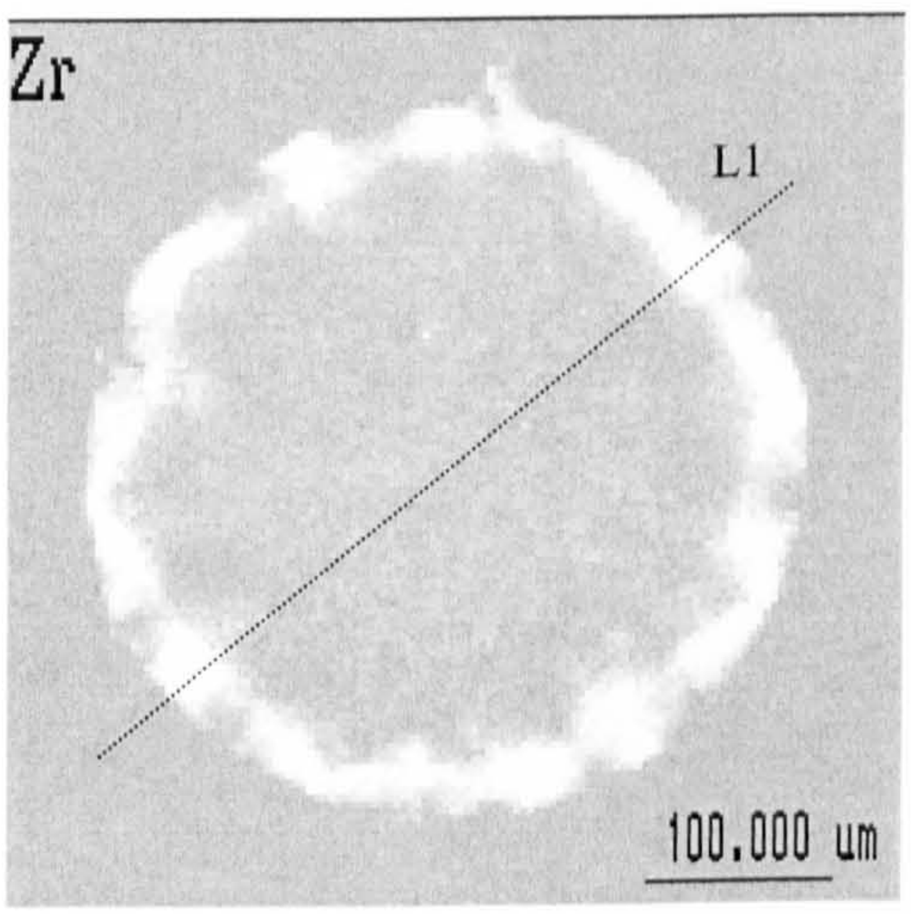

(c)

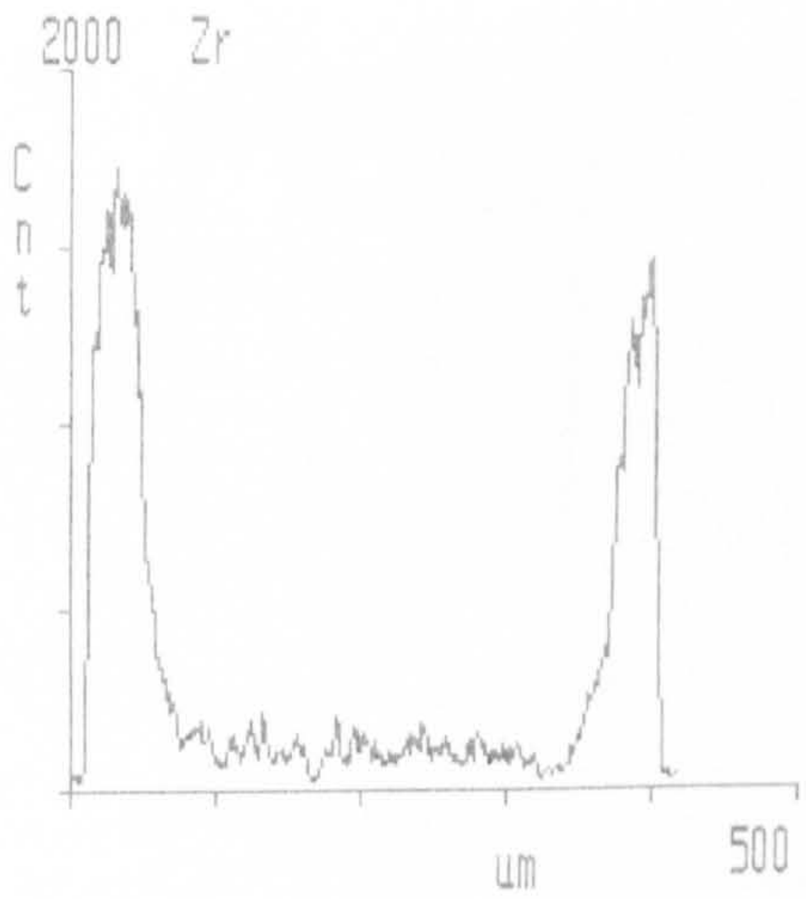

Figure 5.9 A single printed dot on the Type II substrate (S2) as analysed by SEM-EDX (energy dispersive x-ray): (a) image of the dot, (b) dot mapping of Zr, and (c) scan for Zr along line L1 in (b).

(a)

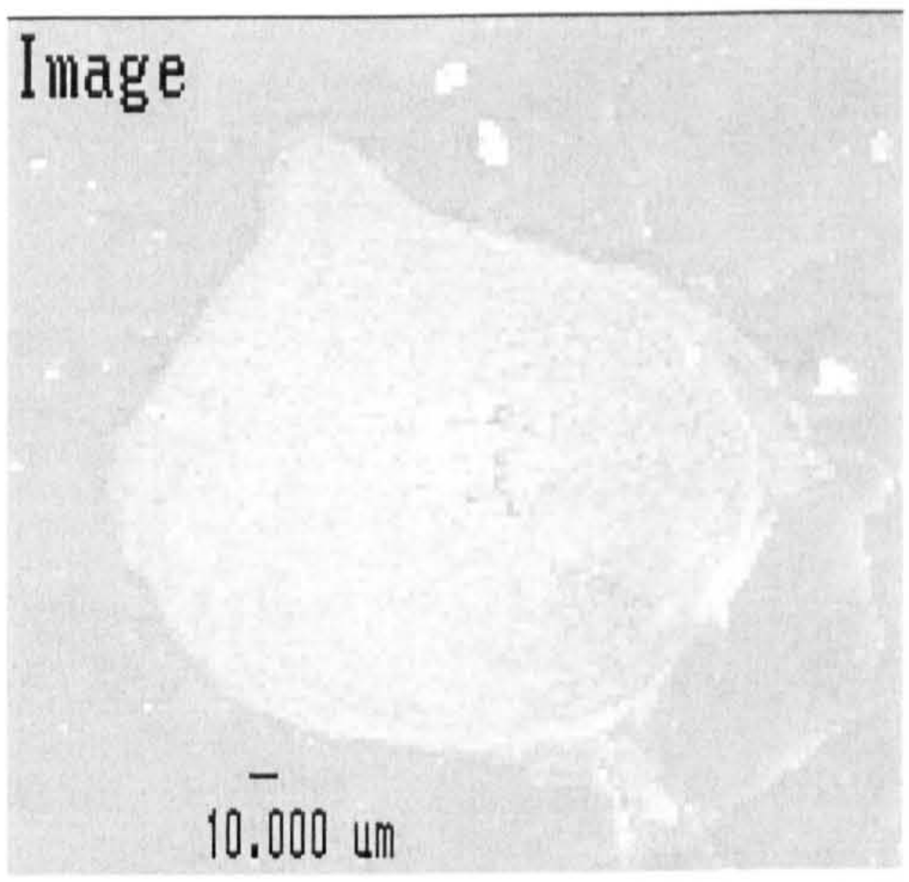

(b)

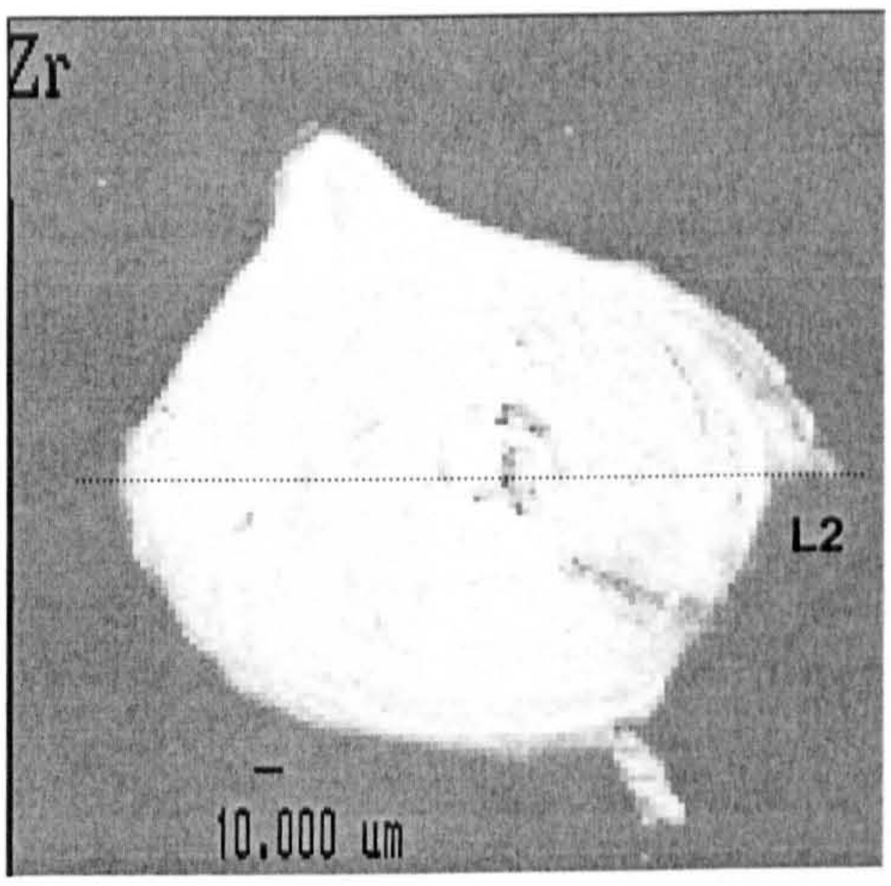

(c)

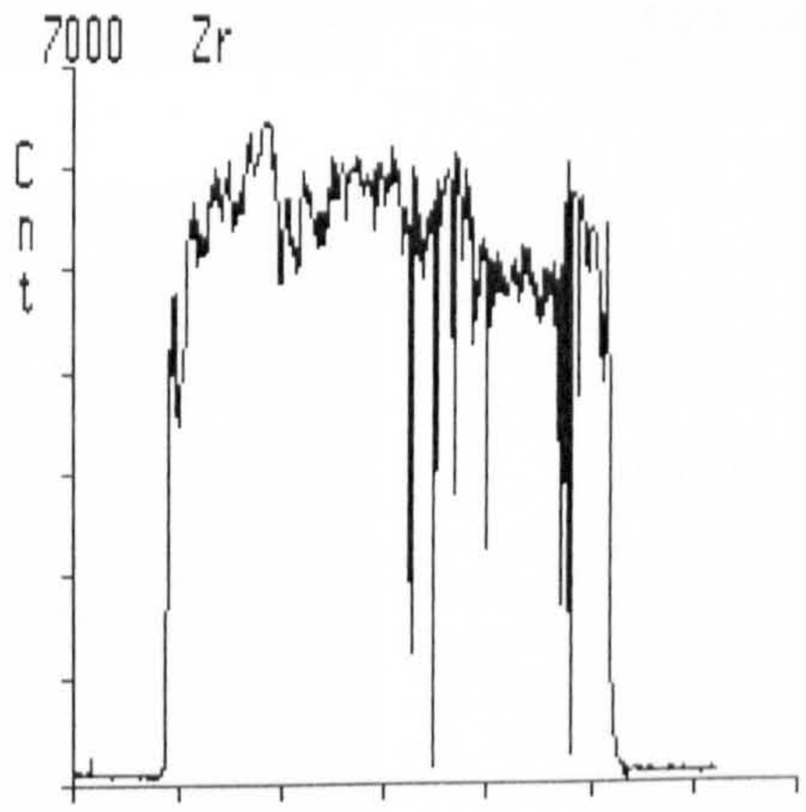

Figure 5.10 A single printed dot on the Type I substrate (S3) as analysed by SEM-EDX: (a) image of the dot, (b) dot mapping of Zr, and (c) scan for Zr along line L2 in (b).

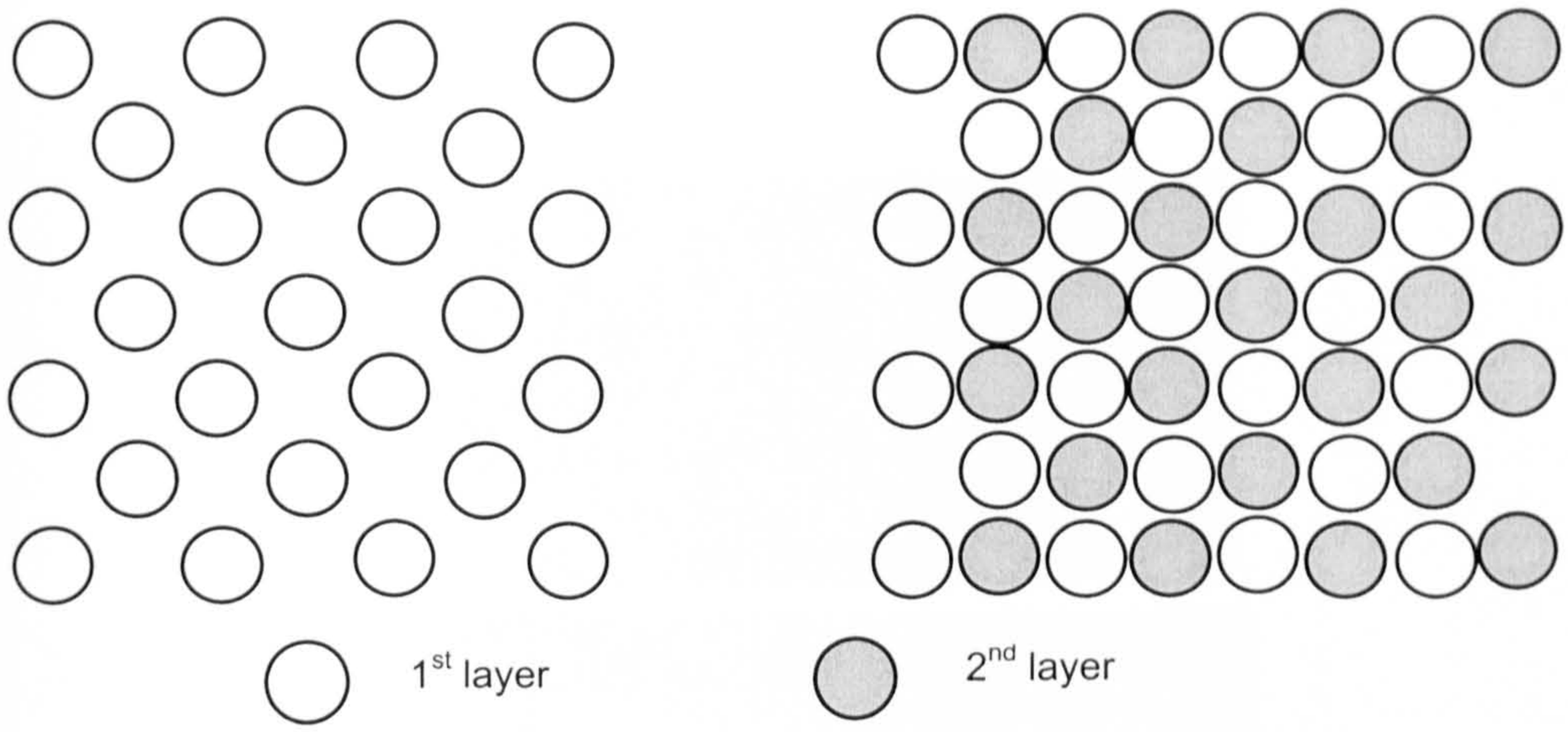

Figure 5.11 Proposed printing algorithm for Type I substrate.

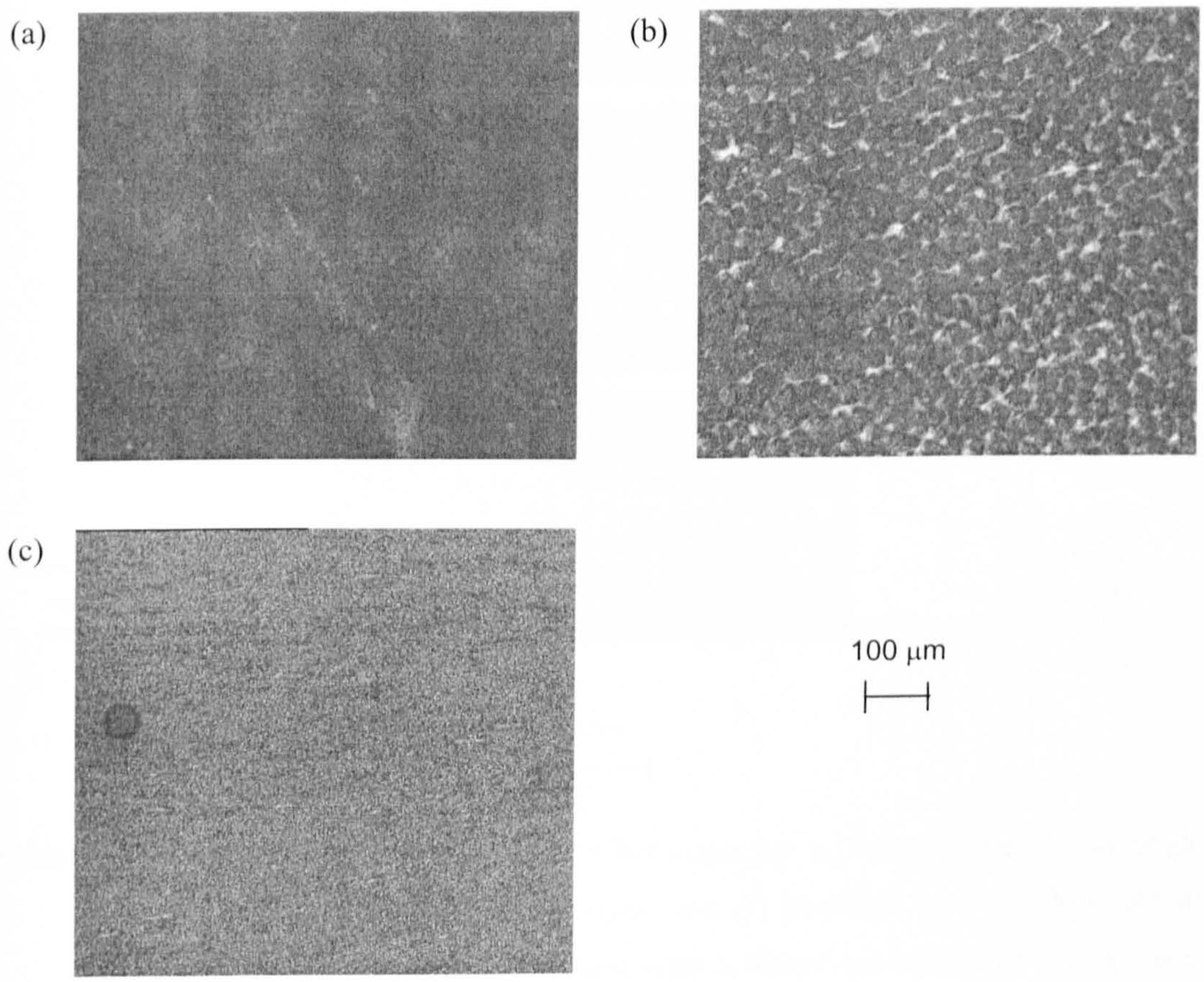

Figure 5.12 Single layer print dried under different conditions: (a) natural convection, (b) forced convection of cool air directed at print and (c) forced convection of cool air flowing across the print.

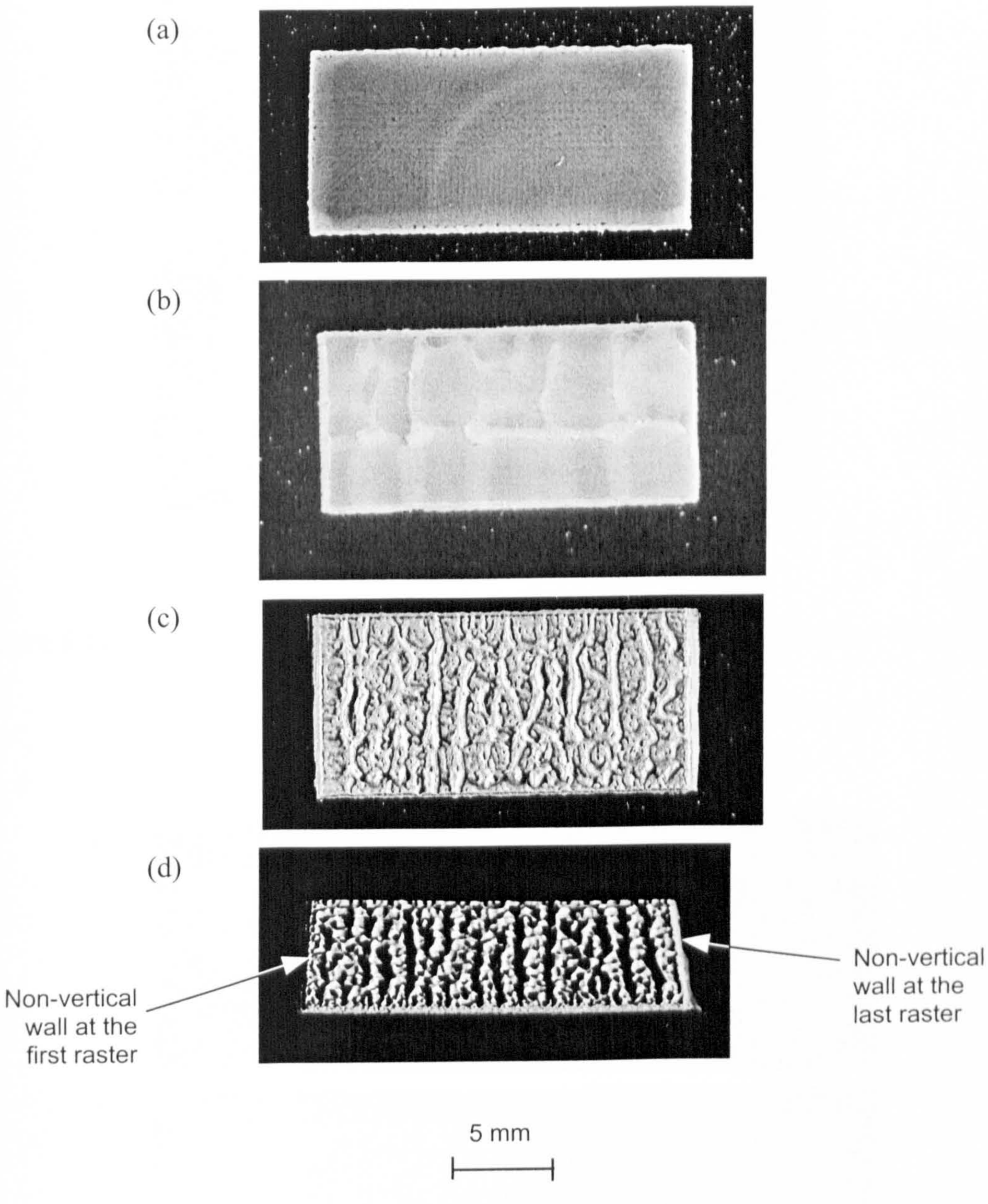

Figure 5.13 Test pattern 3 printed at 3543 x 3660 dots per m^2 on substrate S2: (a) single layer, (b) nine layers, (c) 100 layers and (d) isometric view of 300 layers of overprint. A 15 s of drying time with a forced convection of cool air was allowed between consecutive prints of (b) - (d). The scale bar is for (a), (b) and (c) only.

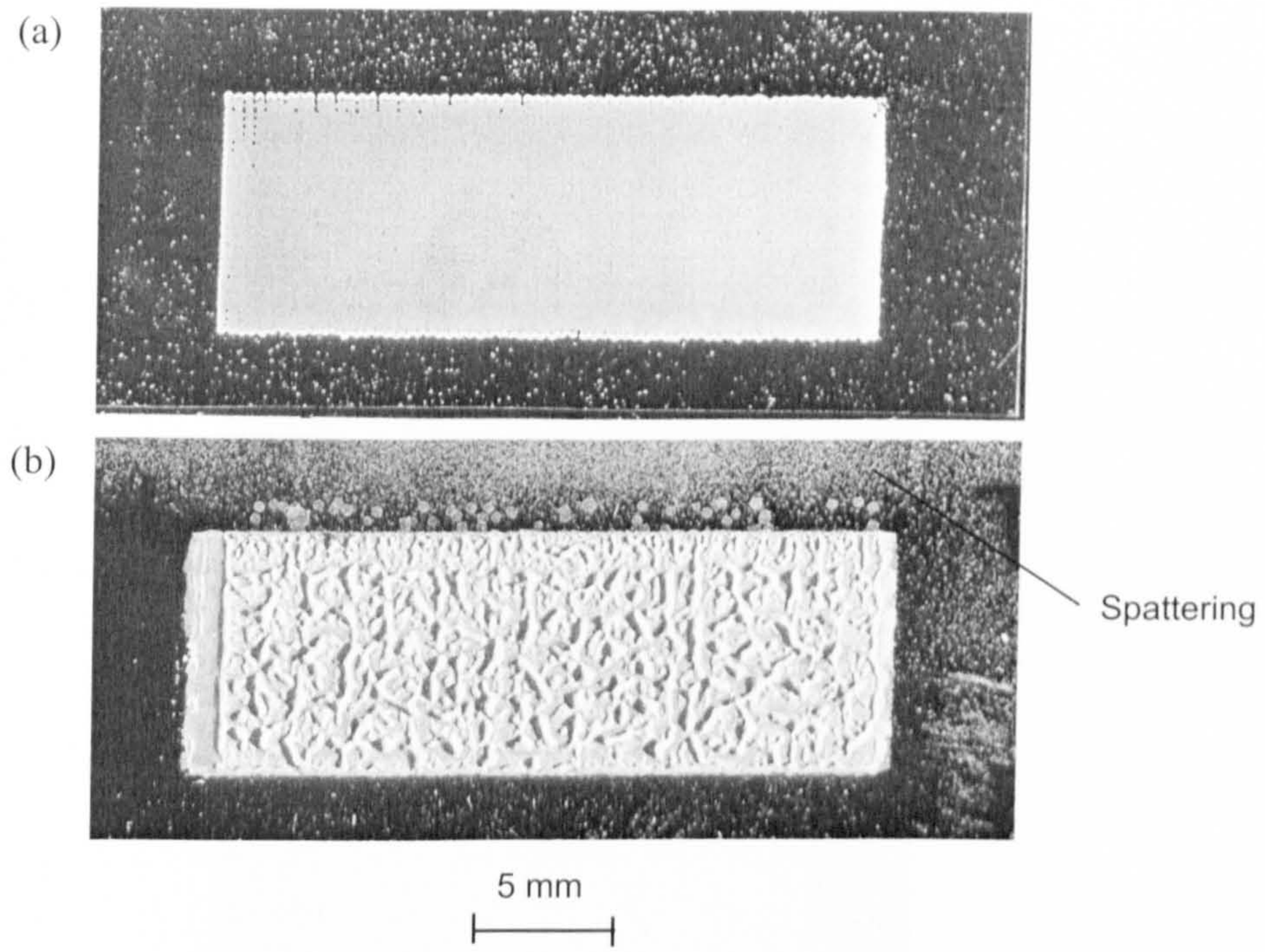

Figure 5.14 Test pattern 3 printed at 2638 x 3660 dots per m^2 on substrate S2: (a) single layer and (b) 100 layers.

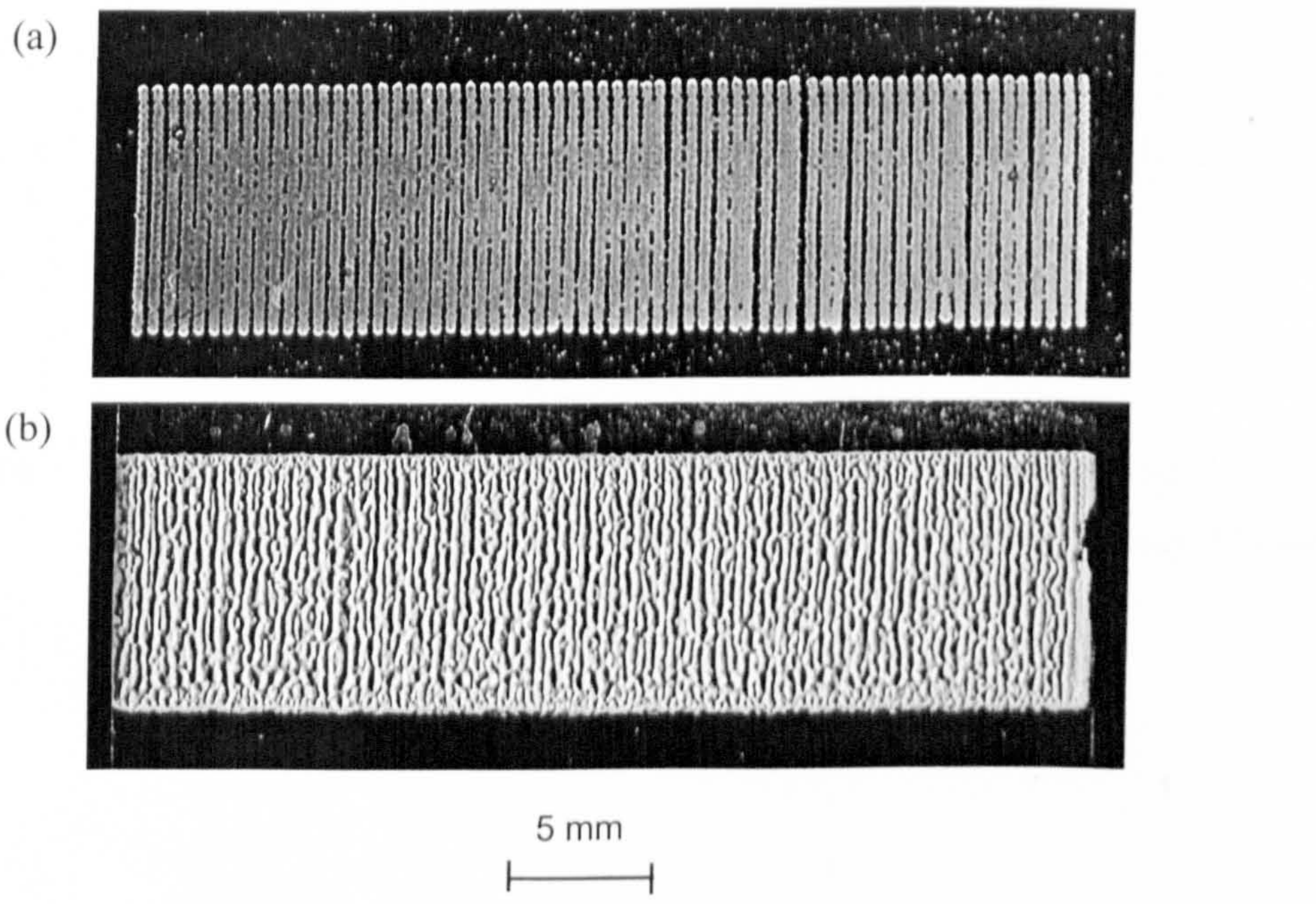

Figure 5.15 Test pattern 3 printed at 1930 x 3660 dots per m^2 on substrate S2: (a) single layer and (b) 100 layers.

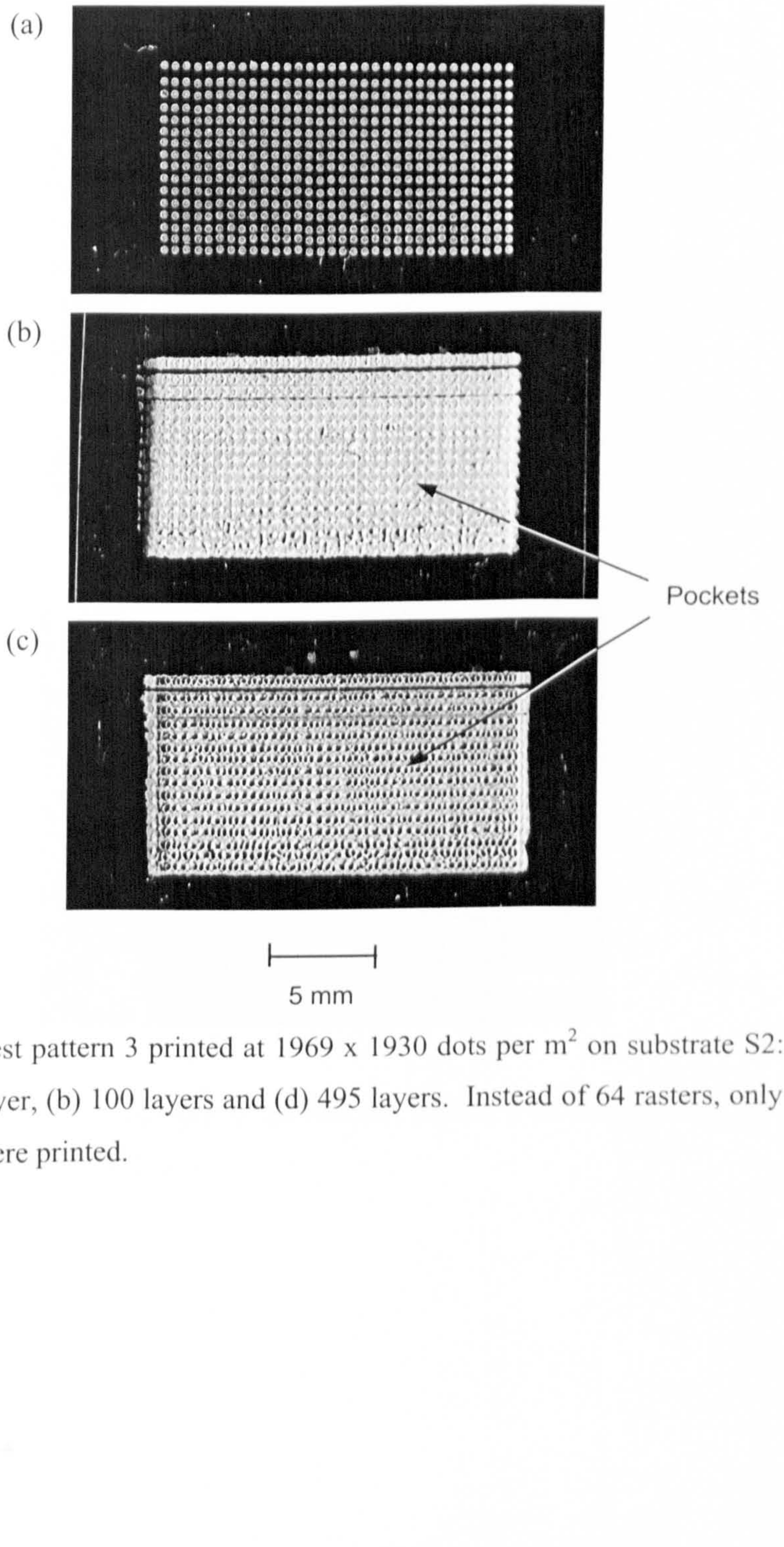

Figure 5.16 Test pattern 3 printed at 1969 x 1930 dots per m^2 on substrate S2: (a) single layer, (b) 100 layers and (d) 495 layers. Instead of 64 rasters, only 32 rasters were printed.

(a)

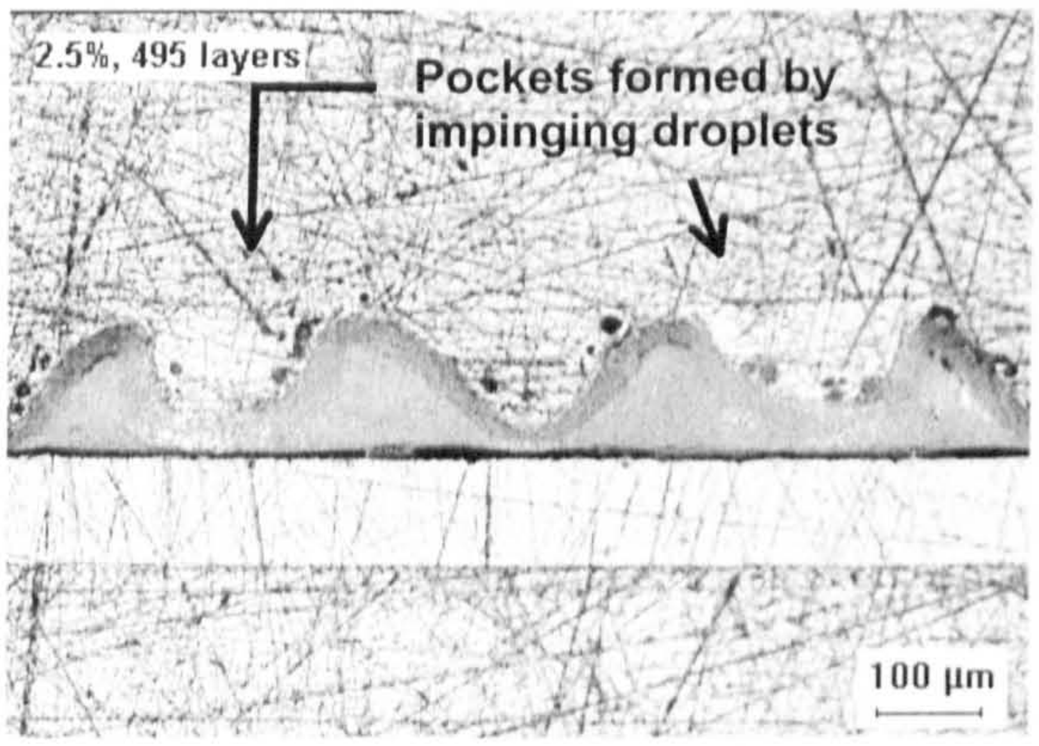

(b)

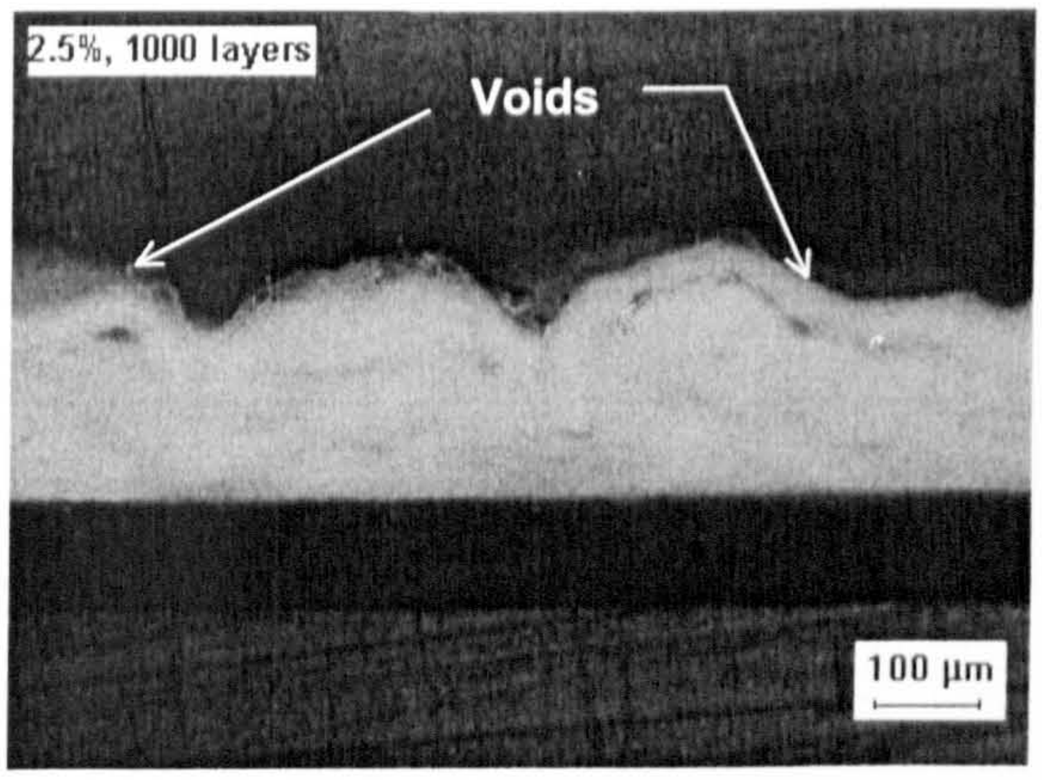

Figure 5.17 Optical micrographs of printed test pattern 3 on substrate S2: (a) 495 layers and (b) 1000 layers.

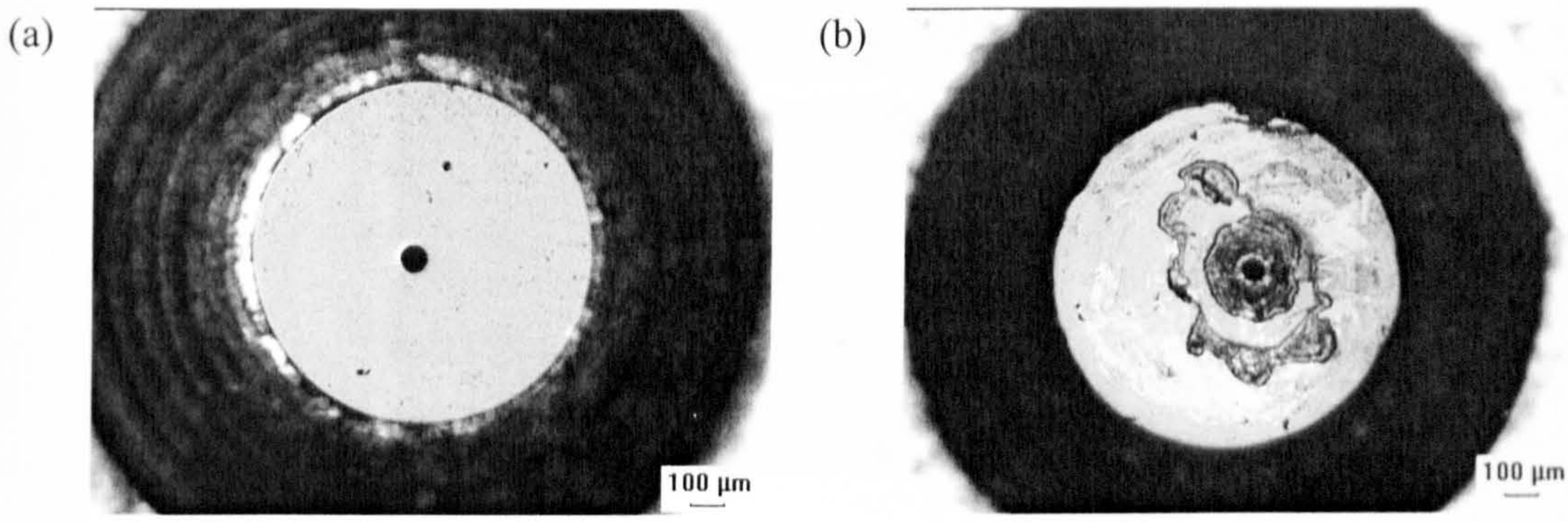

Figure 5.18 Printer nozzle: (a) before use and (b) after 1800 layers of printing.

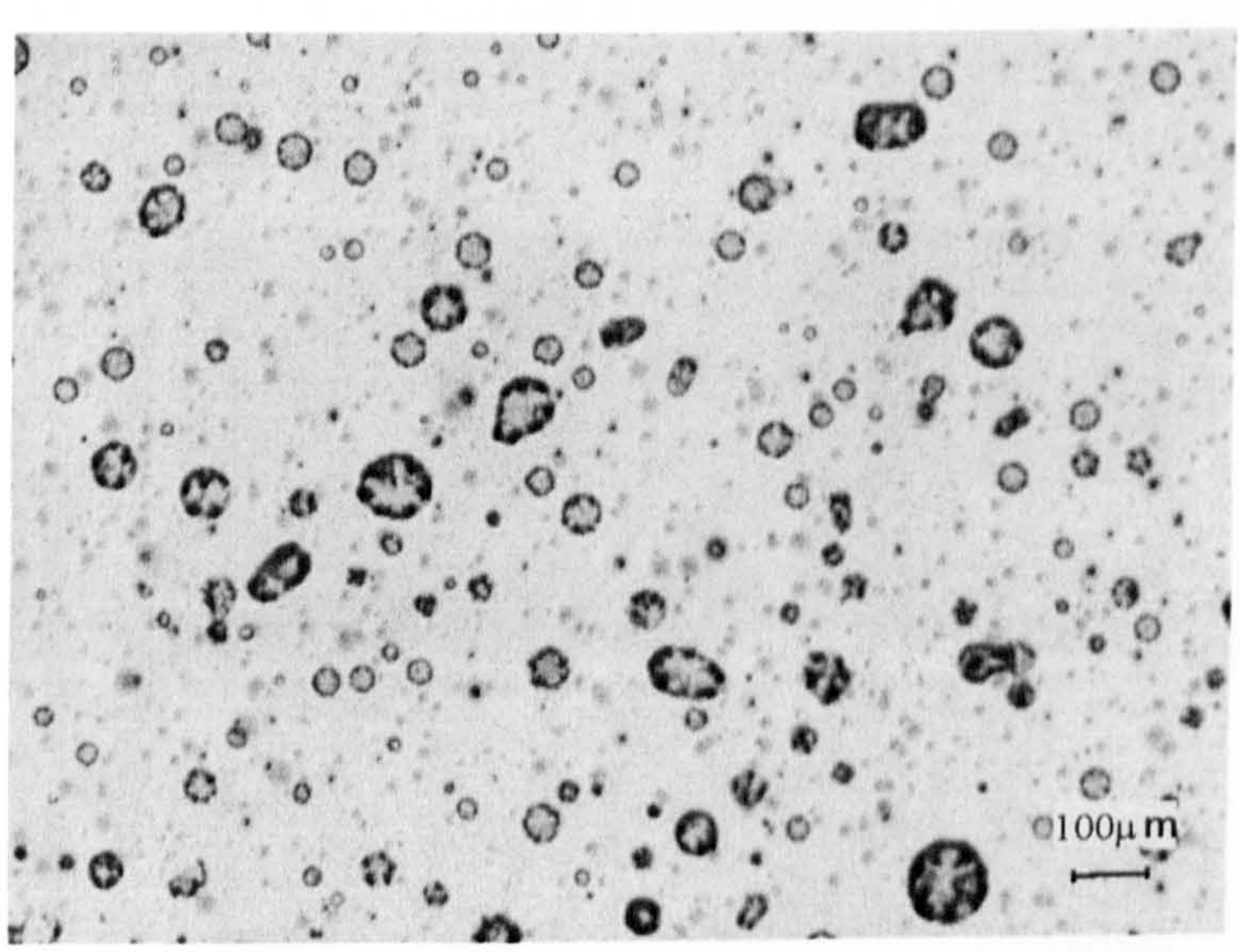

Figure 5.19 Stray drops deposited close to the printed pattern.

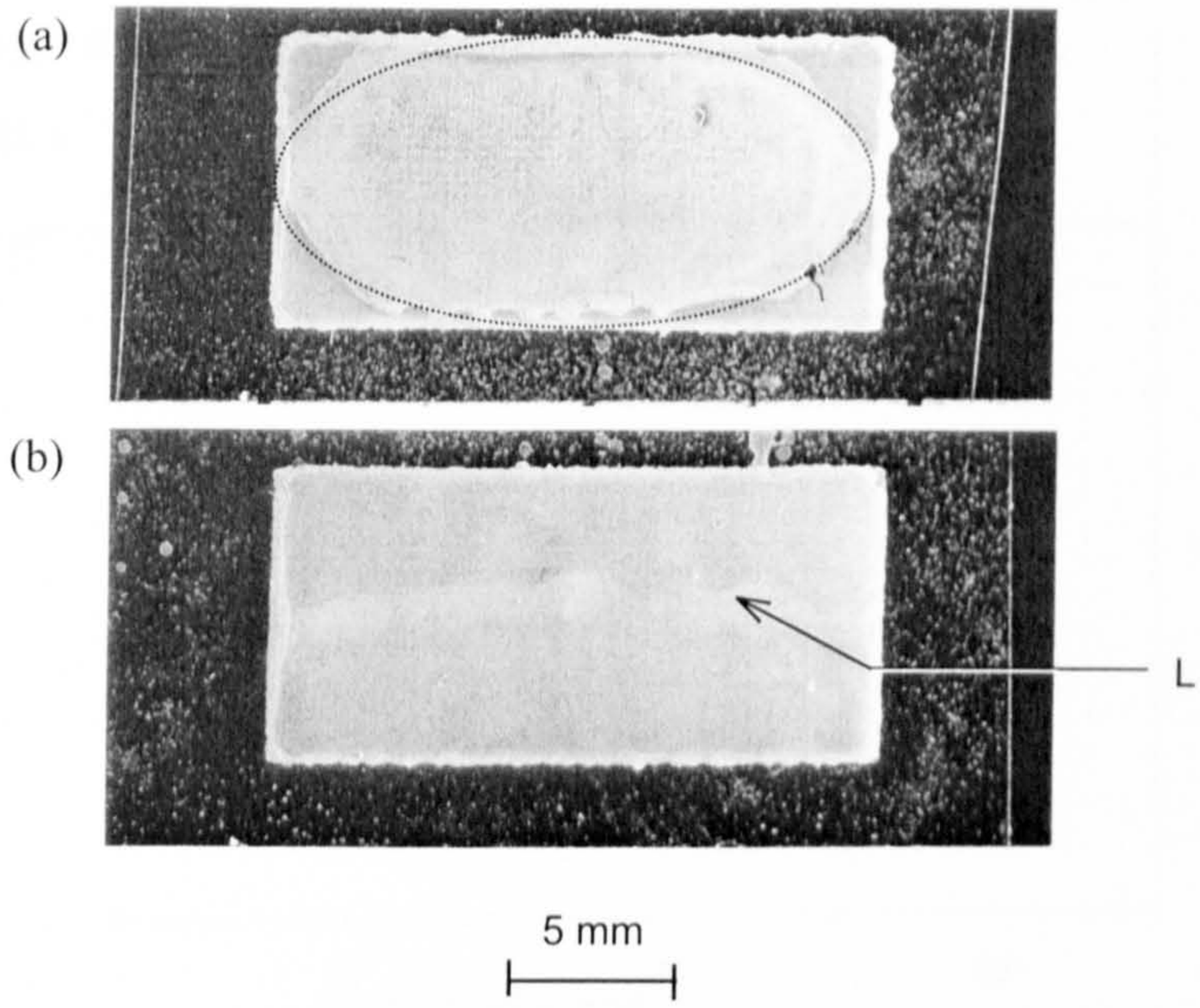

Figure 5.20 Defects appearing on overprinted parts of area 18 x 8.5 mm^2 printed at 3543 x 3660 dots per m^2 on substrate S2: (a) 4 layers of prints with frozen cooling front, t_{print} = 5 s, the dotted line indicates the boundary of the 'frozen' cooling front (b) powder accumulated at the line L after 7 layers of prints, t_{print} = 60 s.

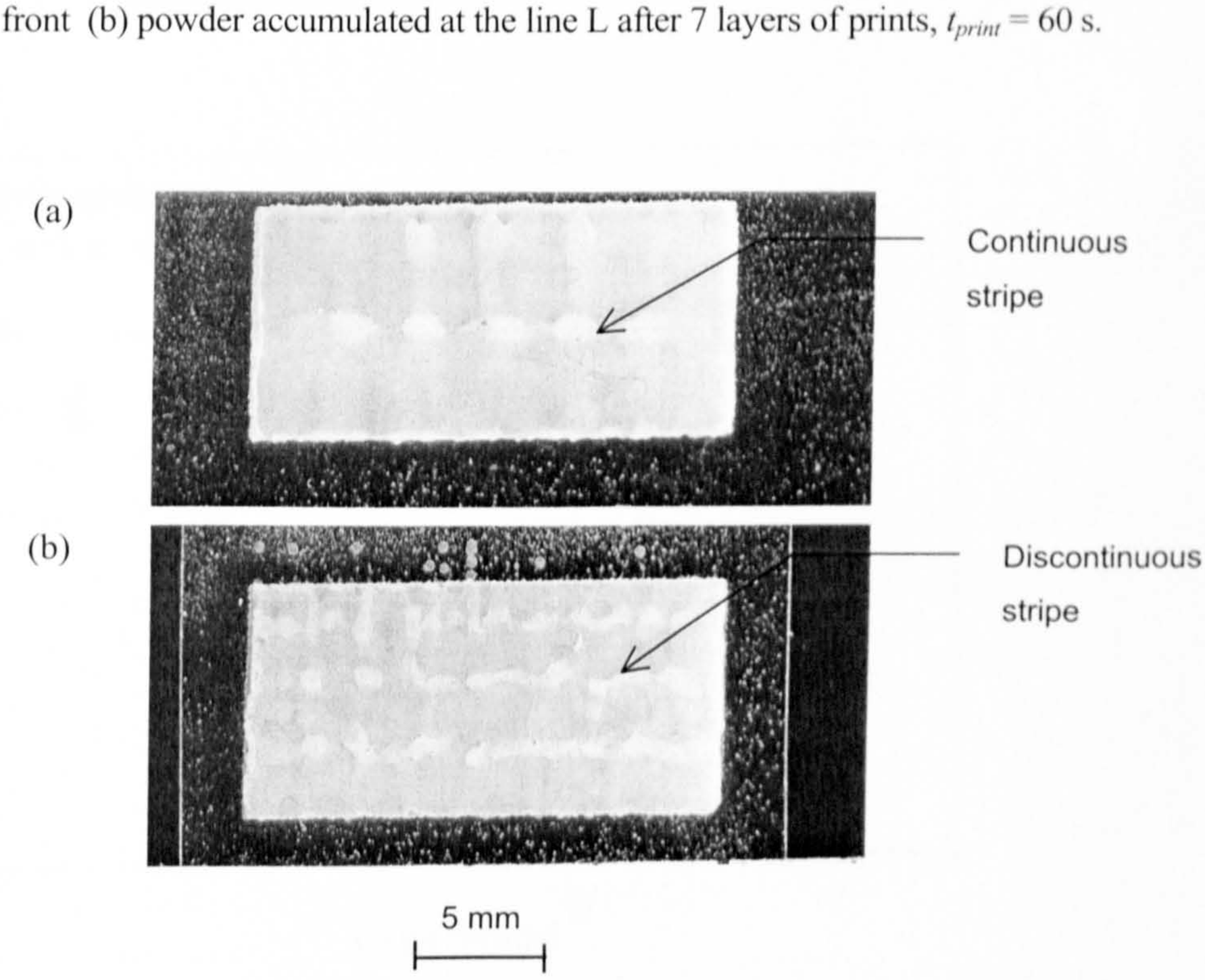

Figure 5.21 Examples of defects as of printed parts of A= 18 x 8.5 mm^2, t_{print} = 15 s: (a) forced convection of cool air (b) heated substrate.

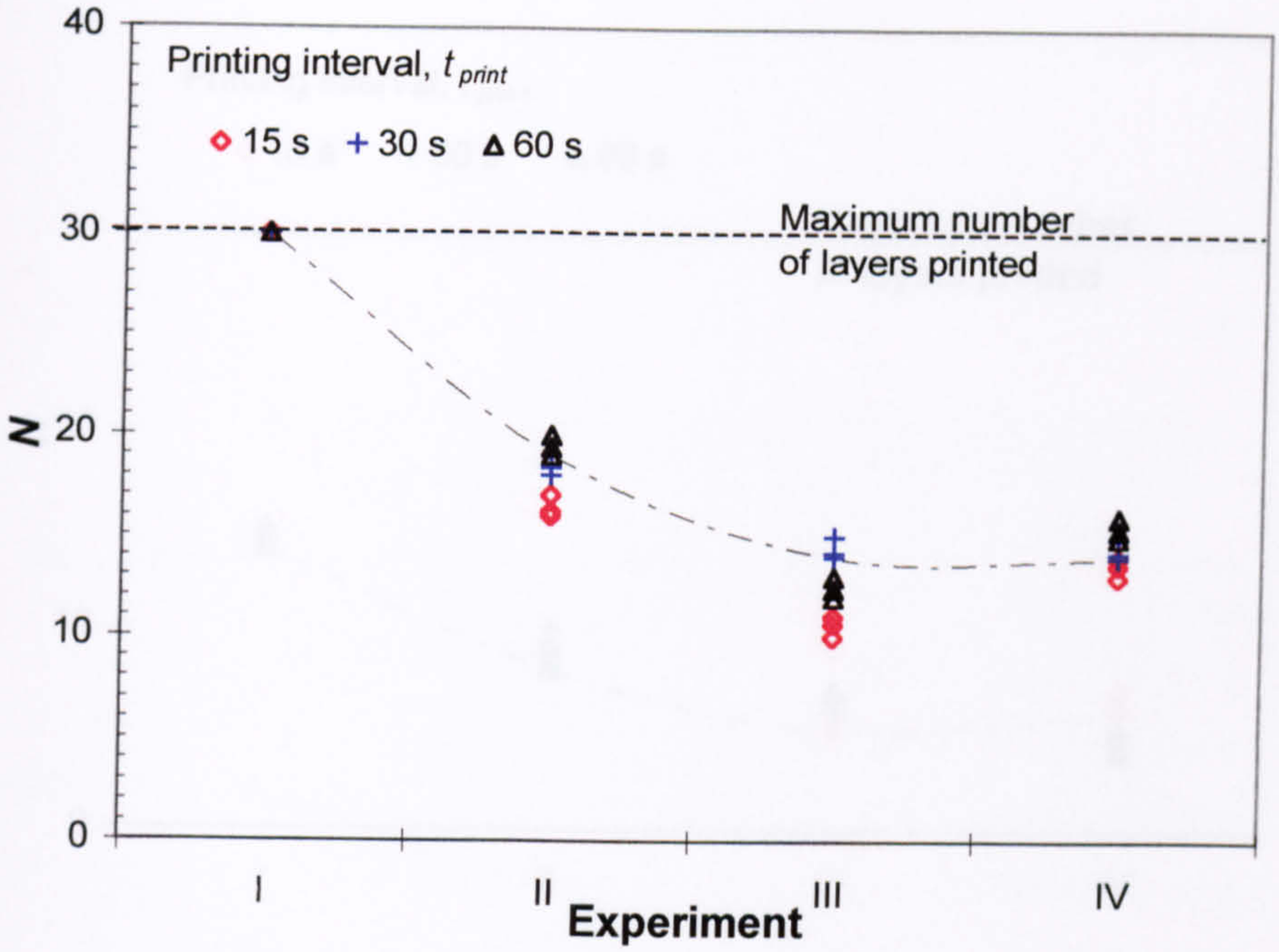

Figure 5.22 Number of layers printable (N) on a 2.2 x 2.2 mm^2 area without the occurrence of defects under different drying conditions (Experiments I to IV).

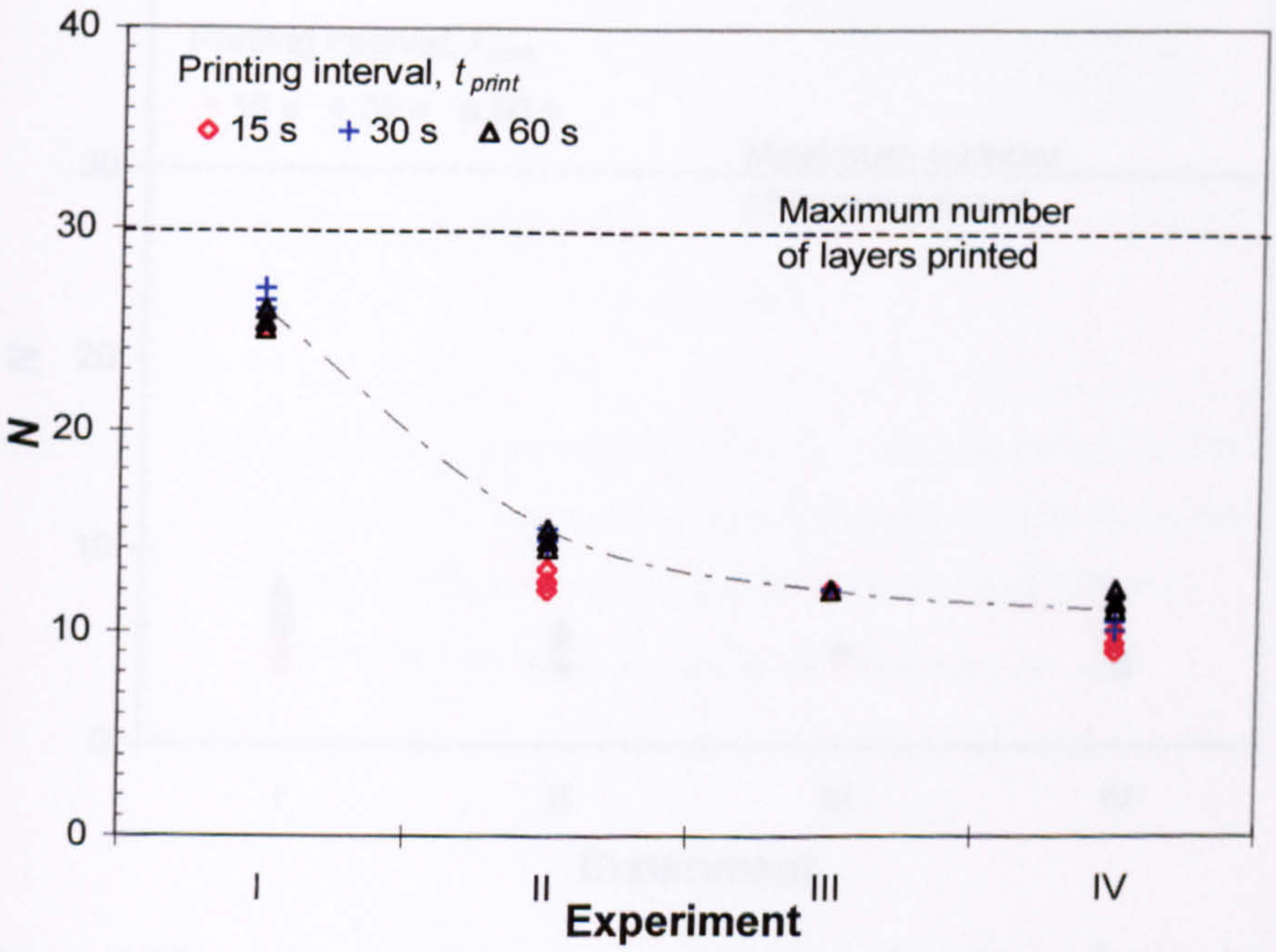

Figure 5.23 Number of layers printable (N) on a 4.5 x 2.2 mm^2 area without the occurrence of defects under different drying conditions (Experiments I to IV).

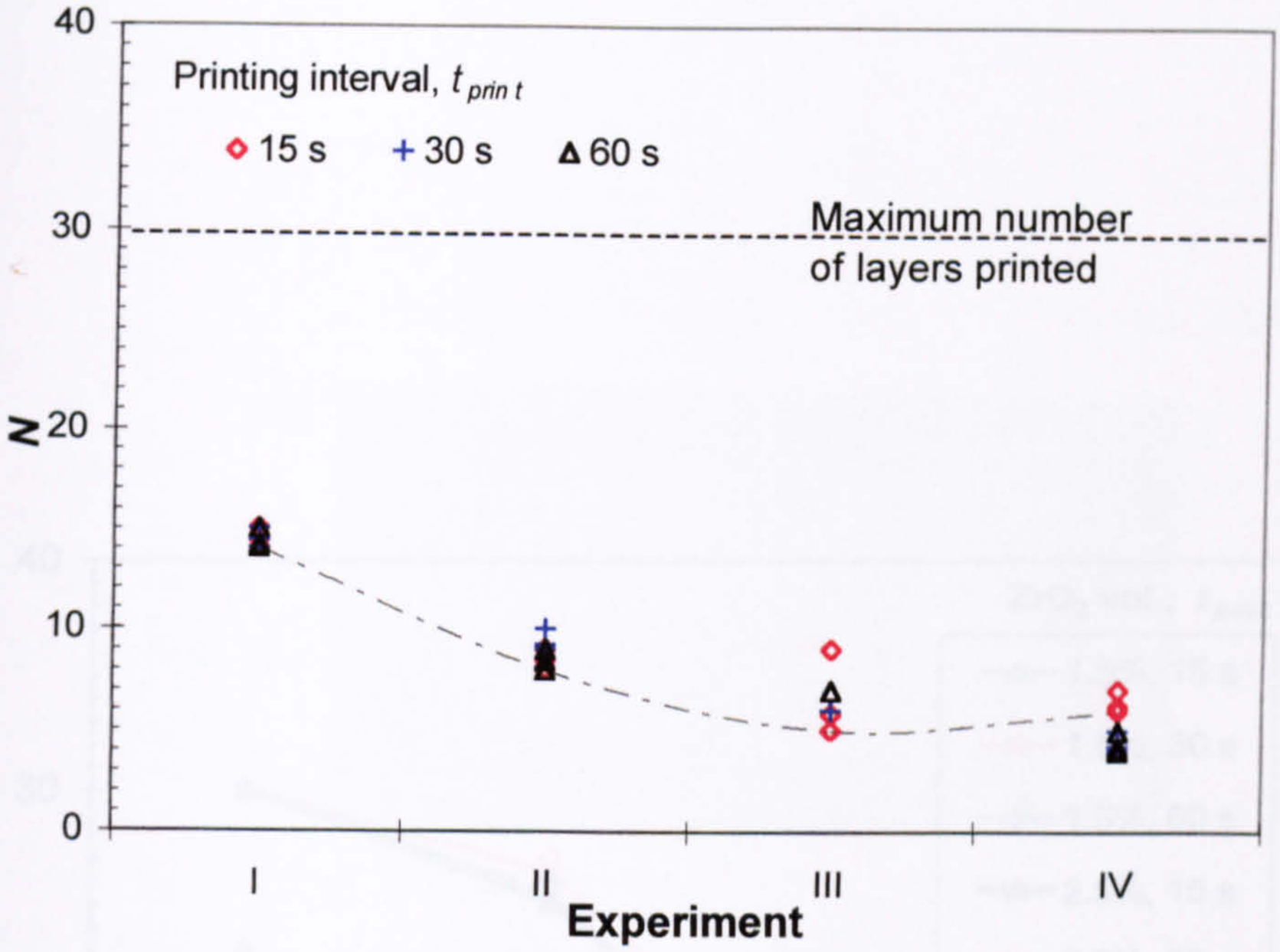

Figure 5.24 Number of layers printable (N) on a 9 x 4.5 mm^2 area without the occurrence of defects under different drying conditions (Experiments I to IV).

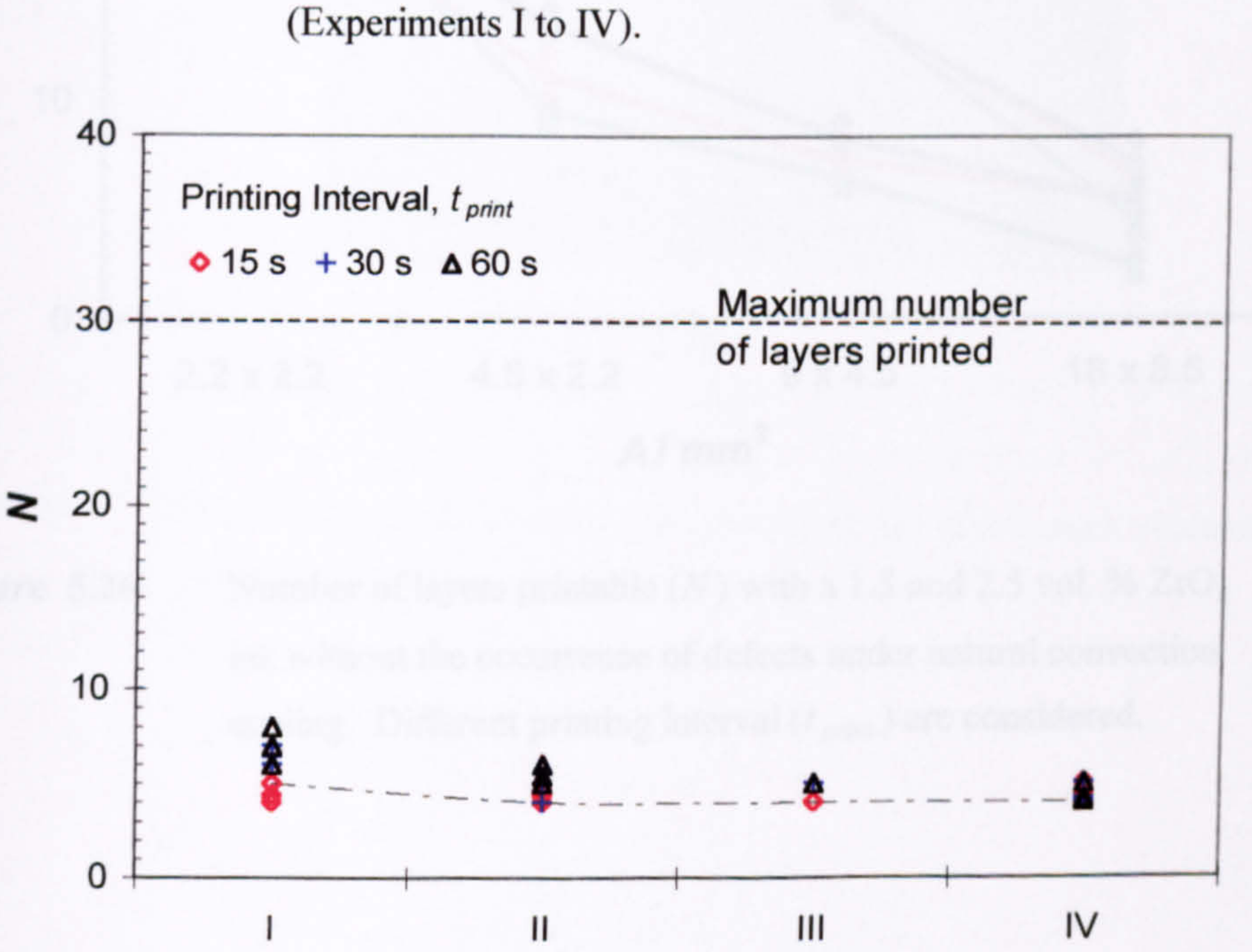

Figure 5.25 Number of layers printable (N) on a 18 x 8.5 mm^2 area without the occurrence of defects under different drying conditions (Experiments I to IV).

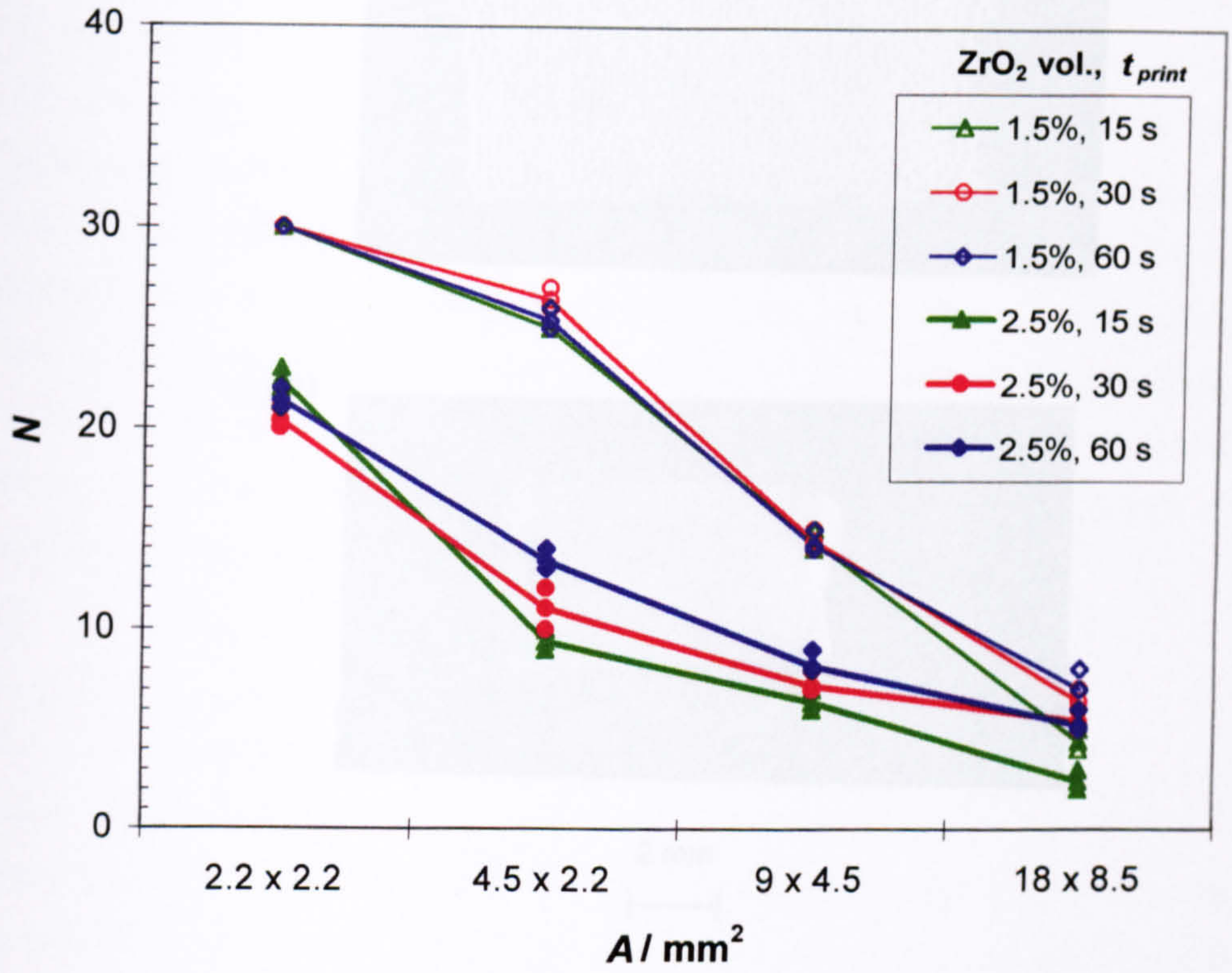

Figure 5.26 Number of layers printable (N) with a 1.5 and 2.5 vol. % ZrO_2 ink without the occurrence of defects under natural convection cooling. Different printing interval (t_{print}) are considered.

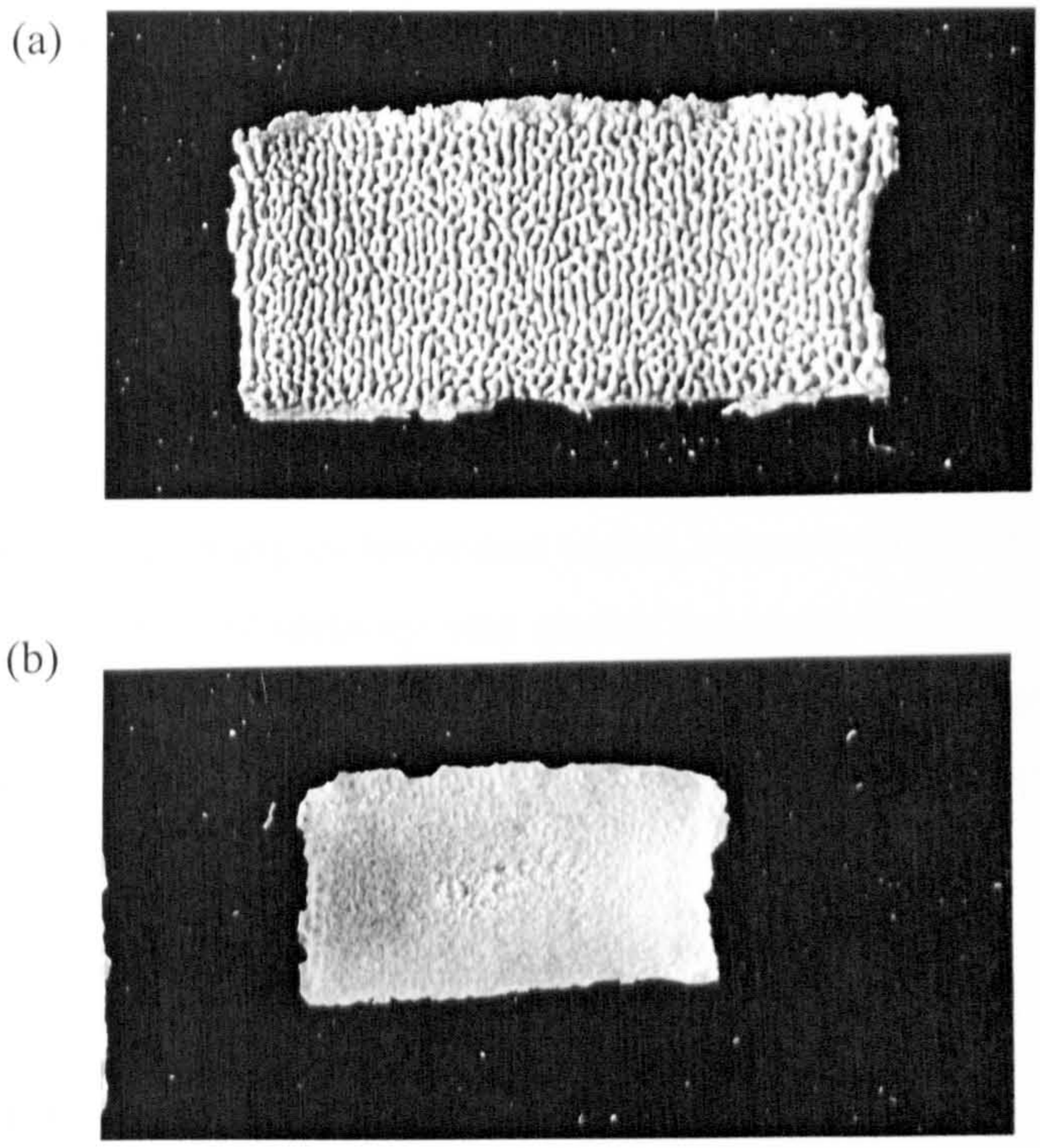

Figure 5.27 Improved surface quality after sintering (a) green part printed with 1800 layers and (b) sintered part.

Chapter

6

Geometrical Changes in a Ceramic Ink Droplet

In this chapter, the wettability and shrinkage of zirconia ink droplets deposited on substrates are investigated. The ink was previously used for Direct Ceramic Ink-Jet Printing via a continuous jet printer, as discussed in Chapters 4 and 5. Two different types of substrates were used to deposit the ink droplets. Silicone release paper (Type I) and acetate sheet (Type II) have surface free energies lower and higher, respectively, compared to the surface tension of the ceramic ink. Wettability was studied by observing the variations in contact angle and the width of ink-substrate interface. The variation of droplet height was also observed. These changes were recorded continuously on video and thus the volume shrinkage of the droplet could be calculated.

6.1 Properties

6.1.1 Ceramic Ink

ZrO_2 ink of 2.5 vol. %, which was used previously for printing in Chapter 5, was employed in this study. Table 6.1 is a summary of the composition of the ink before deposition. The average volume fraction of the ZrO_2 powder in the ink was determined at 2.5 vol. % (18 wt. %) for five samples. The average surface tension of the ink (before deposition), determined from five samples with a Wihelmy plate, was 24 mN m^{-1}.

Table 6.1 Composition of ink before deposition.

Constituent	Description	Before dilution	After dilution
		Vol. %	Vol. %
Ceramic	ZrO_2	37.6	2.5
Dispersant	Zephrym PD3315	15.2	1.0
Resins	Polyvinylbutyral and dibutyl sebcate	40.6	2.7
Electrolyte	NH_4NO_3	6.6	0.4
Solvent	Industrial methylated spirit	-	93.4

6.1.2 Substrates

Droplets of ZrO_2 ink were deposited on silicone release paper (substrate S3) and acetate sheet (substrate S2). The silicone release paper (Type I substrate) has a surface free energy, γ_{sv} lower than the surface tension of the ink. The acetate sheet (Type II substrate) has a higher γ_{sv} than the surface tension of the ink. The values are given in Table 6.2. Further details of S2 and S3 were given in Table 5.2.

Table 6.2 Surface free energies of substrates S2 and S3.

Type	Description	γ_{sv} / mN m^{-1}
I	Silicone release paper (S3)	20
II	Acetate sheet for photocopying and laser printing (S2)	42

6.1.3 Mass Loss

Figure 6.1 shows the mass loss during evaporation. Mass loss occurred at a constant rate for about 130 s but then is faster on the Type II substrate due to more spreading of the ink on it as discussed below.

6.1.4 Swelling Test

Both substrates were immersed in industrial methylated spirit for 250 s and their thickness was measured every 5 s. There was no significant swelling in these substrates (Figure 6.2) over this period and the corresponding change in thickness was negligible. Therefore, it can be assumed that the droplets, which were deposited on both substrates in this study, dried by evaporation.

6.2 Initial contact

After the droplet detached from the syringe tip and came into contact with the substrate, it spread during the first 2 s (Figure 6.3). Concurrently, there were rapid reductions in θ and H on the Type II substrate but on Type I, a slight increase in θ and H was observed. θ and H are the average contact angle and height of the deposited droplet on the substrate, respectively (see also Figure 3.12).

The increase of θ and H on the Type I substrate was the result of vibration in the droplet when it came into contact with the substrate. A careful examination of the droplet after initial contact in Figure 6.4a shows blurring of the image at the top. Thus, the droplet was still in motion when detached from the needle tip and only stabilised after about 2.5s (Figure 6.4b). In a separate experiment, where the droplet was released from a height of 30 mm, as shown in Figure 6.5, there was severe deformation of it on impact with the substrate. This phenomenon was not detected for ink droplets landing on the Type II substrate. In substrate Type II, with a higher surface free energy than the ink's surface tension, there was greater wettability, i.e. lower θ. The movement of liquid due to the increased wettability helped to establish stability rapidly when the droplet was deposited. This resulted in a higher W (which is the width of the base of the deposited droplet) and lower H values to begin with (Table 6.3), and indeed, a higher W/H ratio. Thus, a stable droplet with a lower centre of gravity was accommodated on substrate Type II and this dampened vibration in it.

Table 6.3 Values of volume, average contact angle (θ), width (W) and height (H) of stabilised ceramic ink droplets deposited on each substrate (also see Figure 3.12). The average values for width and height are taken as W_o and H_o, respectively.

Substrate	V / mm^3	θ / degree	W / mm	H / mm
I	1.7	36	2.97	0.48
	2.0	37	3.12	0.53
	2.1	38	3.07	0.52
Average	*1.9 ±0.2*	*37±1*	*3.05 ±0.08*	*0.51 ±0.03*
II	2.5	29	3.65	0.46
	3.0	31	3.79	0.47
	2.3	30	3.49	0.45
Average	*2.6 ±0.4*	*30 ±1*	*3.64 ±0.15*	*0.46 ±0.01*

6.3 Geometrical Changes during Drying

The volume (V) of the spherical cap of ink on the substrate is calculated by Erbil [1999] as:

$$V = \pi W^3 (2 - 3\cos\theta + \cos^3\theta) / (24\sin^3\theta) \qquad (6.1)$$

After detachment from the syringe and deposition on the substrate, the volume of the stabilised ink droplet was calculated using Equation 6.1. There was a 1° variation in θ measurements, as shown in Table 6.3, for three droplets deposited with varying volume V_o. Theoretically, the value of θ on a homogenous solid surface is independent of V [Zisman, 1964] and hence in this experiment, the surface of the substrate can assumed to be uniform.

The variation of θ during drying of the ceramic ink droplet deposited on both types of substrate is shown in Figure 6.6. Variations of W and H were normalised with respect to their respective values at zero time (Table 6.3) and plotted in Figures 6.7 and 6.8, respectively.

The droplet retained the spherical profile except after 120 s and 65 s for the Type I and II substrates, respectively. Within these periods where the spherical profile was maintained, θ,

W and H values showed a maximum standard deviation of <±5%, expressed as a percentage of the average value. When the spherical fit could not be used, θ_l, θ_r, W and H were measured manually and there were larger variations in the data collected with the maximum standard deviation, expressed as a percentage of the average value, amounting to ±12%, ±5% and ±10%, for θ, W and H, respectively. θ_l and θ_r are the left and right, respectively, contact angle of the droplet (Figure 3.12)

Using variations in θ, W and H, the dynamics of shrinkage of the ceramic ink droplets on the two types of substrate are illustrated in Figures 6.9 and 6.10 and discussed as follows.

(a) Type I Substrate

After the droplet has stabilised, it remained stationary with W virtually constant (Figure 6.9a). At the same time, θ and H were decreasing due to evaporation. After about 10 s, the droplet started to shrink as an entity, as illustrated in Figure 6.9b while θ remained virtually constant. Concomitantly, W and H were reduced. Subsequently, there was a reduction in θ with W remaining constant (Figures 6.9c and d).

(b) Type II Substrate

The shrinkage of the ceramic ink droplet during drying on the Type II substrate was markedly different. The high surface free energy of this substrate induced an immediate and rapid spreading of suspension soon after deposition. This caused difficulty in printing arrays of droplets close to one another because there is a tendency for the neighbouring droplets to coalesce. Thus, a rapid decrease in θ and an increase in W were observed initially (Figure 6.10a). This resulted in a greater area for evaporation and H decreased at rate $R1$, as shown in Figure 6.8. After the initial wetting and spreading of the suspension in the first 2 s, W remained constant throughout the rest of the experiment (Figure 6.10b) because of pinning at the contact line of the droplet and accumulation of zirconia at the droplet's periphery. Pinning and powder migration have also been observed during ink-jet printing, where the droplets were released with an initial velocity of 22.3 m s^{-1} (Section 5.3.3). These restricted evaporation and drying took place only in the H direction, as evidenced by its decrease (Figure 6.10) and the reduction in θ (Figure 6.8).

Instead of one continuous line with very small variation in slope as in Type I substrate, *H* was reducing at three different linear rates *R1*, *R2* and *R3* for droplets deposited on Type II substrate during the period of study, with *R1* > *R2* > *R3*. From 70 to 90 s, H decreases at a rate *R3*, which is the slowest and at this stage, the droplet has departed from its spherical fit apart from a central region.

(c) Further Drying

Continuation of drying of the ceramic ink droplets on both substrates (>160 s for Type I and >90 s for Type II) resulted in significant deviation from the spherical-cap shape (Figure 6.11). The affixation of a 'foot' around the edge of the droplet described by Parisee and Allain [1997] was observed on both substrates. Parisee and Allain [1997] also detected an advance of particles into the middle of the droplet and this resulted in an 'outgrowth'. In this work, no 'outgrowth' was observed in the middle of the dried droplet deposited on both substrates.

6.4 Shrinkage

The volumetric shrinkage of the ink droplets over 160 s and 90 s for Type I and II substrates, respectively, was calculated using Equation 6.1 and is plotted in Figure 6.12. In the case of the Type I substrate, only data collected after the droplet has stabilised (after 2.5 s) were considered. The ink droplet experienced two distinctively different shrinkage rates on both substrates with *SR1* > *SR2* as shown in Figure 6.12. In the case of the Type II substrate, *SR1* presided over a shorter duration (of 2 s). Approximately the same average volumetric shrinkage of 70% was experienced on both substrates at the end of 160 s for Type I and 90 s for Type II. The ink droplet deposited on Type II substrate thus shrank about twice as fast compared with those on the Type I substrate.

6.5 Summary and Conclusions

Ceramic ink droplets containing 2.5 vol. % of ZrO_2 particles used in jet printing were deposited on two substrates of different levels of surface free energy in comparison to the surface tension of the ink. The evolution of contact angle, width of the ink-substrate

interface and droplet height was measured as a function of time from digital images of the droplet captured on video. The dynamics of shrinkage of the ink was found to be different.

(i) Droplets deposited on a substrate with lower surface free energy than the surface tension of the ink (Type I) underwent a short period of expansion-contraction before it stabilised. It then shrank with the ink-substrate interface width remaining constant while the contact angle and droplet height decreased. This was followed by a second stage of shrinkage where the contact angle remained constant while the contact interface width and droplet height reduced. The droplet then continued to shrink further, but with a stationary contact interface width and a reducing contact angle and droplet height.

(ii) When deposited on a substrate with higher surface free energy than the surface tension of the ink (Type II), the droplet shrank rapidly with an expanding contact interface width and a decreasing contact angle and droplet height. In the second stage of shrinkage, the contact angle and droplet height decreased while maintaining a constant contact interface width.

(iii) The overall shrinkage rate of the ceramic ink deposited on the Type II substrate was faster than that on the Type I substrate by almost two times.

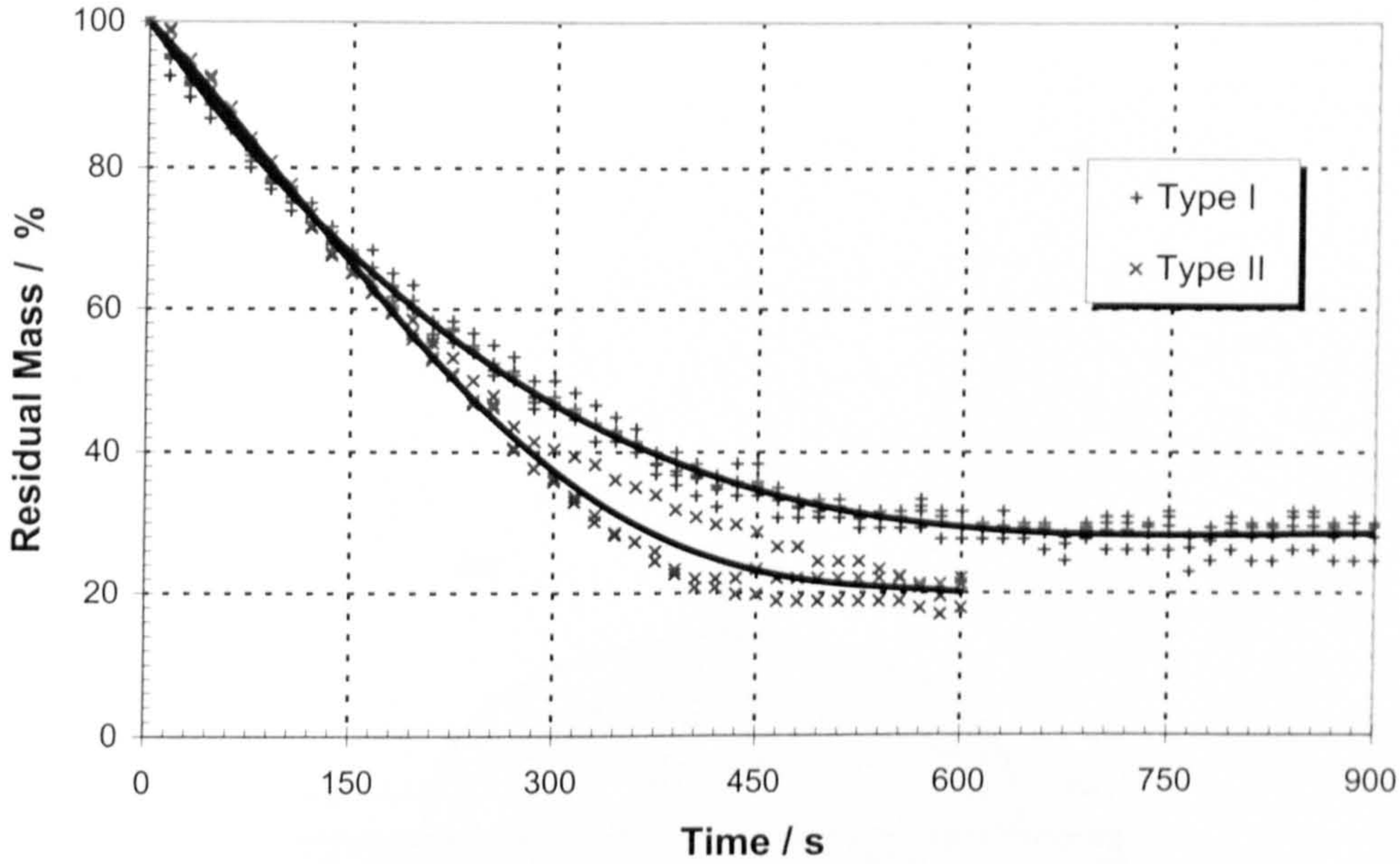

Figure 6.1 Mass changes of ceramic ink droplets placed on Type I and II substrates at 21°C during evaporation. Initial droplet volumes are 7 mm^3 and 10 mm^3 for Type I and II substrates, respectively.

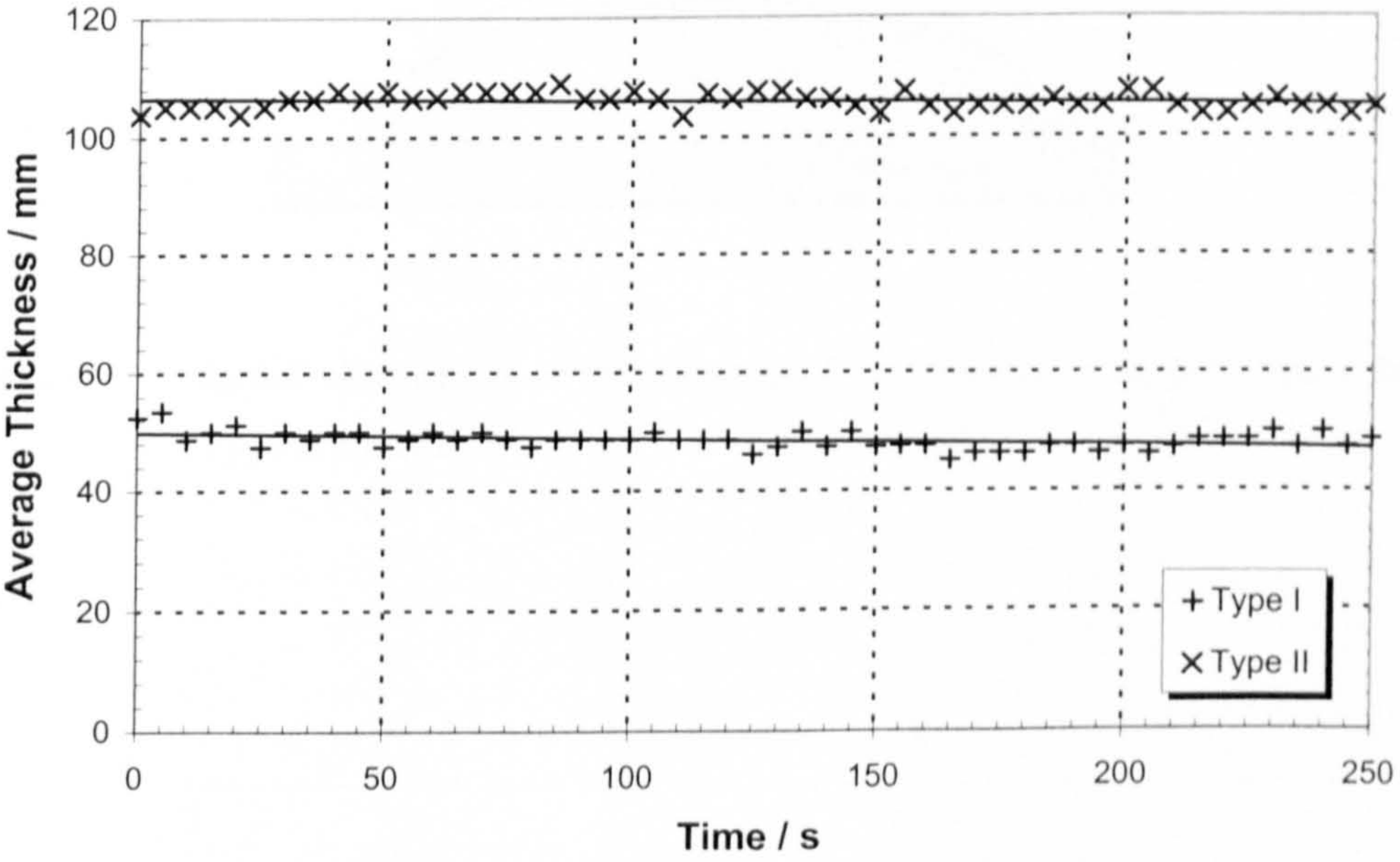

Figure 6.2 Changes of thickness of Type I and II substrates immersed in industrial methylated spirit.

(a)

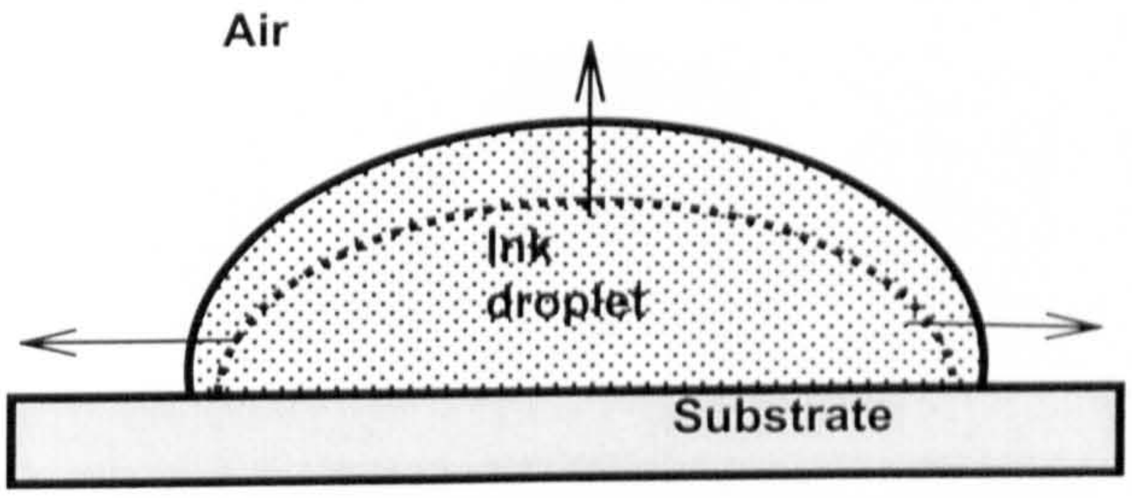

(b)

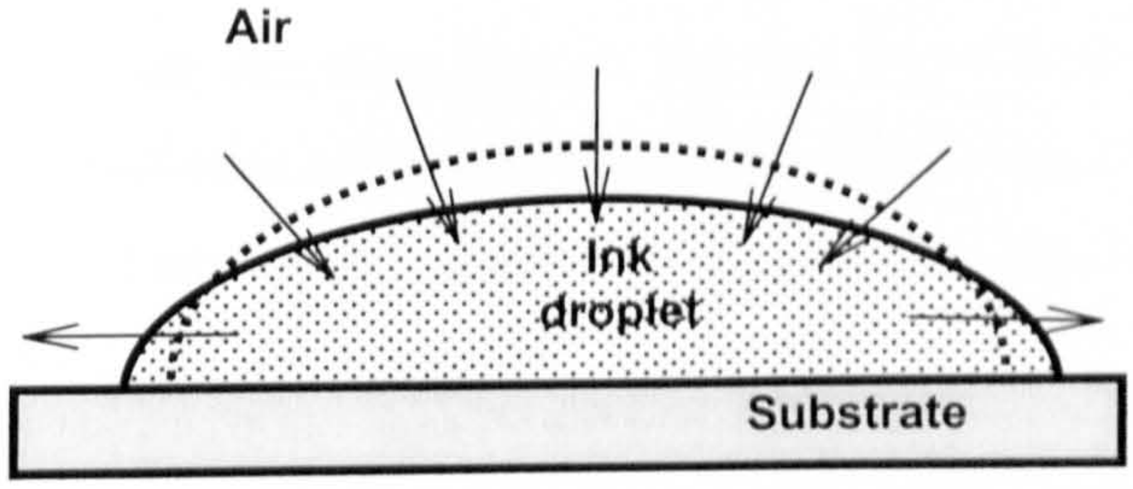

Figure 6.3 Initial observation of ink droplets after detachment on (a) Type I and (b) Type II substrates.

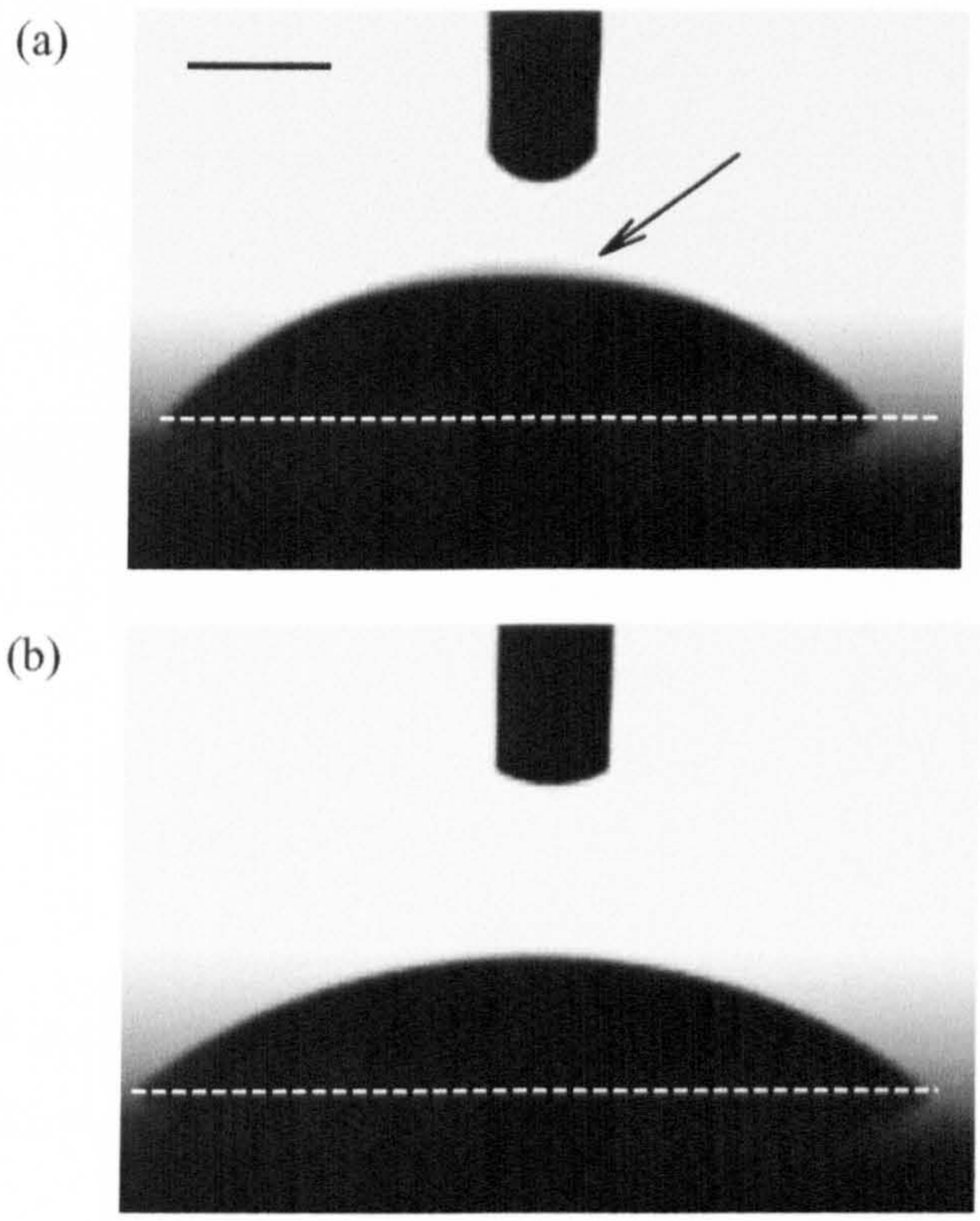

Figure 6.4 Ceramic ink droplet in contact with the Type I substrate: (a) immediately after detachment and (b) stabilised drop. The arrow shows blurring at the top in (a) and the dotted line indicates the baseline. The length of the bar on top left-hand side is 0.5 mm.

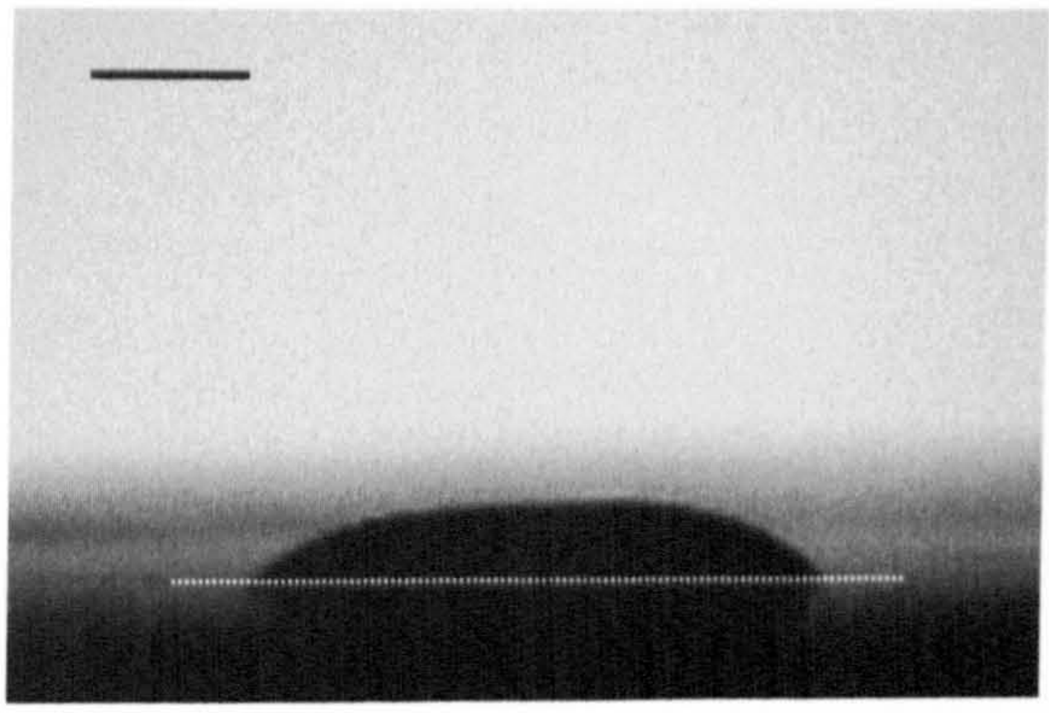

Figure 6.5 Severe deformation of a ceramic ink droplet released from a height of 30 mm onto Type I substrate. The dotted line indicates the baseline. The length of the bar on top left-hand side is 1.0 mm.

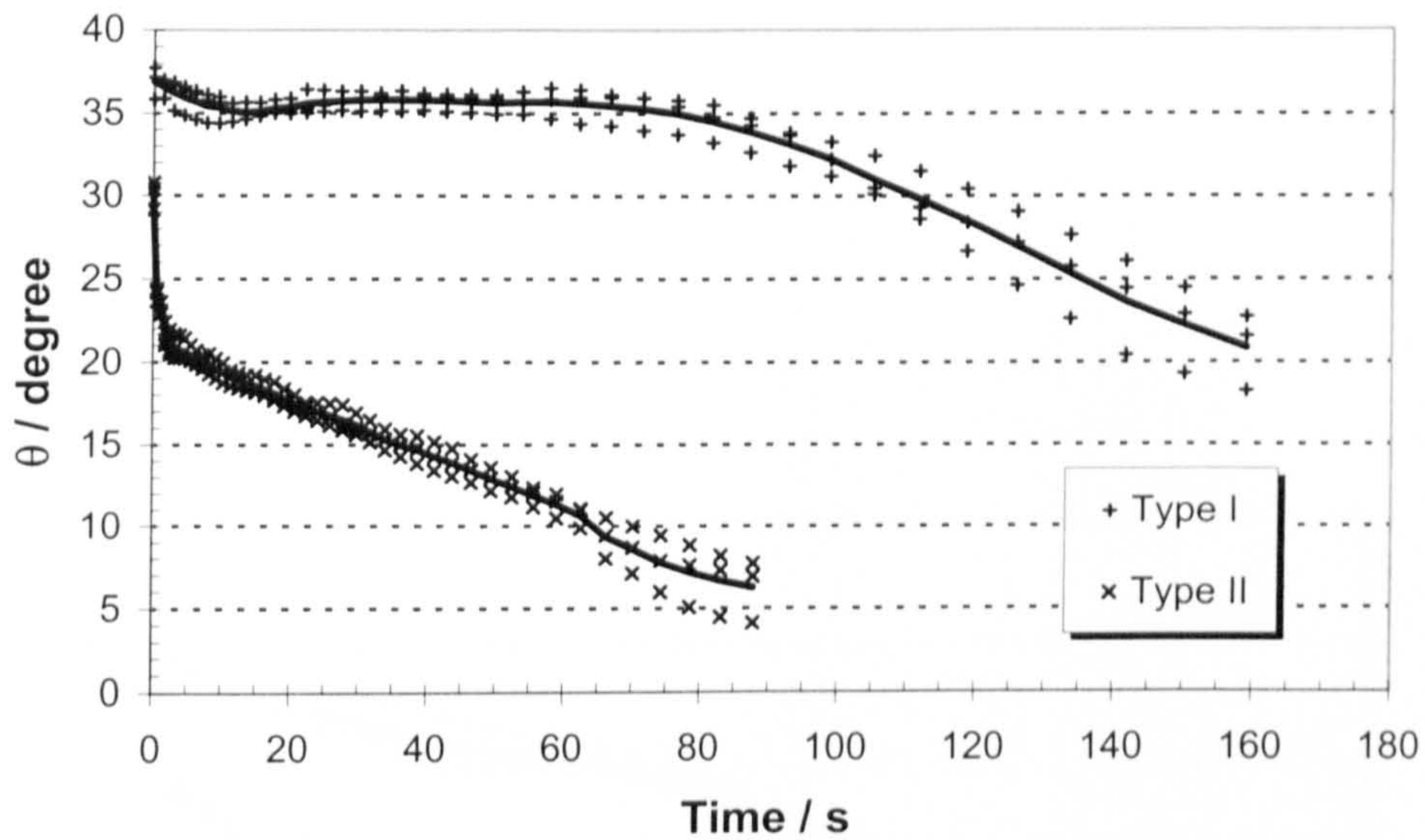

Figure 6.6 Variation of contact angle (θ) of ceramic ink droplets deposited on Type I and II substrates.

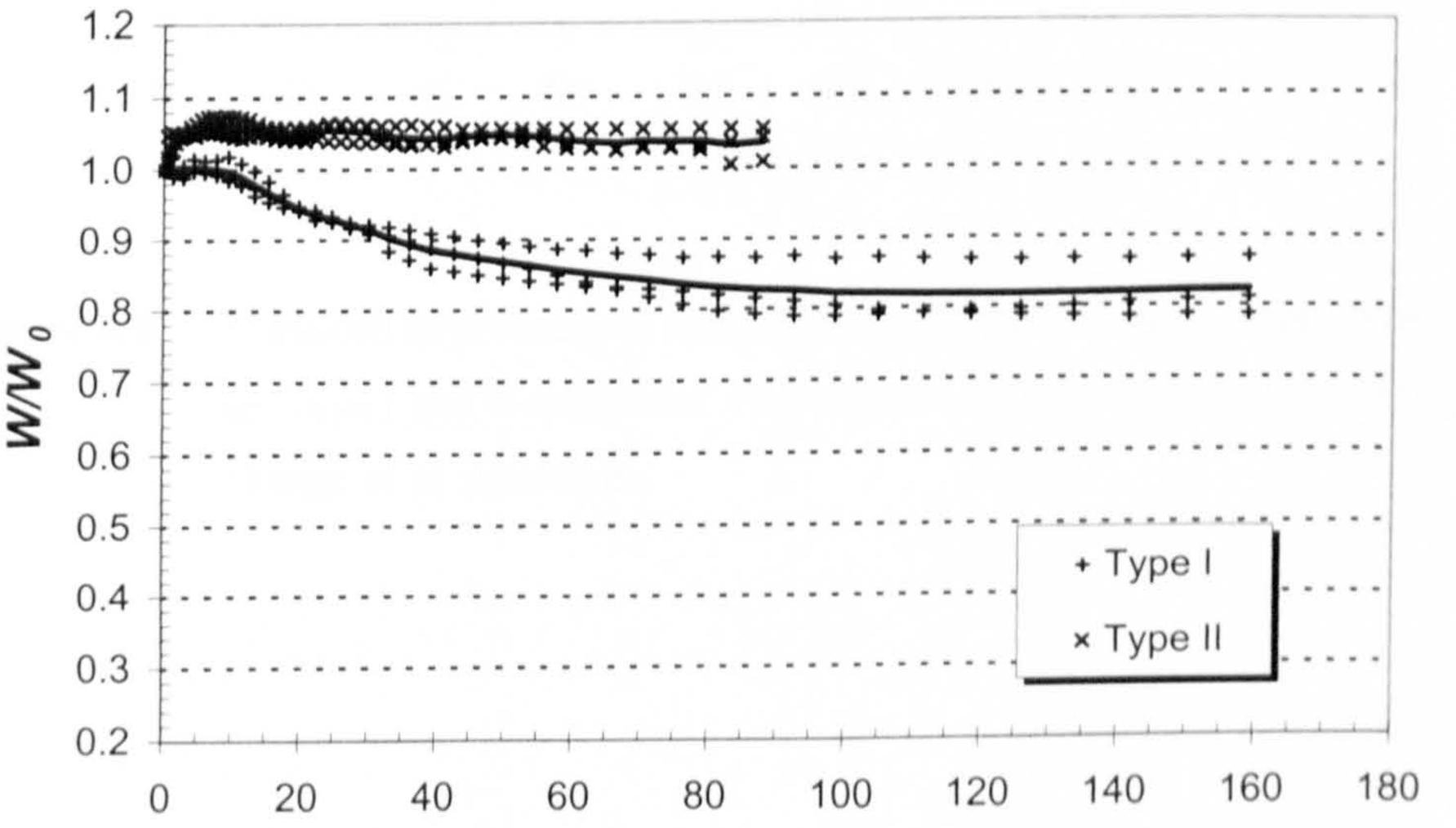

Figure 6.7 Variation of normalised width (W/W_0) of ceramic ink droplets deposited on Type I and II substrates. W_0 is given in Table 6.3.

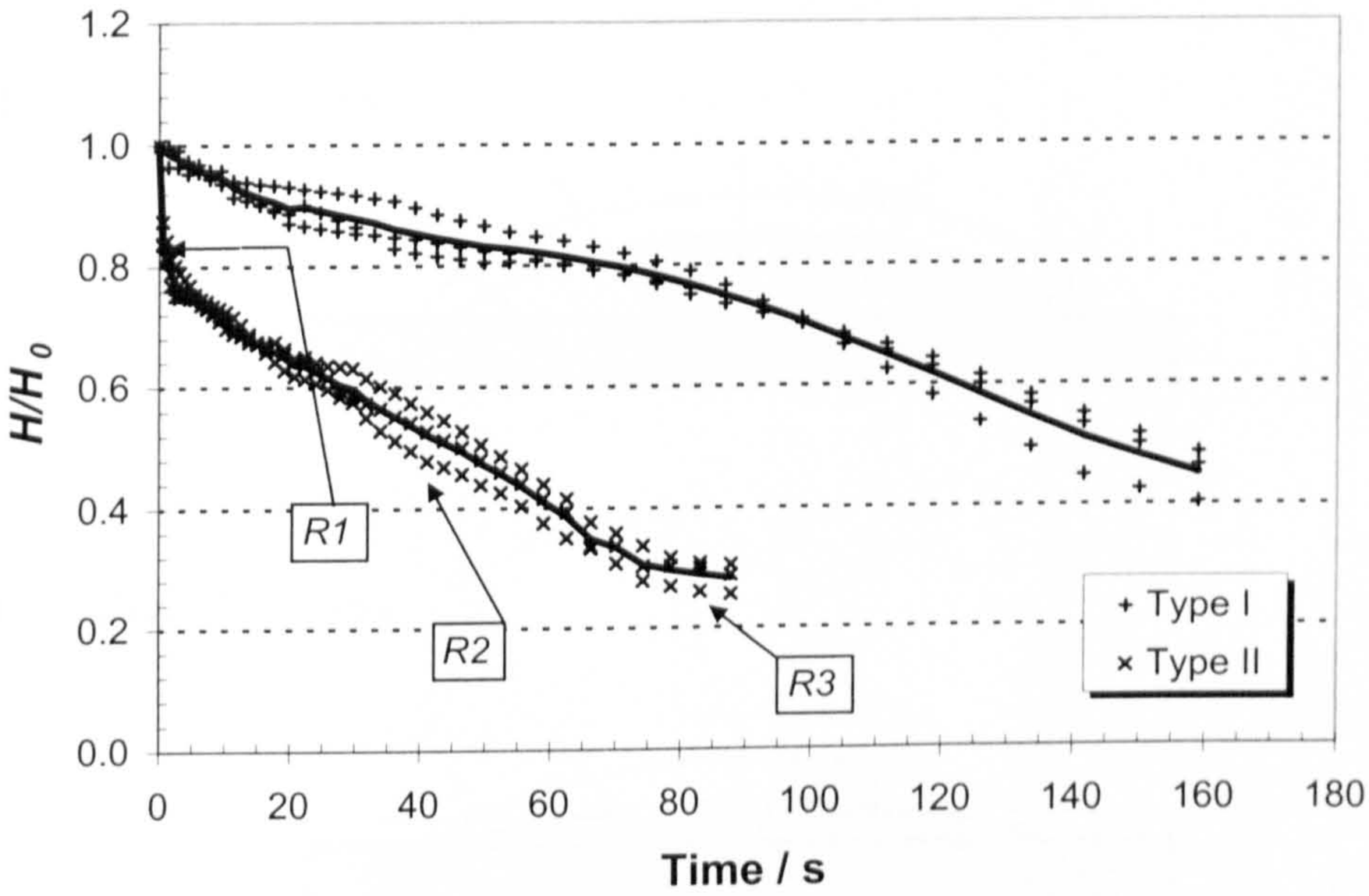

Figure 6.8 Variation of normalised width (H/H_0) of ceramic ink droplets deposited on Type I and II substrates. H_0 is given in Table 6.3. R is the rate of change of H with time.

(a) Time: 0 to 10 s

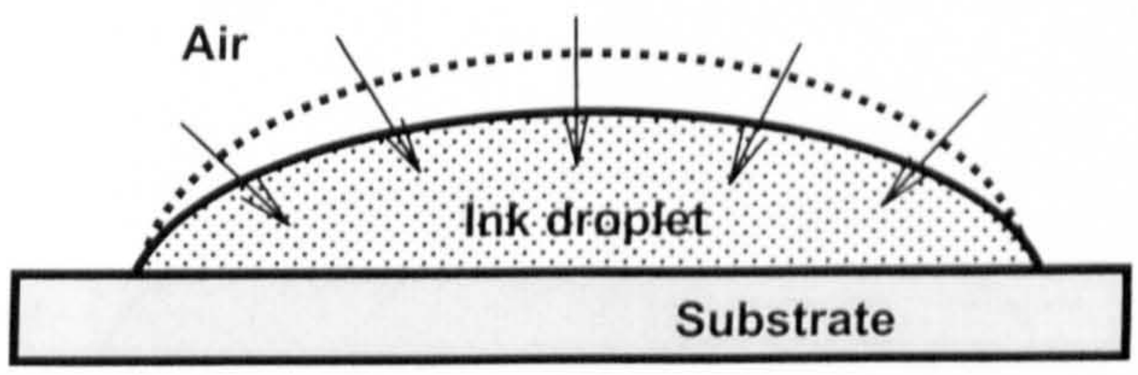

(b) Time: 10 to 75 s

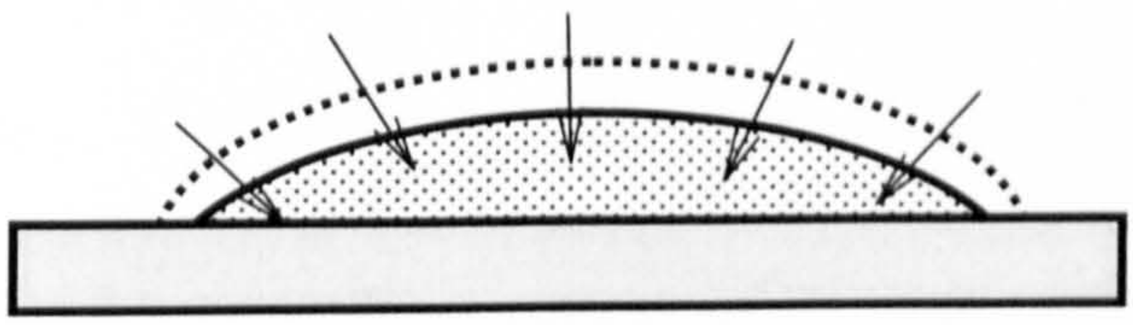

(c) Time: 75 to 120 s

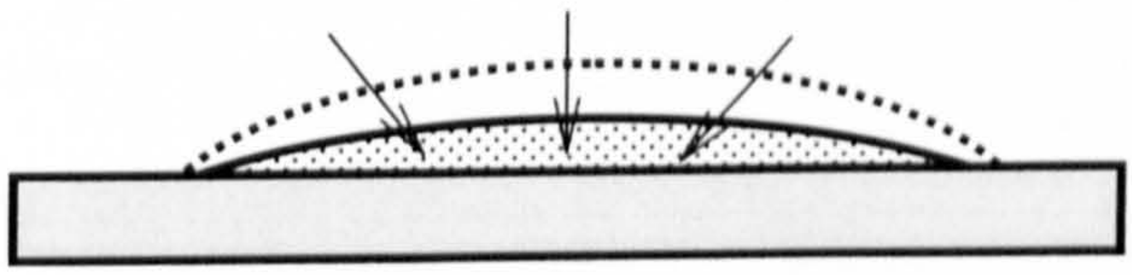

(d) Time: 120 to 160 s

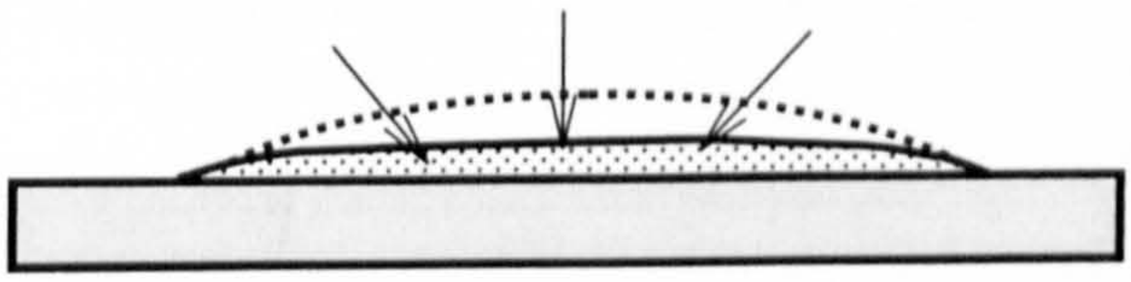

Figure 6.9 Schematic representation of drying of a ceramic ink droplet on Type I substrate at different times. The dotted and solid lines indicate the droplet contour at starting and finishing times, respectively, of each period in (a) - (d).

(a) Time: 0 to 2 s

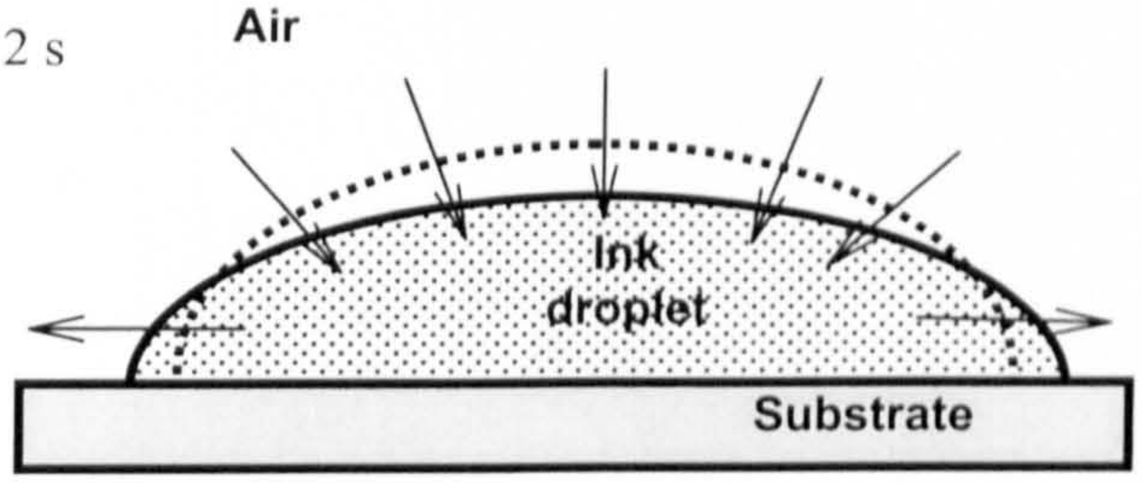

(b) Time: 2 to 70 s

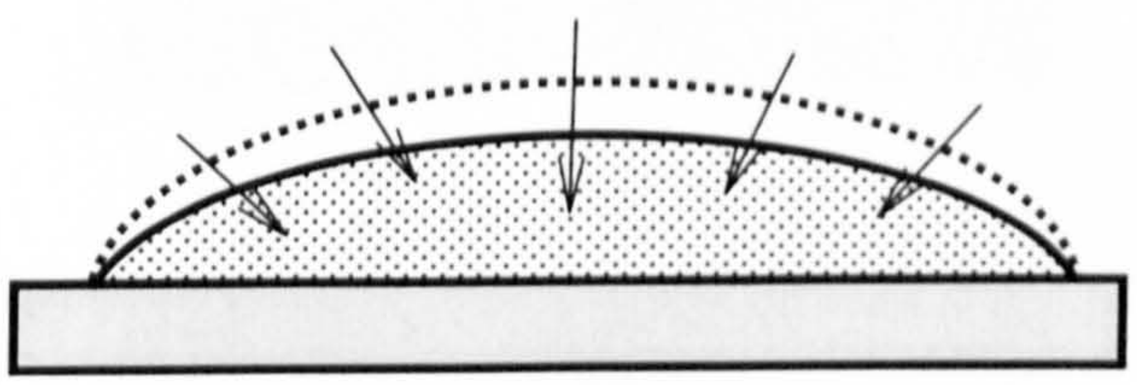

(c) Time: 70 to 90 s

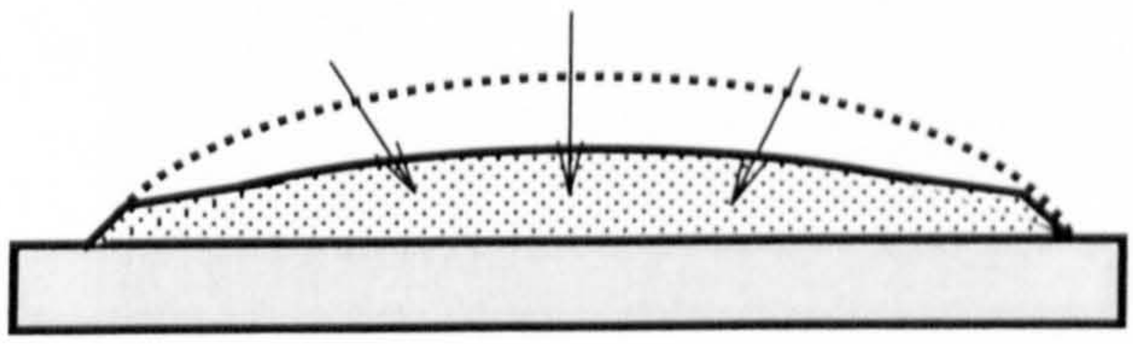

Figure 6.10 Schematic representation of drying of a ceramic ink droplet on Type II substrate at different times. The dotted and solid lines indicate the droplet contour at starting and finishing times, respectively, of each period in (a) - (c).

(a)

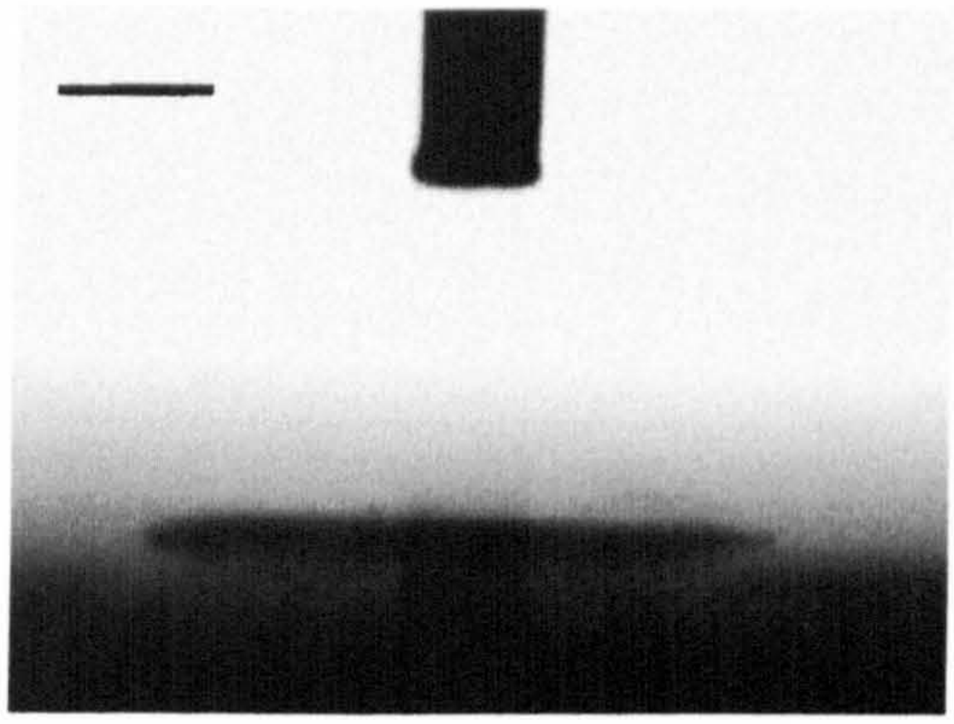

(b)

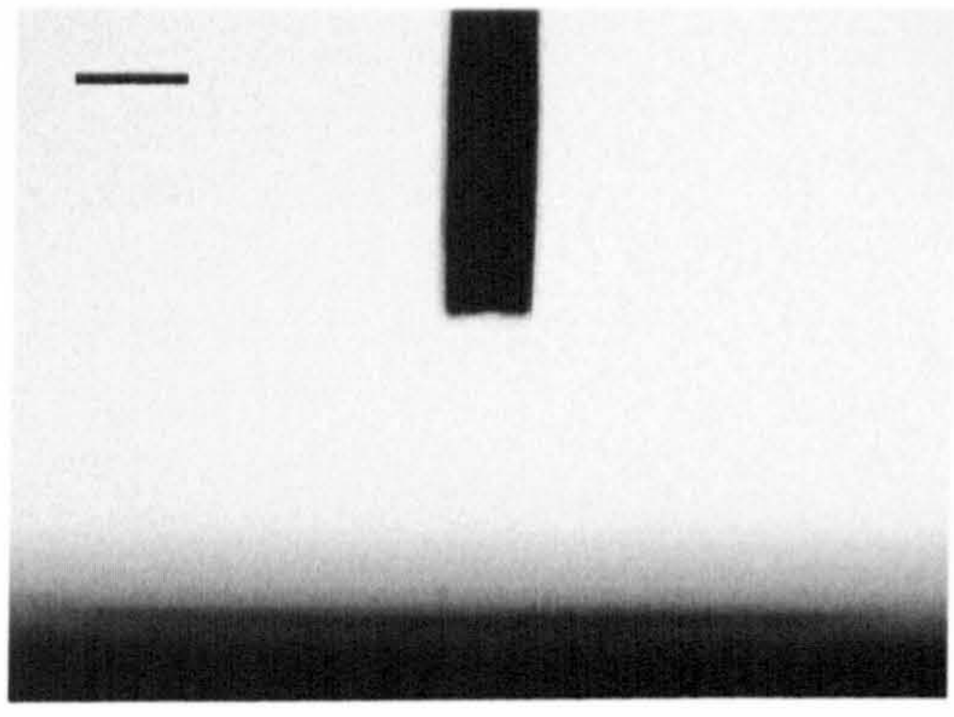

Figure 6.11 Ceramic relics on (a) Type I substrate after 295 s and (b) Type II substrate after 202 s. The length of the bar on top left-hand side is 0.5 mm.

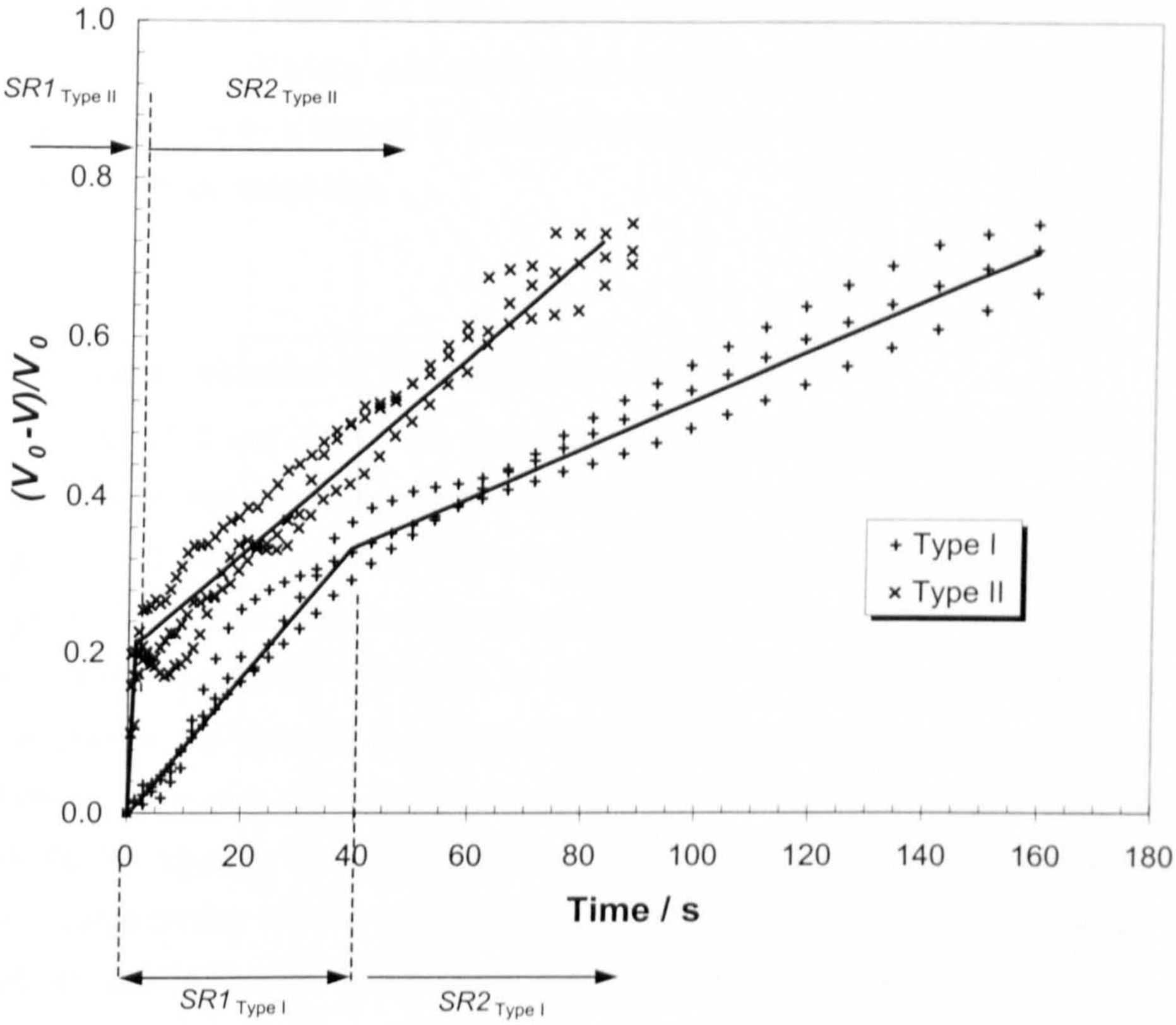

Figure 6.12 Volumetric shrinkage of ceramic ink droplets on both substrates. V_0 and V represent the initial and instantaneous volumes, respectively. SR refers to the shrinkage rate on different types of substrate.

Chapter 7

Dispersion and Stability of Silver Inks

This chapter presents result and discussion on the development of silver inks using three types of dispersant. Various inks made using different amount of dispersant and powder loading of silver were subjected to ultrasonic disruption. The dispersion and stability of these inks are investigated here.

7.1 Characteristics of Dispersants

Both Atphos 3202 and 3205E are phosphate ester-based, anionic dispersants with good stability in water and organic solvents. In addition, Atphos 3202 contains a higher content of phosphoric acid. When used in a polar solvent, the dispersant adsorbs onto the particle and charges it. The particles then electrostatically repel one another and this helps in achieving a stable colloidal suspension. However, in a nonaqeuous medium of low dielectric constant such as ethanol, the electrical barriers preventing aggregation are largely ineffective as the medium has a low ionic concentration and steric stabilisation prevails [Rosen, 1989; Wang *et al.*, 1997]. By adjusting the ionic strength of the solution, it is possible to create substantial surface charge density in order for electrostatic stabilisation to predominate [Widegren and Bergström, 2000]. This can be done by adding an acid or a base [Wang *et al.*, 1997].

Zephrym PD7000 is primarily a polymeric dispersant made from a polyoxyalkene amine derivative. It is weakly cationic, which is attributed to the amine group, but the material is more like non-ionic in nature in terms of its dispersing mechanism [Dehyuvyne, 2001]. As any polymeric dispersant, a molecule of Zephrym PD7000 contains an anchor group and a polymeric chain. The anchor group is adsorbed onto the particle surface where a weak bond is formed; while the polymeric chain penetrates into the solvent and provides a barrier that prevents strong interactions between the particles.

The viscosities of the dispersants as determined by the Hakke RheoStress 150 were 684.5, 354.6 and 260.6 mPa s at shear rate 1000 s^{-1} for Atphos 3202, Atphos 3205E and Zephrym PD7000, respectively.

Uniqema, the supplier of the dispersants, recommended a usage of 1.5 x 10^{-6} - 2.5 x 10^{-6} kg of dispersant per specific area of metal powder (in m^2). Given that the specific surface area of the Ag powder at 3.62 m^2 g^{-1}, this is equivalent to 0.5 - 0.9 wt. % of the Ag powder used. In this study, the amount of dispersant used, or *WPD*, in formulating the Ag ink was varied from 0.5, 1.5, 2.5 to 5 wt. %. This is expressed as a percentage with respect to the weight of the Ag powder.

7.2 Basis of Assessing the Degree of Flocculation

In this study, inks of 2 and 5 vol. % of Ag were used. With the Ag concentration > 1 vol. %, settling of particles is hindered by liquid moving upwards, hence Stokes law cannot be applied [Shaw, 1996]. The sedimentation of the inks and hence its flocculation that are discussed here are influenced by a number of factors including particle size, particle-particle interaction, particle-solvent interaction, density difference and initial powder concentration [Tiller and Khatib, 1984].

A high sediment volume is an indication of increased flocculation. However, the determination of the final sediment volume is difficult as sedimentation may take a considerable time to come to equilibrium. The volume or height of the sediment normally varies asymptotically with time during sedimentation. The half-value time ($t_{1/2}$), which is the time at which the change in sediment volume has reached half its final value, may be used as a measure of the degree of flocculation in the dispersion [Bell and Crowl, 1973].

The gravitational sedimentation behaviour of the Ag inks over a period of 8.64 x 10^5 s (10 days) was studied by monitoring the evolution of the volumes of sediment, suspension and cloudy liquid/solvent at regular interval. The behaviour can be categorised into two basic modes as illustrated in Figure 7.1. For Mode I, the sediment volume increased during sedimentation whereas this decreased in Mode II.

Mode I:

At the beginning of sedimentation, only two layers were observed, corresponding to the sediment and the suspension. As the study continued, the sediment volume increased (Figure 7.1a) and a cloudy liquid containing Ag powder also separated from the suspension gradually. By the end of the 10-day period, there were three zones in the test tube. Bell and Crowl [1973] considered this type of sedimentation to be typical of a deflocculated dispersion.

Mode II:

This mode, where the sediment decreased, is typical of a flocculated dispersion [Bell and Crowl, 1973; Chartier *et al.*, 1996]. Three patterns were noted. Mode (II,a) began with three layers corresponding to the sediment, suspension and cloudy liquid (Figure 7.1b). As sedimentation proceeded, a layer of clear liquid appeared on top of the cloudy liquid. At the same time, the cloudy liquid increased at the expense of the suspension and became increasingly more dilute. At the end of the 10-day period, there was only a thin layer of suspension sandwiched between the sediment and cloudy zone.

As in Mode (II,a), Mode (II,b) also started with three layers (sediment, suspension and cloudy liquid) at the beginning of the study. However, all the powders in the cloudy liquid zone settled gradually and transformed to a layer of clear liquid above the suspension. The suspension was also contracting. By the end of the 10-day period, only the sediment and the clear liquid remained in the test tubes (Figure 7.1c).

Mode (II,c) is typical of a completely flocculated dispersion (Figure 7.1d). Once sedimentation started, most of the dispersed Ag powders settled immediately. This left a layer of clear liquid above the sediment within the first 8.64×10^4 s (24 hour).

7.3 Sedimentation Behaviour

The variation of the volumes of the sediment, suspension, cloudy liquid and clear liquid with time are recorded in Figures 7.2 - 7.5. There was no clearly defined boundary between the cloudy liquid and clear liquid in the inks experiencing sedimentation Modes (II,a) and (II,b). As such, these two layers were considered as one zone in the sedimentation curves (Figures 7.2 - 7.5). The behaviour of each ink is summarised in Table 7.1.

Table 7.1 Sedimentation behaviour and final sediment volume ($V_{s,10}$) of the inks prepared at various wt. % of dispersant. The shadings highlight dispersions that were completely flocculated.

Dispersant	Ag Loading vol. %	$V_{s,10}$ at various *WPD* ml			
		0.5 wt. %	**1.5 wt. %**	**2.5 wt. %**	**5.0 wt. %**
Atphos 3202	2	0.9 Mode (I)	2.0 Mode (I)	2.9 Mode (II,a)	2.4 Mode (II,c)
		→ Increased flocculation			
Atphos 3202	5	3.3 Mode (II,a)	4.2 Mode (II,b)	3.3 Mode (II,c)	4.4 Mode (II,c)
		→ Increased flocculation			
Atphos 3205E	5	2.8 Mode (II,a)	3.1 Mode (II,a)	3.2 Mode (II,b)	3.3 Mode (II,c)
		→ Increased flocculation			
Zephrym PD7000	2	0.9 Mode (I)	1.0 Mode (I)	1.2 Mode (I)	2.1 Mode (II,c)
		→ Increased flocculation			

As shown in Table 7.1, increasing the amount of dispersant in the ink increased flocculation, regardless of the type of dispersant used and the vol. % of Ag. At the highest wt. % of dispersant used (5 wt. %), a completely flocculated ink was produced where most of the Ag powder settled within the first 8.64 x 10^4 s (24 hours) of sedimentation, leaving a layer of clear liquid above the sediment. The increased flocculation at higher amount of dispersant was also observed during the preparation of glass-based slurries [Kinoshita *et al.*, 1997]. It may be attributed to the excess dispersant adsorbed on the monolayer of dispersant. This can neutralise the effect of the monolayer, which provides optimum coverage over the particle, and the particles are likely to agglomerate [Pashley and Israelachvili, 1981]. With the stabilisation effect annihilated, the agitation force (by ultrasonic disruption), which was intended originally to disperse the powder, can cause agglomeration and lead to increased volume of floc [Kinoshita *et al.*, 1997]. Hence, as shown in Table 7.1, the sedimentation behaviour of the 2 vol. % Ag inks that contained Atphos 3202 shifted from Mode (II,a) to Mode (II,c) as *WPD* was increased from 2.5 to 5 wt. %. Similarly, that of the inks

containing Zephrym PD7000 also digressed from Mode I to Mode (II,c) for the same increment in *WPD*.

7.3.1 Increased Powder Loading

When the amount of Ag powder in the ink was increased from 2 to 5 vol. %, the inks transformed to a flocculated series. This is illustrated in Table 7.1 in both the 2 and 5 vol. % inks dispersed with Atphos 3202. At 2 vol. %, only two out of the four inks were experiencing a Mode II sedimentation, whereas all the four inks of the 5 vol. % underwent the similar behaviour. Irrespective of the amount of dispersant used, the sediment volume of the 5 vol. % Ag ink dispersed in Atphos 3202 reached its final value within the first 8.64×10^4 s (24 hour). The final volume at the end of the 10-day period was also more than that of the 2 vol. % inks. Furthermore, flocculation was greater during the initial 8.64×10^4 s, with the interface of the suspension-cloudy liquid moving downwards rapidly (comparing Figures 7.2a with 7.3a and Figures 7.2b with 7.3b). This increased flocculation in the 5 vol. % ink might be due to an insufficient energy employed at ultrasonic disruption. The same level of energy of 39W used for the 2 vol. % ink might not be insufficient to break down the agglomerates present in the 5 vol. % ink. As such, individual powder was not adequately coated with the dispersant. Although a higher level of ultrasonic energy may break down the agglomerates, it will inevitably increase the temperature. The effect of increased temperature on dispersion is rather complicated. It may lead to either an increase or decrease in adsorption on the particle surface, depending on the type of stabilisation mechanism and the dispersant-solvent interaction [Rosen, 1989]. Furthermore, a higher level of ultrasonic energy will increase the mixing temperature close to the boiling point of the solvent where volatility is increased and change the composition of the ink. Other high shear mixers such as twin or triple roll mill can be used to break down the agglomerates in the powder. However, processing aids such as plasticiser, binder and anti-oxidant are required for handling and to coat the powder surface to prevent its oxidisation.

Comparing the two series of inks at 5 vol. % of Ag, Atphos 3205E yielded a lower sediment volume than Atphos 3202. The former also promoted deflocculation, for example, it produced a partly flocculated ink at *WPD* = 2.5 wt. % (Figure 7.4c), but a completely flocculated ink was obtained with the same *WPD* of Atphos 3202 (Figure 7.3c). However, at both lowest (0.5 wt. %) and highest (5 wt. %) levels of dispersant used, the same sedimentation modes were observed for these two series of inks. Overall, an increased

amount of phosphoric acid (in Atphos 3202) did not improve the deflocculation of the Ag powder in industrial methylated spirit (IMS). This is probably due to high ionic strength which compressed the double layer to such an extent that the van der Waals attractions induced flocculation [Widegren and Bergström, 2000].

7.3.2 Dispersion by Steric Stabilisation

As shown in Table 7.1, the use of Zephrym PD7000 produced a series of deflocculated inks except when *WPD* = 5 wt. %. The amount of the final sediment was < that of inks dispersed with Atphos 3202 at the same vol. % Ag, except when *WPD* = 0.5 wt. %. This indicates improved deflocculation with Zephrym PD7000. When *WPD* = 0.5 wt. %, inks dispersed with these two dispersants yielded the same final sediment volume (Figures 7.2a and 7.5a). However, the rate of increase of the sediment was slower during the initial 8.64×10^4 s for the ink made using Atphos 3202 (will be discussed further in Section 7.4). Correspondingly, the downward movement of the interface of the suspension-cloudy liquid was also slower. As in the case of the Atphos 3202, if the quantity of Zephrym PD7000 was too high (5 wt. %), a completely flocculated ink was obtained due to the reason described previously.

7.4 Degree of Flocculation

The sediment volume (V_s), as a function of time, and $t_{1/2}$ were calculated using the following assumptions:

(i) In the case of Mode I sedimentation behaviour, V_s was approximated with a logarithmic law relationship and at $t = 0$, $V_s = 0$.

(ii) In the case of Mode II sedimentation behaviour, V_s was approximated with a power law relationship and at $t = 0$, $V_s = 10$ ml.

(iii) The sediment volume at equilibrium ($V_{s,eq}$) was approximated by that at the end of 10th day ($V_{s,10}$), i.e. $V_{s,eq} \approx V_{s,10}$.

Comparisons of V_s for the different inks are given in Figures 7.6 – 7.8. Table 7.2 shows the $t_{1/2}$ values of the inks with the exclusion of those that were completely flocculated, i.e. exhibiting Mode (II,c) behaviour.

Table 7.2 Half-value time, $t_{1/2}$, of inks dispersed with different types of dispersant at different powder loadings.

Type of dispersant	Ag loading	*WPD*	$V_{s,eq}$	Equation fitted		$t_{1/2}$
	vol. %	wt. %	ml			s
Atphos 3202	2	0.5	0.9	V_s =	0.15 ln(t) + 0.09	3.91×10^4
		1.5	2.0	V_s =	0.41 ln(t) - 0.21	2.52×10^4
		2.5	2.9	V_s =	$3.35\ t^{-0.04}$	7.20×10^{-4}
		5.0	Completely flocculated ink			
Atphos 3202	5	0.5	3.3	V_s =	$6.32\ t^{-0.14}$	2.52×10^3
		1.5	4.2	V_s =	$6.10\ t^{-0.09}$	6.12×10^2
		2.5	Completely flocculated ink			
		5.0	Completely flocculated ink			
Atphos 3205E	5	0.5	2.8	V_s =	$6.32\ t^{-0.14}$	3.31×10^3
		1.5	3.1	V_s =	$6.17\ t^{-0.15}$	2.38×10^3
		2.5	3.2	V_s =	$5.34\ t^{-0.12}$	5.76×10^2
		5.0	Completely flocculated ink			
Zephrym PD7000	2	0.5	0.9	V_s =	0.11 ln(t) + 0.36	8.71×10^3
		1.5	1.0	V_s =	0.09 ln(t) - 0.58	1.58×10^3
		2.5	1.2	V_s =	0.05 ln(t) + 0.99	1.80×10^2
		5.0	Completely flocculated ink			

The smaller the $t_{1/2}$ value, the greater is the flocculation. Therefore, as shown in Table 7.2, there was increased flocculation with *WPD* in each series of ink. This agreed with the observations made from the sedimentation patterns (Table 7.1). There was also a correlation between $t_{1/2}$ and $V_{s,eq}$, or $V_{s,10}$, within the same series of ink, with $t_{1/2}$ inversely proportional to $V_{s,eq}$.

$t_{1/2}$ was further used to assess the degree of flocculation between different series of ink. With the largest $t_{1/2}$ value of 3.91×10^4 s, the 2 vol. % ink dispersed with 0.5 wt. % of Atphos 3202 therefore was the least flocculated. Its $t_{1/2}$ value is about 4.5 times higher than that of a 2 vol. % ink containing 0.5 wt. % of Zephrym PD7000. Similar observation was also made in Section 7.3.2 that although both inks had the same $V_{s,10}$, the rate of increase of V_s was faster at the beginning of sedimentation for the latter and this resulted in a smaller $t_{1/2}$. As a smaller $t_{1/2}$ is an indication of lesser flocculation, the stabilisation provided by Atphos 3202 was therefore more effective than that by Zephrym PD7000. $t_{1/2}$ can also be used to compare

two inks dispersed with different types and quantities of dispersant, such as the 5 vol. % inks that are dispersed at 0.5 wt. % of Atphos 3202 and 2.5 wt. % of Atphos 3205E. For these inks, V_s offered no extra information as both inks yielded approximately the same value. However, a higher $t_{1/2}$ in the former indicated lesser flocculation. This is also corroborated qualitatively by their sedimentation behaviours (Table 7.1).

Increased flocculation with Ag content in the inks that were dispersed by Atphos 3202 was also corroborated by $t_{1/2}$, which reduced drastically at 5 vol. % Ag. The lower $t_{1/2}$ value of the inks dispersed with Atphos 3202 than those with Atphos 3205E also validated the detrimental effect of the higher ionic strength in the former that seemed to induce flocculation.

One important point to take note is that the calculation of $t_{1/2}$ is highly dependent on the accuracy of the measured V_s, especially when V_s is approaching its equilibrium value. In this study, V_s was measured to an accuracy of ±0.1 ml and a more accurate $t_{1/2}$ can be obtained if the degree of accuracy is improved.

7.5 Rheological Behaviour

The viscosity of the inks during sedimentation was measured at 0 s, 2.59 x 10^5 s (day 3), 5.18 x 10^5 s (day 6) and 7.78 x 10^5 s (day 9) to investigate their stability. Measurements were made at three shear rates: 100, 500 and 1000 s^{-1}.

7.5.1 Initial Observations

Figures 7.9 - 7.12 show the viscosity-shear rate graphs of the four series of inks made using various dispersant types and contents.

(a) Effect of increased shear rate

Most of the inks displayed pseudoplastic flow behaviour within the range of shear rate tested, i.e. the viscosity decreased with increased shear rate. As prepared, the attractive interaction between the Ag powder induced flocs in the ink, which caused solvent immobilisation [Shaw, 1992]. Under the action of a higher shear rate, the flocs would be broken down. This facilitated the mobility of solvent between the powder and yielded a lower viscosity. The viscosity of the inks containing 2 vol. % Ag were closer to Newtonian

(Figures 7.9 and 7.12) than those at 5 vol. % (Figures 7.10 and 7.11). This was due to a lower Ag content, reduced powder interaction and lesser flocs in them, indicating better dispersion within the ink. An exception to the pseudoplastic behaviour was the ink dispersed with 5 wt. % of Zephrym PD7000, which displayed dilatant behaviour. At the end of viscosity measurement of this ink, powder was found to segregate at the centre of the plate of the rheometer and circumscribed by a rim of solvent. The segregation was induced under the action of high shear rate and was probably due to the little interaction between the solvent and Ag powder. This led to the 'apparent' increase in viscosity at 1000 s^{-1}.

(b) Effect of increased WPD

No general trend could be derived between the viscosity of the inks and the amount of dispersant. This appear to be dependent on the mode of stabilisation interaction (electrostatic or steric), powder loading and the state of dispersion in the ink (flocculated or deflocculated). For the 2 vol. % inks containing Atphos 3202, a higher *WPD* can result in a greater number of flocs or bigger flocs [Kinoshita *et al.*, 1997], either of these can bring forth a higher viscosity (Figure 7.9). The effect of increased *WPD* on inks was discussed previously in Section 7.3.

At a higher powder loading of 5 vol. % (Figure 7.10), the completely flocculated ink (*WPD* = 2.5 and 5 wt. %) 'appeared' to be less viscous than the partly flocculated inks (*WPD* = 0.5 and 1.5 wt. %). Within each subset of ink, the viscosity increased with *WPD*. In the subset of inks that was completely flocculated, the flocs could be touching each other. For flow to start, sufficient stress or strain must be applied to overcome the bonds between the individual flocs [Bingham, 1922]. The increase in viscosity from 2.5 to 5 wt. % of dispersant could be attributed to an increased number of flocs, bigger flocs and the free dispersant molecules that remained in the solvent [Kinoshita *et al.*, 1997].

The same observation was made in the series of ink dispersed with Atphos 3205E (Figure 7.11). For inks dispersed with *WPD* < 5 wt. %, which were not completely flocculated (Figure 7.4), the viscosity increased with *WPD*. Ink with *WPD* = 5 wt. % was completely flocculated and behaved in a similar manner as the completely flocculated inks containing Atphos 3202, which were described in the preceding paragraph. The ink appeared to be less viscous than those with *WPD* < 5 wt. % during viscosity measurement.

There was little variation in the inks dispersed with Zephrym PD7000 as *WPD* was increased (Figure 7.12). This correlates well with the small changes in sediment volume with *WPD* (Table 7.1). The near Newtonian behaviour also indicates that the interaction between the powder in the ink was weak and hence, lesser flocculation.

7.5.2 Stability of Inks

The discussion in Chapter 4 highlights the importance of the stability of the ink for continuous printing. In additional, the Linx 6200S Jet Printer also stipulated that the ink viscosity should be within 3 - 4 mPa s. In the present study, viscosity was measured every 2.59×10^5 s (3 days) to investigate ink stability. Viscosity of the 2 vol. % Ag inks dispersed with various *WPD* of Atphos 3202 at 0, 2.59×10^5, 5.18×10^5 and 7.78×10^5 s are shown in Figures 7.13 - 7.16. Similar results for Zephrym PD7000 can be found in Figures 7.17 - 7.20. As for the 5 vol. % inks, the viscosity measurements made on 2.59×10^5, 5.18×10^5 and 7.78×10^5 s were mostly < 2 mPa s, which is the lowest measurement limit of the rheometer (Section 3.4.3). Hence, they were not reported nor discussed here. In these inks, the flocculation was so rapid that most of the Ag powder settle in 5.18×10^5 s (6 days), leaving a dilute ink of low viscosity that comprised mainly of solvent.

(a) 2 vol. % Ag dispersed in Atphos 3202

At *WPD* = 0.5 wt. %, the ink exhibited pseudoplastic behaviour on days 0, 2.59×10^5, 5.18×10^5 and 7.78×10^5 s (Figure 7.13). From 2.59×10^5 (day 3) onwards, the ink showed a stable viscosity value. From 0 to 2.59×10^5 s, there was an 18% reduction in viscosity at shear rate 1000 s^{-1}, whereas only a 2% variation was detected between $2.59 \times 10^5 - 7.78 \times 10^5$ s. This agrees well with the time that the sediment volume took to achieve its constant value (Figure 7.2a).

A reduced stabilisation at higher *WPD* of 1.5 and 2.5 wt. % was also noted with the viscosity values still fluctuating between $2.59 \times 10^5 - 7.78 \times 10^5$ s. Moreover, the reduction in viscosity from 0 to 2.59×10^5 s (Figures 7.14 and 7.15) was great. It amounted to 31% at 1000 s^{-1} for both inks, compared to only 18% at *WPD* = 0.5 wt. %. These two inks also had a smaller $t_{1/2}$ value than the ink with *WPD* = 0.5 wt. % (Table 7.2), indicating greater flocculation which induced faster settling of the Ag powder. Furthermore, the flow behaviour of these two inks was increasingly more Newtonian after 2.59×10^5 s. For

example, at *WPD* = 2.5 wt. %, the percentage drop in viscosity on increasing the shear rate from 500 to 1000 s^{-1} was only 7.5, 8 and 13% for measurements taken on 2.59 x 10^5, 5.18 x 10^5 and 7.78 x 10^5 s, respectively; but this was 21% at 0 s.

From 2.59 x 10^5 s to 7.78 x 10^5 s, ink dispersed with *WPD* = 5 wt. %, contained a large proportion of the solvent, from which the Ag powder separated and flocculated to form the sediment. There was thus little changes in the viscosity measured during this period, as shown in Figure 7.16.

(b) 2 vol. % Ag dispersed in Zephrym PD7000

Most of the inks displayed pseudoplastic behaviour. For inks prepared with *WPD* < 5 wt. %, the percentage reduction viscosity from 0 to 2.59 x 10^5 s was 10 - 19%. However, this was < 5% from 2.59 x 10^5 s to 5.18 x 10^5 s and 2.59 x 10^5 s to 7.78 x 10^5 s. This small variation in viscosity indicates that the inks had reached their stability by 2.59 x 10^5 s.

7.6 Summary and Conclusions

The dispersion of Ag particles with Atphos 3202, Atphos 3205E and Zephrym PD7000 in industrial methylated spirit was studied over 8.64 x 10^5 s (10-day period). Both the effects of the amount of dispersant used and powder loading of the inks were also investigated. Flocculation in the inks was compared using the sedimentation graphs and the half-value time ($t_{1/2}$) of the sediment volume. The stability of the inks with respect to their viscosity behaviour during the period of study was also investigated.

(i) Two modes of sedimentation behaviour were observed. The first mode was observed in deflocculated ink where the sediment volume was increasing. No clear liquid was formed during the period of study. The ink was prepared with a lower Ag loading with smaller amounts of dispersant. The second mode was typical of a flocculated ink where the sediment volume was decreasing and a clear liquid was formed above the sedimenting layers during sedimentation.

(ii) Dispersing the ink at the recommended value of 0.5 wt % of dispersant normally produced a deflocculated ink at 2 vol. % Ag. When the amount of disperant used was increased beyond the recommended value, there was greater flocculation and reduced

stability in the inks. With a high value of 5 wt. % of dispersant was used, most of the Ag powder settled immediately at the commencement of sedimentation.

(iii) It was observed that increasing the powder loading of Ag in the ink increased flocculation in the ink. This is due to undispersed agglomerates in the powder, which prevented the powder from being effectively coated by the dispersant. Flocculation did not improve when a dispersant with a higher content of acid was used.

(iv) $t_{1/2}$ was found to be a useful parameter to assess the flocculation in the Ag inks. Its use was qualitatively corroborated by the sedimentation behaviour of each ink.

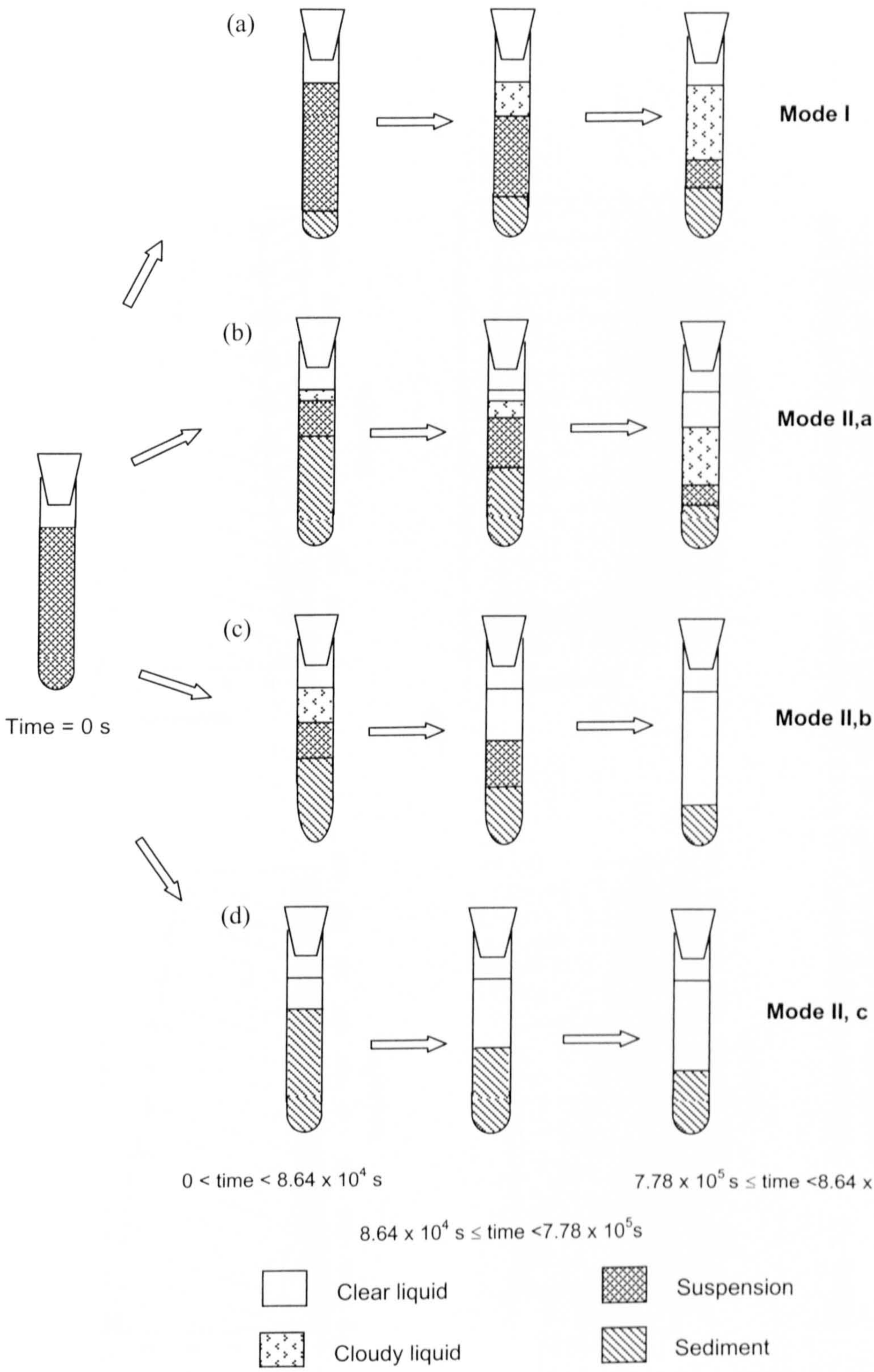

Figure 7.1 Sedimentation behaviour of Ag inks: (a) Mode I, (b) Mode (II,a), (c) Mode (II,b) and (d) Mode (II,c).

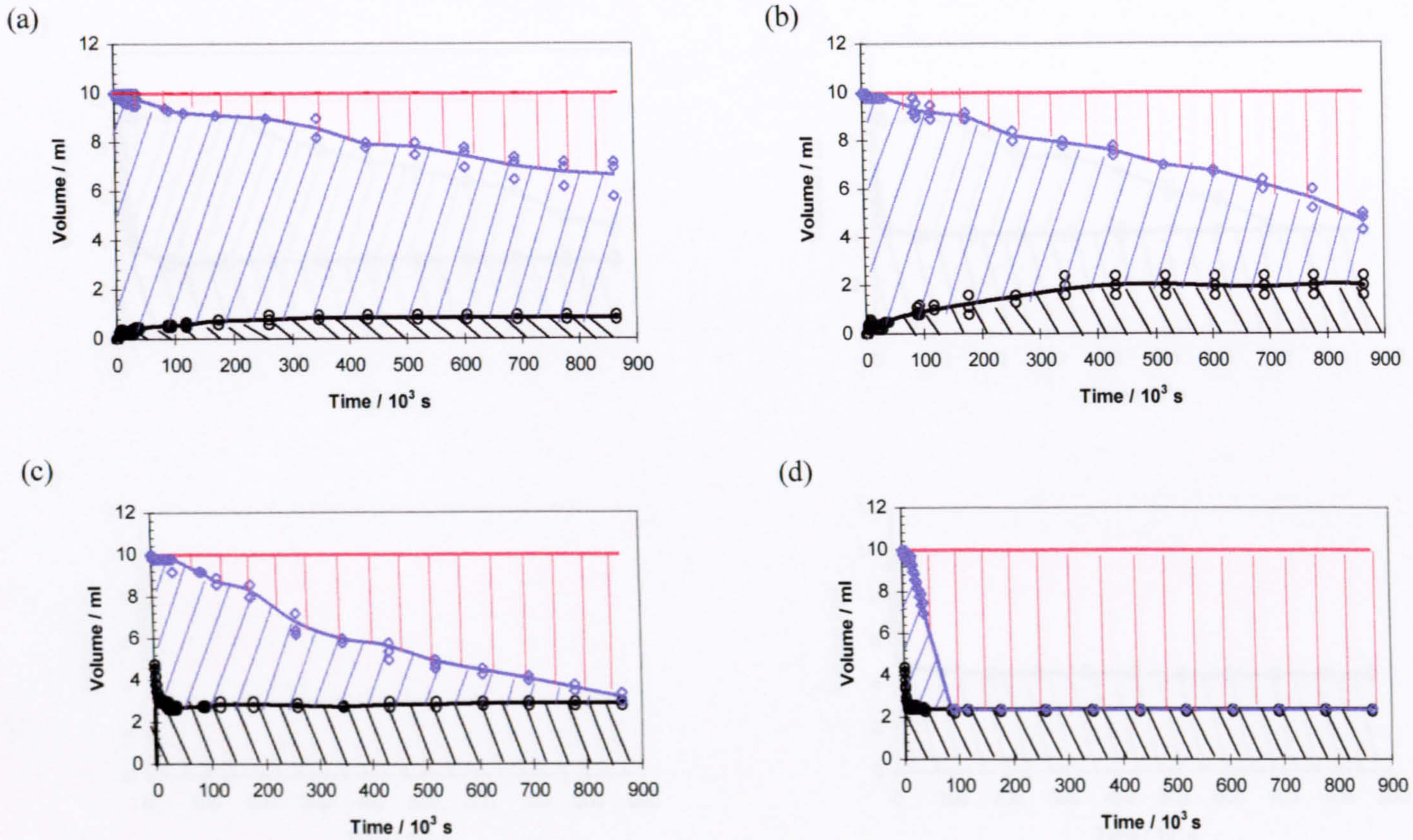

Figure 7.2 Sedimentation behaviour of 2 vol. % Ag inks dispersed with different amounts of Atphos 3202: (a) 0.5 wt.%, (b) 1.5 wt. %, (c) 2.5 wt. % and (d) 5 wt. %. Cloudy/clear liquid zone ( ), suspension volume ( ) and sediment volume ( ).

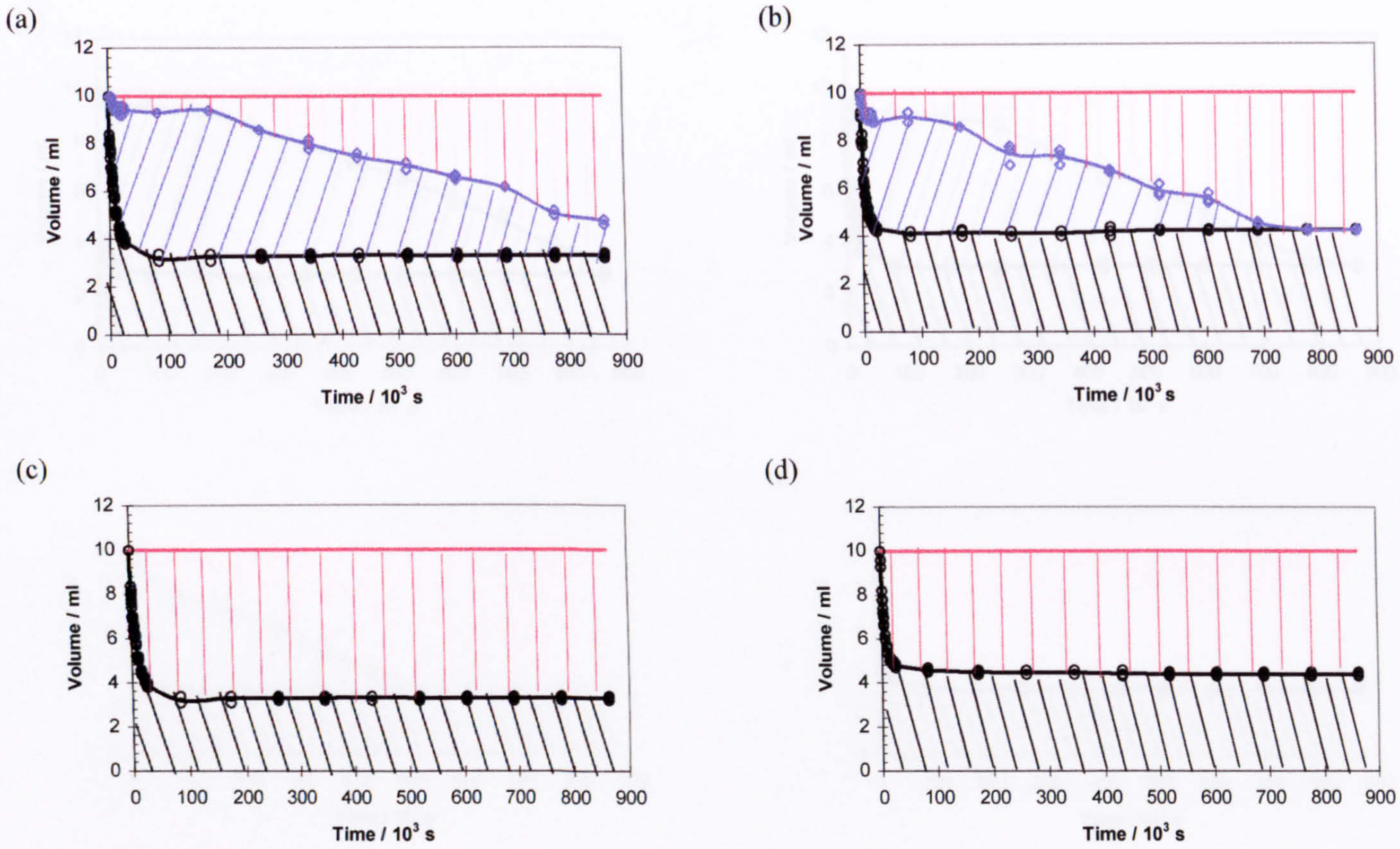

Figure 7.3 Sedimentation behaviour of 5 vol. % Ag inks dispersed with different amounts of Atphos 3202: (a) 0.5 wt.%, (b) 1.5 wt. %, (c) 2.5 wt. % and (d) 5 wt. %. Cloudy/clear liquid zone ( ), suspension volume ( ) and sediment volume ( ).

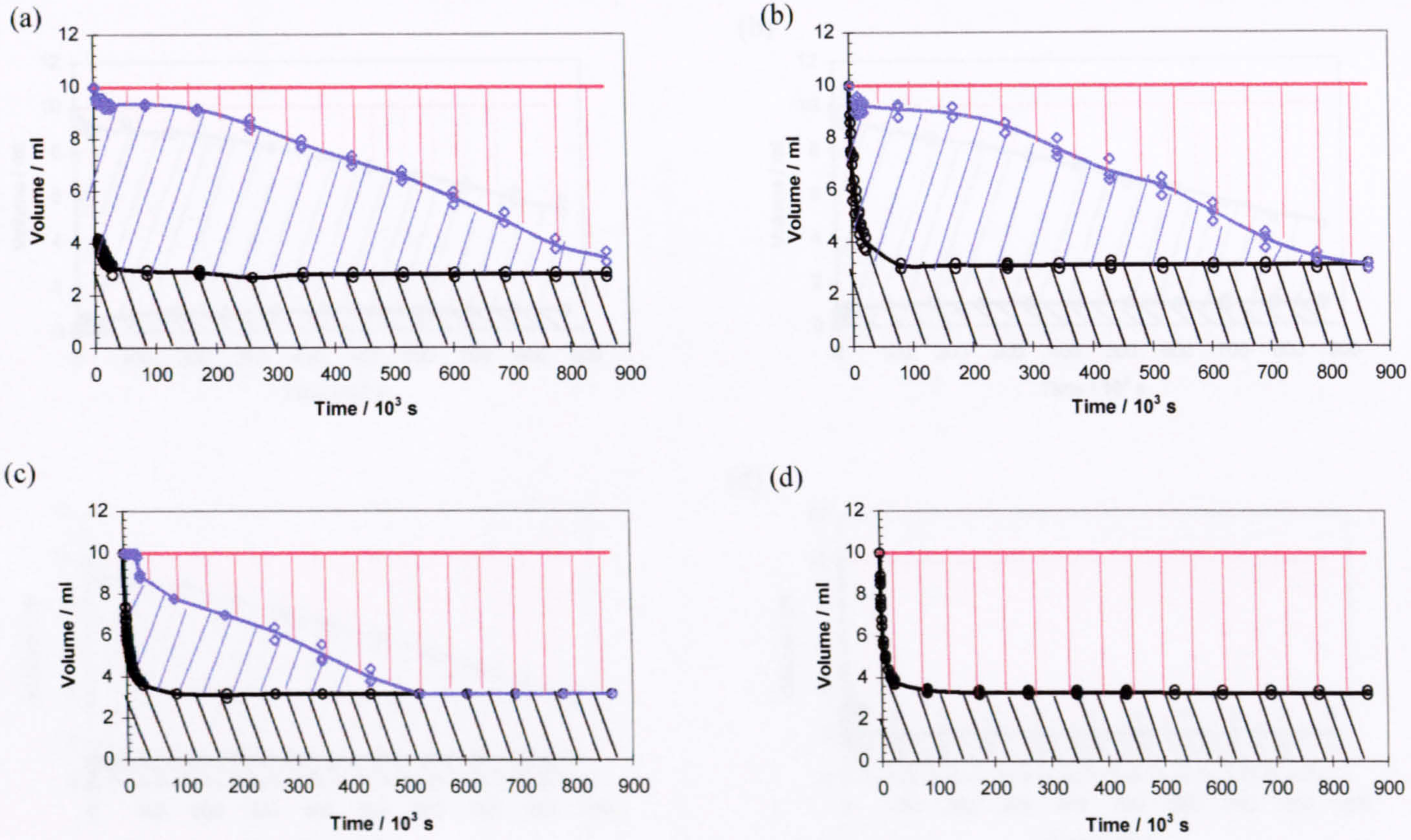

Figure 7.4 Sedimentation behaviour of 5 vol. % Ag inks dispersed with different amounts of Atphos 3205E: (a) 0.5 wt.%, (b) 1.5 wt. %, (c) 2.5 wt. % and (d) 5 wt. %. Cloudy/clear liquid zone ( ), suspension volume ( ) and sediment volume ( ).

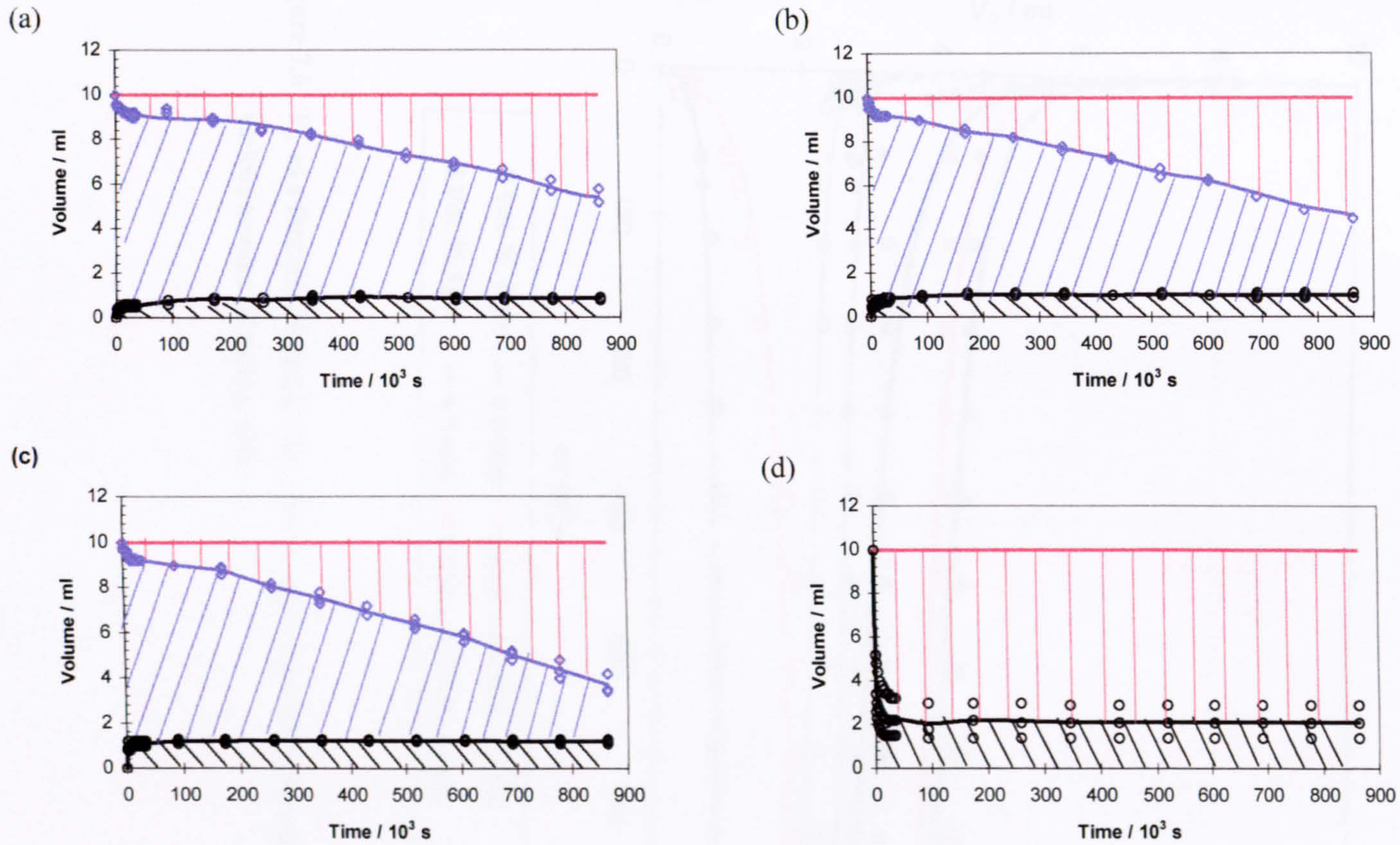

Figure 7.5 Sedimentation behaviour of 2 vol. % Ag inks dispersed with different amounts of Zephrym PD7000: (a) 0.5 wt.%, (b) 1.5 wt. %, (c) 2.5 wt. % and (d) 5 wt. %. Cloudy/clear liquid zone ( ), suspension volume ( ) and sediment volume ( ).

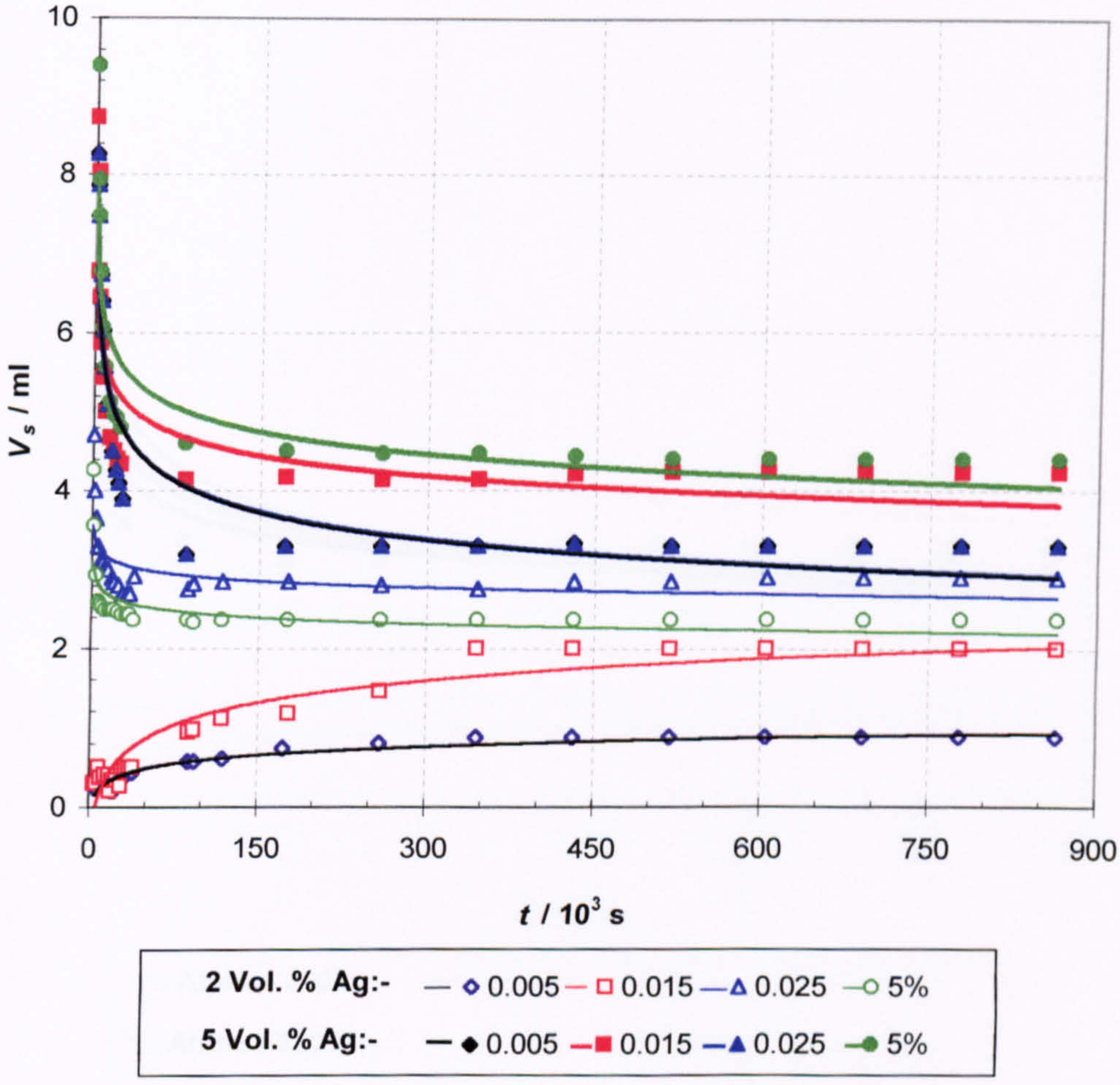

Figure 7.6 V_s as a function of time (t) for 2 and 5 vol.% Ag inks dispersed using various amount of Atphos 3202.

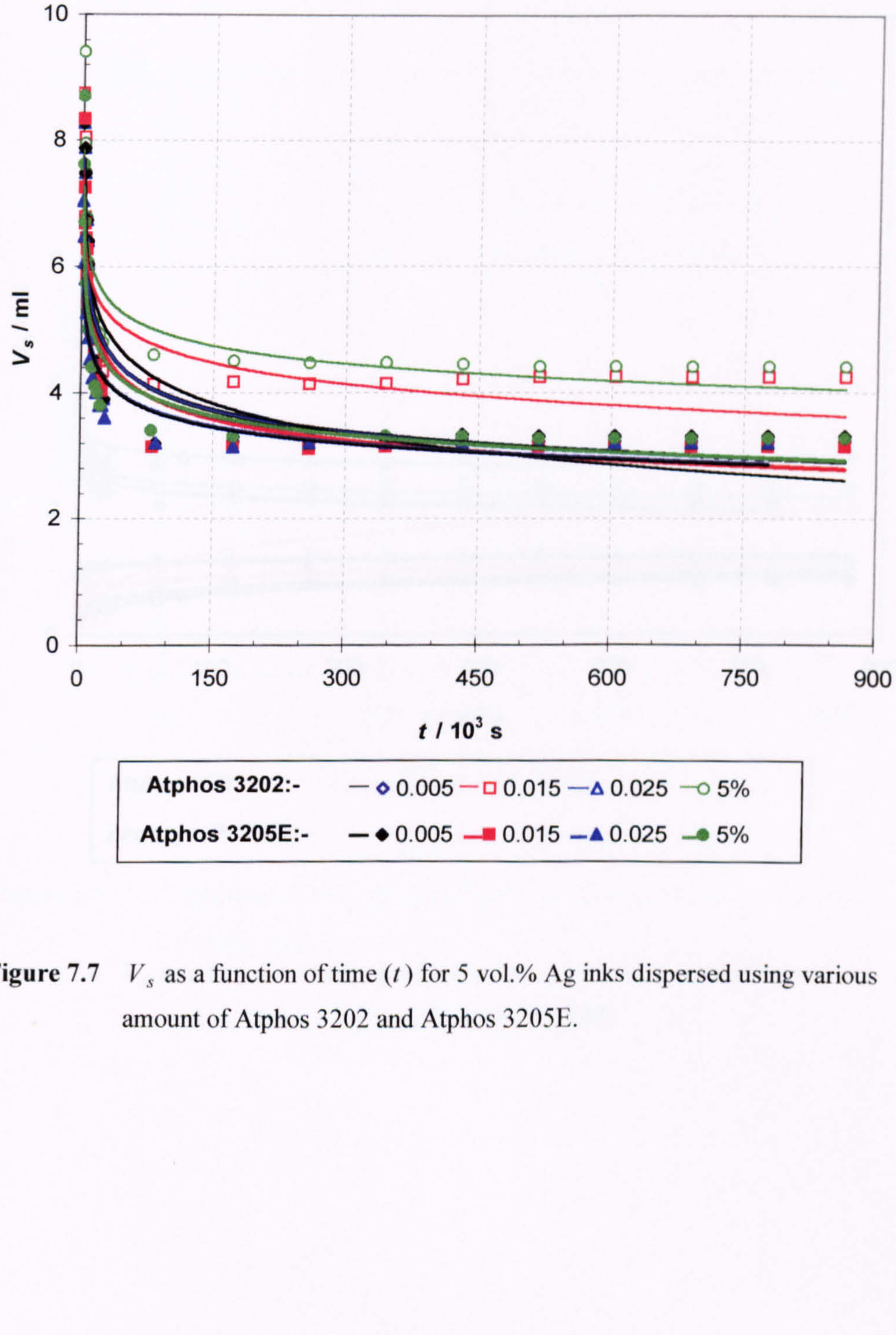

Figure 7.7 V_s as a function of time (t) for 5 vol.% Ag inks dispersed using various amount of Atphos 3202 and Atphos 3205E.

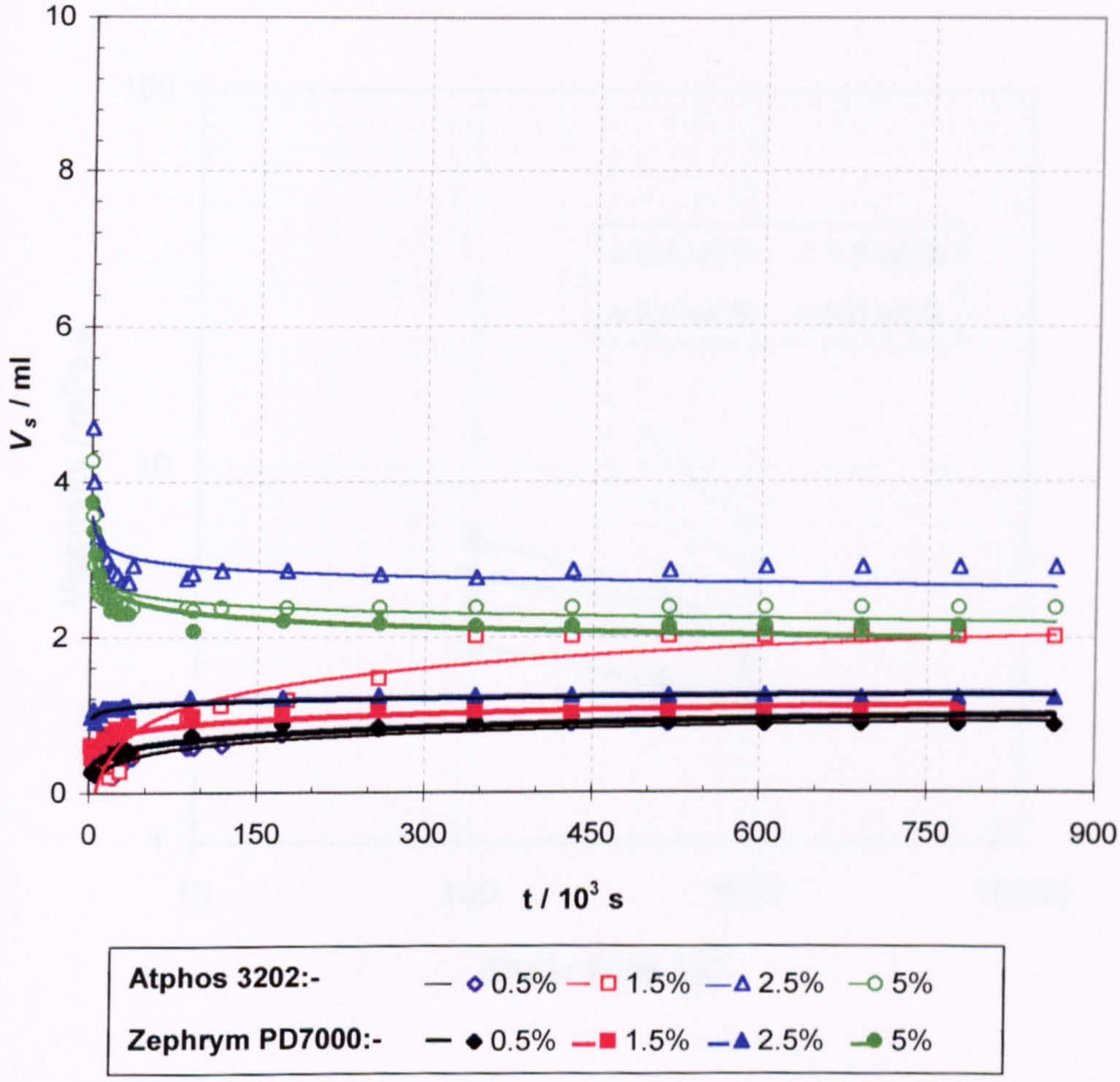

Figure 7.8 V_s as a function of time (t) for 2 vol.% Ag inks dispersed using various amount of Atphos 3202 and Zephrym PD7000.

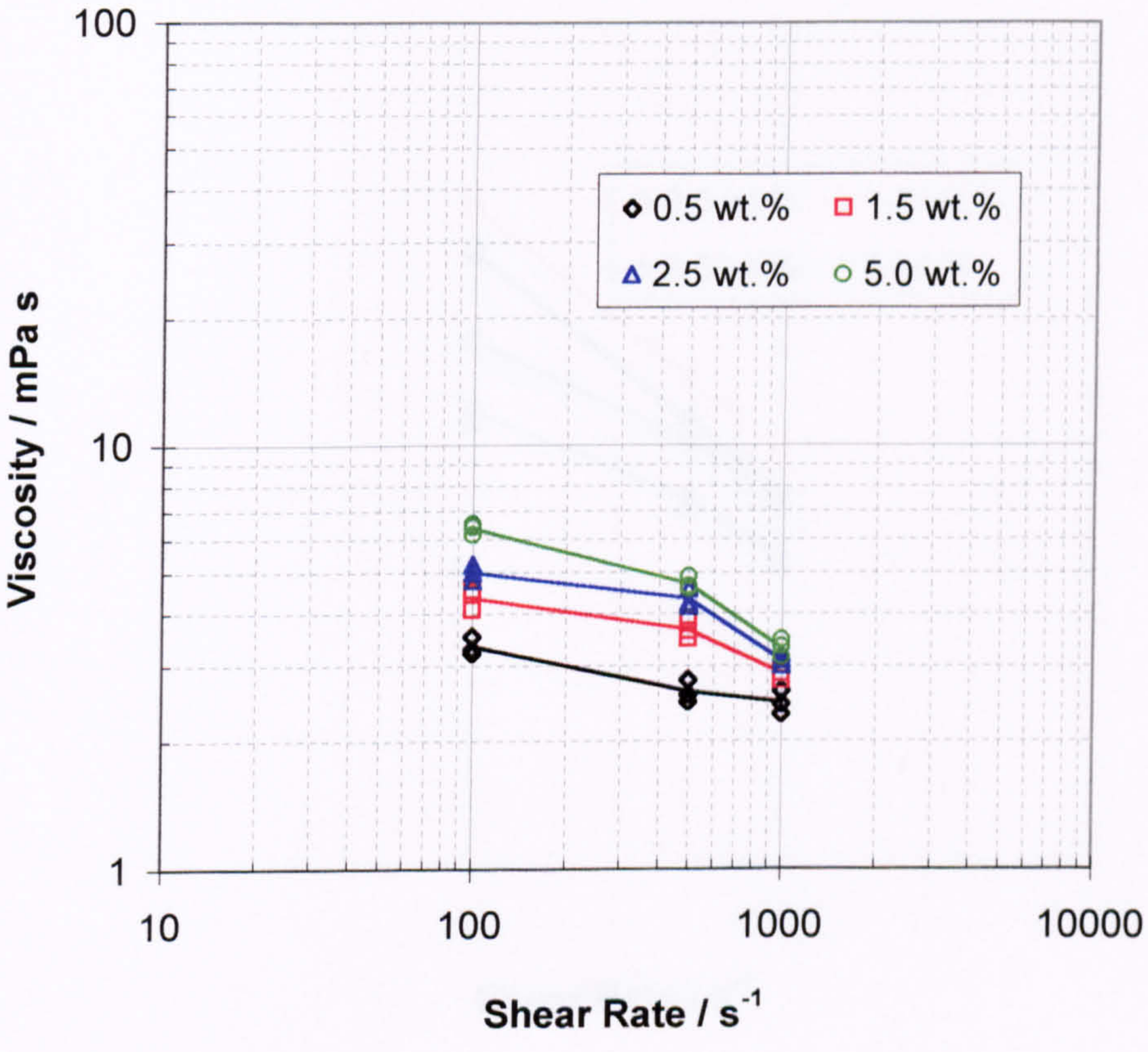

Figure 7.9 Viscosity of 2 vol. % Ag inks dispersed using various amount of Atphos 3202 at 0 s.

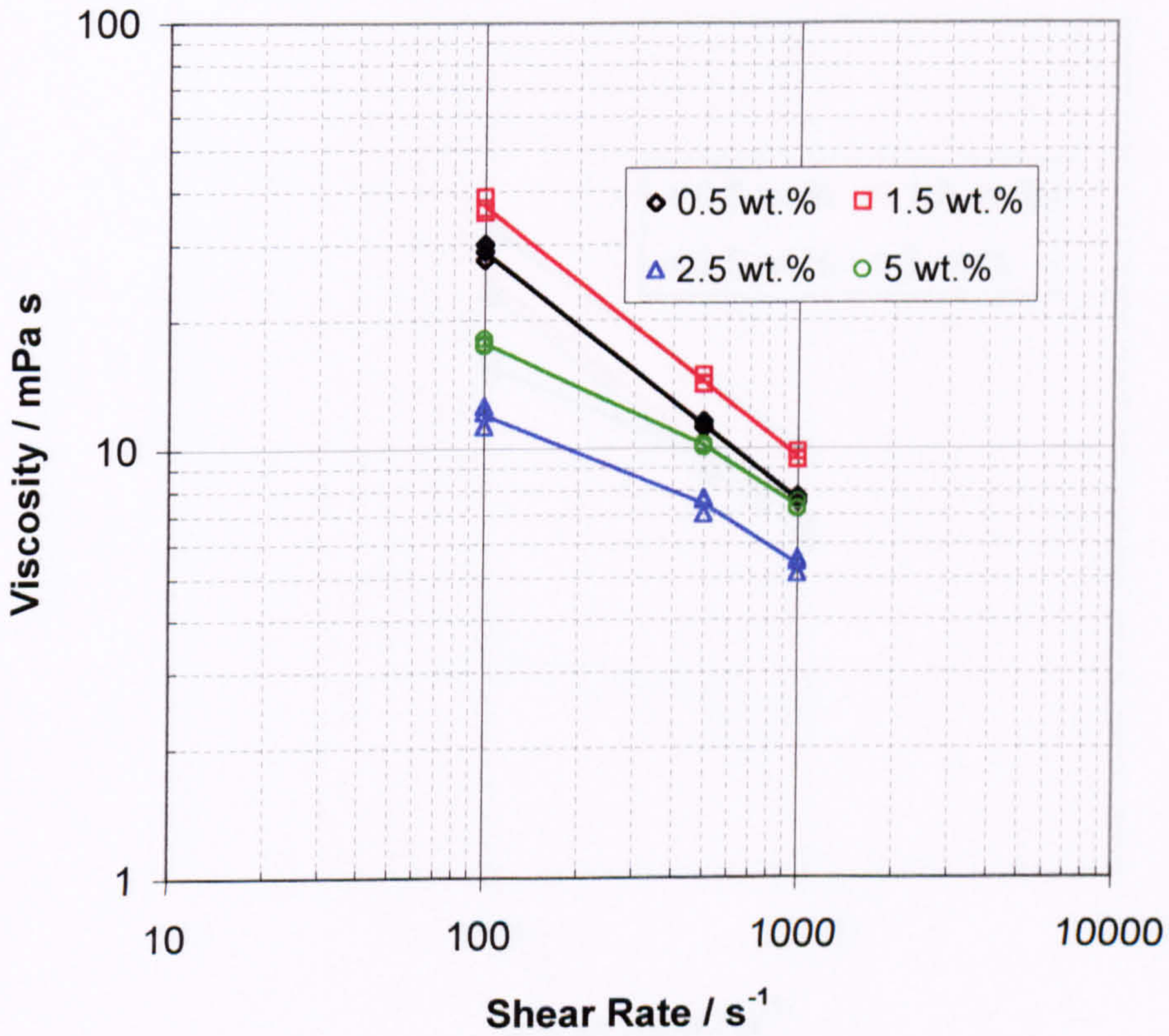

Figure 7.10 Viscosity of 5 vol. % Ag inks dispersed using various amount of Atphos 3202 at 0 s.

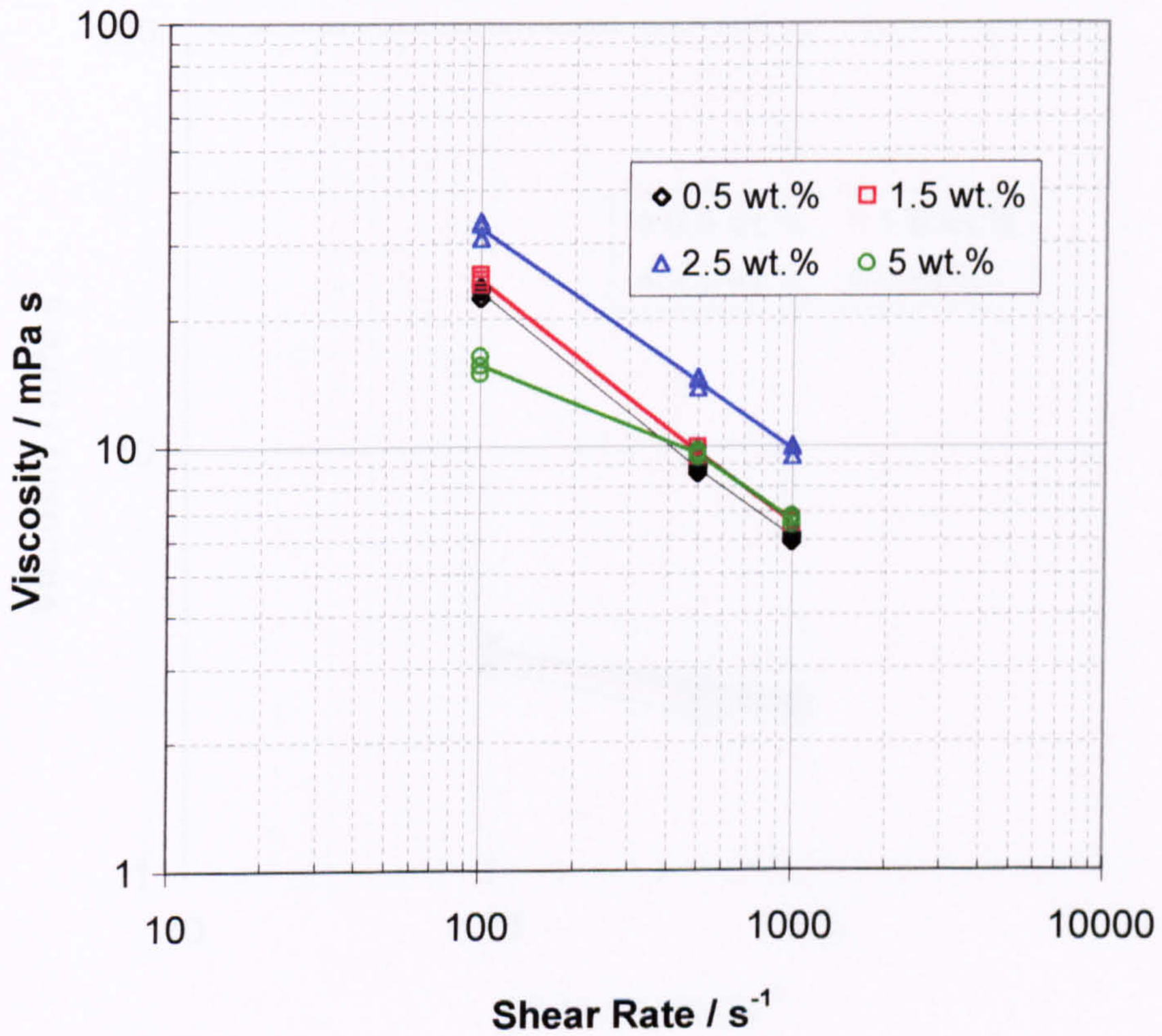

Figure 7.11 Viscosity of 5 vol. % Ag inks dispersed using various amount of Atphos 3205E at 0 s.

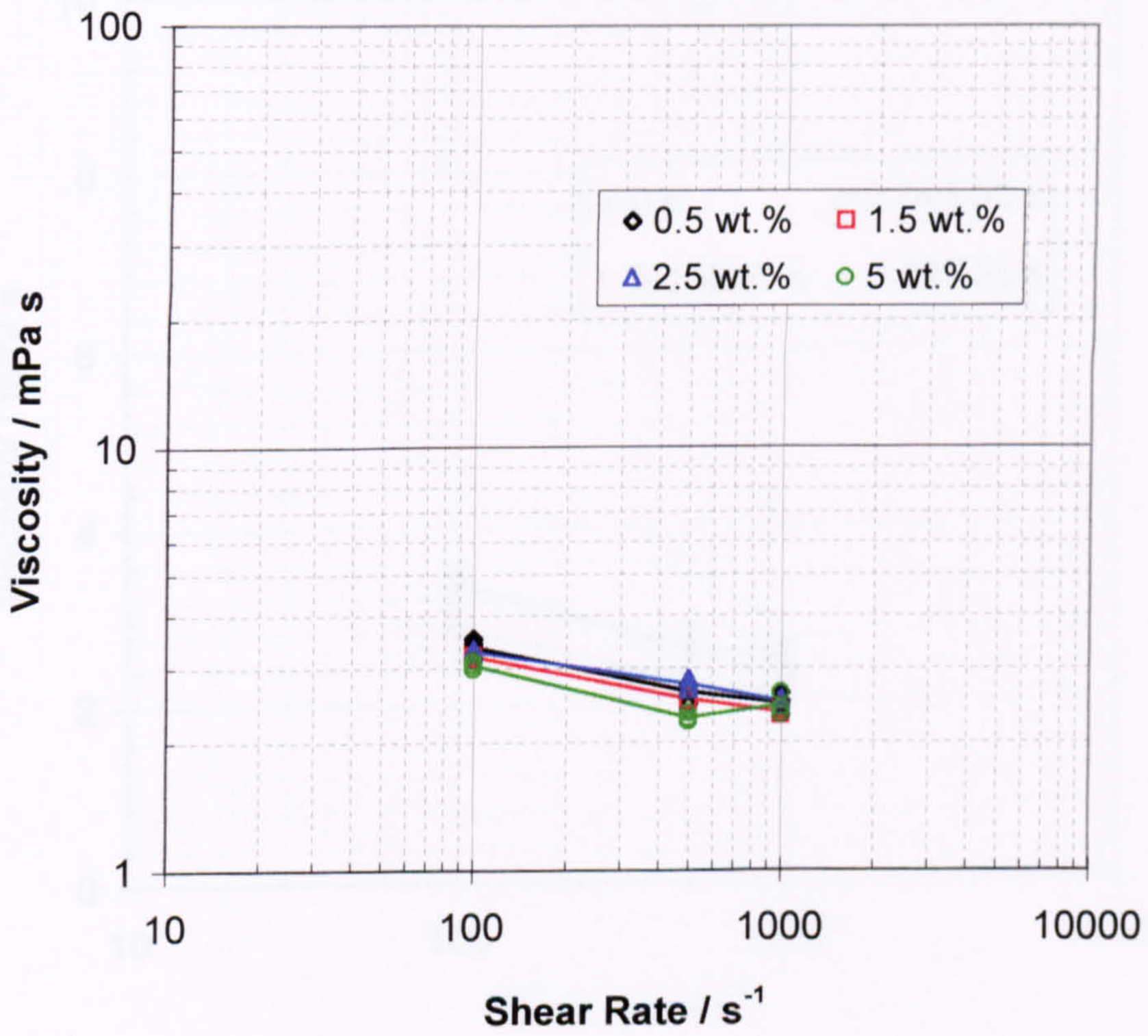

Figure 7.12 Viscosity of 2 vol. % Ag inks dispersed using various amount of Zephrym PD7000 at 0 s.

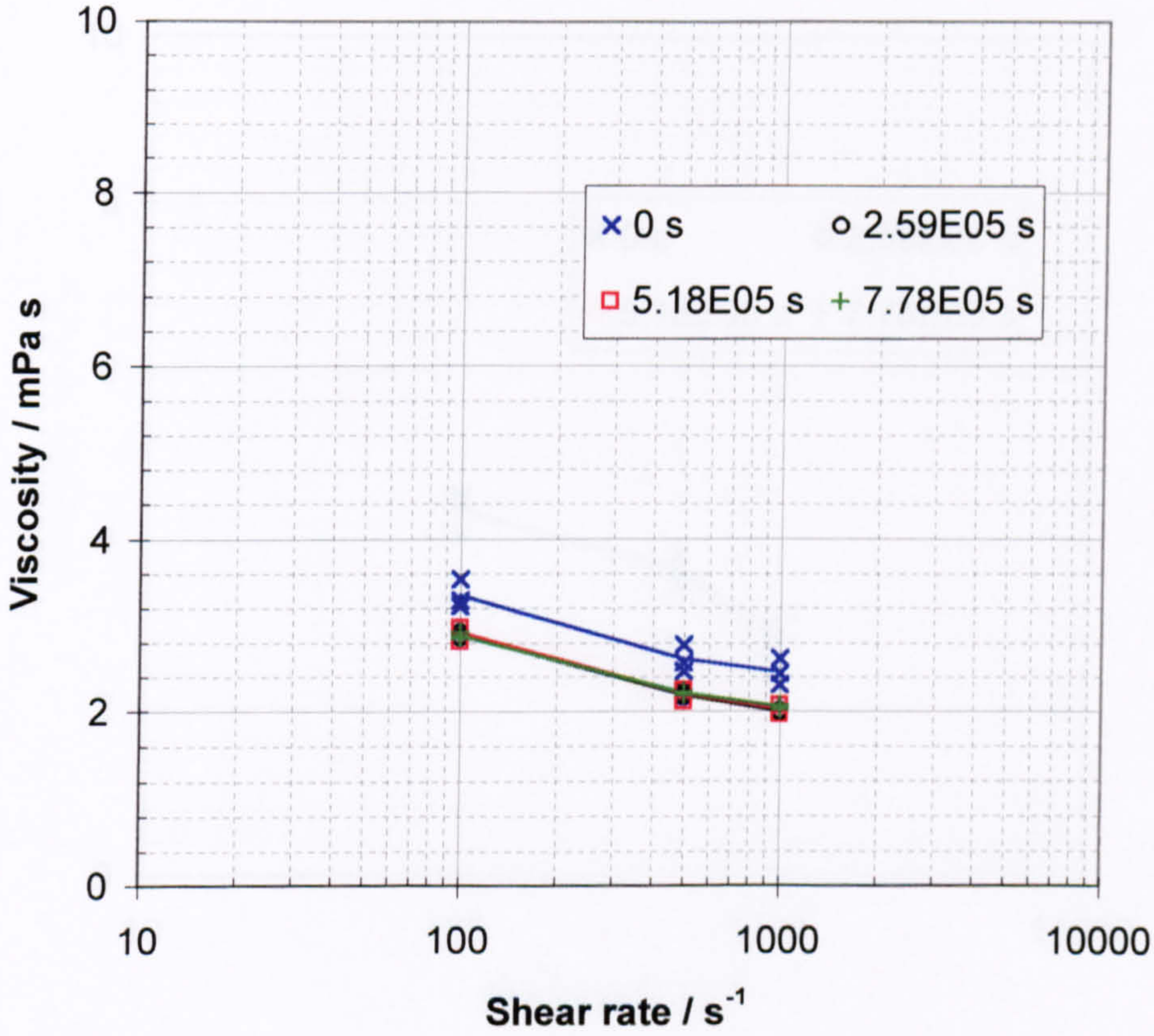

Figure 7.13 Variation of viscosity-shear rate with time for 2% vol. Ag inks made using 0.5 wt. % of Atphos 3202.

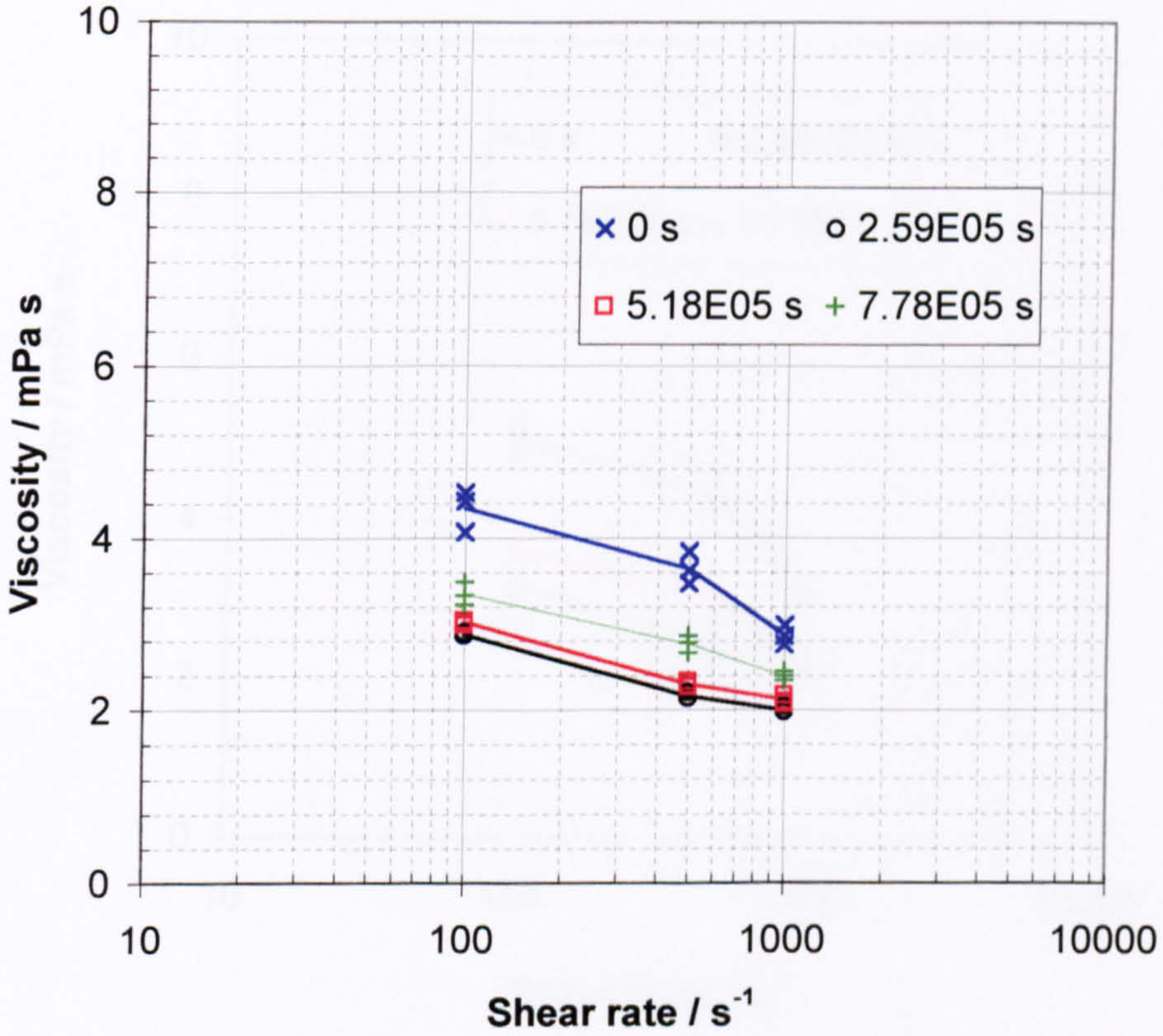

Figure 7.14 Variation of viscosity-shear rate with time for 2% vol. Ag inks made using 1.5 wt. % of Atphos 3202.

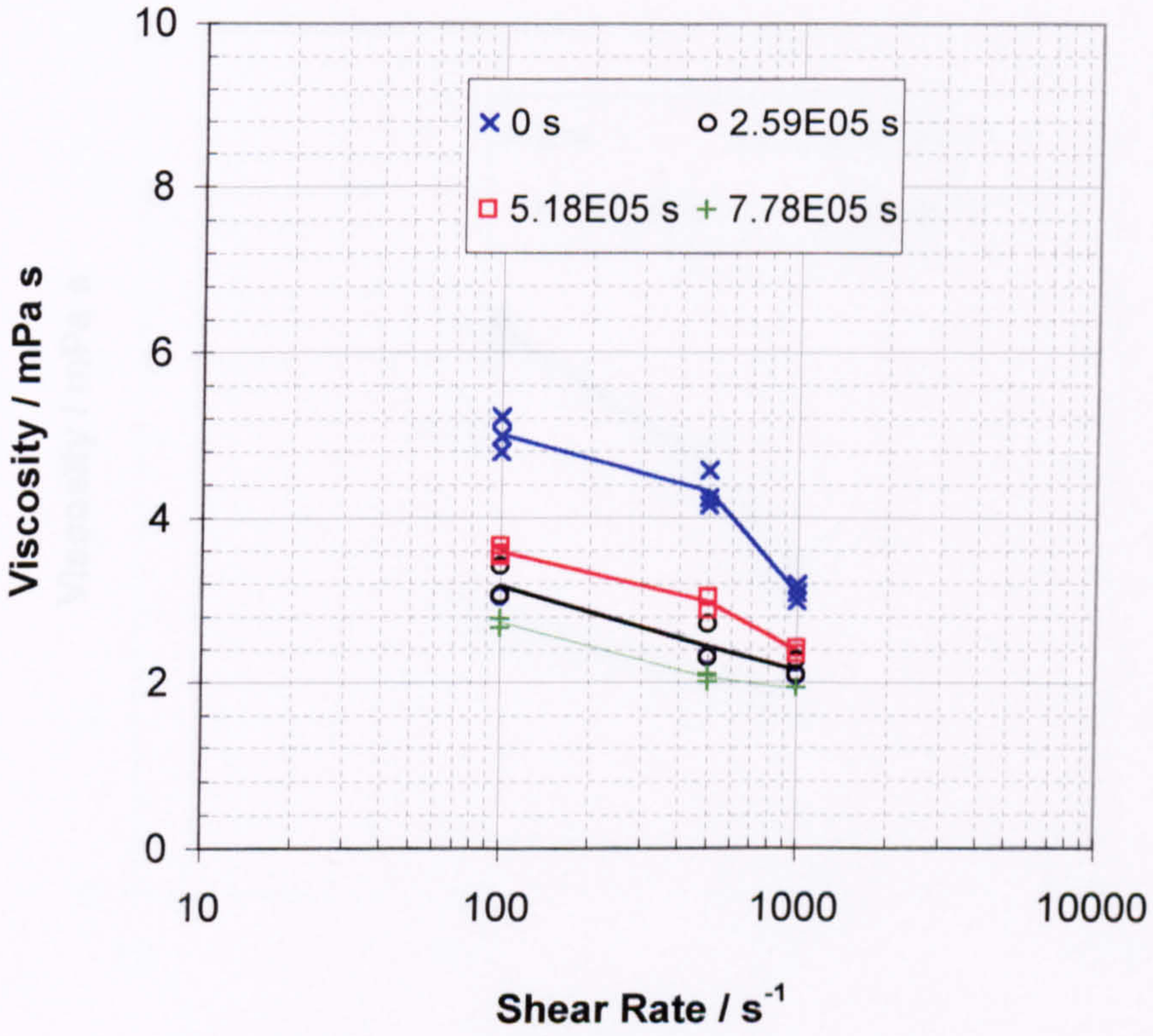

Figure 7.15 Variation of viscosity-shear rate with time for 2% vol. Ag inks made using 2.5 wt. % of Atphos 3202.

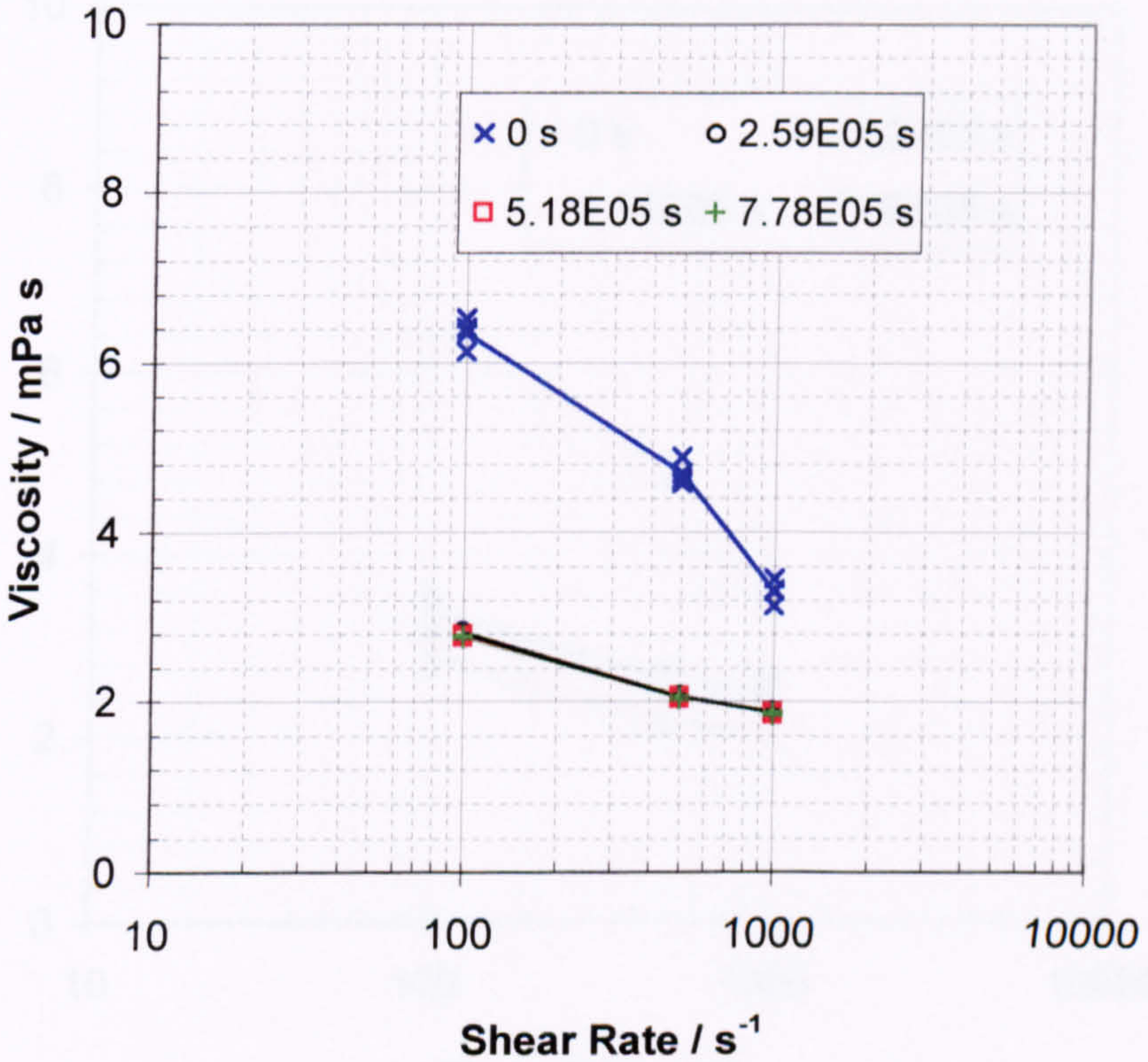

Figure 7.16 Variation of viscosity-shear rate with time for 2% vol. Ag inks made using 5 wt. % of Atphos 3202.

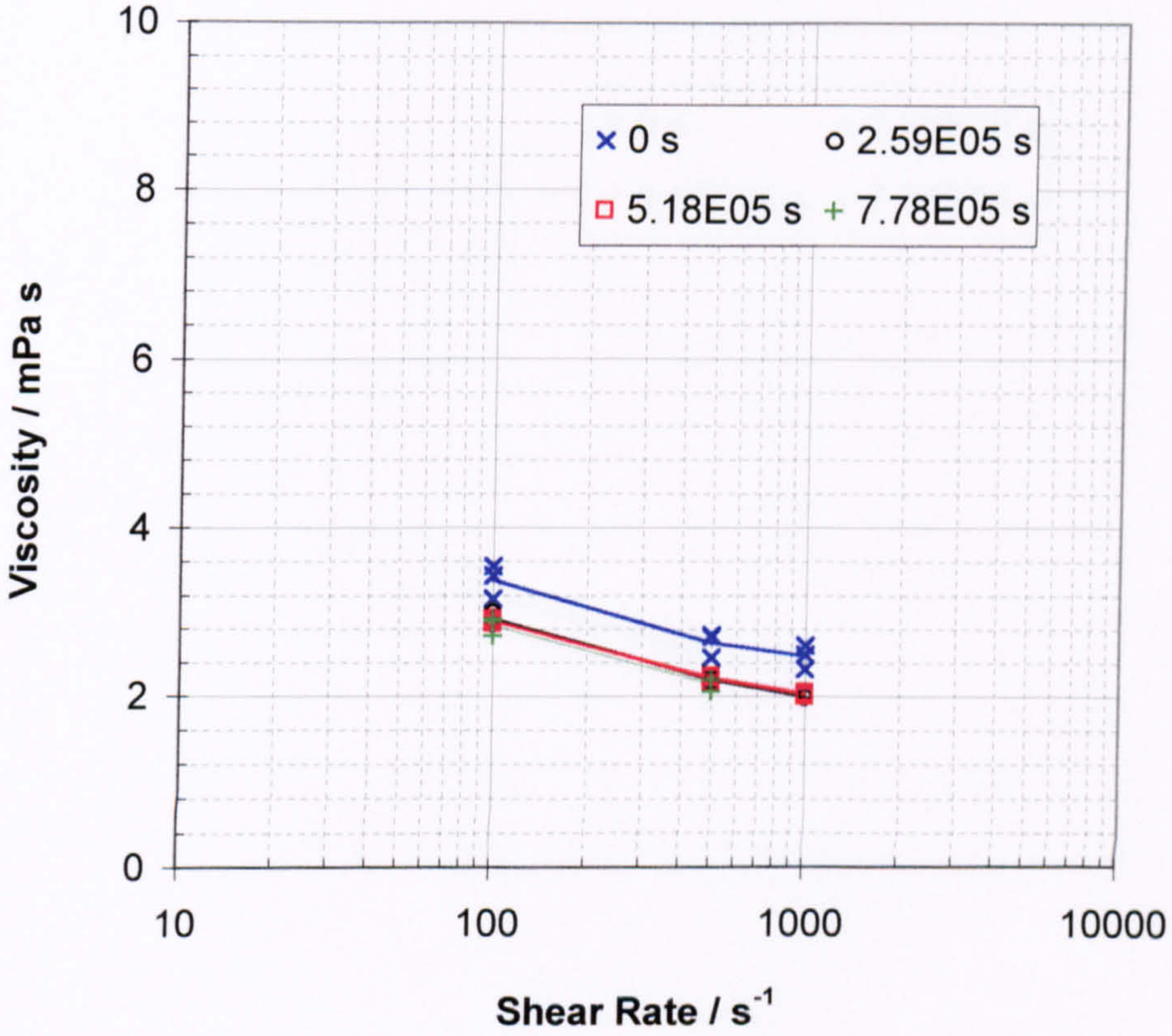

Figure 7.17 Variation of viscosity-shear rate with time for 2% vol. Ag inks made using 0.5 wt. % of Zephrym PD7000.

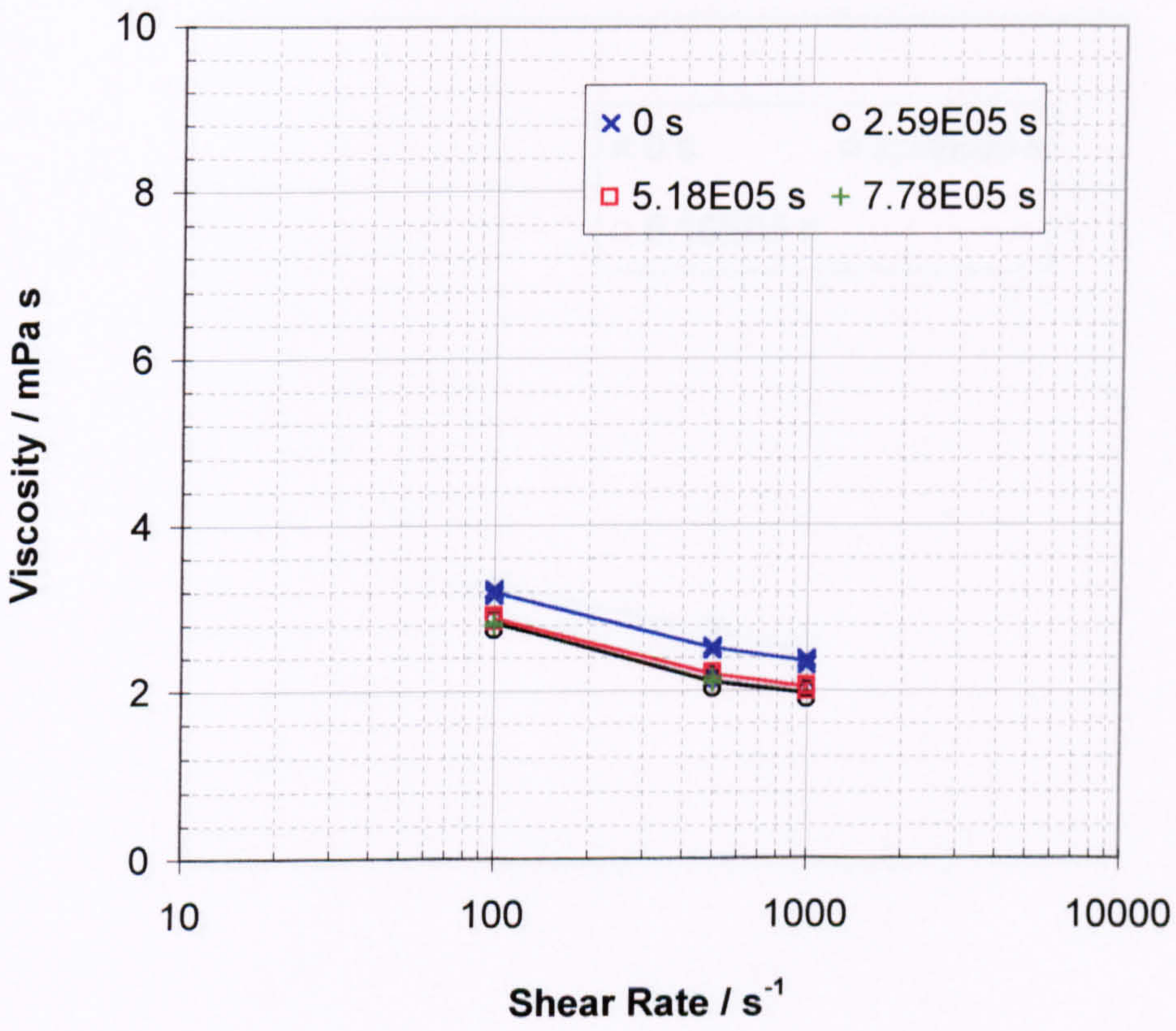

Figure 7.18 Variation of viscosity-shear rate for 2% vol. Ag inks made using 1.5 wt. % of Zephrym PD7000.

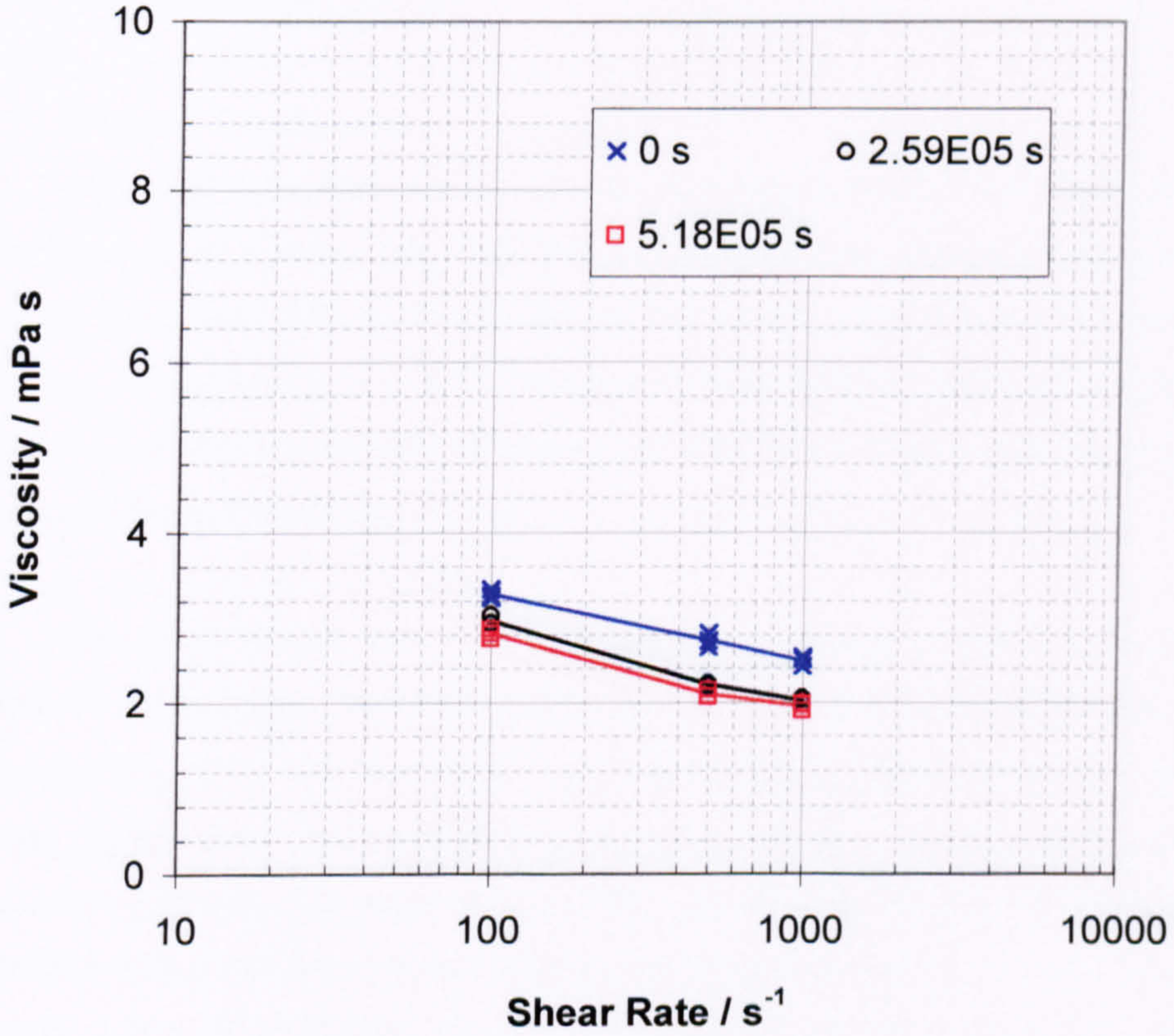

Figure 7.19 Variation of viscosity-shear rate with time for 2% vol. Ag inks made using 2.5 wt. % of Zephrym PD7000. The measured values at 7.78×10^5 s are < 2 mPa s and not reported.

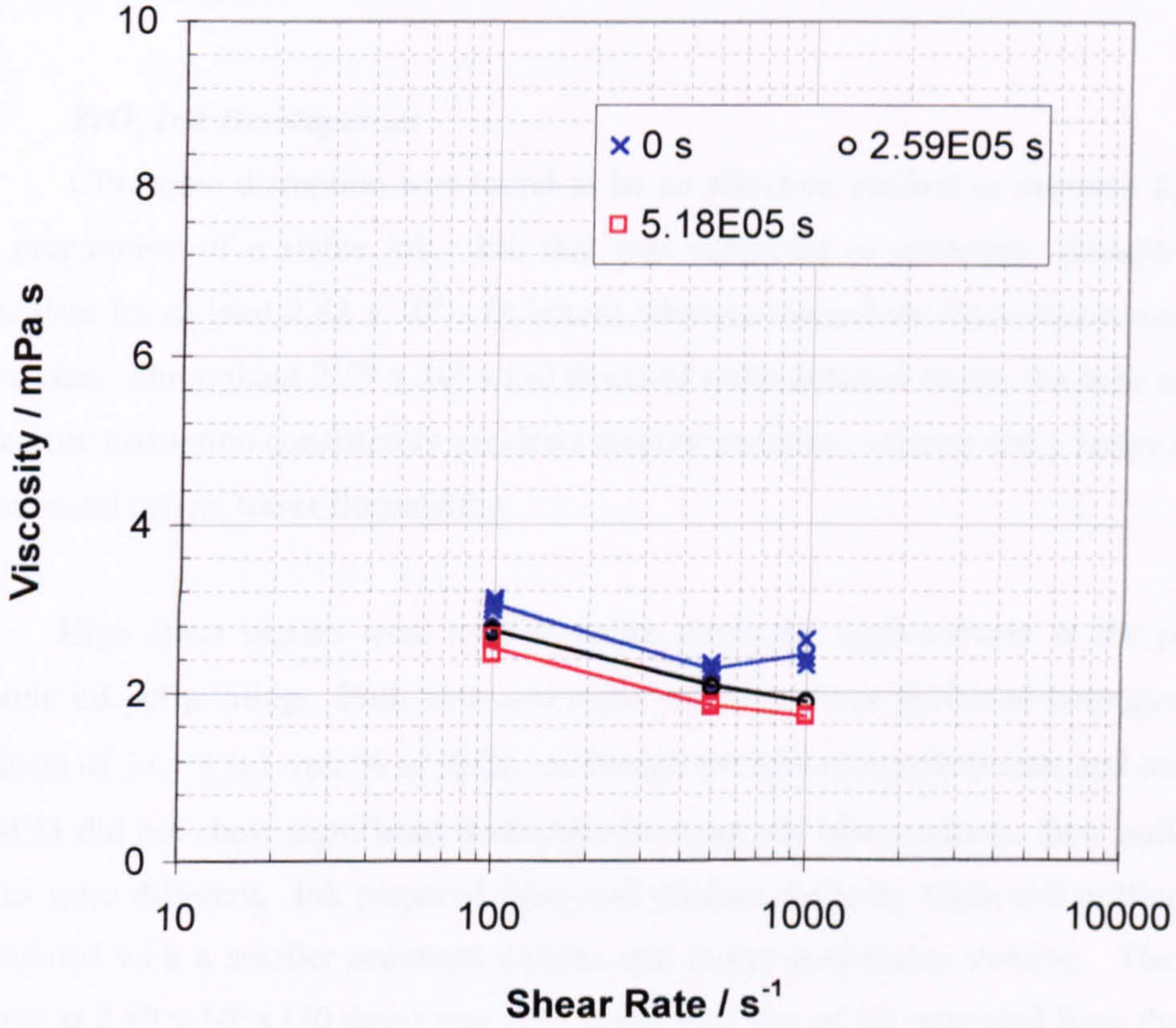

Figure 7.20 Variation of viscosity-shear rate with time for 2% vol. Ag inks made using 5 wt. % of Zephrym PD7000. The measured values at 7.78×10^5 s are < 2 mPa s and not reported.

Chapter 8

Conclusions and Further Work

8.1 Conclusions

(a) ZrO_2 Ink Development

(i) Ultrasonic disruption was found to be an effective method to disperse ZrO_2 ink for the preparation of a stable ink. Ink that was subjected to ultrasonic disruption did not flocculate for at least 2.88×10^4 s (8 hours) whereas immediate flocculation was observed otherwise. Throughout 2.59×10^6 s (30 days) of sedimentation study, the inks subjected to ultrasonic disruption consistently yielded a smaller sediment volume and a larger suspension volume and hence, lesser flocculation.

(ii) High shear mixers were used to break down the agglomerates in the powder for ceramic ink-jet printing. Both twin and triple roll mills have produced homogeneous mill products of 53.1 ± 0.1 vol. % of ZrO_2. Although the loss-on-ignition tests and micrographs by SEM did not show significant distinction between the two products, their sedimentation results were different. Ink prepared from mill product made by triple roll milling was less flocculated with a smaller sediment volume and larger suspension volume. The sediment volume at 2.59×10^6 s (30 days) was 17% lower than that of ink prepared from the twin roll mill product.

(iii) The addition of electrolyte (NH_4NO_3) in the ZrO_2 ink to improve its electrical conductivity, which was necessary for a continuous jet printer, was found to increase flocculation in the ink. Although the ink did not flocculate for a short period of 7.20×10^3 s (2 hours), it yielded a larger sediment volume and smaller suspension volume compared with inks not containing NH_4NO_3. Furthermore, increasing the volumetric ratio of powder to polymer (dispersant, polyvinylbutyral and dibutyl sebacate) from 50% to 60% or 70% also increased flocculation in the ink.

(iv) The ink preparation procedure for 5 vol. % (nominal) ZrO_2 ink was established. The agglomerates in the powder were broken down mechanically by a triple roll mill followed by subjecting the ink to ultrasonic disruption. The ink was further subjected to 1.73 x 10^5 s (2 days) of sedimentation where the hard sediment was removed and the remaining ink suspension was filtered in two stages with a 10 μm and then 5 μm filters. The ink suspension, which comprised of 37.6 vol. % ZrO_2 (excluding solvent), was printed continuously for at least 1.73 x 10^5 s (2 days) on a commercial continuous jet printer. Nozzle blockage did not occur during printing.

(b) Continuous Jet Printing

(i) The modulation frequency for printing was optimised at 70 kHz, i.e. 70,000 droplets were generated per second. At this frequency, the jet emerging from the nozzle broke down into a series of pear-shaped, symmetrical droplets in the middle of the charge electrode and no satellite droplets were observed. On output, all the droplets were placed correctly with clear prints having a well defined boundary.

(ii) Printing substrates of surface free energy (γ_{sv}) 20 - 74 mN m^{-1} have been used for the deposition of ZrO_2 ink of surface tension ($\gamma_{l,ink}$) of 24 mN m^{-1} using the continuous jet printer. There was little ink spreading when the droplet was deposited on substrate where $\gamma_{sv} < \gamma_{l,ink}$. The printed dot was thus smaller. Hence details can be reproduced on this substrate. On the other hand, there was greater spreading on substrates where $\gamma_{sv} > \gamma_{l,ink}$. This led to coalescence of neighbouring dots.

(iii) ZrO_2 powder was also found to migrate to the periphery of printed dot, giving rise to a 'ring' appearance when a droplet of ZrO_2 ink was deposited on substrates where $\gamma_{sv} > \gamma_{l,ink}$ by jet printing at a velocity ~ 22 m s^{-1}. However, no powder migration was observed on substrate where $\gamma_{sv} < \gamma_{l,ink}$ with identical printing condition.

(iv) The surface of green parts produced using substrates where $\gamma_{sv} > \gamma_{l,ink}$ was influenced by the print resolutions in the horizontal and vertical directions. Green parts were made using print resolutions of 3543 x 3660, 2638 x 3660, 1930 x 3660 and 1969 x 1939 dots per m^2 in the horizontal and vertical directions. When a high print resolution of 3543 x 3660 dots

per m^2 was used, enmeshed ridges were obtained in both horizontal and vertical directions. These can be eliminated by reducing the print resolutions in the respective directions. A 1800-layer green part of 0.6 mm in thickness was printed, debound and sintered. The total shrinkages were 17%, 29% and 18% in height, width and thickness, respectively.

(v) The requirements of efficient drying and surface quality of the printed part on substrates where $\gamma_{sv} > \gamma_{l,ink}$ are in competition with each other. Although the use of assisted drying (by forced convection or heated substrate) removed solvent at a faster rate, it also produced thinner defect-free parts compared with those using natural convection. The influence of the type of drying was significant when the print area was smaller.

(c) Wettability and Dynamic Shrinkage

(i) The dynamics of shrinkage of ZrO_2 ink droplets containing 2.5 vol. % of powder, which were slowly released onto substrates, were found to be different on substrates of different level of surface free energy (γ_{sv}) in comparison with the surface tension of the ink ($\gamma_{l,ink}$).

(ii) Droplet deposited on substrates where $\gamma_{sv} < \gamma_{l,ink}$ experienced a short period of instability and vibrated. After it had stabilised, the droplet shrank with decreasing contact angle and droplet height while the ink-substrate interface width remained constant. This was followed by a second stage of shrinkage where the contact angle remained constant while the contact interface width and droplet height reduced. The droplet then continued to shrink further but with a stationary contact interface width and a reducing contact angle and reducing droplet height.

(iii) When $\gamma_{sv} > \gamma_{l,ink}$, the droplet shrank rapidly with an expanding contact interface width and a decreasing contact angle and decreasing droplet height. In the second stage of shrinkage, the contact angle and droplet height decreased while maintaining a constant contact interface width.

(iv) The overall shrinkage rate of the ceramic ink deposited on the substrates where $\gamma_{sv} > \gamma_{l,ink}$ was faster by almost two times.

(d) Development of Silver Ink

(i) Three dispersants, Atphos 3202, Atphos 3205E and Zephrym PD7000, were used to disperse 2 and 5 vol. % of Ag powder in industrial methylated spirit. Both deflocculated or flocculated inks were produced. The former has its sediment volume increased with no clear liquid formed during sedimentation. Generally, they belonged to the 2 vol. % inks made with low dispersant amount at 0.5 wt. %. The flocculated inks, in which a clear liquid was formed during sedimentation, prevailed among inks prepared at 5 vol. % Ag and/or higher dispersant amount.

(ii) The half-value time ($t_{1/2}$) was used successfully to assess the degree of flocculation in the Ag inks. A larger $t_{1/2}$ value is an indication of lesser flocculation. This was validated, qualitatively, by the sedimentation results of the inks investigated and, quantitatively, by the final sediment volumes. The 2 vol. % ink made with 0.5 wt. % of Atphos 3202 had the highest $t_{1/2}$ value of 3.91×10^4 s. This ink also yielded the lowest sediment volume.

(iii) Regardless of the type of dispersant used and the vol. % of Ag, increasing the amount of dispersant beyond the recommended 0.5 wt. % increased flocculation in the ink and, hence, an increased final sediment volume and a smaller $t_{1/2}$. This may be attributed to the excess amount adsorbed over the monolayer of dispersant and neutralised any stabilisation effect provided. A deflocculated ink was produced at the lowest dispersant amount (0.5 wt. %) for a 2 vol. % Ag ink whereas a completely flocculated ink was resulted at the highest dispersant amount of 5 wt. %. In the latter, most of the Ag powders settled immediately soon after sedimentation started.

(iv) Varying amount of Atphos 3202 was also used to prepare Ag inks at 2 and 5 vol. %. With the same ultrasonic energy used, it was found that flocculation was more significant in the 5 vol. % ink with more completely flocculated ink produced of smaller $t_{1/2}$ value. This is due to low ultrasonic energy, which was insufficient to break down the agglomerates. A higher amount of ultrasonic energy was not used to disperse the 5 vol. % ink as this will increase the solvent temperature near its boiling point.

(v) In preparing the 5 vol. % Ag inks, using a less acidic dispersant, such as Atphos 3205E (compared with Atphos 3202), yielded inks with a lower final sediment volume and

larger $t_{1/2}$ values. The resultant inks were less flocculated. It is thus possible to alter the state of flocculation in the Ag ink by adjusting the pH of the inks.

(vi) Viscosity measurements were used to assess the stability of the inks prepared over a period of 8.64×10^5 s (10 days). As prepared, most of the inks displayed pseudoplastic flow behaviour. The variation of their viscosity with respect to the amount of dispersant used was found to depend the powder loading and the state of dispersion in the ink. Two Ag inks at 2 vol. % were successfully prepared with 0.5 wt. % of Atphos 3202 and Zephrym PD7000. Both inks displayed a stable sediment volume after 8.64×10^4 s (1 day) and stable viscosity values after 2.59×10^5 s (3 days).

(vii) Based on the their $t_{1/2}$ values, inks prepared with Atphos 3202 were less flocculated than those with Zephrym PD7000. The $t_{1/2}$ value of the former was 4.5 times higher than that of the latter.

8.2 Contributions of the Research

This research established the conditions to enable continuous printing of a dilute suspension of ZrO_2 ink on a commercial continuous jet printer. The ink preparation procedure was developed with the production of well-dispersed ink with properties matching the printer requirements. The ink could be printed continuously for at least 1.73×10^5 s (2 days) without interruption. This paves the way to prototyping.

A basic understanding of the printing condition and ink-substrate interaction, which will affect dimensional accuracy of the printed part, was gained. For satisfactory droplet placement, the liquid jet should be modulated such that it is broken down into a series of pear-shaped, symmetrical droplets. It was found that powder migration to the dot periphery occurred in droplets deposited by jet printing on substrates with surface free energy higher than the surface tension of the ink. This significantly affected layer building and surface quality of the part. However, powder migration was not observed on substrate with lower surface free energy relative to the surface tension of the ink. The dynamics of shrinkage of a ZrO_2 droplet deposited on these two types of substrate were also different.

Silver-based ink was also developed with suitable viscosity values matching the printer specifications. This opens opportunities to extend the applications of DCIJP to freeforming metallic parts.

8.3 Recommendations for Further Work

(a) Direct and Continuous Jet Printing of ZrO_2

(i) The amount of ZrO_2 in the ink began with 50 vol. % (excluding solvent) at formulation stage but reduced to 37.6 vol. % at printing. This loss of 13 vol. % as sediment was mainly caused by flocculation. The work has shown that the addition of NH_4NO_3 as an electrolyte increased flocculation in the ink. The flocculation in the ink may be reduced by optimising the electrolyte concentration in the ink. However, it is also important to take into consideration that the amount of electrolyte must impart an electrical conductivity value matching the printer requirements. Other substitutes for NH_4NO_3, e.g. citrus acid, may be considered.

(ii) The sediment was normally disposed as waste. From the environmental and cost perspectives, it may be possible to salvage the hard sediment by re-dispersing it in solvent to make up the right composition for printing. However, its composition and content need to be analysed and ascertained. It is possible that the sediment is devoid of electrolyte and a suitable amount must be added to enable printing on a continuous jet printer.

(iii) The issue of drying of overprinted part is a 'bottleneck'. The study showed that accelerated removal of solvent by forced convection or increasing substrate's temperature is detrimental to the surface of parts printed on substrates where $\gamma_{sv} > \gamma_{l,ink}$. Other modes of drying such as ultra-violet, infrared, microwave or those that involve chemical reaction may be explored. However, their selection will depend on the type of ink. It may be possible to use a solvent with a higher volatility but this requires a systematic study of the properties of ink for printing, compatibility with other components in the ink formulation, its handling, health and safety and environmental factors.

(iv) A higher powder content in the printing ink (> 5 vol. % of ZrO_2) is desirable as this will improve the rate of component building and therefore shorter production times. However, the high viscosity associated with a high powder content poses a challenge, in particular, to continuous jet printer such as the Linx 6200S, which is designed for low viscosity inks. Attempting to print high viscosity ink in this printer will invoke its control to dilute the ink until the viscosity fell within its working range of 3 - 4 mPa s. Although the incorporation of wax in the ink will reduce viscosity, there is a limit to which this can attain. Therefore, any effort to improve the powder loading in ink should be developed in parallel with printer control.

(v) With the ink-jet printer demonstrating printing of ZrO_2 ink continuously and directly, it is worthwhile to implement modern Computer Aided Design (CAD) capabilities to extend present applications. This should serve at least two purposes. The first is to extend the present two-dimensional geometrical capabilities of the software in the printer system. The second is the automation of the overprinting process to minimise human intervention. Currently, overprinting is performed manually and this is the only reason limiting the number of layers that has been printed. Automating the printing process will pave the way for mass production and thicker components. For the latter, due consideration should be given to compensate for the reduction in printhead-to-part distance with increased printed layers. With the addition of appropriate hardware, parts can be prototyped on substrates where $\gamma_{sv} < \gamma_{l,ink}$. In addition, more than one nozzle and ink reservoir can be installed in the printer. Different material systems may be used in each nozzle for the purpose of printing functionally graded materials or overhang features.

(b) Development of Ag Ink

(i) Successful Ag inks containing 2 vol. % of powder, which were prepared with 0.5 wt. % of Atphos 3202 and Zeprhym PD7000, have viscosity levels within the viscosity specification of Linx printer. However, they are yet to be test printed on the printer and their electrical conductivity must be characterised prior to this. Alternately, the inks may be test printed on a drop-on-demand printer, which does not require conductive ink.

(ii) A difference in sedimentation behaviour and flocculation was observed in the 5 vol. % silver ink dispersed with the Atphos 3202 and 3205E dispersants, which have different ionic strength. It is thus possible to improve the state of flocculation by altering the ionic strength of the dispersion. This can be done by increasing the surface charge on the powder to a high enough level for stabilisation by the application of an acid or base.

(iii) Increased flocculation was observed in the inks with 5 vol. % of Ag due to the undispersed agglomerates in the powder. High shear mixers such as twin or triple roll may be employed to break down the agglomerates. However, it is important to include processing aids such as plasticiser and binder to bind the powders and anti-oxidant to prevent oxidisation of Ag.

(iv) If handling of the printed green bodies is expected, an appropriate resin should be added to the Ag ink. In this event, the properties of the ink, in particular the viscosity, has to be evaluated carefully.

References

ABRAHAM, T., 2000. U.S. emerges as dominant force in ceramic powders. *Am. Ceram. Soc. Bull.*, **79**(6), pp. 41-44.

ADAMSON, A.W. and GAST, A.P., 1997. *Physical Chemistry of Surfaces*, 6th edn.. New York: John Wiley & Sons, pp. 23-24.

AGARWALA, M.K, BANDYOPADHYAY, A., WEEREN, R. van, LANGRANA, N.A., SAFARI, A., DANFORTH, S.C., JAMALABAD, V.R., WHALEN, P.J., DONALDSON, R. and POLLINGER, J., 1996a. Fused deposition of ceramics (FDC) for structural silicon nitride components. *Proc. solid freeform fabrication symposium,* Austin, Texas, USA, Aug 1996. Austin: University of Texas at Austin, 1996, pp. 326-334.

AGARWALA, M.K, BANDYOPADHYAY, A., WEEREN, R. van, SAFARI, A., DANFORTH, S.C., LANGRANA, N.A., JAMALABAD, V.R. and WHALEN, P.J., 1996b. FDC, rapid fabrication of structural components. *Am. Ceram. Soc. Bull.*, **75**(11), pp. 60-65.

AGARWALA, M.K, WEEREN, R. van, BANDYOPADHYAY, A., WHALEN, P.J., SAFARI, A., and DANFORTH, S.C., 1996c. Fused deposition of ceramics and metals: an overview, (Online). Available: *http://www.caip.rutgers.edu/sff* (Accessed 8 Aug, 1998).

ALVIN, M.A., 1996. Advanced ceramic materials for use in high-temperature particulate removal systems. *Ind. Eng. Chem. Res.*, **35**(10), pp. 3384-3398.

ANON, 1996. World advanced ceramics. *Canad. Ceram. Soc. J.*, **65**(1), pp. 21-22.

ANON, 1999. Shaping with screen printing. *Ceram. Forum Int.*, **76**(11-12), pp. 20-21.

ASTM D1331-89, 1989. Standard test methods for surface and interfacial tension of solutions of surface-active agents. *1989 annual books of ASTM standards, section 15, vol. 15.04.* Philadelphia: American Society for Testing Methods, 1989, pp. 115-117.

ATKINSON, A., DOORBAR, J., JUDD, A., SEGAL, D.L. and WHITE, P.J., 1997. Continuous ink-jet printing using sol-gel 'ceramic' inks. *J. Sol-Gel Sci. Technol.*, 8(1-3), pp. 1093-1097.

BANDYOPADHYAY, A., PANDA, R.K., McNULTY, T.F., MOHAMMADI, F., DANFORTH, S.C. and SAFARI, A., 1998. Piezoelectric ceramics and composites via rapid prototyping techniques. *Rapid Prototyping J.*, **4**(1), pp. 37-49.

BAO, X. and EDIRISINGHE, M.J., 1998. Use of trichlorophenylsilane in the synthesis of polymeric precursors for silicon carbide. *J. Mater. Sci. Lett.*, **17**(19), pp. 1641-1643.

BARON, D.M. and PERRY, J.R., 1983. The fabrication of spark plugs. *Proc. Brit. Ceram. Soc.*, **3**(33), pp. 79-87.

BEAMAN, J.J., BARLOW, J.W., BOURELL, D.L., CRAWFORD, R.H., MARCUS, H.L. and McALEA, K.P, 1997. *Solid Freeform Fabrication: A New Direction in Manufacturing.* Massachusetts: Kluwer Academic Publishers, pp. 1-49, 121-165.

BELL, S.H., and CROWL, V.T., 1973. Assessment of the state of dispersion. *In:* G.D. PARFITT, ed. *Dispersion of powders in liquids.* London: Applied Science Publishers, Ltd., 1973, pp. 267-307.

BIEHL, S., DANZEBRINK, R., OLIVEIRA, P. and AEGERTER, M.A., 1998. Refractive microlens fabrication by ink-jet process. *J. Sol-Gel Sci. Technol.*, **13**(1-3), pp. 177-182.

BINGHAM, E.C., 1922. *Fluidity and Plasticity.* New Yori: McGraw Hill, 1922, p. 228.

BIRDI, K.S. and VU, D.T., 1993. Wettability and the evaporation rates of fluids from solid surfaces. *In:* K.L. MITTAL, ed. *Contact angle, wettability and adhesion.* The Netherlands: Utrecht, 1993, pp. 285-293.

BIRKENSHAW, J.W., 1999. Printing processes. *In:* R.H. LEACH, R.J. PIERCE, E.P. HICKMENA, M.J. MACKENZIE and H.G. SMITH, eds. *The printing ink manual,* 5th edn.. Netherlands: Kluwer Academic Publishers, 1999, pp. 14-85.

BIRMINGHAM, B.R., TOMPKINS, J.V., HARRISON, S.L. and MARCUS, H.L., 1995. Solid freeform fabrication laser beam processing using gas phase approaches. In: T.S. SRIVATSAN and J.J. MOORE, eds. *Proc. 2nd Int. Conf. Beam Processing Adv. Mater.,* Cleveland, Ohio, USA, Oct 30 - Nov 2, 1995. Warrendale: Minerals, Metals and Materials Society, 1996, pp. 105-117.

BLAZDELL, P.F., EVANS, J.R.G., EDIRISINGHE, M.J., SHAW, P. and BINSTEAD, M.J., 1995. The computer aided manufacture of ceramics using multilayer jet printing. *J. Mater. Sci. Lett.*, **14**(22), pp. 1562-1565.

BLAZDELL, P.F. and KURODA, S., 2000. Plasma spraying of submicron ceramic suspensions using a continuous ink jet printer. *Surf. Coat. Tech.*, **123**(2-3), pp. 239-246.

BOSE, A., 1995. The technology and commercial status of powder injection moulding. *JOM*, **47**(8), pp. 26-30.

BOSSEL, C., DUTTA, J., HOURIET, R., HILBORN, J. and HOFMANN, H., 1995. Processing of nano-scaled silicon powders to prepare slip cast structural ceramics. *Mater. Sci. Eng.*, **A204**, pp. 107-112.

BRINKER, C.J. and SCHERER, G.W., 1990. *Sol-Gel Science: The Physics and Chemistry of Sol-Gel Processing.* Boston: Academic Press, pp. 839 – 880.

BS 733: Part 2 : 1987. *Pyknometers. Methods for Calibration and Use of Pyknometers.* London: British Standard Institution.

BS 5600, 1981. *Powder Metallurgical Materials and Products.* London: British Standard Institution.

BUEHNER, W.L., HILL, J.D., WILLIAMS, T.H. and WOODS, J.W., 1977. Application of ink jet technology to a word processing output printer. *IBM J. Res. Develop.*, **21**(1), pp. 2-9.

BUNNELL, D.E., DAS, S., BOURELL, D.L., BEAMAN, J.B. and MARCUS, H.L., 1995. Fundamentals of liquid phase sintering during selective laser sintering. *In:* H.L. MARCUS, J.J. BEAMAN, D.L. BEAMAN, D.K. BOURELL, J.W. BARLOW and R.H. CRAWFORD, eds. *Proc. solid freeform fabrications symp.*, Austin, Texas, USA, Aug 7-9, 1995. Austin: University of Texas at Austin, 1995, pp. 440-447.

CANNON, W.R., MORRIS, J.R. and MIKESKA, K.R., 1986. Dispersants for nonaqueous tape casting. *In:* J.R. BLUM and W.R. CANNON, eds. *Advances in ceramics, vol. 19 - multilayer ceramic devices.* Columbus: American Ceramic Society, 1986, pp. 161-174.

CARRION, A., 1997. Technology forecast on ink-jet head technology applications in rapid prototyping. *Rapid Prototyping J.*, 3(3), pp. 99-115.

CAWLEY, J.D., 1997. Computer-aided manufacturing of laminated engineering materials (CAM-LEM) and its application to the fabrication of ceramic components without tooling. *Proc. int. gas turbine and aeroengine congress and exhibition,* Orlando, Florida, USA, Jun 2-5, 1997. New York: American Society of Mechanical Engineers, 1997, pp. 1-6.

CAWLEY, J.D., HEUER, A.H., NEWMAN, W.S. and MATHEWSON, B.B., 1996. Computer-aided manufacturing of laminated engineering materials. *Am. Ceram. Soc. Bull.*, **75**(5), pp. 75-79.

CHANDRA, S., Di MARZO, M., QIAO, Y.M. and TARTARINI, P., 1996. Effect of liquid-solid contact angle on droplet evaporation. *Fire Safety J.*, **27**(2), pp. 141-158.

CHARTIER, T., SOUCHARD, S., BAUMARD, J.R. and VESTEGHEM, H., 1996. Degradation of dispersant during milling. *J. Eur. Ceram. Soc.*, **16**(12), pp. 1283-1291.

CHEDIAK, J.A., 1996. Ceramic engineers in the 21st century. *Am. Ceram. Soc. Bull.*, **75**(1), pp. 52-55.

CHEONG, M.H. and WAGNER, S., 2000. Inkjet printed copper source/drain metallisation for amorphous silicon thin-film transistors. *IEEE Electron Dev. Lett.*, **21**(8), pp. 384-386.

CHOU, K. and LEE., L., 1989. Effect of dispersants on the rheological properties and slip casting of concentrated Al_2O_3 slurry. *J. Am. Ceram. Soc.*, **72**(9), pp. 1622-1627.

CIMA, M.J., YOO, J., KHANUJA, S., RHYNERSON, M. and NAMMOUR, D., 1995. Structural ceramic components by 3D printing. *In:* H.L. MARCUS, J.J. BEAMAN, D.L. BEAMAN, D.K. BOURELL, J.W. BARLOW and R.H. CRAWFORD, eds. *Proc. solid freeform fabrications symp.*, Austin, Texas, USA, Aug 7-9, 1995. Austin: University of Texas at Austin, 1995, pp. 479-488.

CONLEY, J.G. and MARCUS, H.L., 1997. Rapid prototyping and solid free form fabrication. *J. Manuf. Sci. Engrg.- Trans. ASME,* **119**(4B), pp. 811-816.

CRUMP, S.S., 1991. Fast precise, safe prototypes with FDM. *In:* A. BACHI and J.J. BEAMAN, eds. *PED-Vol. 50: Intelligent design and manufacturing for prototyping.* New York: American Society of Mechanical Engineers, 1991, pp. 53-60.

CURODEAU, A., SACHS, E. and CALDARISE, S., 2000. Design and fabrication of cast orthopaedic implants with freeform surface textures from 3-D printed ceramic shell. *J. Biomed. Mater. Res.*, **53**(5), pp. 525-535.

DAIICHI KIGENSO KAGAKU KOGYO CO. LTD., 1998. *Certificate of Analysis for Zirconium Dioxide Grade 'HSY-3'.* Osaka: Daiichi Kigenso Kagaku Kogyo Co. Ltd, Jun 3, 1996.

DEEGAN, R.D., BAKAJIN, O., DUPONT, T.F., HUBER, G., NAGEL, S.R. and THOMAS, T.A., 1997. Capillary flow as the cause of ring stains from dried liquid drops. *Nature*, **389**(6653), pp. 827 - 829.

DENKOV, N.D., VELEV, D.D., KRALCHEVSKY, P.A., IVANOV, I.B., YOSHIMURA, H. and NAGAYAMA, K., 1992. Mechanism of formation of two-dimensional crystals from latex particles on substrates. *Langmuir*, **8**(12), pp. 3183-3190.

DEHUVYNE, B. (bart.dehuvyne@uniqema.com), Mar 9, 2001. *Re: Dispersants*. Email to B.Y.Tay (b.y.tay@qmw.ac.uk).

DISLICH, H., 1983. Glassy and crystalline systems from gels: chemical basis and technical applications. *J. Non-Cryst. Solids*, **57**(3), pp. 371-380.

DREITREK, INC., 1997. Ceramic thin tape casting 5 microns. *Am. Ceram. Soc. Bull.*, **76**(9), p. 164.

EDIRSINGHE, M.J., 1990. Injection moulding of ceramics. *Metals and Ceramics*, **6**(6), pp. 367-370.

EDIRISINGHE, M.J., 1997. Freeforming ceramics. *Mater. World*, **5**(3), pp. 138-140.

EDIRISINGHE, M.J., 1998. Solid freeform fabrication of ceramics. *In:* T.S. SRIVATSAN and K.A. KHOR, eds. *Proc. 1998 TMS fall meeting*, Rosemont, Illinois, USA, Oct 11 - 15, 1998. Warrendale: The Minerals, Metals and Materials Society, 1998, pp. 139-150.

ELLOIT, G. and SARTIN, A., 1997. The increasing use of ceramic filters in air pollution control applications. *Filtr. Separat.*, **34**(4), pp. 331-335.

ERBIL, H.Y., 1999. Determination of the peripheral contact angle of sessile drops on solids from the rate of evaporation. *J. Adhesion Sci. Technol.*, **13**(12), pp.1405-1413.

EVANS, J.R.G., 1994. Interfacial aspects of ceramic injection moulding. *In:* R.J. PUGH and L. BERGSTRÖM, eds. *Surface and colloid chemistry in advanced ceramics processing*. New York: Marcel Dekker, 1994, pp. 309-351.

FERBER, M.K. and TENNERY, V.J., 1991. Structural applications for technical, engineering and advanced ceramics. *In:* S.J. SCHNEIDER, Jr, volume chairman *Engineering materials handbook, vol. 4 - ceramics and glasses*. Ohio: American Society for Metals, International, 1991, pp. 959-960.

FILLMORE, G.L., BUEHNER, W.L. and WEST, D.L., 1977. Drop charging and deflection in an electrostatic ink jet printer. *IBM J. Res. Develop.*, **21**(1), pp. 37-47.

FREIMAN, S.W. and ONODA, G.Y. Jr., 1997. Advanced ceramics in the U.S. for the 21st century: prospects and challenges. *Ceram. Engrg. Sci. Proc.*, **18**(3A), pp. 21-27.

FUSTER, N.P., 1997. Rapid development. *Assembly Automation*, **17**(3), pp. 525-540.

GERMAN, R.M. and BOSE, A., 1997. *Injection Moulding of Metals and Ceramics.* Princeton: Metal Powder Industrial Federation, 1997.

GILBERT, J.M., ELLIINER, G.R., KEY, P.H., SNELLING, H.V., HARRSION, D. and HARREY, P., 1999. Via and embedded resistor production in low cost lithographically printed substrates. *Proc. 49th electronic components and technology conference,* San Diego, California, USA, Jun 1 - 4, 1999. Piscataway: IEEE, 1999, pp. 160-166.

GLOWACKI, B.A., 2000. Preparation of $Bi_2Sr_2CaCu0_{8-x}$ tracks and thick films by jet printing. *Supercond. Sci. Technol.*, **13**(5), pp. 584 -591.

GOODS, R.J., 1992. Contact angle, wetting and adhesion: a critical review. *In*: K.L. MITTAL, ed. *Contact angle, wettability and adhesion.* The Netherlands: Ultrechi, 1992, pp. 3-36.

GRAULE, T.J., GAUCKLER, L.J. and BAADER, F.H., 1996. Direct coagulation casting, a new green shape technique, part i: processing principles. *Ind. Ceram.*, **16**(1), pp. 31-34.

GREUL, M., 1996. Innovative economic process for the rapid prototyping of near net shape metal and ceramic parts. *Mat. Tech.*, **11**(4), pp. 140-142.

GRIFFIN, A., McMILLIN, S., GRIFFIN, C. and BARTON, K., 1997. Bioceramic RP materials for medical models. *In:* A.J. LIGHTMAN, R.P. CHARTOFF, M.K. AGARWALA and F. PRING, eds. *Proc. of the 7th int. conf. on rapid prototyping - 1997,* San Francisco, California, USA, Mar 31 - Apr 3, 1997. Dayton: University of Dayton, 1997, pp., 355-359.

GRIFFIN, E.A., MUMM, D.R. and MARSHALL, D.B., 1996. Rapid prototyping of functional ceramic composites. *Am. Ceram. Soc. Bull.*, **75**(7), pp. 65-68.

GRIFFITH, M.L. and HALLORAN, J.W., 1996. Freeform fabrication of ceramics via stereolithography. *J. Am. Ceram. Soc.*, **79**(10), pp. 2601-2608.

HAKKE, 1998. *Instruction Manual: Rotovisco® RT20, RheoStress® RS75/RS80 and RS150, Part No. 003-3633.* Karlsruhe: Hakke Mess-Technik, GmbH, u. Co., May 1998.

HALLORAN, J.W., 1999. Freeform fabrication of ceramics. *Brit. Ceram. Trans.*, 98(6), pp. 299-303.

HARGREAVES, I., 1999. Ultra-violet and electron-beam curing systems. *In:* R.H. LEACH, R.J. PIERCE, E.P. HICKMENA, M.J. MACKENZIE and H.G. SMITH, eds. *The printing ink manual*, 5th edn.. Netherlands: Kluwer Academic Publishers, 1999, pp. 636-677.

HARKINS, W.D. and JORDAN, H.F., 1930. A method for the determination of surface and interfacial tension from the maximum pull on a ring. *J. Am. Chem. Soc.*, **52**(5), pp. 1751-1772.

HARNBY, N., 1992. The mixing of cohesive powders. *In:* N. HARNBY, M.F. EDWARDS and A.W. NIENOW, eds. *Mixing in the process industries*, 2nd edn.. Oxford: Butterworth-Heinemann, 1992, pp. 82-94.

HAYES, D.J., COX, W.R. and GROVE, M.E., 1998. Micro-jet printing of polymers and solder for electronics manufacturing. *J. Electron. Manuf.*, 8(3), pp. 209-216.

HAYES, D.J., COX, W.R. and GROVE, M.E., 1999. Low-cost display assembly and interconnect using ink-jet printing technology, (Online). Available: *http://www.microfab.com/papers/paper-pdf/displayworks-99.PDF* (Accessed 8 Aug 2000).

HEBNER, T.R., WU, C.C., MARCY, D., LU, M.H. and STURM, J.C., 1998. Ink-jet printing of doped polymers for organic light emitting devices. *App. Phys. Lett.*, **72**(5), pp. 519-521.

HERMAN, H. and SAMPATH, S., 1996. Thermal spray coatings. *In:* K.H. STERN, ed. *Metallurgical and ceramic protective coatings*. London: Chapman and Hall, 1996, pp. 261-289.

HEUSCH, R. and REIZLEIN, K., 1987. Disperse systems and dispersants. *In:* W. GERHARTZ, Y.S. YAMAMOTO, L. KAUDY, R. PFETTERKORN and J. R. ROUNSAVILLE, eds. *Ullmann's encyclopaedia of industrial chemistry, vol. A.8 - coronary therapeutics to display technology*, 5th edn.. Weinheim: VCH Publishers, 1987, pp. 577-600.

HIGASHITANI, K., YOSHIDA, K., TANISE, N. and MURATA, H., 1993. Dispersion of coagulated colloids by ultrasonication. *Colloid Surf. A: Phsysiochem. Eng.*, **81**, pp. 167-175.

HILMAS, G., 1996. Innovative technique for rapidly prototyping parts of polymers, metals, ceramics, composites and functionally graded materials. *Mat. Tech.*, **11**(6), pp. 226-228.

HONG, C.M. and WAGNER, S., 2000. Inkjet printed copper source/drain metallization for amorphous silicon thin-film transistors. *IEEE Elect. Device Lett.*, **21**(8), pp. 384-386.

HORN, R.G., 1990. Surface forces and their action in ceramic materials. *J. Am. Ceram. Soc.*, **73**(5), pp. 1117-1135.

HOTZA, D. and CREIL, P., 1995. Review: aqueous tape casting of ceramic powders. *Mater. Sci. Eng. A - Struct.*, **202**(1-2), pp. 206-217.

HUDD, A., 1999. Ink-jet inks. *In:* R.H. LEACH, R.J. PIERCE, E.P. HICKMENA, M.J. MACKENZIE and H.G. SMITH, eds. *The printing ink manual*, 5th edn.. Netherlands: Kluwer Academic Publishers, 1999, pp. 678-698.

ICI SURFACTANTS, 1997. *Atsurf 3315: P64-34E.* Belgium: ICI Europe Ltd., Oct 1997.

IPPOLITO, R., LULIANO, L., di TORINO, POLITECNICO, and GATTO, A., 1995. Benchmarking of rapid prototyping techniques in terms of dimensional accuracy and surface finish. *CIRP Annals*, **44**(1), pp. 157-160.

JANNEY, M.A., OMATETE, O.O., WALLS, C.A., NUNN, S.D., OGLE, R.J. and WESTMORELAND, G., 1998. Development of low-toxicity gelcasting systems. *J. Am. Ceram. Soc.*, **81**(3), pp. 581-591.

JETHANANDANI, R., 1997. Surface-engineered ceramics – an improved lot. *Am. Ceram. Soc. Bull.*, **76**(4), pp. 90-92.

JONES, R.L., 1996. Thermal barrier coatings. *In:* K.H. STERN, ed. *Metallurgical and ceramic protective coatings*. London: Chapman and Hall, 1996, pp. 194-235.

JORGE, E., CHARTIER, T. and BOCH, P., 1990. Ultrasonic dispersion of ceramic powders. *J. Am. Ceram. Soc.*, **73**(8), pp. 2552-2554.

KAMO, R., 1991. Adiabatic diesel engines. *In:* S.J. SCHNEIDER Jr, volume chairman *Engineering materials handbook, vol. 4 - ceramics and glasses*. Ohio: American Society for Metals, International, 1991, pp. 987-994.

KATSTRA, W.E., PALAZZOLO, R.D., ROWE, C.W., GIRITLIOGLU, B., TEUNG, P. and CIMA, M.J., 2000. Oral dosage forms fabricated by Three Dimensional Printing™. *J. Controlled Release*, **66**(1), pp. 1-9.

KEELING, M.R., 1981. Ink jet printing. *Phys. Technol.*, **12**(5), pp.196-203.

KENNARD, F., 1991. Cold isostatic pressing. *In:* S.J. SCHNEIDER Jr, volume chairman *Engineering materials handbook, vol. 4 - ceramics and glasses*. Ohio: American Society for Metals, International, pp. 147-152.

KIM, S.J. and McKEAN, D.E., 1998. Aqueous TiO_2 suspension preparation and novel application of ink jet printing technique for ceramic patterning. *J. Mater. Sci. Lett.*, **17**(2), pp. 141-144.

KIMURA, T., SAKAMOTO, T., LEVEQUE, J., SOHMIYA, H., FUJITA, M., IKEDA, S. and ANDO, T., 1996. Standardisation of ultrasonic power for sonochemical reaction. *Ultrason. Sonochem.*, **3**(3), pp. S157-S161.

KINOSHITA, M., SATOU, M. and UEMATSU, K., 1997. Dispersant affects glass-based multicomponent slurries. *Am. Ceram. Soc. Bull.*, **76**(10), pp. 55-58.

KLEIN, L.C., 1991. Sol-gel processing. *In:* S.J. SCHNEIDER Jr, volume chairman *Engineering materials handbook, vol. 4 - ceramics and glasses*. Ohio: American Society for Metals, International, 1991, pp. 209-214.

KLOCKE, F., 1997. Modern approaches for the production of ceramic components. *J. Eur. Ceram. Soc.*, **17**(2-3), pp. 457-465.

KLOSTERMANN, D., CHARTOFF, R., OSBORNE, N. and GRAVES, G., 1997. Laminated object manufacturing, a new process for the direct manufacture of monolithic ceramics and continuous fibre CMCs. *Ceram. Eng. Sc. Proc.*, **18**(4B), pp. 113-120.

KLOSTERMANN, D., CHARTOFF, R.P., OSBORNE, N.R., GRAVES, G.A., LIGHTMAN, A., HAN, G., BEZEREDI, A., RODRIGUES, S., PAK, S., KALMANOVICH, G., DODIN, L. and TU, S., 1998. Direct fabrication of ceramics, CMC by rapid prototyping. *Am. Ceram. Soc. Bull.*, **77**(10), pp. 69-74.

KRIEGESMANN, J., 1991. Processing of advanced bulk ceramic materials. *In:* P. VINCENZINI, ed. *Fundamentals of ceramic engineering.* Essex: Elsevier Science Ltd., 1991, pp. 147-152.

KRUSS, 1985. *Kruss K10 Tensiometer Manual.* Hamburg: Kruss, GmbH, 1985.

KRUTH, J.P., 1991. Material incress manufacturing by rapid prototyping techniques. *Annals of the CIRP*, **40**(2), pp. 603-614.

KRUTH, J.P., LEU, M.C. and NAKAGAWA, T., 1998. Progress in additive manufacturing and rapid prototyping. *CIRP Annals*, **47**(2), pp. 525-540.

KUHN, L. and MYERS, R.A., 1979. Ink-jet printing. *Am. Scientist*, **240**(4), pp. 120-132.

LABRINCHA, J.A., MENG, L.J., DOS-SANTOS, M.P., MARQUES, F.M.B. and FRADE, J.R., 1993. Evaluation of deposition techniques of cathode materials for solid oxide fuel cells. *Mater. Res. Bull.*, **28**(2), pp. 101-109.

LANGE, F.F, 1989. Powder processing science and technology for increased reliability. *J. Am. Ceram. Soc.*, **72**(1), pp. 3-15.

LANGE, F.F. and CLAUSSEN, N.E., 1984. Some processing requirements for transformation toughened ceramics. *In:* L. HENCH and D.R. ULRICH, eds. *Ultrastructure processing of ceramics, glasses and composites*. New York: John Wilegy & Sons, Inc., 1984, pp. 493-506.

LAU, W.W.Y. and BURNS, C.M., 1973. Kinetics of spreading. Polystyrene melts on plane glass surfaces. *J. Colloid Interface Sci.* **45**(2), pp. 295-302.

LE, H.P., 1998. Progress and trends in ink-jet printing technology. *J. Imaging Sci. Tech.*, **42**(1), pp. 49-62.

LEACH, R.H. and PIERCE, R.J., 1999. The nature of printing ink. *In:* R.H. LEACH, R.J. PIERCE, E.P. HICKMENA, M.J. MACKENZIE and H.G. SMITH, eds. *The printing ink manual*, 5th edn.. Netherlands: Kluwer Academic Publishers, 1999, pp.1-13.

LEE, F.C., MILLS, R.N. and TULKE, F.E., 1984. The application of drop-on-demand ink jet technology to colour printing. *IBM J. Res. Develop.*, **28**(3), pp. 307-313.

LEE, S-F.F., SACHS, E. and CIMA, M., 1995. Layer position accuracy in powder-based rapid prototyping. *Rapid Prototyping J.*, **1**(4), pp. 24-37.

LEWIS, J.A., 2000. Colloidal processing of ceramics. *J. Am. Ceram. Soc.*, **83**(10), pp. 2341-2359.

LEWIS, W.A. Jr., 1996. Dry pressing technical ceramics. *Am. Ceram. Soc. Bull.*, **75**(4), pp. 103-106.

LI, Y., TANG, Z.L., ZHANG, Z.T. and GONG, J.H., 1999. Electrical conductivity of zirconia stabilised with yttria and calcia. *J. Mater. Sci. Lett.*, **18**(6), pp. 443-444.

LIN, J.C. and WANG, C.Y., 1996. Effects of surfactant treatment of silver powder on the rheology of its thick-film paste. *Mater. Chem. Phys.*, **45**(2), pp. 136-144.

LINX PRINTING TECHNOLOGIES, PLC, 1996. *User Manual for Linx 6200 Series, MP65138.* Cambridge: Linx Printing Technologies, Plc., 1 May 1996.

LLOYD, W.J. and TAUB, H.H., 1988. Ink-jet printing. *In:* R.C. DURBECK and S.SHERR, eds. *Output hardcopy devices.* Boston: Academic Press, Inc., 1988, pp. 311-370.

MAENOSONO, S., DUSHKIN, C.D., SAITA, S. and YAMAGUCHI, Y., 1999. Growth of a semiconductor nanoparticle ring during the drying of a suspension droplet. *Langmuir,* **15**(4), pp. 957-965.

MANAS-ZLOCZOWER, I., 1991. Mixing in high-intensity batch mixers. *In:* C. RAUWENDAAL, ed. *Mixing in polymer processing.* New York: Marcel Dekker, Inc., 1991, pp. 323-376.

MARK, H.F., BIKALES, N.M., OVERBERGER, C.G. and MENGES, G., 1988. *Encyclopaedia of Polymer Science and Engineering, Vol. 13: Poly(phenylene) Ether to Radical Polymerisation.* New York: John Wiley & Sons, Inc., 1988, pp. 312-345.

MARSH, R., 1988. Inks for special purposes. *In:* R.H. LEACH, R.J. PIERCE, E.P. HICKMENA, M.J. MACKENZIE and H.G. SMITH, eds. *The printing ink manual,* 4th edn.. London: Van Nostrand Reinhold, 1988, pp. 562-591.

MASON, T.J., LORIMER, J.P. and BATES, D.M., 1992. Quantifying sonochemistry: casting some light on a 'black art'. *Ultrasonics*, **30**(1), pp. 40-42.

MAXWELL, J. and PEGNA, J., 1995. Gas phase laser induced pyrolysis of tapered microstructures. *In:* H.L. MARCUS, J.J. BEAMAN, D.L. BEAMAN, D.K. BOURELL, J.W. BARLOW and R.H. CRAWFORD, eds. *Proc. solid freeform fabrications,* Austin, Texas, USA, Aug 7-9, 1995. Austin: University of Texas at Austin, 1995, pp. 143-150.

McALEA, K., FORDERHASE, P., HEJMADI, U. and NELSON, C., 1997. Materials and applications for the selective laser sintering process. *In:* A.J. LIGHTMAN, R.P. CHARTOFF, M.K AGARWALA and F. PRING, eds. *Proc. 7th int. conf. rapid prototyping,* San Francisco, California, USA, Mar 31 - Apr 3, 1997. Dayton: University of Dayton, 1997, pp 23-33.

McENTIRE, B.J., 1991. Dry pressing. *In:* S.J. SCHNEIDER Jr, volume chairman *Engineering materials handbook, vol. 4 - ceramics and glasses*. Ohio: American Society for Metals, International, 1991, pp. 141-145.

McHALE, A.E., 1991. Processing additives. *In:* S.J. SCHNEIDER Jr, volume chairman *Engineering materials handbook, vol. 4 - ceramics and glasses*. Ohio: American Society for Metals, International, 1991, pp. 115-121.

MECHOLSKY, J.J., Jr., 1989. Engineering research needs of advanced ceramics and ceramic-matrix composites. *Am. Ceram. Soc. Bull.*, 68(2), pp. 367-375.

MELVIN III, L.S. and BEAMAN, J.J., 1991. The electrostatic application of powder for selective laser sintering. *In:* H.L. MARCUS, ed. *Proc. solid freeform fabrication symposium*, Austin, Texas, USA, Aug 1991. Austin: The University of Texas at Austin, 1991, pp. 171-177.

MELVIN, L.S, III and BEAMAN, J.J., 1992. The application of an artificial body forces to the selective laser sintering process. *In:* H.L. MARCUS, K.J. BEAMAN, J.W. BARLOW, D.L. BOURNELL and R.H. CRAW, eds. *Proc. solid freeform fabrication 3rd symposium,* Austin, Texas, USA, Aug 3 - 5, 1992. Austin: the University of Texas at Austin, 1992, pp. 118-123.

MISTLER, R.E., 1998. Tape casting: past, present, potential. *Am. Ceram. Soc. Bull.*, 77(10), pp. 82-86.

MIKESKA, K. and CANNON, W.R., 1984. Dispersants for tape casting pure barium titanate. *In:* J.A. MANGELS and G.L. MESSING, eds. *Advances in ceramics, vol. 9, forming of ceramics*. Boston: American Ceramic Society, 1984, pp. 255-275.

MOLONEY, V.M.B., PARRIS D. and EDIRISINGHE, M.J., 1995. Rheology of zirconia suspensions in a nonpolar organic medium. *J. Am. Ceram. Soc.*, 78(12), pp. 3225-3232.

MORNEO, R., 1992. The role of slip additives in tape-casting technology: part i - solvents and dispersants. *Am. Ceram. Soc. Bull.*, 71(10), pp 1521-1531.

MOTT, M. and EVANS, J.R.G., 1999. Zirconia/alumina functionally graded material made by ceramic ink jet printing. *Mater. Sci. Eng. A - Struct.*, 271 (1-2), pp. 344-352.

MOTT, M. and EVANS, J.R.G., 2001. Solid freeforming of silicon carbide by inkjet printing using a polymeric precursor. *J. Am. Ceram. Soc.*, 84 (2), pp. 307-313.

MOTT, M., SONG J. and EVANS, J.R.G., 1999. Microengineering of ceramics by direct ink-jet printing. *J. Am. Ceram. Soc.*, **82**(7), pp. 1653-1658.

NANOPOWDERS INDUSTRIES LTD., 2000. *Technical Specification for Silver #562, Lot nr. 0008-1.* Kfar Saba: NanoPowders Industries Ltd., Nov 13, 2000.

NAPPER, D.H., 1983. Polymeric Stabilisation of Colloidal Dispersions. London: Academic Press, 1983, pp. 4-13.

OMATETE, O.O., JANNEY, M.A. and STREHLOW, R.A., 1991. Gelcasting - a new ceramic forming process. *Am. Ceram. Soc. Bull.*, **70**(10), pp. 1641-1649.

OWENS, D.K. and WENDT, J., 1969. Estimation of the surface free energy of polymers. *J. Appl. Polym. Sci.*, **13**, pp 1741-1747.

PARFITT, G.D. and BARNES, H.A., 1992. The dispersion of fine particles in liquid media. *In:* N.HARNBY, M.F. EDWARDS and A.W. NIENOW, eds. *Mixing in the process industries*, 2nd edn.. Oxford: Butterworth-Heinemann, 1992, pp. 99-117.

PARISEE, F. and ALLAIN, C., 1996. Shape changes of colloidal suspension droplets during drying. *J. Phys. II France*, **6**(7), pp. 1111-1119.

PARISEE, F. and ALLAIN, C., 1997. Drying of colloidal suspensions: experimental study and profile renormalisation. *Langmuir,* **13**(14), pp. 3598-3602.

PARISH, M. and JEFFERY, J.B., 1995. Ceramic filter elements with tailored macro- and microstructures. *Filtr. Separat.*, **32**(1), pp. 31-35.

PASHLEY, R.M. and ISRAELACHVILI, J.N., 1981. A comparison of surface forces and interfacial properties of mica in purified surfactant solutions. *Colloids Surf.*, **2**(2), pp. 169-187.

PAUL, B.K. and BASKARAN, S., 1996. Issues in fabricating manufacturing tooling using powder-based additive freeform fabrication. *J. Mater. Processing Technol.*, **61**(1-2), pp. 168 - 172.

PEUCKERT, M., VAAHS, T. and BRÜCK, M., 1990. Ceramics from organometallic polymers. *Adv. Mater.*, **2**(9), pp. 398-404.

PHAM, D.T. and GAULT, R.S., 1998. A comparison of rapid prototyping technologies. *Int. J. Mach. Tools Manuf.*, **38**(10-11), pp. 1257-1287.

PIMBLEY, W.T. and LEE, H.C., 1977. Satellite droplet formation in a liquid jet. *IBM J. Res Develop.*, **21**(1), pp. 21-30.

PORTER, M.R., 1994. *Handbook of Surfactant,* 2nd edn. Glasgow: Blackie Academic and Professional, 1994, pp. 26-93.

RAMSEY, B.J., EVANS, P.S.A. and HARISSON, D.J., 1997. Conductive lithographic films, (Online). Available: *http://www.brunel.ac.uk/research/cleaner/CLF.html* (Accessed June 5, 2000).

RANCE, D.G., 1982. Thermodynamics of wetting: from its molecular basis to technological application. *In:* D.M. BROWNS, ed. *Surface analysis and pretreatment of plastics and metals*. Essex: Applied Science, 1982, pp. 121-152.

RAY, A.K., LEE, J. and TILLEY, H.L., 1988. Direct measurements of evaporation rates of single droplets at large Knudsen numbers. *Langmuir,* 4(3), pp. 631-637.

RAYLEIGH, L., 1882. On the equilibrium of liquid conducting masses charged with electricity. *Philos. Mag.*, **14**, pp. 184-186.

REED, J.S., 1995. *Principles of Ceramic Processing*, 2nd edn.. New York: John Wiley & Sons, 1995, pp. 201 - 211, 397-398, 418-449, 492 -524, 583 - 624.

REIS, N., SEERDEN, K.A.M., DERBY, B., HALLORAN, J.W. and EVANS, J.R.G., 1999. Direct inkjet deposition of ceramic green bodies: ii – jet behaviour and deposit formation. *Mat. Res. Soc. Symp. Proc.*, **542**, pp. 147-152.

RICE, W., 1983. Ceramics from polymer pyrolysis, opportunities and trends - a materials perspective. *Am. Ceram. Soc. Bull.*, **62**(8), pp. 889-892.

RICHARDS, V.L. II., 1989. Adsorption of dispersants on zirconia powder in tape-casting slip compositions. *J. Am. Ceram. Soc.*, **72**(2), pp. 325-327.

RICHERSON, D.W., 1991. Forming and predensification and nontraditional densification processes. *In:* S.J. SCHNEIDER Jr, volume chairman *Engineering materials handbook, vol. 4 - ceramics and glasses*. Ohio: American Society for Metals, International, 1991, pp. 123-124.

RICHERSON, D.W., 1992. *Modern Ceramic Engineering: Properties, Processing and Use in Design*, 2nd edn.. New York: Marcel Dekker, 1992, pp. 478-488, 519-595.

ROCK, S.J., GILMAN, C.R. and MISIOLEK, W.Z., 1997. Freeform powder moulding: from CAD model to part without tooling. *Int. J. Powder Metall.*, **33**(6), pp. 37-44.

ROSEN, M.J., 1989. *Surfactants and Interfacial Phenomena*, 2nd edn. New York: John Wiley & Sons, 1989, pp. 56-57, 349-362.

RUPPEL, I., 1991. Extrusion. *In:* S.J. SCHNEIDER Jr, volume chairman *Engineering materials handbook, vol. 4 - ceramics and glasses*. Ohio: American Society for Metals, International, 1991, pp. 166-172.

RUST, R.D., 1995. Process characterisation and control. *In:* C.F.COOMBS, Jr., ed. *Printed circuits handbook*, 4th edn.. New York: McGraw Hill, 1995, pp 25.1-25.18.

SACHS, E., CIMA, M., CORNIE, J., BRANCAZIO, D., BREDT, J., CURODEAU, A., FAN T., KHANUJA, S., LAUDER, A., LEE, J. and MICHAELS, S., 1993. Three dimensional printing: the physics and implications of additive manufacturing. *CIRP Annals*, **42**(1), pp. 257- 260.

SACHS, E., CIMA, M., WILLIAMS, P., BRANCAZIO, D. and CORNIE, J., 1992. Three dimensional printing: rapid tooling and prototypes directly from a CAD model. *J. Eng. Ind.*, **114**(4), pp. 481-488.

SAITO, S., 1985. *Fine Ceramics*. Essex: Elsevier Science Ltd., 1985, pp. xv-xxii.

SCALTER, N., 1999. *Electronics Technology Handbook*. New York: McGraw-Hill, pp. 509-522.

SCHILLING, C.H. and AKSAY, I.A., 1991. Slip casting. *In:* S.J. SCHNEIDER Jr, volume chairman *Engineering materials handbook, vol. 4 - ceramics and glasses*. Ohio: American Society for Metals, International, 1991, pp.153-160.

SCHREDIER, J.M., LINDBLAD, N.R., HENDRICKS, C.D., Jr., and CROWLEY, J.M., 1967. Stability of an electrified liquid jet. *J. Appl. Phys.*, **38**(6), pp. 2599- 2605.

SCHWARTZ, M.M., 1992. *Handbook of Structural Ceramics*. New York: McGraw Hill, pp. 8.1-8.91.

SCOTT, H.G., 1975. Phase relations in the zirconia-yttria system. *J. Mater. Sci.*, **10**(9), pp 1527-1535.

SEBASTIAN, P.J., GOMEZDASA, O. and NAIR, P.K., 1993. Screen printed ZnCdS films for opto-electronic applications. *Eng. Optics*, **6**(1), pp. 117-119.

SEERDEN, K.A.M., REIS, N., DERBY, B., GRANT, P.S., HALLORAN, J.W. and EVANS, J.R.G., 1999. Direct ink-jet deposition of ceramic green bodies: i – formulation of build materials. *Mat. Res. Soc. Symp. Proc.*, **542**, pp. 141-146.

SEPULVEDA, P., 1997. Gelcasting foams for porous ceramics. *Am. Ceram. Soc. Bull.*, **76**(10), pp. 61-65.

SHANEFIELD, D.J., 1995. *Organic Additives and Ceramic Processing.* Amsterdam: Kluwer Academic Publishers, 1995, pp. 91-114.

SHANNAHAN, M.E.R. and BOURGES, C., 1994. Effects of evaporation on contact angles on polymer surfaces. *Int. J. Adhesion Adhesives,* **14**(3), pp. 201-205.

SHAW, D.J., 1996. *Introduction to Colloid and Surface Chemistry*, 4th edn.. Oxford: Butterworth-Heinemann, 1996, pp. 1-20, 169-173, 244-261.

SHIMODA, H., 1995. An overview of the status of the fine ceramics industry in Japan. *Ind. Ceram.*, **15**(3), pp. 187-190.

SIGMUND, W.M., BELL, N.S. and BERGSTRÖM, L., 2000. Novel powder-processing methods for advanced ceramics. *J. Am. Ceram. Soc.*, **83**(7), pp. 1557-1574.

SKIDMORE, C., 1998. Zirconium oxides/chemicals - a review of raw materials, markets and future prospects. *Int. Ceram.*, (2), pp 17-22.

SLADE, C.E. and EVANS, J.R.G., 1998. Freeforming ceramics using a thermal jet printer. *J. Mater. Sci. Lett.*, **17**(19), pp. 1669-1671.

SMITH, V., DECKMAN, B. and BRUECK, D., 1994. Advanced ceramics: where do we go from here? *Am Ceram. Soc. Bull.*, **73**(12), pp. 49-52.

SONG, J.H., EDIRISINGHE, M.J. and EVANS, J.R.G., 1999. Formulation and multilayer jet printing of ceramic inks. *J. Am. Ceram. Soc.*, **82**(12), pp. 3374-3380.

STEINLAGE, G.A., ROEDER, R.K., TRUMBLE, K.P. and BOWMAN, K.J., 1996. Centrifugal slip casting of components. *Am. Ceram. Soc. Bull.*, **75**(5), pp. 92-94.

STINTON, D.P., BESMANN, T.M., LOWDEN, R.A. and SHELDON, B.W., 1991. Vapour deposition. *In:* S.J. SCHNEIDER Jr, volume chairman *Engineering materials handbook, vol. 4 - ceramics and glasses.* Ohio: American Society for Metals, International, 1991, pp. 215 - 222.

SUBRAMANIAN, P.K. and MARCUS, H.L., 1995. Selective laser sintering of alumina using aluminium binder. *Mater. Manuf. Processes*, **10**(4), pp. 689-706.

SUYAMA, Y. and YAMAGUCHI, T., 1991. Products for advanced ceramics: characterisation and synthesis. *In:* P. VINCENZINI, ed. *Fundamentals of ceramic engineering.* Essex: Elsevier Science Ltd., 1991, pp. 121-151.

SWARTZ, S.L., SHROUT, T.R. and TAKENAKA, T., 1997a. Electronic ceramics R&D in the US, Japan, part i: patent history. *Am. Ceram. Soc. Bull.*, **76**(7), pp. 59-63.

SWARTZ, S.L., SHROUT, T.R. and TAKENAKA, T., 1997b. Electronic ceramics R&D in the US, Japan, part ii: Japanese view. *Am. Ceram. Soc. Bull.*, **76**(8), pp. 51-55.

TAIT, R.B., HUMPHRIES, R. and LORENZ, J., 1994. Thick film heater elements and temperature sensors in modern domestic appliances. *IEEE Trans. Indust. Appl.*, **30**(3), pp. 573-577.

TENG, K.F. and VEST, R.W., 1987. Liquid ink jet printing with MOD inks for hybrid microcircuits. *IEEE Trans. Comp. Hybrids and Manuf.Tech.*, **12**(4), pp. 545-549.

TENG, K.F. and VEST, R.W., 1988. Metallization of solar cells with ink jet printing and silver metallo-organic inks. *IEEE Trans. Comp. Hybrids and Manuf. Tech.*, **11**(3), pp. 291-297.

TENG, R.K.F., AZADPOUR, A.M. and KARIM, A., 1990. Study of solar cell fabrication using an electrostatic thick-film printing method. *IEEE Trans. Ind. Electron.*, **37**(5), pp. 419-423.

TENG, W.D., 1997. *Solid freeform fabrication of ceramics: continuous direct ink-jet printing and electrostatic atomisation.* Ph.D. dissertation. Uxbridge: Brunel University, 1997.

TENG, W.D. and EDIRISINGHE, M.J., 1998. Development of ceramic inks for direct continuous jet printing. *J. Am. Ceram. Soc.*, **81**(4), pp. 1033-1036.

TENG, W.D., EDIRISINGHE, M.J. and EVANS, J.R.G., 1997. Optimisation of dispersion and viscosity of a ceramic jet printing ink. *J. Am. Ceram. Soc.*, **80**(2), pp. 486-494.

TILLER, F.M. and KHATIB, Z., 1984. The theory of sediment volumes of compressible, particulate structures. *J. Collod. Inter. Sci.*, **100**(1), pp. 55-67.

TURNER, S.W., 1991. Sol-gel process - principles and applications. *Am. Ceram. Soc. Bull.* **70**(9), 1487-1490.

UZIEL, Y., 1997. Eliminating prototype tooling in metal casting yields a seamless transition from CAD to manufacturing – a case study. *SME technical paper PE98-117-2*, pp. 1-8.

VEST, R.W., 1986. Materials science of thick film technology. *Am. Ceram. Soc. Bull.*, **65**(4), 631-636.

VINCENZINI, P, 1991. Ceramics: some approaches to the meaning of the term and research prospects. *In:* P. VINCENZINI, ed. *Fundamentals of ceramic engineering.* Essex: Elsevier Science Ltd., 1991, pp. 1-25.

WALIG, L.R., 1988. Image transfer. *In:* C.F.COOMBS, Jr, ed. *Printed circuits handbook*, 3rd edn.. New York: McGraw Hill, 1988, pp 11.1 - 11.37.

WANG, G. and KRSTIC, V.D., 1998. Rapid prototyping of ceramic components - review. *J. Canad. Ceram. Soc.*, **67**(3), pp. 52-57.

WANG, G., SARKAR, P. and NICHOLSON, P.S., 1997. Influence of acidity on the electrostatic stability of alumina suspensions in ethanol. *J. Am. Ceram. Soc.*, **80**(4), pp. 965-972.

WANG, S.R., DOUGHERTY, J.P., HUEBNER, W. and PEPIN, J.G., 1994. Silver-palladium thick film conductors. *J. Am. Ceram. Soc.*, **77**(12), pp. 3051-3072.

WEBER, C., 1939. Zum zerfall eines flussigkeisstrahles. *Z. Angew. Math*, **11**, pp. 136-154.

WEST, R.C., ASTLE, M.J. and BEYER, W.H., 1985. *CRC Handbook of Chemistry and Physics*, 66th edn.. Florida: CRC Press, Inc., p. F-32.

WIDEGREN, J. and BERGSTRöM, L., 2000. The effect of acids and bases on the dispersion and stabilisation of ceramic particles in ethanol. *J. Eur. Ceram. Soc.*, **20**(6), pp. 659 - 665.

WILLIAMS, S (Swilliam@linx.co.uk), Oct 7, 1998. *Re: Linx Printer.* Email to B.Y. Tay (B.Y.Tay@lboro.ac.uk).

WILLIAMS, S (Swilliam@linx.co.uk), Jan 18, 2000. *Re: Linx Printer.* Email to B.Y. Tay (B.Y.Tay@qmw.ac.uk).

WINDLE. J. and DERBY, B., 1999. Ink jet printing of PZT aqueous ceramic suspensions. *J. Mater. Sci. Lett.*, **18**(2), pp. 87-90.

WRIGHT, M.J. and EVANS, J.R.G., 1999. Ceramic deposition using an electromagnetic jet printer station. *J. Mater. Sci. Lett.*, **18**(2), pp 99-101.

XIANG, Q.F., EVANS, J.R.G., EDIRISINGHE, M.J. and BLAZDELL, P.F., 1997. Solid freeforming of ceramics using a drop-on-demand jet printer. *P. I. Mech. Eng. B - J. Eng. Manuf.*, **211**(3), pp. 211-214.

YAJIMA, S., 1983. Special heat-resisting materials from organometallic polymers. *Am. Ceram. Soc. Bull.*, **62**(8), pp. 893-903.

YANAGIDA, H., KOUMOTO, K. and MIYAGAMA, M., 1996. *The Chemistry of Ceramics*. Chichester: John Wiley & Sons, 1996, pp. 147-149, 168-170, 174.

YANG, Y., CHANG, S., BHARATHAN, J. and LIU, J., 2000. Organic/polymeric electroluminescent devices processed by hybrid ink-jet printing. *J. Mater. Sci. - Mater. Electron.*, **11**(2), pp. 89-96.

YOO, J., CHO, K.M., BAE, W.S., CIMA, M. and SURESH, S., 1998. Transformation-toughened ceramic multilayers with compositional gradients. *J. Am. Ceram. Soc.*, **81**(1), pp. 21-32.

ZHOU, J.G., 2000. Editorial. *Mater. Design*, **21**(2), pp. 61-63.

ZISMAN, W.A., 1964. Relation of the equilibrium contact angle to liquid and solid constitution. *Adv. Chem. Ser.*, **43**, pp. 1-51.

Appendix

Power Estimation at Ultrasonic Disruption

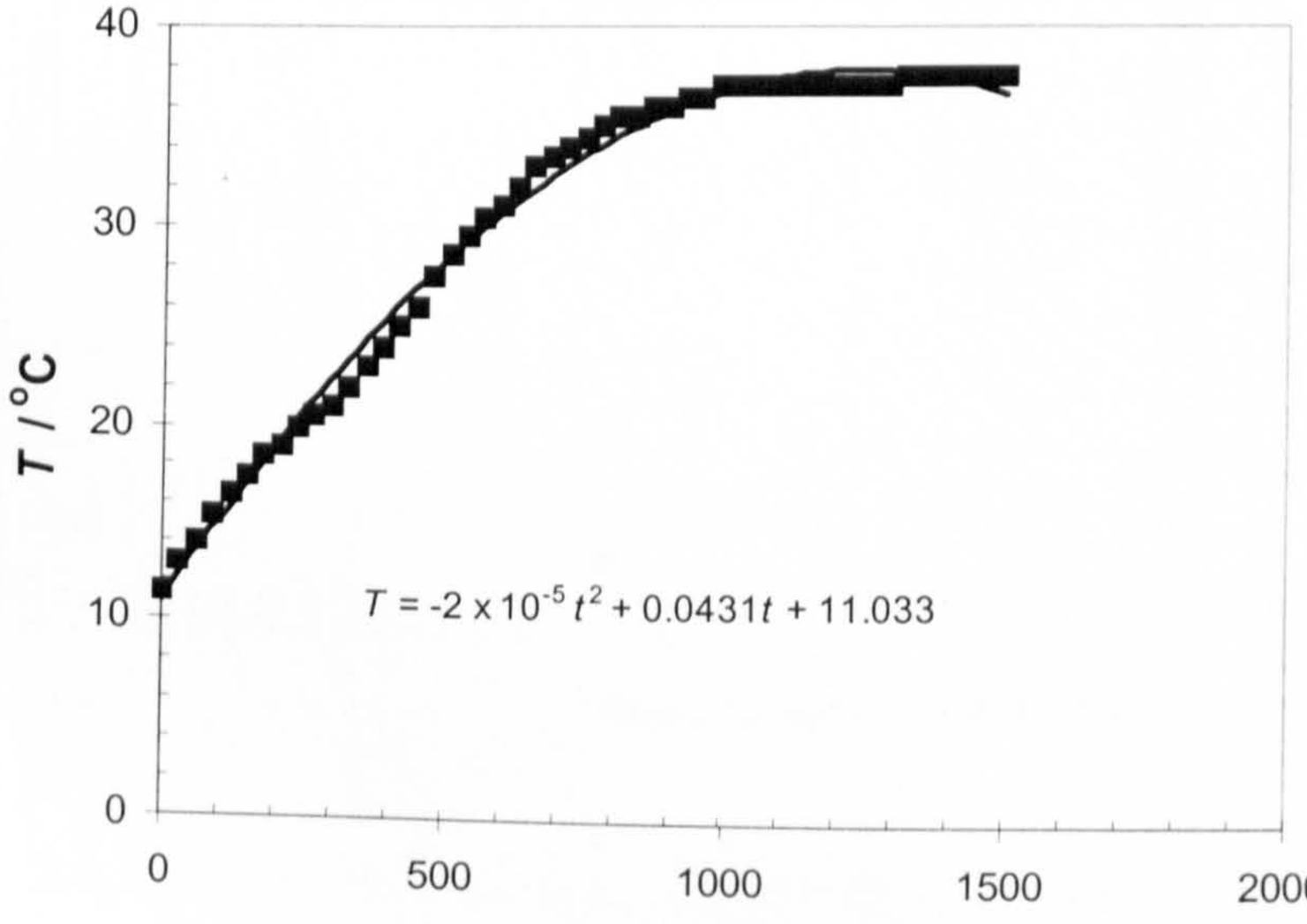

Figure A.1 Temperature T versus time t curve of ceramic ink during ultrasonic disruption.

For a single batch of ink,

Mass, m	=	0.7103 kg
C_p	=	2450 J kg^{-1} K^{-1}
$(dT/dt)_0$	=	0.0431 °C s^{-1}

From Equation 3.1

P_{diss}	=	2450 x 0.7103 x 0.0431
	=	75 W

Appendix

B

Viscosity Measurements of IPA

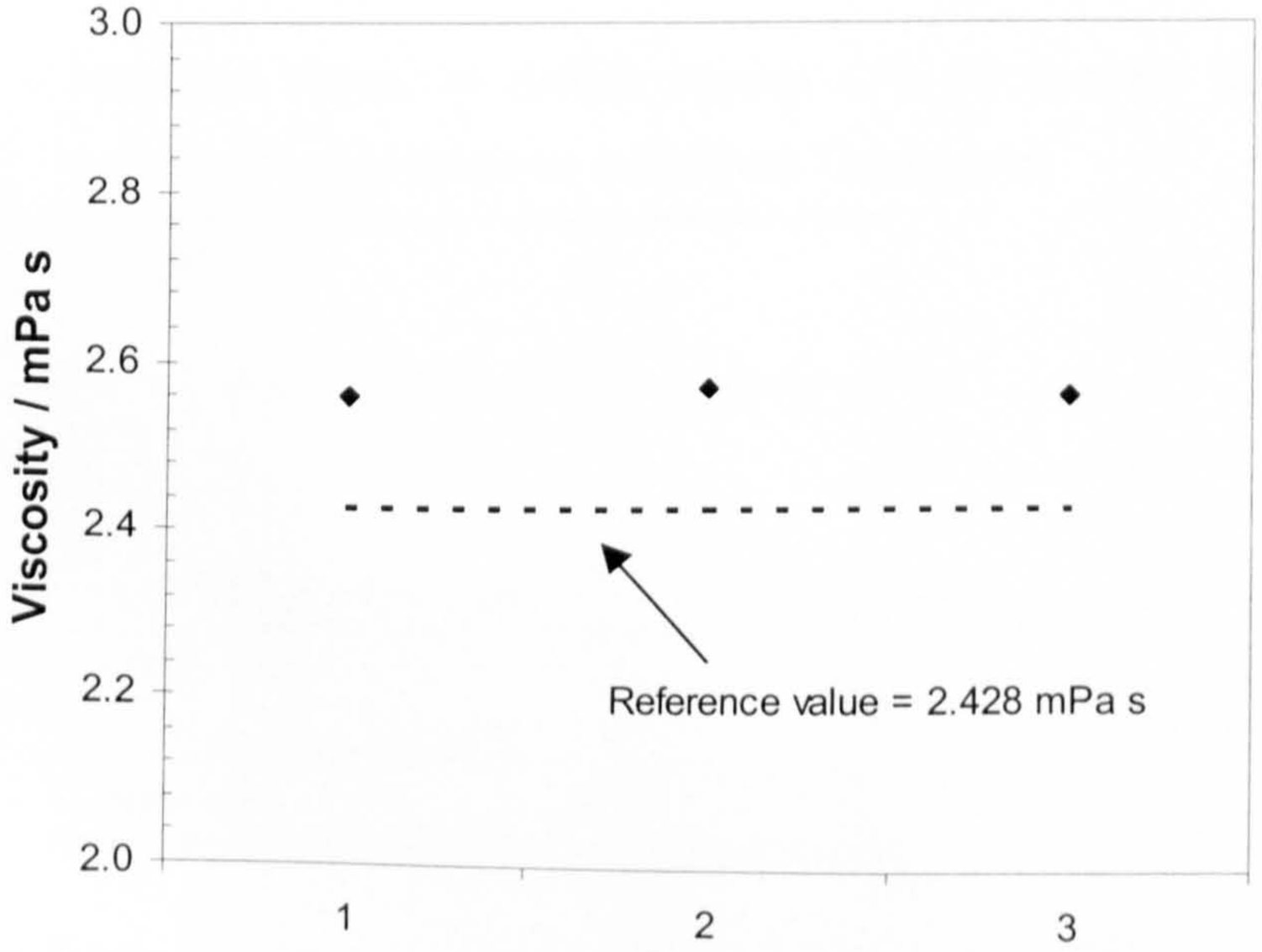

Figure B.1 Measurement of IPA (AnalR Propan-2-ol, Merck, Leicestershire, UK) by Hakke RheoStress 150 at 20°C, 1000 s^{-1}. The average variation from the handbook value of 2.428 mPa s [West *et al.*, 1989] is 5.6%.

Appendix

C

Surface Tension Measurement using Ring Method

Table A.1 Measured values of surface tension (γ^*) for ceramic ink over five consecutive measurements with Kruss Tensiometer.

S/N	γ^* / mN m^{-1}
1	25.1
2	25.1
3	25.1
4	25.1
5	25.1
Average	**25.1**

According to Kruss Tensionmeter manual [Kruss, 1985] the real surface tension, $\gamma_{l,ink}$, is:

$$\gamma_{l,ink} = C\,\gamma^*\,F$$

Where F is the linear compensation factor for the instrument, which is 1.07

C, Harkins and Jordan's correction factor [Harkins and Jordan, 1930]

From Table VIIIE of reference [Harkins and Jordan, 1930]. for the ring configuration of $R = 9.545$ mm, $R/r = 51.6$, $C = 0.875$.

Therefore,

$$\gamma_{l,ink} = 0.875 \times 25.1 \times 1.07$$
$$= 23.5 \text{ mN m}^{-1}$$